University of Southampton

Faculty of Social and Human Sciences

Geography and Environment

Analysis of Vegetation Dynamics and Application in Agriculture Using MERIS Terrestrial Chlorophyll Index

BY

LINGQUAN ZHOU

A thesis submitted for the degree of Doctorate of Philosophy (PhD)

Supervisors:

J. Dash and P.M. Atkinson

April 2018

UNIVERISTIY OF SOUTHAMPTON

Abstract

FACULTY OF SOCIAL AND HUMAN SCIENCE

Geography and Environment

Thesis for the degree of Doctor of Philosophy

Analysis of Vegetation Dynamics and Application in Agriculture Using MERIS Terrestrial Chlorophyll Index

LINGQUAN ZHOU

Vegetation phenological stages are important indicators for monitoring vegetation growth, evaluating climate change impacts on vegetation, control atmospheric general circulations and carbon sequestration. Traditional phenology observations rely on fixed-point visual inspection. However, this method is labour-intensive and subjective, and often limited to few species. Remote sensing technology using vegetation indices provides a more objective, long-term, continuous and efficient way to monitor land surface phenology from regional to world wide scale. The European Space Agency (ESA)'s Medium Resolution Imaging Spectrometer (MERIS) data in red/NIR (near infrared) were used to produce the level-2 product of MERIS Terrestrial Chlorophyll Index (MTCI). The MTCI, is strongly linked with the red edge position (REP) in vegetation spectra, and in turn the foliar chlorophyll content, making the MTCI a useful product of vegetation phenology indicator.

In this thesis the MTCI data with different resolutions were applied to monitor vegetation phenological variables over mainland China, namely onset of greenness (OG) and end of senescence (ES). Then they were correlated with climatic factors of temperature and precipitation, demonstrated the main drives for major vegetation types in climate zones. Both MTCI and NDVI time-series captured the growth patterns for major vegetation types, the OG estimates were more consistent than the ES, and overall the NDVI gave later ES estimates than the MTCI. 9-year phenology maps showed that the OG was advanced and the ES was delayed in general. The OG was more related with latitude than the ES especially in the north China, while

it was the opposite for the ES. And it was found in north China, the temperature was the main driver for the earlier OG, while in the south precipitation played a prominent role in advancing the OG. For the ES, both precipitation and temperature influenced partially. In Qinghai-Tibet Plateau, the precipitation was the main driver for both shifting OG and ES of grass, while less influenced by temperature. Among the vegetations that were examined, the broadleaf forest had the strongest correlation with climatic factors; the needle leaf forest was also greatly influenced by climate in cold temperate zone; the grass was highly affected by climate, while the mixed forest and crops were at moderate level.

In the light of the abilities of MTCI in monitoring vegetation phenology, MTCI was applied into specific situations to test the performance on phenology-based applications, including mapping paddy rice in northeast China and predict rice yield. The results were well consistent with the statistical data on the prefectural level and county level in spatial distribution and quantity from 2007 to 2011. The crop yield regression models indicated that the maximum value of MTCI time-series has a better correlation with rice yield.

In summary, MTCI has its own advantages than popular index such as normalised difference vegetation index (NDVI). It is more sensitive to high values of chlorophyll content and less sensitive to spatial resolution and atmospheric effects. Although the MERIS was not in operation anymore in May 2012, the successor, the Sentinel satellites were launched, with a wider range of wavelength from blue to shortwave infrared, including red edge bands. Therefore, index for estimating foliar chlorophyll can be produced to combine with other Sentinel products in agricultural, biological, and ecological studies.

Table of Contents

Table of Figures

List of Tables

Author's Declaration

I, Lingquan Zhou

declare that the thesis entitled

Analysis of Vegetation Dynamics and Application in Agriculture Using MERIS Terrestrial Chlorophyll Index

and the work presented in the thesis are both my own, and have been generated by myself as the result of my own original research. I confirm that:

- This work was done wholly or mainly while in candidature for a research degree at University of Southampton;
- Where any part of this thesis has previously been submitted for a degree or any other qualification at this University or any other institution, this has been clearly stated;
- Where I have consulted the published work of others, this is always clearly attributed;
- Where I have quoted from the work of others, the source is always given.
- I have acknowledged all main sources of help;
- Where the thesis is based on work done by myself jointly with others, I have made clear exactly what was done by others and what I have contributed myself.

Signed:

Date:

Acknowledgements

It is an honour for me to express my sincere gratitude to people who have made this happen.

I owe the deepest appreciation to my supervisor Professor Jadu Dash and Professor Peter Atkinson. Their constant guidance, support and inspiration have been invaluable. Especially thanks to Professor Jadu Dash, he created an ambiance that encouraged innovation and made me develop good study habits. He also shared his extraordinary experiences throughout the work. Without his unflinching encouragement and help, it would have been impossible for me to finish this thesis.

And I would like to thank my family, my mum, dad and my wife, for their constant support and backing in helping me achieve this goal.

1.Introduction

1.1 A definition of phenology

Phenology is defined by the International Biological Program (IBP) as "the study of the timing of recurrent biological events, the causes of their timing with regard to biotic and abiotic forces, and the interrelation among phases of the same or different species" (Lieth 1974). Phenology as a word was introduced in 1853 by the Belgian botanist Charles Morren and derived from the Greek word *phaino*, which means to show or to appear (Fenner 1998; Haggerty 2008; Koch et al. 2007; Schwartz 2013). In practical terms, phenology is the study of measuring the timing of periodic biological events in the animal and plant lifetime, and how they are influenced by the environment. For example, sprouting and flowering of plants in the spring, colour changes of leaves in the autumn, bird migration and nesting, insect hatches, and animal hibernation are all phenological events (Dube et al. 1984). In the case of flowering plants, more specifically, the life cycle events or phenophases include leaf budburst, first flower, last flower, first ripe fruit, and leaf shedding, among others. Therefore, phenologists record the dates of the event occurrences or phenophases to study how environmental conditions such as temperature and precipitation affect their timing.

Phenology has strong links with human knowledge and its studies may be as old as civilisation itself. As a result of agriculture farmers started to reside in one place with continuous agricultural activities such as planting seeds, observing crop growth, and carrying out the harvest year after year. In ancient periods, phenology was recorded as empirical knowledge and stories up to 3000 years ago in China as well as in the Christian Bible (Schwartz 2013). However, this empirical knowledge could not be translated into systematic data which provide the impetus for the early development of phenology to become an integrated scientific endeavour and discipline, while for a long time the field remained in agricultural applications and generally it was only deemed practical on the local scale.

Ancient inhabitants in China and Europe recorded the activities of plants and animals to mark the seasons (Battey 2000). A large quantities of fragmentary phenology related information was delivered in Chinese folk, poetry, chronicles, almanacs, and monographs on agriculture or herbalism, and also similar forms of

literature are found in European history, especially on agriculture, demonstrating the early origin of phenological knowledge is linked closely with agriculture practices closely (Liang 2009). The longest written phenological record originated in Japan at the Royal court of Kyoto, since the 8th century, as a part of the national festival tradition to record cherry flowering time (Aono and Kazui 2008), and the most vital and broadest tradition of phenological observation is found in Europe in light of long-term data sets in numerous European countries (Menzel 2002).

Modern phenological studies are thought to have been initiated in Europe in the mid-18th century. In 1736 Robert Marsham constantly recorded the "indications of Spring" on his family estate in Norfolk, Britain, to improve timber production by learning more about the timing of plant and animal life cycles such as the first occurrence of leafing, flowering, and insect emergence. After he passed away, his descendants kept making these records until 1947, making it one of the longest phenological monitoring records in Europe (Haggerty 2008). Today, phenology becomes an integrating scientific discipline. Many recent phenological studies are carried out by scientists from various fields including population biologists, community ecologists, climatologists, hydrologists, and specialists of remote sensing (Haggerty 2008). However, as phenology is being paid more and more attention by individuals from many different scientific backgrounds, the full benefits of disciplinary combination still need to be demonstrated and realised in the future (Schwartz 2013).

1.2 The role of vegetation phenology

Phenology has a long traditional history in agriculture. Historical interest in phenology came from an interest in the development of farming and its relation to the climate (Ruml and Vulić 2005). Knowledge of the timing of phenological events and their variability can be helpful for improving stable crop quality and yields by implementing suitable and sustainable crop management including timely irrigation, fertilising and crop protection. Complex environmental interactions and genetic factors determine the dynamics of phenology. Among the vegetation phenological phases such as germination, vegetative, flowering, fruiting, and senescence, flowering time is the most often considered, for it is simple to record and easy to

interpret. It has been found that temperature is the dominant reason for the dynamics of flower time and other phenological phases. Nevertheless, temperature is not the only reason for explaining all the variation in plant growth. Photoperiod, rainfall, and solar radiation have all been reported as important factors often modifying the phenology of plants (Günter et al. 2008; Richardson et al. 2013a; Ruml and Vulić 2005; Schwartz 2013). Although the soil plays a less important role in influencing plant growth than climate (Wielgolaski 2001), sometimes soil temperature, water content, soil type and nutrient supply can also be significant for plant growth (Wielgolaski 1999).Recently, there has been an increase in interest in phenology primarily due to changes in the timing of different phenological phases in plants and animals, connected to climate change (Menzel and Fabian 1999; Peñuelas et al. 2002) Moreover, phenology can contribute to various scientific disciplines from biodiversity, agriculture, and forestry to human health. For example, phenology studies provide significantly valuable data for land-use planning, crop zonation, agricultural, forestry and domestic pest species control, conservational species protection and pollen release information (Khwarahm et al. 2017), and their relations to human health.

It is becoming widely documented that earlier onset of spring phenological events and a lengthening of the growing season is occurring at many locations across the globe because of global warming (Menzel 2000; Menzel 2002). For example, Menzel and Fabian (1999) found an average lengthening of the growing season of about 11 days for tree species in Europe, from the early 1960s to the end of the 20th century. The IPCC (International Panel on Climate Change) in its Third Assessment Report (2002) concluded that many physical and biological systems were already reacting to changing temperatures, such as hydrology, glaciers and ice, vegetation, insects, birds and mammals. Vitasse et al. (2011) predicted that the dates of tree flushing would advance from 0 to 2.4 days per decade, and the senescence would delay from 1.4 to 2.3 days per decade. Guo et al. (2013) found that the first flowering dates of chestnut in Beijing advanced by 1.6 days per decade and the growing season expanded by 4.3 days per decade, during 1963 to 2008. All of these studies demonstrate that climate change is changing the seasonality of our ecosystems significantly, especially in the middle and higher northern latitudes (Smetacek and Nicol 2005; Tucker et al. 2001; Zhang et al. 2004).

The importance of phenology lies in its ability to monitoring effectively the impacts of climate change on plants and animals. Records on observations of plant phenological events such as leaf unfolding, flowering, fruit ripening, leaf colouring, and leaf fall, provide an indication that climatic change is advancing event occurrences by about 2.3 to 5.2 days per decade in the last 30 years, according to (Alcamo and Olesen 2012). Sparks and Menzel (2007) suggested that some effects on vegetation would happen in the future including (i) ranges extending towards the Polar Regions and higher altitudes; (ii) changes in land cover density and vegetation composition; (iii) longer growing seasons; and (iv) more shifting phenological events such as earlier plant flowering, earlier breeding times, earlier egg laying in the year. Among these, changes of growing seasons and phenological events can be well depicted by phenology, which is in close relation to climate and weather conditions, especially temperature in spring and summer (Sparks et al., 2001). Unlike range extension or ecosystem composition change, which can be confounded by other factors such as land use change, temperature is the dominant influence. In addition, changes in the cycle of phenological events and lengthening of the growing season can significantly affect: (i) the global carbon and water cycle (Baldocchi et al. 2005; Churkina et al. 2005; Piao et al. 2007); (ii) shifts in agricultural zoning (Fischer et al. 2005; Fischer et al. 2002); (iii) changing response of vegetation to the atmospheric boundary layer (Schwartz and Crawford, 2001); (iv) plant competition and biodiversity (Rathcke and Lacey, 1985; Schwartz 2003); (v) pest and disease control (Schwartz, 2003); and (vi) pollen flight forecasts (Tormo et al., 2011). Phenology, therefore, has been suggested by Sparks and Menzel (2003), and Walther et al. (2002) as the simplest and most effective means of observing the influence of temperature change which, in turn, makes phenology a significant tool in global change research.

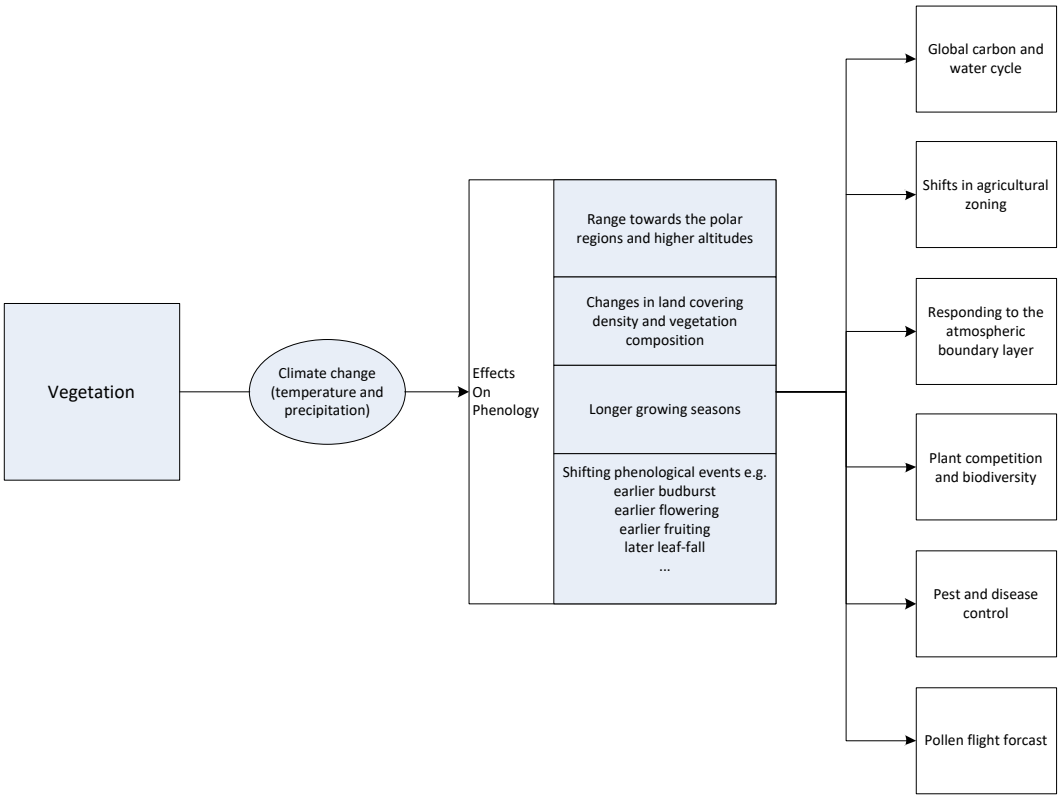

Figure 1 Climate change impacts on vegetation and its responses to the environment.

1.3 The role of remote sensing

The vegetation phenology including bud burst, leaf development, senescence, and growing season length, can be used to document and evaluate the effect of climate change impacts on phenological events. Therefore, long-term observation and recording of vegetation phenological changes is valuable for monitoring and understanding the trends in regional and global climate changes, providing opportunities for reconstructing past climate variation, evaluating the magnitude of climate change impacts on vegetation growth, and predicting biological responses to future climate scenarios (Zhang et al. 2012b).

Conventional long-term observations of species level have been used widely in revealing local and regional climate change for decades (Chen et al. 2005b). For example, budburst and flowering dates could be recorded and associated with air temperature for finding variation in climate over the long-term period. Land surface phenology (LSP) is usually defined as the seasonal variation in vegetated land surface, which is measurable by earth observation satellites (de Beurs and Henebry 2010; Han and Xie 2014; Helman 2018; Jones et al. 2014; Luo et al. 2014; Moody

and Johnson 2001; White and Nemani 2006). It is distinguished from the traditional vegetation or plant phenology that usually is monitored by species in-situ, because LSP is based on regional-to-global scale observations of phenology, which can be directly compared with regional climate information. Therefore, LSP remote sensing data is able to serve as key biological indicators for detecting the response of terrestrial system to climate change. Spectral vegetation indices derived from satellite sensor data are usually used to extract LSP information, such as the Normalised Difference Vegetation Index (NDVI), provide an indication for leaf chlorophyll content, leaf area, canopy cover, and structure, which constitutes canopy greenness. However, the NDVI had been demonstrated to saturate at high level of greenness biomass and concentrations of chlorophyll (Dash et al. 2010b; Huete et al. 2002; Mutanga and Skidmore 2004). Therefore, more accurate chlorophyll-based vegetation indices such as MERIS Terrestrial Chlorophyll Index (MTCI) have been developed to overcome the problem.

By using satellite sensor image derived vegetation indices, remote sensing provides an opportunity to study plant growing conditions and observe vegetation covering large areas over time, and to understand the effects of climate change from local to global scales. For example, Botta et al. (2000) combined leaf onset dates retrieved from NOAA/AVHRR satellite NDVI with climate data and a land cover map to identify appropriate models for predicting the onset date of leaf growth for the decade 1983 to 1993. Maignan et al. (2008) used AVHRR NDVI data to monitor the inter-annual variation of vegetation phenology globally for 18 years from 1982 to 1999. Zhang et al. (2006b) used the enhanced vegetation index (EVI) derived from NASA's Moderate Resolution Imaging Spectroradiometer to study global vegetation phenology including green-up, maturity, senescence, and dormancy, for the period 2001 to 2003. Zhang et al. (2012b) used a two-band enhanced vegetation index (EVI2) derived from the AVHRR and MODIS Climate Modelling Grid (CMG) records to represent global vegetation phenology for three decades (1982-1989, 1990-1999, and 2001-2009).

Many phenology studies were also conducted in China at local to regional scales. Conventional ground observations were often used within conservation or forestry regions for specific species, to study the phenological variation caused by climate

change (Du et al. 2010; Luo et al. 2007; Zhang et al. 2006a; Zhang et al. 2010). However, such conventional approaches are commonly limited by the number of *in situ* observation sites and labour intensity; therefore, it is very hard to obtain information on vegetation response to climate change at the biomes scale. In addition, phenological stations and conventional phenological data are comparatively scarce (Chen and Pan 2002).

1.4 Aims and objectives

The overall aim of this research was to test the performance of the MTCI in monitoring phenology and phenology-based agricultural applications over China at a range of temporal and spatial resolutions. The specific objectives are proposed as follows:

1. To investigate the performance of using the MTCI to monitor vegetation phenology at large and regional scales for different vegetation types.
2. To estimate vegetation phenology over a 9-year period across mainland China by using the MTCI data.
3. To quantify vegetation phenological variation at the regional scale and investigate the drivers of this variation.
4. To evaluate the potential of using phenological information derived from MTCI in specific applications such as agricultural mapping and crop yield forecasting, in conjunction with other indices.

1.5 Thesis structure

After Chapter 1 (*Introduction*), Chapter 2 reviewed the use of remote sensing in monitoring vegetation phenology. Including sources of remote sensing data, processing data, and phenological extraction techniques.

Chapter 3 (*compare MTCI with NDVI*) computed MTCI from 2010 MERIS 300 m 8-day data, and extracted phenological metrics including Onset of Greenness (OG) and End of Senescence (ES) at the regional level within mainland China, for four major vegetation types. The chapter concluded with a summary of the advantage and disadvantage for the MTCI in monitoring vegetation phenology, compared to widely used NDVI.

Chapter 4 (*mapping vegetation phenology over mainland China*) adopted 4.6 km MTCI data from 2003 to 2011 to extract key phenological variables including OG, ES, and LGS at the national level of mainland China. By the end of this chapter, the produced phenology maps were ready to be used for further analysis.

Chapter 5 (*analyse phenology change with climate change*) studied phenology changes in related to climatic factors of precipitation and temperature over a period from 2003 to 2011 based on the phenology maps produced in the last chapter, for eight vegetation-climate zones in mainland China.

Chapter 6 (*use MTCI and other vegetation indices to map paddy rice in northeast China*) utilised 1km MTCI data from 2007 to 2011, coupling with MODIS NDVI and $LSWI_{1640}$, by using a combined conditions method to map paddy rice fields distribution at northeast China. At the end of this chapter, rice maps were generated for the year 2007 to 2011. These rice maps were validated with NLCD 2010 dataset and statistical records from the yearbook.

Chapter 7 (*using rice map to predict yield*) established a linear regression relationship between phenological variables extracted from MTCI time-series data and yield records from the statistical yearbook. This was validated by using leave-one-year-out-approach.

Chapter 8 *(discussion)* reviewed the findings from the previous chapters, and discussed the benefits of the MTCI in land surface phenology-based applications, as well as the limitations.

Chapter 9 (*conclusions and future work*) summarised the novel contributions made in this thesis, discussed the advantages and disadvantages of using MTCI in monitoring land surface phenology, and in phenology-based applications.

2.Literature Review

2.1 Climate change and vegetation phenology

There is a substantial body of evidence showing Earth has warmed since the middle of the 19th century, it can result from natural causes, human activities through the emission of greenhouse gases such as CO_2 and methane, and land use. (Wheeler and von Braun 2013). Climate warming has brought the spring earlier and delayed the arrival of winter (Menzel et al. 2006; Peñuelas et al. 2009). It changes the growing cycle of plants between years, which leads to many consequences for ecological processes, agriculture, forestry, human health, and the global economy (Myneni et al. 1997). Studies on the impact of plant responds to climate change suggest that the phenological shifts in turn affect climate (Fang et al. 2002; Ganjurjav et al. 2016; Menzel et al. 2006; Richardson et al. 2013b; Vitasse et al. 2011; Wang et al. 2017b; White et al. 2005). Longer growing seasons have effects on biochemical processes and physical properties of vegetated land surfaces. CO_2 uptake is the main biochemical process in photosynthesis, in which plant traps CO_2 from the atmosphere to produce glucose for growth and respiration (Polgar and Primack 2011). An extended plant growing season increases the amount of biospheric CO_2 uptake and thus decreases the concentration of CO_2 in the atmosphere, which contributes to the greenhouse effect. Furthermore, the extended plant activity increases the total emission amount of biogenic volatile organic compounds (BVOCs), which may also contribute to the complex processes associated with global warming (Delbart et al. 2008; Hollister et al. 2005). In addition, the shifts in all the phenophases have impacts on regional microclimate, by altering surface albedo, CO_2 fluxes and evaporation, and in the longer term, global climate (Menzel 2002).

The scientific discipline of phenology has a long history, it was firstly known as records of how and when plants and animals responded to seasonal changes by early farmers (Demarée and Rutishauser 2009). In recent decades, many modelling and empirical studies demonstrating that plant phenology can serve as an indicator of the long-term biological impacts of climate change on ecosystems, especially temperature on the timing of plant phenophases (Donnelly and Yu 2017; Richardson et al. 2013b). Further, not only are plant phenophases impacted by climate change, but also plant growth responds to climate system with, for example, influences on

carbon flux to the atmosphere (Richardson et al. 2013b). Menzel et al. (2006) highlighted the impacts on the environment by using long-term (1971-2000) pan-European (21 countries) phenological data. They found that 78% of all leafing, flowering, and fruiting records advanced and only 3% were significantly delayed, while the average advance of spring/summer was 2.5 days decade^{-1} in Europe. Piao et al. (2006b) examined the effects from climate changes on vegetation phenology during 1982 to 1999 in temperate China. The results showed that a warming in the early spring by 1°C would cause an earlier green-up date of 7.5 days, whereas a delayed dormancy of 3.8 days in autumn. Guo et al. (2013) evaluated long-term (1963-2008) climate responses of chestnut phenology season from Beijing, China. The results showed that the first flowering date in Beijing was advanced by high temperature, but delayed during autumn and winter in warm conditions. Leaf colouring was advanced by warm weather, but delayed by high temperature in autumn.

Climate change has a direct impact on food security by altering the global patterns of precipitation and temperature that determine the location of arable land and the quality and quantity of crops (Ostberg et al. 2018). Global warming also increases the probabilities of extreme weather events, such as droughts, floods, and heat waves, which may increase the variability in crop yields and trigger the fluctuations in crop price (Mendelsohn et al. 2007; Tadesse et al. 2014). Anthropogenic emissions of greenhouse gases influence crop yield in several ways. On the one hand, climate changes alter the length of growing season, water availability, and heat stress (Eyshi Rezaei et al. 2014; Lobell et al. 2012; Schlenker and Roberts 2009); and on the other hand, higher concentrations of atmospheric CO2 increase the water use efficiency and enhance the photosynthesis rate in wheat, rice, and maize (Darwin and Kennedy 2000). Therefore, it is necessary to monitor and evaluate the impacts from global warming to crops.

2.2 The means to observe vegetation phenology

As phenology provides significant evidence of climate impacts, showed in IPCC reports 2001 and 2007, time-series-data of phenological events at different scales, are crucially important to be collected for a greater understanding of how vegetation

systems respond to climatic fluctuations, and to develop new or improved strategies for effective management. Traditional plant phenological observations are based on direct measurements, record specific phenophases such as flowering or fruiting, and are commonly carried out by a limited number of observers over a limited geographic area or at one specific site (Ricotta and Avena 2000). On the other hand, remotely sensed satellite sensor data are used to quantify the seasonal patterns derived from plants' development and senescence, at a coarse spatial and temporal resolution over a regional or global scale (White and Nemani 2006). Moreover, the use of inexpensive digital cameras for proximal sensing of phenological events is becoming more common (Zhao et al. 2012).

2.1.1 Conventional ground observation of vegetation phenology

Field phenological observations provide details of plant seasonal development for specific species. In fact, phenological ground observations have a long history, some up to centuries (Rutishauser et al. 2007). For example, it can be extended back for thousands of years in China (Zhu and Wan 1963), and traced back to the early 1700s in Europe (Sparks and Carey 1995), and 1800s in Japan (Lauscher 1978). Traditionally, plant phenological observations are mainly about recording the occurrence dates for key events such as first leaf opening, first flowering, full bloom, and end of bloom, by long-term observations. There are several networks of phenology observation in the world. The most notable are the PlantWatch in Canada (https://www.naturewatch.ca/plantwatch/), the National Phenology Network in the USA (NPN, https://www.usanpn.org/usa-national-phenology-network), the Nature's Calendar in the UK (https://naturescalendar.woodlandtrust.org.uk/), and the Japan phenological Eyes Network (PEN, http://pen.agbi.tsukuba.ac.jp/index_e.html).

To acquire accurate dates for the key events, frequent observations over the whole growing season are needed. As a result, ground-based recording phenological dates is relatively labour intensive and costly (Sparks et al. 2006). Furthermore, in the interest of obtaining reliable observation series and comparable data, a standardised protocol is required. However proficient skills and the effort of observers largely determines the quality of the phenology data, but it increases the susceptibility to subjective inaccuracy (Booth et al. 2006; Menzel 2002). Although phenological

time-series data can be collected by single or multiple observers at a specific location or via phenological networks for different locations on the same species (Bertin 2008), direct observations of plant phenology are sometimes discontinuous for many reasons such as weather and climatic reasons and observer personal reasons, and sometimes the observations are also geographically limited so that there is a significant decline in long-term observation sites.

2.1.2 Remote sensing techniques of land surface phenology observation

Satellite sensor imagery also has been used for a wider spatial scale, primarily based on the normalised spectral reflectance in the red and near-infrared regions of the electromagnetic spectrum, for delineating phenological patterns of key events such as the so-defined 'leafing out' in spring (Botta et al. 2000; Studer et al. 2007). For example, the satellite-derived NDVI can be used to estimate the amount of actively transpiring vegetation, which increases during the green-up phase. This widely used index provides a measure of the extent, density, and vigour of land vegetation (Schwartz and Karl 1990). Compared with a labour-intensive ground observation, a satellite-based method can provide estimated data for a large area with relatively lower cost. However, remotely sensed satellite sensor data still depend on ground observation data for validation. Nevertheless, it is hard to correlate ground observations with satellite sensor observations, primarily because the data are at a different scale for ground (fine scale) and satellite (coarse scale) observations (Fisher and Mustard 2007). Moreover, satellite sensor observations are affected by other factors such as clouds, aerosols and other atmospheric characteristics as well as sensor-related reasons, all of which result in limited temporal and spatial coverage for satellite sensor images (Ahl et al. 2006; Fisher and Mustard 2007; Studer et al. 2007; Zhang et al. 2006b; Zhang et al. 2004).

Non-commercial satellite sensors in use for monitoring land surface phenology

The advantages of applying remote sensing techniques for phenology are the ability to capture continuous phenology events at large scale in an economic way (Langley et al. 2001; Nordberg and Evertson 2005; Xie et al. 2008) and the ability to retrospectively estimate the phenology from archived satellite sensor data from the

present time to over several decades back (Xie et al. 2008). Therefore, many approaches adopting a variety of satellite remote sensing products has been used to monitor the timing of phenology events.

Over the past half-century, several airborne and space-borne sensors (multispectral or hyperspectral) with a wavelength ranging from the visible to the microwave, spatial resolutions ranging from sub-metre to kilometres, temporal resolutions from 30 min to weeks or months have been used in phenological studies (Xie et al. 2008). Since different sensors have their own spatial, temporal, spectral and radiometric characteristics, it is significant to choose appropriate sensors for mapping vegetation phenology. Generally, it can be summarised into four major related factors: (I) the mapping objective. Normally the species of vegetation and the expected mapping accuracy need to be considered first. In general, coarse resolution images are usually adopted when higher level of vegetation class needs to be identified, while the finer resolution images are commonly used for fine-detailed classification of vegetation. (II) The cost of images. Under normal conditions, remote sensing imagery may be expensive especially for fine spatial and temporal resolution remote sensing composites which are often sold by retailers authorised by satellite companies. For example, a Canadian company, Prairie Geomatics, usually produces NDVI vegetation maps derived from India IRS-1D, French SPOT, or U.S. Landsat satellite photos for approximately 47 per acre. However, more and more free satellite sensor imagery is available online, including data from the European Space Agency's Sentinel series of satellite sensors (III) The climate conditions (especially atmospheric conditions). Sometimes, to obtain cloud-free time-series images, different sources of satellite images need to be considered because of their various spatial, temporal and radiometric characteristics (Soudani et al. 2006). (IV) The technical issues for image interpretation. Technical specifics need to be paid attention to regarding image quality, pre-processing, and interpretation when choosing suitable sensors.

Many onboard sensors carried by satellites with various spectral, spatial, and temporal characteristics have been utilised for vegetation phenology studies, as shown in table 1.

Satellite	Sensor	Operation	Resolution	Frequency
Landsat	MSS (Landsat 1-3)	1972–1983	80m	18 day
	TM (Landsat 4 and 5)	1982–1993(4)	30 m for multispectral bands	16 day
		1984–2013(5)	120 m for the thermal infrared band	
	ETM+ (Landsat 7)	1999–present	15 m for panchromatic bands	16 day
			30 m for multispectral bands	
			60 m for the thermal infrared band	
	OLI and TIRS (Landsat 8)	2013-present	15 m for panchromatic bands	16 day
			30 m for multispectral bands	
			10 0m for the thermal infrared band	
NOAA	AVHRR	1978–present	1.1 km	1 day
SPOT	Vegetation (SPOT 4 and 5)	1998–present	1 km	1 day
Terra	MODIS	1999–present	250 m (Band1-2), 500 m (Band3-7), 1 km (Band8-36)	1-2 day
Aqua	MODIS	2002–present	250 m (Band1-2), 500 m (Band3-7), 1 km (Band8-36)	1-2 day
Envisat	MERIS	2002–2012	300m	3 day
Sentinel	C-SAR (Sentinel-1)	2014-present	SM: 5×5 m, IW: 5×20 m, EW: 25×100 m, WV: 5×20 m	12 day
	MSI (Sentinel-2)	2015-present	10 m (VNIR), 20 m (REP & SWIR), 60 m (atmospheric correction bands)	5 day
	OLCI(Sentinel-3)	2016-present	300 m (FR), 1.2 km (RR)	0.5-2 day

Table 1 Characteristics of low or no- cost satellite sensors utilised for vegetation phenology studies.

Landsat

The Landsat sensor images might be the most widely adopted products to offer the world longest continuous and consistent Earth monitoring satellite sensor imagery (Droogers and International Water Management 2002; Xie et al. 2008). The first Landsat satellite was launched in 1972, and afterwards a series of more sophisticated multispectral imaging sensors, named MSS (Multispectral Scanner) and TM (Thematic Mapper) were equipped onto Landsat 4 (1982), 5 (1984), 6 (1993, launch failed), 7 (1999 with Enhanced Thematic Mapper Plus, ETM+), 8 (2013 with Operational Land Imager, OLI, and Thermal Infrared Sensor, TIRS), and 9 is planned to launch in late 2020. The Landsat TM and ETM+ imaging sensors have archived millions of images with medium-to-coarse spatial resolution since they were incepted. For example, Landsat TM imagery has a spatial resolution of 30 m for the multispectral bands and 120 m for the thermal infrared band; while Landsat ETM+ imagery has a spatial resolution of 30 m for multispectral bands and 60 m for the thermal infrared band, and the latest Landsat 8 has a finer resolution at 15 m for the panchromatic bands.

The Landsat series of satellites offer two primary advantages: a finer spatial resolution at 30 m which is appropriate for landscape characterisation and a long-term observation time-series back to the 1970s. However, Landsat's 16-day revisit cycle is relatively too long and misses some details for observation during rapidly changing phenological stages such as leaf unfolding or flowering. Since Landsat data are free for download from the U.S. Geological Survey (USGS) website, which makes Landsat imagery accessible to all researchers and developers, researchers are developing new methodologies that fuse Landsat data with other satellite remote sensing data, to potentially overcome the shortcomings of low temporal frequency of Landsat series. For instance, Schmidt et al. (2012) applied STARFM (Spatial and Temporal Adaptive Reflectance Fusion Model) to long-term MODIS and Landsat TM/TM+ data from February 2000 to September 2007 at a test area within the North Queensland Savannas in Australia. Tewes et al. (2015) applied the ESTARFM (Enhanced Spatial and Temporal Adaptive Reflectance Fusion Model) algorithm to MODIS 250 m and RapidEye 5 m for monitoring rangeland dynamics in a semi-arid environment located in South Africa. He et al. (2015a) merged the MODIS and

Landsat TM data to create a dataset of vegetation dynamics with both fine spatial resolution and temporal resolution, for two ranches in southwestern Texas.

Landsat products have been adopted for vegetation mapping mainly at a regional scale. Because of the long time-series of Landsat dataset, it is very helpful and convenient to map long-term vegetation distributions and study spatiotemporal vegetation changes over the time (Xie et al. 2008). For example, Fisher et al. (2006) compiled 57 Landsat scenes from southern New England from 1984 to 2002 to extract phenological metrics by a logistic-growth simulating sigmoid curve, and the accuracy was qualified with direct field measurements. The results indicated that the variability of local satellite-derived phenological metrics was close with multiple springtime ground observation with r^2=0.91, and the deciduous forest in the Providence leaf out 5-7 days earlier than comparable rural areas; Bhandari et al. (2012) synthesised Landsat TM images through 2003 to 2008 using the STARFM for assessing vegetation phenology in Eucalyptus woodland and open forest environments in Australia. The results showed no significant difference in trend and less than 16 days for key phenological parameters, compared with MODIS NDVI; Kovalskyy et al. (2012) compared NDVI data derived from three-year flux tower data with Landsat NDVI, and MODIS nadir bidirectional reflectance distribution function-adjusted reflectance (NBAR) NDVI data to assess the suitability of freely available satellite sensor data for phenological monitoring, at two flux tower sites in the United Sates. The results suggested that the 30 m Landsat NDVI data had a larger correlation with the flux tower NDVI data than the MODIS 500 m NBAR NDVI data, and the derived vegetation green-up and maximum-greenness onset dates from Landsat were closer to those derived from the flux tower NDVI data than from MODIS NDVI; Dong et al. (2015a) developed an automated Landsat-based paddy rice mapping system (Landsat-RICE) that used time-series Landsat images and a phenology-based algorithm identifying paddy rice fields during the transplanting/flooding period, in northeast China from 1986 to 2010. The results showed overall accuracies from 84% to 95%, and the Kappa coefficients ranged from 0.6 to 0.9.

SPOT

The SPOT (***S****atellite* ***P****our l'****O****bservation de la* ***T****erre*, in French) Earth Observation

satellite sensor imagery has been widely used for studying, monitoring, forecasting, and managing natural resources and human activities (Xie et al. 2008). SPOT 1 to 5 were launched, respectively, in the years of 1986, 1990, 1993, 1998, and 2002, with a full range of resolution of 1 km at the global scale (SPOT vegetation imagery) down to 2.5 m at the local scale. HRV (High Resolution Visible) imaging instruments are equipped on SPOT 1, 2, and 3 and HRVIR (High Resolution Visible and Infrared) is on SPOT 4, and HRG (High-Resolution Geometry) is on SPOT 5. Moreover, the SPOT vegetation (VGT) instrument was installed onto SPOT 4 and 5 as a second imaging instrument. SPOT-VGT imagery is included for scientific studies at both regional and global scales over long time periods at a spatial resolution of 1 km and a temporal resolution of 1 day. Therefore it is very helpful to use SPOT-VGT products to observe and analyse the evolution of land surfaces and understand land cover changes over a large area (Saint 1994).

With multiple onboard sensors and high revisit frequencies, the SPOT satellite sensors can capture an image of any place on the Earth every day and especially suitable for mapping vegetation at various scales (regional, national, continental, or global). For example, Kaptué Tchuenté et al. (2011) proposed a new classification of ecosystems based on an 8-year (2000-2007) analysis of NDVI datasets from SPOT VGT at the African continental scale; Cong et al. (2012) performed a multi-method investigation of the spring vegetation growth onset phenology for temperate China (north of 30°N) at the regional scale with NDVI data produced from SPOT satellites over the period 1999-2009.

AVHRR

The first Advanced Very High-Resolution Radiometer (AVHRR) was a 4-channel radiometer, carried aboard TIROS-N (launched October 1978), one of NOAA's Polar Orbiting Environmental Satellite series. It was subsequently improved to a 5-channel instrument (AVHRR/2) initially carried on NOAA-7 (launched June 1981), while AVHRR/3 is the latest 6-channel instrument carried on NOAA-15 (launched May 1998). One of the primary advantages of AVHRR is its relatively long-term continuity. It has been providing data since the 1980s and it is planned to continue to be on duty into the 2020s with National Oceanic and Atmospheric Administration (NOAA) and the European Organisation for the Exploitation of Meteorological

Satellites (EUMETSAT) sharing operations. AVHRR provides pre-processed data for Earth surface observations. Several products are available nowadays for vegetation phenology studies at no charge. For example, twice monthly (15-day composite) data at 8 km spatial resolution at a global scale are available for free download from 1982 to 2012; weekly and bi-weekly composites at 1 km resolution at the country scale for the United States are available since 1989, according to the USGS (U.S. Geological Survey); and recently, Pinzon and Tucker (2014) constructed the "third generation" GIMMS (Global Inventory Monitoring and Modelling System) NDVI. The latest version (3g.v1) of the NDVI3g dataset has a temporal coverage from July 1981 to December 2015, a regular 1/12°×1/12° spatial resolution (about 8 km), and contains maximum NDVI values at 15-day intervals. However, AVHRR imagery has a limitation in calibration, geometry, orbital drift, limited spectral coverage and variation in spectral coverage, especially in the early period of application, which may bring in substantial errors (Hastings and Emery 1992; Huh 1991; Xie et al. 2008).

Because of the long history image archive (since 1978 when the first AVHRR was launched), it is very useful to study long-term vegetation change. For example, Duchemin et al. (1999) monitored two key phenological stages of deciduous forests—budburst and senescence—using NDVI derived from NOAA/AVHRR in France for the period of 1989 to 1994; Sehgal et al. (2011) used NOAA/AVHRR NDVI data from 1981 to 2001 to derive the spatial patterns of temporal trends in phenology metrics and productivity of crops, in the Indo-Gangetic Plains of India (IGP); Wang et al. (2016) investigated the spatial variability and temporal trends of vegetation phenology including beginning of growing season (BGS), end of growing season (EGS), and length of growing season (LGS), over the Northern Hemisphere by using AVHRR NDVI data from 1982 to 2012.

MODIS

Moderate Resolution Imaging Spectroradiometer (MODIS) is a key instrument on the Terra (EOS AM, launched 1999) and Aqua (EOS PM, launched 2002) satellites, collecting data in 36 spectral bands between 0.405 μm and 14.385 μm, with the first seven bands designed for land surface observation (in visible and infrared regions). MODIS has a 250 m, 500 m or 1000 m spatial resolution over Earth's surface every

1-2 days, and it is processed into a variety of data products including surface reflectance, vegetation indices, land surface temperature and others (Justice et al. 1998). Terra's orbit around the Earth is timed so that it passes from north to south across the equator in the morning, while Aqua passes south to north over the equator in the afternoon, therefore Terra MODIS and Aqua MODIS together can observe the entire earth's surface every 1 to 2 days. Due to the relatively coarse spatial resolution and a long-term data range (from 2002 to present), MODIS is commonly used for vegetation mapping and monitoring at large scales. For example, Zhang et al. (2003) developed a new method by using a series of piecewise logistic functions to monitor vegetation phenology from time-series satellite sensor data at large scale, on the basis of MODIS data, tested in the northeast United States. Multiple indices were calculated from MODIS surface reflectance data including EVI, NDVI, Land Surface Water Index (LSWI), to map paddy rice planting area in Southern China and Northeast Asia (Xiao et al. 2006; Xiao et al. 2005). Ahl et al. (2006) calculated NDVI and EVI from MODIS, also Leaf Area Index (LAI) and Fraction Intercepted Photo-synthetically Active Radiation (FIPAR) MODIS products were used to monitor spring canopy phenology for a deciduous broadleaf forest in northern Wisconsin. Ren et al. (2008) estimated crop yield in Jining, Shandong Province, China, based on 250 m spatial resolution MODIS NDVI data. Le et al. (2014) derived multi-cropping information in China, based on MODIS EVI data, by adopting a smoothing method of adaptive Savitzky-Golay filter first and then identifying the cropping cycles with an iterative moving-window method.

As mentioned before, image fusion by combining finer spatial resolution data such as Landsat satellite sensor data can possibly improve mapping results. For example, Cammalleri et al. (2013) generated a fine resolution daily evapotranspiration (ET) map by fusing daily MODIS 1 km and 30 m biweekly Landsat imagery. The accuracy of the fused Landsat-MODIS daily ET maps was evaluated over Iowa using observations collected from eight flux towers, which were in corn and soybean fields in 2002. A significant increase was founded in ET accuracy (reducing errors from 0.75 to 0.58 mm d^{-1} on average), compared to the Landsat-only case. The increase was further evident at the seasonal timescale, where a 3% error was obtained using Landsat-MODIS fusion versus a 9% Landsat-only case.

MERIS

Medium Resolution Imaging Spectrometer (MERIS) was a passive imaging sensor flying on Envisat which was launched in 2002 by ESA (European Space Agency) and was in orbit until 2012. MERIS has 15 spectral bands within the visible and near-infrared range, each capable of gathering data at a resolution of 260 m across track × 300 m along track. The narrow bands of MERIS make it possible to derive more accurate land cover classes and vegetation indices than other sensors such as AVHRR and SPOT VGT. The standard products available through MERIS include radiance, reflectance, and two vegetation indices known as the MERIS Global Vegetation Index (MGVI) and the MERIS Terrestrial Chlorophyll Index (MTCI). Products at a reduced resolution (1040 m x 1160 m) can usually be obtained free of charge over the internet, while full resolution products (260 m x 300 m) usually must be requested. The primary mission of MERIS is to monitor oceans and coastal areas but also has many land applications. Its land mission is to study the role of terrestrial surfaces in climate dynamics and biogeochemical cycles for climate change. For example, Meng et al. (2009) developed a model to estimate certain phenological stages such as the start of season and end of season, for winter wheat, based on MERIS NDVI data, in Fengqiu, Henan Province and Yucheng, Shandong Province, in China. Dash et al. (2010b) used the MTCI to investigate the annual and inter-annual variation in vegetation phenology in India. O'Connor et al. (2012) derived the start of the season (SOS) metric to indicate vegetation seasonality across the island of Ireland, by utilising 10-day MERIS Global Vegetation Index (MGVI) composites, and highlighted how SOS varied according to land cover type. MERIS is replaced by the Ocean and Land colour Imager (OLCI) sensor on board of the Sentinel 3 mission to provide data continuity (Hu and Campbell 2014).

Sentinel

Sentinel satellites, launched in the Copernicus programme, are designed to provide continuous long-term data flow to allow monitoring of environmental parameters with high accuracy (Toming et al. 2017).

Sentinel-1A was launched in April 2014 and Sentinel-1B was in April 2016, by the ESA on a SOYUZ rocket from the Guiana Space Centre in French Guiana, Sentinel-

1 is the first one of the series of earth observation satellites of Copernicus programme. The Sentinel-1 synthetic aperture radar (SAR) operates at a centre frequency of 5.4GHz, offering a 12-day repeat cycle at the equator with 175 satellite orbits per cycle. With Sentinel-1A and 1B operating, a 6-day repeat cycle at the equator will be achieved. Sentinel-1 operates in four exclusive acquisition modes: Stripmap (SM), Interferometric Wide swath (IW), Extra-Wide swath (EW), and Wave mode (WV). Each mode can produce products at SAR level-0, Level-1 single look complex (SLC), Level-1 ground range detected (GRD) and Level-2 Ocean (OCN).

Sentinel-2 programme consists of Sentinel-2A and Sentinel-2B satellites, which were launched in June 2015 and March 2017 respectively. Sentinel-2 carries two multispectral instruments (MSI). The MSI has four bands at 10 m, six bands at 20 m, and three bands at 60 m spatial resolution, and it has a swath width of 290 km by applying a total field of view of approximately 20°. It covers the visible and near-infrared (VNIR) and the shortwave-infrared (SWIR) spectral region, incorporating two spectral bands in the red-edge region, centred at 705 nm and 740 nm with a band width of 15 nm and a spatial resolution of 20 m, which are important for the retrieval of chlorophyll content (Dash and Curran 2004; Delegido et al. 2011).

Sentinel-3A was launched in February 2016 and Sentinel-3B was in April 2018. Both satellites were taken into orbit on a Rockot launcher from the Plesetsk Cosmodrome in northern Russia. The Ocean and Land Colour Instrument (OLCI) on board Sentinel-3 satellites is the successor of MERIS mission (2002-2012) with improved capabilities for measuring sea-surface topography, sea- and land-surface, ocean colour and land colour (Toming et al. 2017). The revisit time of the twin constellation will be less than two days and the full spatial resolution is 300 × 300 m, which is a high temporal and moderate spatial resolution for monitoring coastal areas and water quality.

Vegetation Indices and Plant Monitoring

Remote sensing on vegetation is mainly performed by obtaining the electromagnetic wave (EMR) reflectance information from canopies using passive

sensors. It is well known that the reflectance of light spectra from plants changes with plant type, water content within tissues, and other intrinsic factors, as the EMR spectrum reflected from vegetation is determined by chemical and morphological characteristics of the surface of organs or leaves (Liu et al. 2016a). Leaves absorb the blue and red wavelengths and reflect the green wavelength of sunlight (Khamala 2017). After NIR radiation passes through the first layer of the leaf (the palisade tissue), it reaches the mesophyll and the internal leaf cavities, being reflected by the internal mesophyll structure of leaves upwards (reflected radiation) or downwards (transmitted radiation) (Homolová et al. 2013). The reflection of visible radiation is mainly because of the function of leaf pigments. A healthy plant will absorb blue and red light energy for photosynthesis and generate chlorophyll, while reflecting green light energy. A healthy plant with more chlorophyll reflects more NIR than an unhealthy one (Gitelson and Merzlyak 1998).

The main spectral light in use falls into the visible spectral range of 400 – 700 nm, which is strongly absorbed by chlorophyll in plant leaves during photosynthesis. It contains blue (450 – 495 nm), where the canopy reflectance is minimal and atmospheric aerosol diffusion effects are maximal; green (495 – 570 nm), where it covers the reflectance peak from leaf surfaces (hence the colour green can be seen), and red (620 – 750 nm), which is the most important region for vegetation analysis, and has a higher chlorophyll absorption than other bands. In addition, the near and mid infrared (850 – 1700 nm) is also commonly used, because of its strong reflectance by the cell structure of the leaves. Their usages are shown in **Table** 2.

Band name	Wavelength (nm)	Uses
Visible blue	450 - 495	Penetration of water, smoke plumes detection
Visible green	495 - 570	Measuring plant vigour
Visible red	620 - 750	Vegetation discrimination
Near infrared	850 - 900	Biomass mapping
Middle infrared	1500 - 1700	Moisture content within plants

Table 2 The wavelength (mm) and usage in remote sensing of spectral bands.

Spectral transformations have been commonly used to process remotely sensed data for monitoring vegetation phenology. The transformations are designed to enhance

the spectral reflectance characteristics of vegetation or environmental conditions that are in relation to phenological development (Reed et al. 2009), which include changing leaf area, soil moisture, and vegetation water content. Vegetation indices normally utilise the reflective characteristics of vegetation through adopting band-ratio or differencing of the red and the NIR bands or other reflective wavelengths for the purpose of reducing the effects of atmospheric aerosols or soil ground reflectance (blue) as well as for highlighting leaf water content (shortwave infrared) (Reed et al. 2009).

Common vegetation indices

The Normalised Difference Vegetation Index (NDVI) probably is one of the most widely used and implemented index for vegetation studies. It is a satellite-derived global vegetation indicator obtained from the red to near-infrared (NIR) ratio of vegetation reflectance in the electromagnetic spectrum. The formula is as following (Myneni and Hall 1995; Reed et al. 1994):

$$\boldsymbol{NDVI = \frac{NIR-RED}{NIR+RED}} \qquad (1)$$

The NDVI is strongly coupled to red reflectance, which is related to the photosynthetic capacity of vegetation and biophysical variables such as the fraction of photosynthetically active radiation (FPAR) and fractional green cover (Huete et al. 1997). A direct use of NDVI is to characterise canopy growth or vigour. Thus, the NDVI has been compared to the LAI and other biophysical variables (Fan et al. 2009). Although NDVI has been used widely in many phenological studies to extract phenological variables for quantifying ecosystem response to climate change over continents and decades (eg. Bradley et al. 1994; Maignan et al. 2008; Mašková et al. 2008; Piekielek 2012; White et al. 2009; Zhang et al. 2003; Zhang et al. 2012b). However, NDVI is affected by a number of different sources of noise possibly attributed to image misalignment, sensor miscalibration (Vermote and Kaufman 1995) and unstable atmospheric conditions such as cloud, water, snow or shadow. Therefore, it is challenging to extract phenological variables routinely and reliably from raw NDVI time-series data (Reed et al. 1994). Furthermore, the NDVI varies with both the amount of green vegetation biomass and the concentration of chlorophyll and saturates at high levels of both (Gitelson and Merzlyak 1998; Huete

et al. 2002; Mutanga and Skidmore 2004).

Other vegetation indices such as the Soil Adjusted Vegetation Index (SAVI) (Huete 1988) and the Soil and Atmospherically Resistant Vegetation Index (SARVI) (Kaufman and Tanre 1992) were developed for reducing canopy background effects and atmospheric contamination. The SAVI and SARVI are tightly linked to near-infrared reflectance and to structural parameters such as leaf area index (LAI) and biomass (Huete et al. 1997). However, applications of these vegetation indices in phenological studies are limited.

The Enhanced Vegetation Index (EVI) is another widely used vegetation index, which was designed to reduce soil and atmospheric effects, improve sensitivity in high biomass regions, and to reduce the canopy background signal and atmospheric influences It is described as:

$$\boldsymbol{EVI = G\frac{\rho_{NIR} - \rho_{red}}{\rho_{NIR} + C_1\rho_{red} - C_2\rho_{blue} + L}} \qquad (2)$$

Where ρ_{blue}, ρ_{red}, $and\ \rho_{NIR}$ are reflectance values in the corresponding bands respectively; L (=1) is the canopy background adjustment, C_1 (=6) and C_2 (=7.5) are aerosol resistance coefficients, and G (=2.5) is a gain factor. The EVI includes the blue band to correct the influence of atmospheric aerosols on red reflectance, while it remains sensitive to variation in canopy density where NDVI becomes saturated (Huete et al. 2002). For example, Yu et al. (2014) used MODIS EVI data from 2000—2009 to extract forest phenological variables including start of growing season (SOS), end of growing season (EOS), and length of growing season (LGS) in Northeast China by adopting a threshold method. Suepa et al. (2016) used MODIS EVI time-series data, along with field survey data, to quantify phenological patterns and trends in the monsoon in Southeast Asia during 2001—2010 period and assessed their relationship with climate change in the region.

However, there exists requirement for reflectance information in the blue band, which is not available on some satellite sensors such as AVHRR and SPOT-VGT. Therefore, to keep EVI's advantage Jiang et al. (2008) developed a two band (without blue band) EVI (EVI2), which is described as:

$$EVI2 = \frac{G(\rho_{NIR} - \rho_{red})}{\rho_{NIR} + C_3\rho_{red} + L} \quad (3)$$

Where C_3 is a coefficient with a value of 2.4. The EVI2 inherits the function from EVI, which is less sensitive to background reflectance, hence it is very suitable to utilise EVI or EVI2 to monitor vegetation following fire, because canopy reflectance is also influenced by other factors affecting background reflectance including bright soils and non-photosynthetically active vegetation (i.e. litter and woody tissues) (Rocha and Shaver 2009). EVI2 has a stronger sensitivity to aerosol noise than EVI, which can be overcome with improved atmosphere correction (Zhang et al. 2012b). Studies based on EVI2 have been conducted. For example, Rocha and Shaver (2009) adopted both EVI2 and NDVI derived from MODIS to resolve differences in surface greenness and Leaf Area Index (LAI) among three sites located along a burn severity gradient in arctic tundra. The results indicated that EVI2 had several advantages over NDVI including the ability to resolve LAI differences for vegetation with different background soil reflectance.

The MERIS Terrestrial Chlorophyll Index (MTCI)

Chlorophyll is one of the most important biochemicals of the leaf, and it is in a highly positive relation to both the productivity of vegetation and the depth and width of the chlorophyll absorption features in the reflectance spectra. The long wavelength (red) edge of this absorption feature moves to even longer wavelengths with an increase in chlorophyll content (Curran et al. 1990; Filella and Penuelas 1994; Munden et al. 1994). The red edge position (REP) can be defined as the point of maximum change in reflectance along this edge (Horler et al. 1983). However, the methods designed for estimating REP were based on continuous spectra without consideration for standardisation or automation (Dawson and Curran 1998) and due to the asymptotic relationship between REP and chlorophyll content, REP cannot become an accurate indicator of chlorophyll content at high chlorophyll contents (Jago et al. 1999).

The MERIS on the European Space Agency (ESA) Envisat satellite has a fine spectral resolution at 1.8 nm, moderate spatial resolution at a full resolution 300 m and a reduced resolution 1200 m, and a 3-day repeat cycle, making MERIS a potentially valuable sensor to measure and monitor terrestrial environments at

regional-to-global scales. Two techniques have been used to estimate chlorophyll content using the red edge position based on MERIS spectra (band centre at 665, 681.25, 708.75 and 760.625 nm, where wavebands are discontinuous): Lagrangian interpolation (Dawson 2000; Dawson and Curran 1998) and linear interpolation (Clevers et al. 2002). However, both two techniques could not provide an automated and one-step procedure which were quite important and necessary for processing a large quantity of data. A new easy-to-use index, MERIS Terrestrial Chlorophyll Index (MTCI), therefore, was developed for estimating chlorophyll content from MERIS data (Dash and Curran 2004).

The MTCI was developed according to two criteria: At first, it needed to be easy to calculate from MERIS data recorded at the standard band setting; second, it should be sensitive to a wide range of chlorophyll contents (Dash and Curran 2007). The MTCI is calculated as the ratio of the difference in reflectance (R) between band 10 and band 9 and the difference in reflectance between band 9 and band 8 of the MERIS standard band setting, formula as following:

$$\boldsymbol{MTCI} = \frac{\boldsymbol{R_{Band10} - R_{Band9}}}{\boldsymbol{R_{Band9} - R_{Band8}}} = \frac{\boldsymbol{R_{753.75} - R_{708.75}}}{\boldsymbol{R_{708.75} - R_{681.25}}} \qquad (4)$$

Where $R_{753.75}$, $R_{708.75}$, and $R_{681.25}$ are the reflectance in the centre wavelengths of bands 8, 9 and 10, in the MERIS standard band setting.

The MTCI is designed based on the red-edge position (REP), making it one of few related directly to canopy chlorophyll concentration and leaf area index (LAI) (Dash et al. 2010b), and it has limited sensitivity to atmospheric effects as well as soil background and view angle (Dash et al. 2009a). Therefore, the MTCI is also suitable for monitoring vegetation dynamics. Boyd et al. (2011) used MTCI data to construct the phenological profile and extract key phenological event dates from woodland and grass/heathland in Southern England for the period 2003 to 2008. They also compared the results with MERIS global vegetation index (MGVI), MODIS NDVI, and MODIS EVI. Close correspondence between MTCI and canopy phenology as indicated by ground observations and climatic proxy was evident. Differences between MTCI-derived results and those from MGVI, NDVI, and EVI were also observed. Viña et al. (2011) evaluated several vegetation indices

for the remote estimation of the green leaf area index (Green LAI) of two crop types (maize and soybean). The results indicated that among the indices test, Green Chlorophyll Index (Cl_{green}), Red-edge Chlorophyll Index ($Cl_{red\text{-}egde}$), and MTCI exhibited a large and significant linear correlation with Green LAI, and were sensitive across the entire range of Green LAI evaluated.

Although the ESA's Envisat mission ended on 08 April 2012, the MTCI now is still available from Sentinel-3 OLCI level-2 products, known as Terrestrial Chlorophyll Index (OTCI) (https://sentinels.copernicus.eu/web/sentinel/user-guides/sentinel-3-olci/product-types/level-2-land).

2.1.3 Methods for deriving vegetation phenological variables from satellite measurements

It is more and more popular to use high frequency satellite sensor data (e.g. NOAA-AVHRR NDVI and Terra/Aqua-MODIS NDVI or EVI) to detect phenological events, for the use of ecological and climate change studies at large scales. Various methods have been developed for capturing important phenological information from remote sensing data. The common methods usually contain two steps: (1) transform vegetation indices data derived from satellite sensor images into time-series; (2) detect phenological parameters from the time-series data based on different rules.

Time-series satellite sensors data smoothing techniques

A general problem with satellite optical sensor observation is that the data are sometimes affected by atmospheric dust and aerosols, gaseous absorbers, and clouds, leading to reflectance values altered or missing (Atkinson et al. 2012). Therefore, several techniques were applied to estimate the invalid values by making use of valid observed values, for the purpose of reconstructing the plant growth profile. More than 20 techniques have been developed for reducing the noise of time-series vegetation index data from different satellite sensors. Generally, all the techniques can be divided into four categories according to the algorithm they use: (1) Threshold-based approaches, which controls the smoothness of the reconstructed time-series profile by setting a threshold. Typical methods include the Best Index Slope Extraction Algorithm (BISE) (Viovy et al. 1992) and the modified

BISE (M-BISE) (Lovell and Graetz 2001); (2) Filter-based methods, which apply a defined filter to fill the gaps in a moving window according to the valid observations. Common approaches include the Running Medians (Velleman 1980), the Savitzky-Golay (S-G) filter (Chen et al. 2004), the Mean Value Iteration (MVI) (Ma and Veroustraete 2006), the Changing Weight (CW) filter (Zhu et al. 2012), and the adapted local regression filter (Moreno et al. 2014); (3) Curve-fitting methods, which fit the vegetation growing profile with a mathematical curve, such as the harmonic analysis of time-series (HANTS) (Roerink et al. 2000), the double logistic function (DL) (Beck et al. 2006), the Asymmetric Gaussian function (A-G) (Jonsson and Eklundh 2002); (4) Other approaches, such as the wavelet transform (Lu et al. 2007), the data assimilation (Gu et al. 2009), and the Whittaker Smoother (WS) (Atzberger and Eilers 2011).

Many studies have been conducted in testing all the gap-filling/smoothing techniques under different circumstances, for the purpose of finding their advantages and disadvantages. Atkinson et al. (2012) assessed four techniques including Fourier analysis, asymmetric Gaussian model, double logistic model and the Whittaker filter for smoothing the vegetation growing profile on major vegetation types in India. It was found that the double logistic and asymmetric Gaussian models did not return good results in areas with multiple growing seasons and also demonstrated that independent parameters for each model were necessary. Geng et al. (2014) tested eight time-series reconstruction techniques including the modified best index slope extraction (M-BISE) technique, the Savitzky-Golay (S-G) technique, the mean value iteration filter (MVI) technique, the asymmetric Gaussian (A-G) technique, the double logistic (D-L) technique, the changing-weight filter (CW) technique, the interpolation for data reconstruction (IDR) technique, and the Whittake smoother (WS) technique. Four types of time-series NDVI data were used: AVHRR, Pathfinder AVHRR, SPOT-VGT, and MODIS. These techniques were evaluated by calculating the root mean square error (RMSE), the Akaike Information Criterion (AIC), and the Bayesian Information Criterion (BIC). The result indicated that S-G, CW, and WS techniques performed best, while IDR, M-BISE, and MVI returned less accurate results. Therefore, it is important to select the appropriate data smoothing method before extracting phenological information from time-series satellite sensors data. Wang and Tao (2014) compared

three smoothing methods were compared for simulating the spatial pattern of the start of season of cropland in Northeast China, using NDVI data produced from SPOT Vegetation satellites. The results showed that Asymmetric Gaussians produced the most approximative results of all, followed by Double Logistic algorithm, and Savizky-Gloay algorithm produced earliest estimates.

Phenology extraction techniques

Many approaches to deriving phenological metrics have been addressed since the early 1990s. Reed et al. (1994) identified the onset-of-greenness metrics at the point of time-series AVHRR NDVI data, where the smoothed data crossed the moving average in an upward direction and remained above it for the greatest sustained increase. Schwartz and Reed (1999) used an updated version of the technique reported by Reed et al. (1994) to process AVHRR NDVI into start-of-season dates, and compared with modelled phenology. Schwartz and Chen (2002) employed a simple method of Seasonal Midpoint NDVI (SMN) in which a SMN threshold is defined to determine the start and end of season in case of broad leaf forest. Zhang et al. (2003) identified key phenological phases of vegetation by fitting a continuous logistic function to time-series of MODIS VI data and estimating phenological transition dates based on inflection point of the curve. They used the same approach to produce global maps of annual ecosystem phenology, and compared with in-situ measurements. The results demonstrated that realistic estimates of phenological dates were identified (Zhang et al. 2006b). White and Nemani (2006) used region-specified NDVI threshold to analyse the phenological behaviour of group of pixels.

Many methods for retrieving phenological metrics from satellite sensors data have been developed, since remote sensing has been used widely for monitoring vegetation (Wang et al. 2017a). The methods for deriving phenological parameters from satellite sensors data can be generally classified into two categories: the threshold method and the profile-based derivative methods.

The threshold method has been applied in a range of applications, it sets the threshold for identifying a vegetative growing cycle. For example, Lloyd (1990) used the NDVI threshold method in classifying phenological terrestrial vegetation. Fischer (1994) adopted it in modelling seasonal variation of vegetation. Markon et

al. (1995) employed this method in detecting the characteristics of vegetation phenology with the assumption of a single threshold being applicable across all the vegetation covers, by rescaling the NDVI value range to multiply by 100 then adding 100 (values greater than 100 represented vegetative surfaces). White et al. (1997) determined the onset and end of growing season according to a set threshold of the normalised NDVI ratio, instead of the original NDVI values. The NDVI ratio was developed based on the method of Reed et al. (1994), and then a threshold of 0.5 was set to identify the growing season length. Similarly, the normalised NDVI ratio method is arbitrary relative to the NDVI threshold method, and therefore this method was only used in the north-eastern DBF and some other similar canopy conditions. However, it had been demonstrated by Huete et al. (1997) that the threshold method was limited by the variation in background reflectance of different vegetation types. Therefore, it was not possible to establish a single, meaningful threshold to signify the onset or end of vegetation activity for a range of vegetation covers at large scales.

Comparing with the threshold method, the profile-based derivative methods have a better ability to handle multiple growing cycles and can be applied to range of vegetation types. It is based on the changing derivative before and after the start or end point of a growing season. Moulin et al. (1997) used the time derivative of NDVI to detect three phenological events of a growing season: beginning, maximum and end. It defined that the time derivative before the beginning date should be zero, after the beginning date should be positive and at the end date should be similar with the beginning date. However, this algorithm is quite sensitive to the weight of the derivative term: a larger term would have many short-term signal variations because of residual noise and a small weight of the derivative term, the algorithm would fail for pixels which partly remain green during the year. Duchemin et al. (1999) found that the temporal variation of NDVI during budburst and senescence was nearly linear. The linear segments method is sensitive to a change in the rate of NDVI variation which could be attributed to a temperature fluctuation during budburst in spring, or a severe drought in summer accelerating the senescence. Zhang et al. (2003) identified phenological event dates based on the curvature-change rate of a logistic model for time-series of MODIS vegetation indices. This method has been widely adopted in many studies (Ahl et al. 2006;

Peckham et al. 2008; Zhang et al. 2004). This curvature-change method has an ability to handle multiple growth cycles and is more flexible for study periods such as multi-year growing seasons. However, in the research, it was found that this method still had a challenge: it was hard to determine a single sustained increase and decrease period before the MODIS measurements could be fitted by the logistic model. Studer et al. (2007) compared maximum slope and threshold approach for deriving start-of-season (SOS) metrics, using EFAI-NDVI dataset from the NOAA/NASA Pathfinder NDVI dataset. The result showed that the threshold method was better able to represent the temperature dependent temporal pattern of observed phenology, while the slope method did not reflect several years with a very early spring onset due to little snow and warm temperature.

2.1.4 Automated vegetation phenology observation

Traditional phenological observation is operated by an individual person, recording specific phenophases such as budburst or flowering. Such observations are typically limited to the number of individuals, located within a limited geographic area or a specific site. On the other side, remote sensing observation usually operates at coarse spatial and temporal resolutions, and at a regional or large scale (White and Nemani 2006).

To address the issues of the gap between the direct ground-based and remote sensing phenological monitoring, in recent years, the use of inexpensive visible spectrum digital cameras for proximal sensing of phenological events has become more common. Digital cameras, although not certified as calibrated instruments, can be used successfully, as relatively inexpensive multi-channel imaging sensors (Ahrends et al. 2008; Crimmins and Crimmins 2008; Graham et al. 2006; Graham et al. 2009; Richardson et al. 2009; Richardson et al. 2007). One of the advantages of repeated photography is that it allows samples to be obtained at very high temporal resolutions, often at daily or hourly intervals, for monitoring vegetation phenology. Moreover, mounting these systems on towers or other platforms provides data at an intermediate scale of observation, allowing a contrast between field-based observations and satellite-derived measures (Richardson et al. 2009).

Earlier applications of camera system technologies in phenological studies took

place in the agriculture field: the observation of phenological phases was first tested by Adamsen et al. (1999) to analyse wheat senescence, and by Purcell (2000) to detect changes in wheat and soybean canopies over the growing seasons. Digital camera images, phenology, and satellite-based data were jointly analysed by Fisher et al. (2006), who used multiple photographs, visually classified by independent observers, as validation data for satellite model estimates of phenological development.

The link between leaf pigmentation and digital images was found by Kawashima and Nakatani (1998) who estimated the chlorophyll content in leaves using a video camera. Net CO_2 uptake of moss was analysed by Graham et al. (2006) with a camera based upon the changes in reflected visible light (VIS) during moss drying and hydrating. More recently, commercially available digital web camera systems were installed on CO_2 flux towers across North America to observe deciduous vegetation green-up and to make comparisons to changes in the fraction of the photosynthetically active radiation absorbed by the canopy (Keller et al. 2008). Digital webcam images were used for spring green-up tracking of forests and jointly analysed with FAPAR (fraction of incident photosynthetically active radiation absorbed by the canopy), broadband NDVI and the light-saturated rate of canopy photosynthesis, inferred from eddy covariance measurements at a flux tower site (Richardson et al. 2007). A similar study was carried out by Ahrends et al. (2008), which conducted phenological observation using digital visible-light cameras for a managed mixed forest in northern Switzerland, to identify leaf unfolding dates of the dominant tree species. Dates of leaf emergence were estimated based on the levels of the extracted red, green and blue colours. Comparison on the performance of digital camera and satellite sensor data for canopy greenness observation also was undertaken by Brown et al. (2017). The relationships between the green chromatic coordinate (GCC) derived from near-surface remote sensing and a range of vegetation products derived from MERIS throughout the growing season were investigated. The results indicated that moderate-to-strong relationships were found at deciduous forest sites, and small correlations were found over evergreen forest sites.

2.3 Phenology studies in China

Modern phenological observation and research in China can be traced back to the 1920s, starting with Dr. Kezhen Zhu (Coching Chu) (1890-1974), who is commonly regarded as the founder of modern Chinese phenology. He summarised phenological knowledge from the last 3000 years in China in 1931 and introduced phenological principles such as species selection, phenological observation methods from Europe and the United States from the mid-18th to early 20th century. Moreover, Dr. Coching Chu organised and established the first phenological observation network in China, in 1934. Observations of some 21 species of wild plants, 9 species of fauna, some crops, and several hydro-meteorological events ceased in 1937 due to World War II in China (1937-1945). In the 1970s, the Chinese Academy of Sciences (CAS) established a phenological network nationwide at the first time, under the guidance of Dr. Zhu. The observation began in 1963 and continued until 1996. It resumed in 2003, but with a reduced number of stations, species, and phenophases. In addition, the Chinese Meteorological Administration (CMA) established a countrywide phenological network in the 1980s.

The observation programme of the CAS network includes a total of 173 observed species, of which 127 species of woody and herbaceous plants had a localised distribution. Since 1973, several stations added phenological observations of major crops. These observations were carried out mainly by botanical gardens, research institutes, universities and middle school according to uniform observation criteria. The phenophases of woody plants included bud-burst, first leaf unfolding, 50% leaf unfolding, flower bud or inflorescence appearance, first bloom, 50% bloom, the end of blooming, fruit or seed maturing, fruit or seed shedding, first leaf coloration, full leaf coloration, first defoliation, and the end of defoliation.

The Institute of Geography at the Chinese Academy of Sciences took responsibility for collecting the phenological data and publishing them. Changes to the stations and in observers over the years resulted in data that were spatially and temporally inhomogeneous. The number of active stations has varied over time. The largest number of stations operating was 69 in 1964 and the smallest number occurred between 1969 and 1972 with only four to six stations active. The phenological data

from 1963 to 1988 were published in the form of Yearbooks of Chinese Animal and Plant Phenological Observation.

The CMA phenological network is affiliated with the national-level agro-meteorological monitoring network and came into operation in 1980. The phenological observation criteria for woody and herbaceous plants and fauna were adopted from the CAS network. There are 28 common species of woody plants, one common species of herbaceous plant and 11 common species of fauna. The main phenophases are the same as those of the CAS network. In addition to the natural phenological observations, the network also carries out professional phenological observation of crops based on a specific observation criterion. The main crop varieties include rice, wheat, corn, grain sorghum, millet, sweet potato, potato, cotton, soybean, rape, peanut, sesame, sunflower, sugarcane, sugar beet, and tobacco.

The CMA network is the largest phenological observation system in China at present. There were 587 agro-meteorological measurement stations in 1990. Of these, about 400 stations were undertaking phenological observations. As the phenological and meteorological observations are parallel in this network, the data are especially valuable for understanding phenology-climate relationships. These data can also be used to provide agro-meteorological service and prediction on: crop yield, soil moisture and irrigation amounts, plant diseases and insect pests, and forest fire danger.

Studies based on ground observation

A variety of applications demonstrate the utility of phenological ground observation over China. Lu et al. (2006) observed four species of trees in Northeast China, the North China Plain and the lower and middle reaches of the Yangtze River, Inner Mongolia Plateau in North China, the Loess Plateau in central China, and Yunan-Guizhou Plateau in the southwest, in a period during 1963 to 1988. To determine the significant period of temperature influence on flowering dates, linear regression analysis was applied in their research. The results indicated that the period during which temperature influences flowering time varies from 60 to 90 days for *Robinia pseudoacacia* in the south to 30 to 40 days in the north, due to the shorter warm

period before flowering in the north. The three other species showed similar trends of changes with latitude in the length of the period of temperature influence. Zhang et al. (2010) observed 24 plant species in 14 families at the North Slope of Mt. Qomolangma (Mt. Everest) in Tibet, western China, from early May to late August in 2005. To test the relationship between onset of flowering and fruiting, first dates of flowering and fruiting were converted to calendar days and then analysed by linear regression. The results showed that the species have evolved various phenological strategies as adaptations to the short growing season with limited resources and pollinators in this harsh alpine environment at extremely high elevations. Ma and Zhou (2012) observed 13 woody plant species via 20 observation sites across China from the 1960s to 2000s. By performing linear regression analysis, the existence of linear temporal trends was tested, and *t*-test was applied for the significance testing of regression parameters. The results showed that spring in China had started 2.88±2.33 days earlier per decade since the early 1980s, and on average 4.93±0.26 days earlier per degree Celsius in spring. Tao et al. (2012) observed wheat phenology at more than 100 national agro-meteorological experiment stations throughout China from 1981 to 2007. Accumulated thermal development unit (ATDU) during a development period such as wheat growing period (GP), vegetative growing period (VGP), and reproductive growing period (RGP) was calculated as the methods used by the CROPSIM/CERES-Wheat version 4.0 model in DSSAT 4.0. The results showed that besides the complex influences of agronomic factors, climate change contributed substantially to the shift of wheat phenology. Mean day length during the vegetative growing period had a decreasing trend at most of the investigated stations owing to delay of sowing date or/and advancement of heading date, which counterbalanced the roles of temperature in controlling the duration of the vegetative growth period. In-depth analyses showed that thermal requirements from sowing to almost each development stage increased. However the thermal requirements to complete each single development stage changed differently, which tended to increase yield and adapt to ongoing climate change. Xiao et al. (2013) observed crops at 36 agro-meteorological stations in the North China Plain from 1981 to 2009. A linear regression model was used to determine the time trend in each investigated phenological event of winter wheat. The results showed the dates

of sowing, emergence, and dormancy (start of dormancy) delays on the average by 1.5, 1.7 and 1.5 days decade^{-1}, respectively. On the contrary, the dates of green-up (end of dormancy), anthesis (BBCH 61) and maturity (BBCH 89) occurred early, on average by 1.1, 2.7 and 1.4 days decade^{-1}, respectively.

Studies based on remote sensing

Applications usually focus on vegetation phenology monitoring, vegetation mapping, crop acreage estimation, crop yield prediction, and so on. Wu et al. (2008) investigated variation in the start of growing season (SGS) in China's cropland from 1983 to 2002, using AVHRR NDVI. The results showed that the average date of SGS in China's cropland become progressively later from south to north in China during the past 20 years, corresponding well with the temperature and precipitation gradients. Ren et al. (2008) used MODIS-NDVI data to establish a linear regressive relationship between the spatial accumulation of NDVI and the production of winter wheat in Shandong Province, in China, by using a stepwise regression method. The results showed that the relative errors of the predicted yield ranged from -4.62% to 5.40% and the whole RMSE was 214.16kg ha^{-1} lower than the RMSE (233.35kg ha^{-1}) of agro-climate models in the same study region. Cai et al. (2012) investigated the spatio-temporal dynamics of deciduous broadleaf forest (DBF) in the Khingan Mountain region in northeast China and its phenology changes in relation to climate change and elevation, based on MODIS EVI data. Four phenological variables were extracted. The results showed that the DBF has generally degraded and over 65% of DBF has a shortened growing season, over the past decade. Wei et al. (2012) used AVHRR NDVI data from 1982 to 2006 across China and the TIMESAT program to quantify annual vegetation production and its changing trend. Results identified great spatial variability in vegetation growth and its temporal trend across China in the study period. Ding et al. (2013) analysed spatial-temporal changes in alpine grassland phenology in the terrestrial ecosystem in Qinghai-Tibetan Plateau from 1999 to 2009, based on NDVI data from SPOT VGT. The results showed that the phenology of alpine grassland was closely related to water and heat conditions. Pan et al. (2014) used the TIMESAT program to extract phenology parameters of croplands from Chinese HJ-1 NDVI data, at Guanzhong Plain, China. The results showed that the crop season start and end derived from HJ-1 A/B NDVI time-series

data was comparable with agro-metrological observation based on the small-scale test.

In summary, remote sensing provides an ideal way of observing vegetation phenology. It is less labour intensive and time consuming than the conventional field survey, and it also provides the only feasible means of observing a large portion of Earth's surface at a high temporal frequency in a consistent manner (Almond 2009). Therefore, remote sensing is an important technology for understanding the dynamics of the landscape. MTCI provides crucial information on chlorophyll content, and it has its own advantages compared to the use common NDVI. Therefore, it is important to find its application in monitoring vegetation phenology. Although there are many phenological studies across China, they are mostly concentrated in specific regions or species. Therefore, a detailed understanding of country-scale phenology is needed.

2.4 Mapping rice area and forecasting its yield using remote sensing

Rice the one of the most important crop and staple food for more than 50% of the world population (Khush 2005b). In recent decades, with the increase of world population and changing climate, great pressure was put on the global food demand and its production (Wheeler and von Braun 2013), especially in the heavy rice consuming regions, Asia, where has 60% of the World population and about 90% of the World's total rice production (Mosleh et al. 2015). Under such circumstances, reliable and timely estimates of rice planting area and its yield and production are critical for decision makers to plan for food security.

2.4.1 Review of estimating crop areas

Timely monitoring of rice agriculture is crucial for yield estimation, agricultural resource management and environment sustainability in China and worldwide (Li et al. 2017). In addition, methane (CH_4) is the second important greenhouse gas (GHG) after carbon dioxide (CO_2), and rice paddies have been regarded as one of the major anthropogenic sources of atmospheric CH_4 (Wassmann et al. 1993). The most common and traditional ways for estimating crop cultivated areas are normally

done through seasonal fields surveys based on many sample clusters. Then all the surveys are constituted from county-to-national scale for the measuring cultivated areas during the crop growing season. Each cluster needs to be visited many times and recorded, and then processed for aggregating regional-to-national statistics. This method can reflect invaluable historic trends in rice producing regions. However, it is extremely time-consuming, labour-intensive, less precise, and high cost. In addition, the survey result is easily influenced by human factors (Prasad et al. 2006; Reynolds et al. 2000). For rice yield and production forecasting, it also presents three major weaknesses: (i) it is time-consuming, subjective, and prone to discrepancies because of insufficient field surveys that lead to poor crop yield and production estimation (Mosleh et al. 2015). (ii) the estimations are often available after the harvest to the government and public, and thus less helpful for food security purposes (Mosleh et al. 2015). (iii) Field surveys need huge finance to support, especially when it is implemented at large scales (Bouvet and Le Toan 2011).

In this context, remote sensing-based methods were adopted as effective alternative for mapping crop area. It can provide long-lasting surface information with high frequencies, has a spatial coverage over large geographic area, and its cost is relatively low, some satellite sensors data are freely available (*i.e.*, MODIS, SPOT-VGT, Landsat). Normally, two main kinds of satellites sensors are used to map rice paddies and forecast the yield and production: microwave and optical. Microwave sensors can penetrate through clouds because of the long wavelength; thus, they are suitable for mapping crops in long-term cloudy and rainy weather regions (Bouvet and Le Toan 2011; Miyaoka et al. 2013; Shao et al. 2001; Zhang et al. 2018b; Zhang et al. 2009). However, the available synthetic aperture radar (SAR) imagery is limited (Zhang et al. 2009) and expensive (Li et al. 2012). Frequently used optical satellite sensors include the Multispectral Scanner System/Thematic Mapper/Enhanced Thematic Mapper Plus/Operational Land Imager and Thermal Infrared Sensor (MSS/TM/TM+/OLI and TIRS) (Dong et al. 2015a; Dong et al. 2016; Fang et al. 1998; Jackson et al. 2004; Jin et al. 2015; Kontgis et al. 2015; Liu et al. 2005; Qin et al. 2015; Wang et al. 2015; Zhang et al. 2018a; Zhou et al. 2016), the Moderate Resolution Imaging Spectroradiometer (MODIS) (Clauss et al. 2016; Fontana 2005; Huang et al. 2012; Mkhabela et al. 2011; Shi et al. 2013; Sun et al.

2009; Xiao et al. 2006; Xiao et al. 2005; Zhang et al. 2015a; Zhang et al. 2012a), NOAA's Advanced Very High Resolution Radiometer (AVHRR) (Doraiswamy and Cook 1995; Esquerdo et al. 2011; Fang et al. 1998; Huang et al. 2013; Mkhabela et al. 2005; S. Mkhabela et al. 2005), and SPOT High Resolution Geometrical/High Resolution Visible Infrared/VEGETATION (HRG/HRVIR/VGT) . In addition, to overcome the cloud, a number of studies have explored the advantages of integrating optical and microwave datasets for more efficient and accurate crop monitoring (Mansaray et al. 2017; Onojeghuo et al. 2018; Wang et al. 2015; Zhang et al. 2018b; Zhou et al. 2016).

Mapping crop areas and monitoring crop growth using optical satellite sensor data is primarily based on the crop's physical feature of apparent reflectance in the visible near infrared (VNIR) portions of the electromagnetic spectrum. As crop grows, the reflectance in the near infrared (NIR) reaches the highest value, while in the visible region it reaches the lowest (Kawamura et al. 2018; Mansaray et al. 2017). On the other hand, using microwave (radar) satellite sensor data for agricultural purposes is based on the backscatter response, mainly including surface scattering, volume scattering, and surface scattering attenuated by the vegetation volume (Bouvet and Le Toan 2011; Shao et al. 2001; Shen et al. 2009).

Many studies have been undertaken in China to map paddy rice using satellite sensor data. Only a few studies focused on mapping rice paddies at the national scale with most studies were concentrated on mapping at the regional scale in the main rice-producing regions in northern or southern China. Common methods based on satellite sensor data can be generally divided into two categories: image-based methods and pixel-based methods. Image-based methods normally compare all the pixels in one image for classification or object detection, based on the similarities or differences among them. For these methods, it is still a challenge to collect yearly ground reference data (Zhong et al. 2014). Such methods are often represented by the supervised classification methods that are learning an established classification from the training dataset containing the predictor variables measured in the sample crop fields (Černá and Chytrý 2005). Pixel-based methods usually focus on the time-series data for a single pixel, correlated with the spectral characteristics of different crops. These methods focus on the phenological change

of one vegetation type, using remote sensing data to provide phenology information of land surface (Wang et al. 2015). For these methods, sometimes the sub-pixel phenology information of small crop fields cannot be captured, due to the relatively coarse spatial resolutions. For example, MODIS has a finest 250 m spatial resolution, while in Southern China there are lots of heterogeneous and fragmented agricultural landscapes (Bridhikitti and Overcamp 2012).

2.4.2 Review of forecasting crop yield

Numerous approaches are available for estimating or forecasting crop yield with remotely sensed data, including statistics models (i.e. regression models) and simulation models (i.e. agro-climate models and crop growth models). They are combined with satellite sensors data for more efficient, accurate and real-time crop yield forecasting.

The most common approach to forecast crop yield is to develop direct empirical relationships by generating regression models, between long-term crop yield records and satellite sensors data derived crop parameters such as LAI (Leaf Area Index), NDVI, fPAR (fraction of Photosynthetically Active Radiation), and NPP (Net Primary Production) (Du et al. 2014; Esquerdo et al. 2011; Li et al. 2011b; Mkhabela et al. 2011; Wall et al. 2008; Wei et al. 2013). This approach is based on the capacity that many growing conditions can be reflected by the parameters, which are assumed to be directly related to crop yield (Tucker et al. 1980). However, the actual crop yield depends on many more factors than the ones that parameters can capture (Bastiaanssen and Ali 2003). Tucker et al. (1980) for the first-time identified relationships between NDVI and crop yield using experimental fields and ground-based spectral radiometer measurements. Grain yields were found to be strongly correlated with the NDVI values around the dates of maximum greenness. From then on, a few studies have been conducted based on NOAA AVHRR data. Ramussen (1992, 1997, 1998) established a linear correlation between the time integral of the NDVI and millet yield. Das et al. (1993) found that NDVI measured between flowering and milking stages gave the best prediction for the grain yield. Quarmby et al. (1993) built simple linear relationships between NDVI and yield of wheat, corn, rice, and maize crops. Maselli et al. (1993) tested NDVI maximum value during rainy season and yield of millet and sorghum in the Sahel, and Smith

et al. (1995) reported the relationship between NDVI and wheat yield in Western Australia. More recent, with the development of satellite and remote sensing technologies, remotely sensed data with improved radiometric calibration and finer spatial and temporal resolution are available for example the MODIS. Ren et al. (2008) found the largest correlation between wheat production and accumulated MODIS-NDVI about 40 days ahead the harvest time, in Shandong Province, China. Bolton and Friedl (2013) used satellite sensors data from MODIS to develop empirical models for maize and soybean yield forecast in central United States. Dempewolf et al. (2014) used Landsat data that was about six weeks before harvest, to test four different peak-season MODIS-derived vegetation indices against reported yield values for deriving wheat yield. Qader et al. (2018) used MODIS with official crop statistics to develop an empirical regression-based model to forecast winter wheat and barley production in Iraq. Although most of the results of remote sensing in crop yield estimation and prediction are encouraging and promising, the challenge still exist in small crop fields that are smaller than the spatial resolution of the remotely sensed data used (Khamala 2017). Further, because the empirical regression model is often established between local crop yield records and a satellite-derived VI, the model is not suitable for generalising to other areas (Qader et al. 2018).

Simulation models were developed in the late 1960s for the first time, to emulate the main physiological process of crop growth on daily basis, these models try to integrate multiple factors affecting crop growth, such as water, temperature, etc (Ahmad et al. 2018; Zhou et al. 2017). Nevertheless, in the beginning, the losses caused by pests and disease were not taken into account, which were assumed to be controlled in such models (Lobell 2013). The advantage of these simulation models lies in their ability in simulating the soil-environment-plant interaction, but they are restricted by a number of physiological and pedological parameters are required that are not available or cannot be calibrated in some countries and regions (Zhang et al. 2012a; Zhou et al. 2017). To overcome these problems, the remote sensing is used as a useful method. VIs that derived from satellite sensors data are used to establish relationships with Above Ground Biomass (AGB) of crops, to generate remote sensing-based crop growth models. Examples of the models include the World Food Studies (WOFOST) (de Wit et al. 2019), Simulaterur

mulTIdisciplinaire pour les Culture Standard (STICS) (Brisson et al. 2003), and Crop Systems Simulation (CROPSYST) (Stöckle et al. 2003).

In conclusion, the importance of monitoring plant phenology and its related applications is increasing under the circumstances of climate change these days. Vegetation phenology is an important indicator for monitoring changes in the climate and natural environment (Richardson et al. 2013b). Therefore, it is great significant to study vegetation phenology for understanding the trend of changing natural phenomena and serve for agricultural applications and global change studies(Tang et al. 2015; Wang et al. 2017b).

Since the 1980s, the NDVI has been used widely to evaluate phenological characteristics over large areas. Although NDVI is one of the most common VI for studying vegetation phenology dynamics, however, NDVI is not suitable for the tropical zone due to variations of atmospheric conditions associated with aerosols and clouds (Kobayashi and Dye 2005), and high biomass region with large values of LAI (Mutanga and Skidmore 2004). MTCI is more sensitive to high values of chlorophyll content (Dash and Curran 2004), which is different from NDVI. Because MTCI is derived from the narrow bands in the red-edge-position that is highly related to the chlorophyll content. Therefore, MTCI has a great potential to be used in monitoring vegetation dynamics. However, the amount of literature about applying MTCI in vegetation phenology studies is still limited. How will the MTCI perform in describing vegetation phenology dynamics and how accurate the MTCI can be in agricultural applications, are still need to be tested and verified.

3.Comparison between Phenological Variables Extracted from MERIS Terrestrial Chlorophyll Index and Normalised Difference Vegetation Index

3.1 Background

Phenology is the study of recurring biological events in plants and animals, such as the leafing and flowering of plants, maturation of agricultural crops, the emergence of insects and migration of birds (Haggerty 2008; Schwartz and Chen 2002). Vegetation phenology has a strong association with Earth's climate and hydrologic regimes which can affect the exchange of carbon, water and, the energy between the vegetation and the atmosphere. Therefore, it can be regarded as one of the key indicators that reflect the response of the Earth's biosphere to climate change (Chuanfu et al. 2012; Reed et al. 1994; Xu and Liu 2007; Zhang et al. 2003).

Vegetation phenology can be derived from ground measurements or satellite remote sensing data. Ground-based methods have practical weaknesses such as being subjective, time-consuming and difficult to measure large-scale regions (Dash et al. 2010b); while satellite remotely sensed data have a wider coverage and repeated temporal frequency from daily to monthly, providing an opportunity to measure vegetation phenology at large scales (Zhang et al. 2003). Since the rapid development of satellite technology and use of new sensors, there has been an increasing interest in extracting vegetation phenology from remote sensing data. Many studies used the NDVI derived from long-term remote sensing data such as NOAA AVHRR, Landsat TM/TM+, TERRA MODIS, and SPOT VEGETATION to measure vegetation phenology from regional to global scales (Mašková et al. 2008; Piekielek 2012; White et al. 2009; Zhang et al. 2003; Zhang et al. 2012b). However, those datasets were derived from different satellites and processed by different methodologies. As a result, vegetation phenology data extracted for the same region varied from each other.

The NDVI, calculated from red and infrared band results in a trend of saturation at high levels of vegetation biomass and chlorophyll concentration (Gitelson and Merzlyak 1998; Huete et al. 2002; Mutanga and Skidmore 2004). Unlike NDVI the MERIS Terrestrial Chlorophyll Index (MTCI) is more sensitive to large values of chlorophyll content. It has been applied in many regional to global scale applications as it is the only chlorophyll content product providing an indication of terrestrial vegetation condition. The MTCI provides combined information on both

the LAI (area of leaves per unit area of ground) and the chlorophyll concentration of leaves (the amount of chlorophyll per unit weight of leaf) (Dash et al. 2009a; Dash and Curran 2007; Dash et al. 2010b). The MTCI has been validated at the MERIS spatial resolution with different vegetation types as well as across different regions. The results showed there was a positive relationship between MTCI and chlorophyll content, and they are strongly linked with each other (Almond 2009; Boyd et al. 2011; Dash and Curran 2007; Dash et al. 2010a; Dash et al. 2010b; Dash et al. 2007; Harris and Dash 2010; Jeganathan et al. 2010). Moreover, MTCI is easy to calculate and yet it is sensitive to all notably large values of chlorophyll content (Dash and Curran 2004). It is highly suitable for monitoring vegetation function and condition reliably as the only presently available chlorophyll index from a spaceborne sensor.

Many studies focused on evaluating vegetation phenology extracted from different remote sensing datasets. Huete et al. (1997) evaluated the differences and similarities in sensitivity to vegetation condition by comparing several vegetation indices from Landsat TM and MODIS data. The NDVI showed a high sensitivity to the highly absorbing red band, while other indices were more sensitive to the near-infrared band. Kawamura et al. (2005) compared MODIS NDVI and AVHRR NDVI time-series data and found that the MODIS NDVI time-series depicted the seasonal changes in grassland with a greater fidelity. Soudani et al. (2006) assessed the potential use of IKONOS, Landsat ETM+, and SPOT HRVIR data for estimating LAI in forest, and five vegetation indices were tested. The result indicated that a -10% offset was needed for dense vegetation land cover when using IKONOS NDVI, while no corrections were needed when focusing on bare soils or sparse vegetation regions. Zeng et al. (2011) compared MODIS NDVI and AVHRR NDVI time-series and discovered that the phenology extractions from those two datasets were significantly distinctive, from 2000 to 2008 over the northern high latitudes; Tang et al. (2015) adopted both AVHRR NDVI and MERIS MTCI for extracting phenological metrics including OG and ES at nine regions in China for different land covers. The results showed that both indices performed very well in capturing the vegetation growing patterns, but NDVI detected a later ES than MTCI.

Very few studies have compared the uncertainty in estimating phenological

variables from use of different spectral vegetation indices. Moreover, the ability of MTCI to derive phenological information and any potential advantage compared to the well-established NDVI based method has not been studied. Therefore, the purpose of this chapter was to compare the vegetation phenology extracted from MERIS NDVI and MERIS MTCI at different regions across China, attempt to find the advantages and disadvantages for the MTCI to NDVI for the example. To do so, the ability of the NDVI and the MTCI time-series of capturing the growth pattern for different vegetation types in different regions needs to be investigated and the phenological metrics including OG and ES extracted from the NDVI and the MTCI compared.

3.2 Study Area

The main climate in China is dominated by dry seasons and wet monsoons on one hand, resulting in significant temperature differences in winter and summer. In winter, cold and dry winds come from northern high latitude areas, while in summer warm and moist winds come from lower latitude sea areas. Considering the great latitudinal variation, coastal and continental regions, and orographic variation, climates differ from region-to-region (Chen et al. 2005b). The climate zone changes from tropical, subtropical, warm-temperate, temperate, to cold-temperate from south to north in the eastern part of the country. On another hand China is affected by the continental climate. The climate zone changes from humid to arid from east to west, and it is dry in northwest China. The precipitation declines gradually from the south-eastern part of China to the north-western part. In south-eastern coastal areas, it reaches over 1,500 mm per year, while in the north-western desert areas it drops to below 200 mm per year (Gao et al. 2006). At the same time, China is a mountainous country, with more than half of the territory occupied by mountains and plateaus. The various climate, along with the complicated physiognomy, results in heterogeneous biomes in China.

3.3Data

3.3.1 Remote sensing data

Zhang et al. (2010) indicated that time-series data with a temporal resolution

between 6 and 16 days could be used to estimate vegetation phenology precisely, even if some uncertainties exist in the daily data. Therefore, in this research three data sources were used: (a) 300 m weekly MERIS L3 surface reflectance data from Oct 2009 to Mar 2011 (18 months) to capture the full growing season patterns (requested from http://maps.elie.ucl.ac.be/CCI); (ii) 2010 global land cover map from ESA in 300 m spatial resolution (downloaded from http://maps.elie.ucl.ac.be/CCI/viewer/); (iii) shape file of vegetation regionalisation map of China (obtained from http://www.resdc.cn/data.aspx?DATAID=133).

The surface reflectance (SR) products of MERIS span from 2003 to 2012, the spectral content consists of 13 surface reflectance channels (the atmospheric band 11 and 15 were removed), at a spatial resolution of 300 m for the Full Resolution (FR) and 1000 m for the Reduced Resolution (RR). The dataset is available at 7-day temporal resolution in 5°x5° tiles such as to composite global time-series datasets. The original MERIS L3 surface reflectance data are in NetCDF format. Each file contains variables for 13 bands (except band 11 and 15) and uncertainties for each spectral band, number of observations with clear sky land coverage, water coverage, clear sky snow and ice coverage, cloud coverage and cloud shadow coverage for each pixel during the 7 days. In addition, the data also contains a pixel-level classification including the classes: clear land, clear water, clear snow, cloud, and cloud shadow. Corresponding variables were extracted to calculate MTCI according to Dash and Curran (2004):

$$\boldsymbol{MTCI} = \frac{\boldsymbol{R_{Band10} - R_{Band9}}}{\boldsymbol{R_{Band9} - R_{Band8}}} = \frac{\boldsymbol{R_{753.75} - R_{708.75}}}{\boldsymbol{R_{708.75} - R_{681.25}}} \qquad (5)$$

NDVI was already calculated and stored as a variable in the original NetCDF file, and they were extracted separately. After that all tiles were mosaicked. 76 time-series files for each of the MTCI and NDVI were prepared, and clear land in the current pixel status variable was made as a land mask. However, because of clouds and other reasons, not enough valid data were retrieved to make the required complete time-series datasets. Therefore, a Maximum Value Composite (MVC) procedure was employed to obtain MTCI and NDVI composites for 18 months, with bi-weekly temporal resolution, which created 38 layers from Oct 2009 to Mar 2011.

3.3.2 China climate regionalisation map

The dataset was acquired from the Data Centre for Resources and Environmental Sciences, Chinese Academy of Sciences (RESDC) (http://www.resdc.cn/data.aspx?DATAID=133). The original dataset was divided into 36 sub-zones for more specific vegetation types and climate zones, based on the zonation of vegetation and its related climatic factors. Only the major climate zones were taken into consideration, therefore, it was categorised into six major climate zones (Figure **2**).

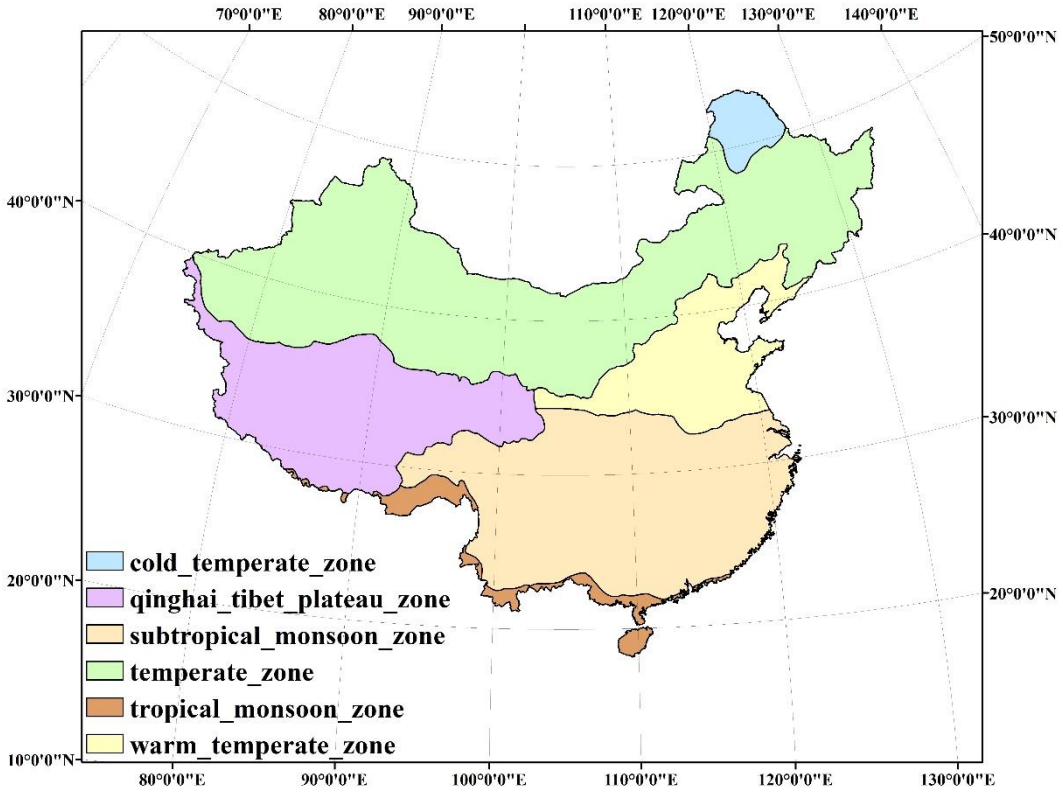

Figure 2 Climate regionalisation map of mainland China.

3.3.2 Land cover map

The land cover map used in this research was derived from ESA's global land cover project using 12 months' worth of data collected from 1 January to 31 December, from Envisat's MERIS instrument at a resolution of 300 m (available from https://www.esa-landcover-cci.org/). The map projection is WGS84 and the classification uses the UN Food and Agriculture Organisation's (FAO) Land Cover Classification System (LCCS) (http://www.esa.int/esaCP/). ESA's land cover map

had an overall accuracy of 73% weighted by area for its 22 land cover classes.

Vegetation types in China differ from region-to-region in response to temperature, precipitation and soil type. The major vegetation types are composed broadly of deciduous, semi-deciduous, and evergreen. The phenology of these vegetation types is often controlled by climatic condition. Therefore, to compare vegetation phenology extracted from NDVI and MTCI under different climatic conditions within different regions, four major types of vegetation were selected: cropland, broadleaf deciduous, mixed evergreen (broadleaf or needle leaf), and grassland (Figure **3**). Each vegetation type was investigated across five climate zones including the warm temperate zone, subtropical zone, tropical monsoon zone, temperate zone, and Qinghai-Tibet plateau zone (Figure **4**), cold temperate zone was not included due to MERIS 300m data was not available in this region.

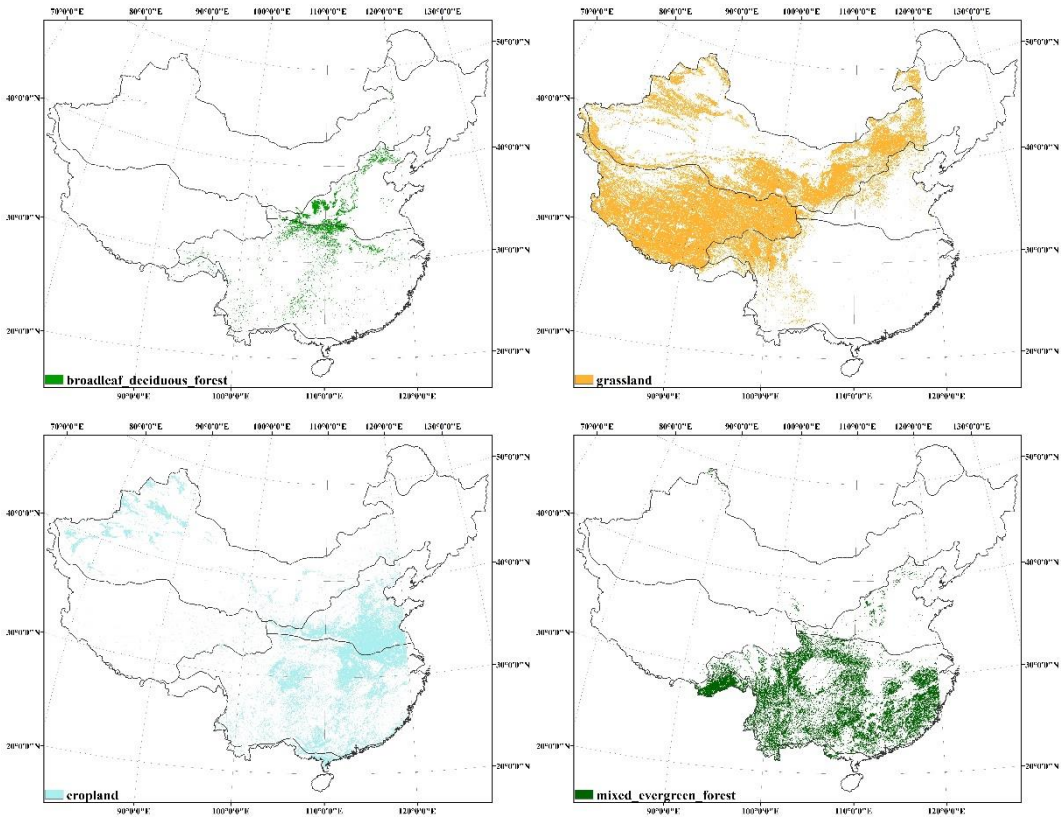

Figure 3 Major land cover types extracted from ESA 2010 Global Land Cover Map: (a) broadleaf deciduous forest; (b) grassland; (c) major cropland (d) mixed evergreen (broadleaf and needle leaf) forest.

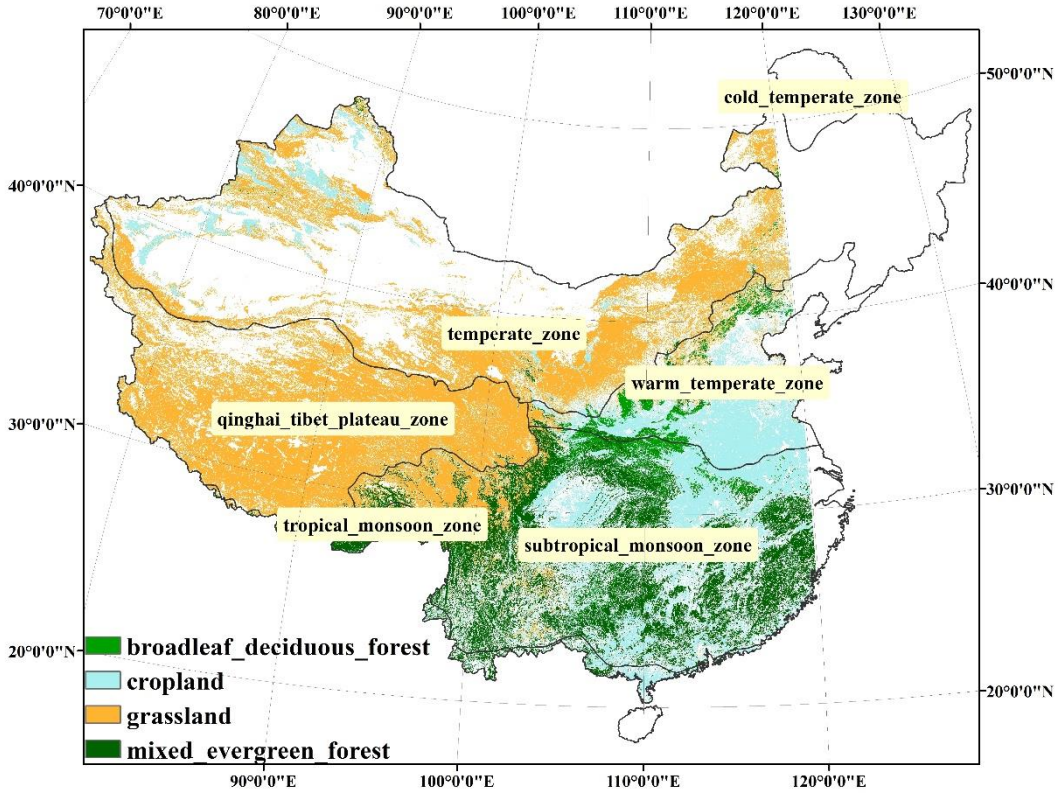

Figure 4 Vegetation distributions and climate zones investigated in this study (non-coloured regions are not available for the MERIS 300 m data).

3.4 Method

In this chapter, three procedures were applied for extracting phenological metrics from both the MTCI and NDVI time-series data. The flowchart of Figure **5** shows the steps: (1) data cleaning; (2) data smoothing; (3) phenological metrics extraction.

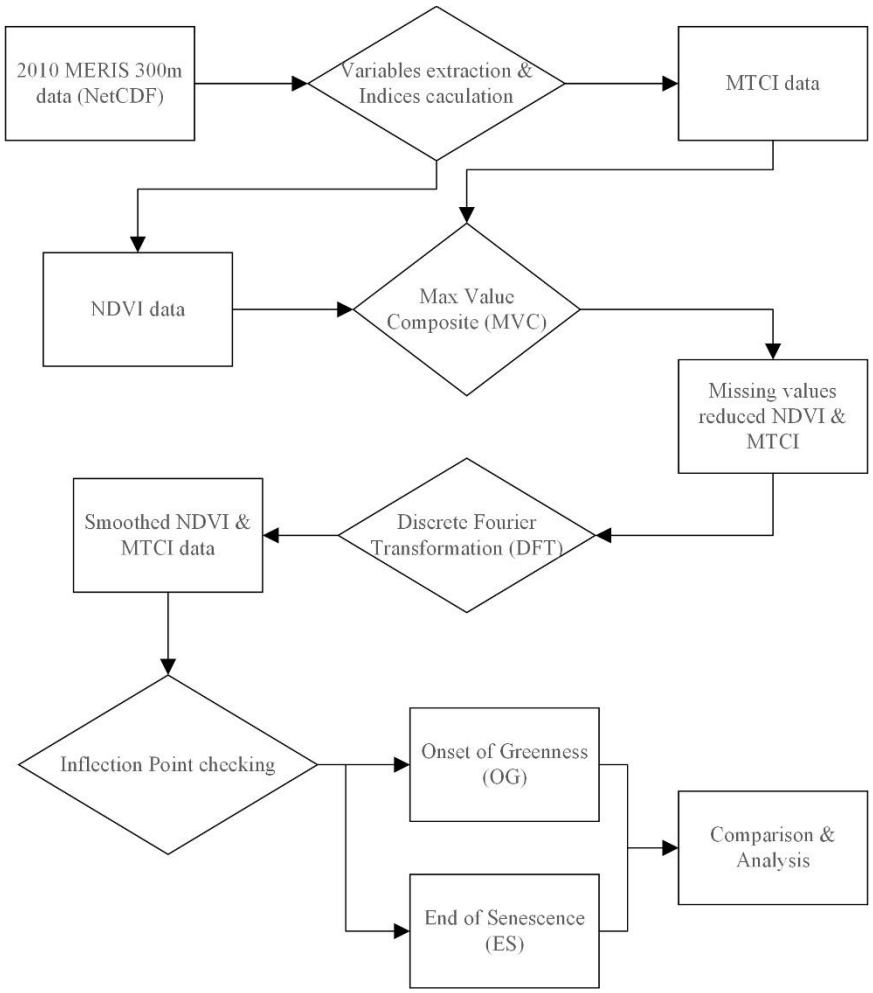

Figure 5 Flowchart of procedures for data processing, phenological metric extraction, and comparison.

3.4.1 Data cleaning

To remove the missing data or outliers, a data cleaning procedure was required after applying the MVC method, which obtained the valid maximum value for every two dates, and transformed the raw data into biweekly interval. Although valid MTCI values range from 1 to 6, and NDVI values from -1 to 1, there may exist erroneous values or missing data creating data dropouts (MTCI=0) and data gaps due to cloud, local climate fluctuations and other atmospheric noise, and residual atmospherically-related noise (Atkinson et al. 2012; Wu et al. 2009). Therefore, the data anomalies and useless data from the temporal data series were also removed. The outcomes of data cleaning were shown in Figure **6**.

3.4.2 Data smoothing

A data smoothing procedure aimed at minimising errors existing in the raw MTCI and NDVI data. There are many different techniques applicable for reducing noise in time-series datasets, such as best index slope extraction (BISE) (Viovy et al. 1992), the asymmetric Gaussian (Jönsson & Eklundh, 2002), Savitzky–Golay (Chen et al. 2004), double logistic functions (Zhang et al. 2004), the Mean Value Iteration (MVI) (Ma and Veroustraete 2006), the Changing Weight (CW) filter (Zhu et al. 2012) and so on. However, most of these techniques require an iterative approach to adjust the model parameters such as a noise-threshold and size of the temporal neighbourhood to achieve reliable smoothing. Comparing with these methods, Dash et al. (2010b) pointed out that Fourier transform-based approaches have the advantage of minimal user input (only need to decide the number of harmonics to reconstruct the time-series) and have been applied successfully to regional-to-global AVHRR time-series datasets (Cui et al. 2010; Loyarte et al. 2008; Moody and Johnson 2001; Roerink et al. 2000). In this research, the discrete Fourier transformation (DFT) was applied, and the smoothed time-series are shown in Figure **6**.

The DFT decomposes any complex waveform into a series of sinusoids of different frequency. Individual sinusoids and their frequencies can be combined into a complex waveform for which noise has been removed. The DFT is calculated as follow:

$$\boldsymbol{F(u) = \frac{1}{N}\sum_{x=0}^{N-1} f(x) \times e^{-2\pi ux/T}} \quad (6)$$

Where $f(x)$ is the *x*th value in the time-series, *u* is the number of Fourier components, *x* is the dekad number, *T* is the length of time period cover (number of dekad), and *T* is equal to *N*.

Eq. (6) consists of two parts: cosine (real) and sine (imaginary), where the cosine part is:

$$\boldsymbol{Fc(u) = \frac{1}{N}\sum_{x=0}^{N-1} f(x) * \cos(2\pi \frac{ux}{T})} \quad (7)$$

And the sine part is:

$$\boldsymbol{Fs(u) = \frac{1}{N}\sum_{x=0}^{N-1} f(x) * \sin(2\pi \frac{ux}{T})} \qquad (8)$$

Using Eqs. (7) and (8), the Fourier magnitude (F_m) can be calculated as:

$$\boldsymbol{Fp(u) = atan2\left(\frac{Fc(u)}{Fs(u)}\right)} \quad (9)$$

The first two harmonics of the Fourier transform usually account for 50-90% of the variability in a dataset (Jakubauskas et al. 2001). However, the first two harmonics can only represent annual and semi-annual cycles, which is not enough to represent all the phenological cycles in China. Jakubauskas et al. (2001; 2002) demonstrated that the first four harmonics could adequately represent unimodal vegetation growth patterns. Dash et al. (2010b) tested the first four harmonics for vegetation in India. It was found that if only the first four harmonics were used, local oscillations could be avoided during the growing season, which were detected by higher harmonics. And six harmonics were used for detecting the double cropping patterns, which is common in India. Therefore, in this study, six harmonics were used in the inverse DFT to generate a smoothed MTCI time-series.

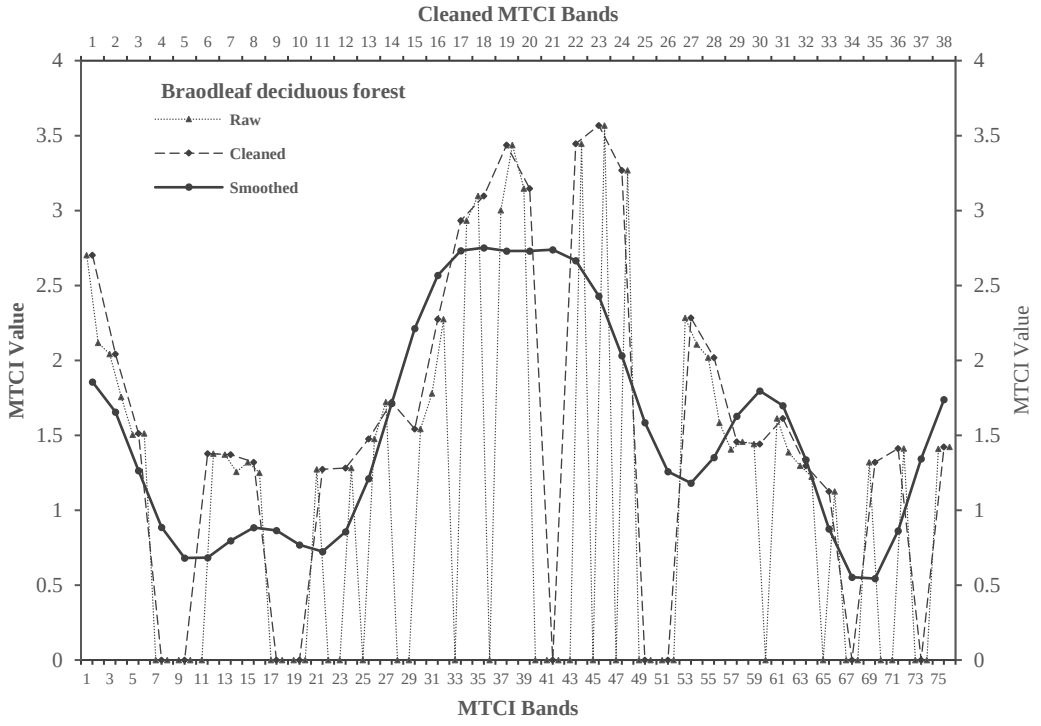

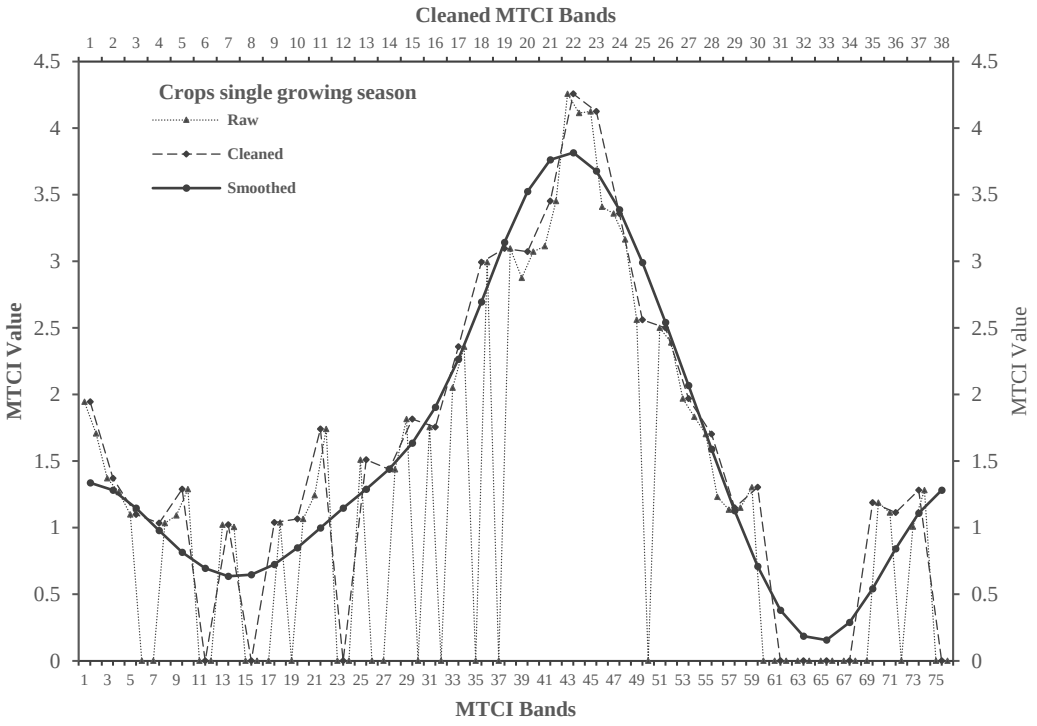
Cleaned MTCI Bands
Crops single growing season
Raw
Cleaned
Smoothed
MTCI Value
MTCI Bands

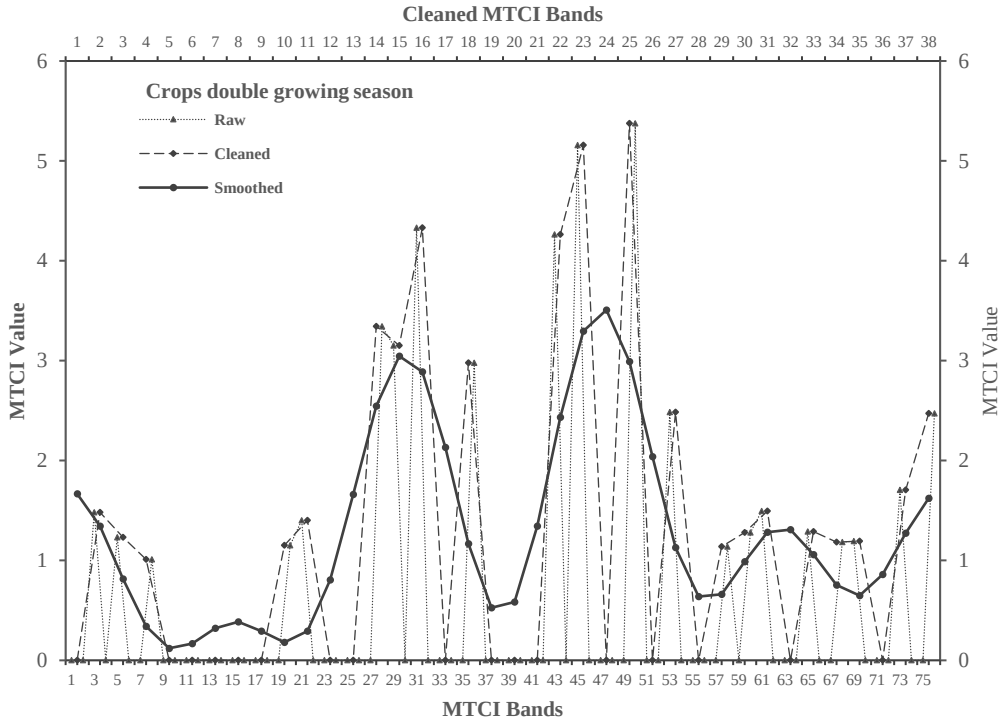
Cleaned MTCI Bands
Crops double growing season
Raw
Cleaned
Smoothed
MTCI Value
MTCI Bands

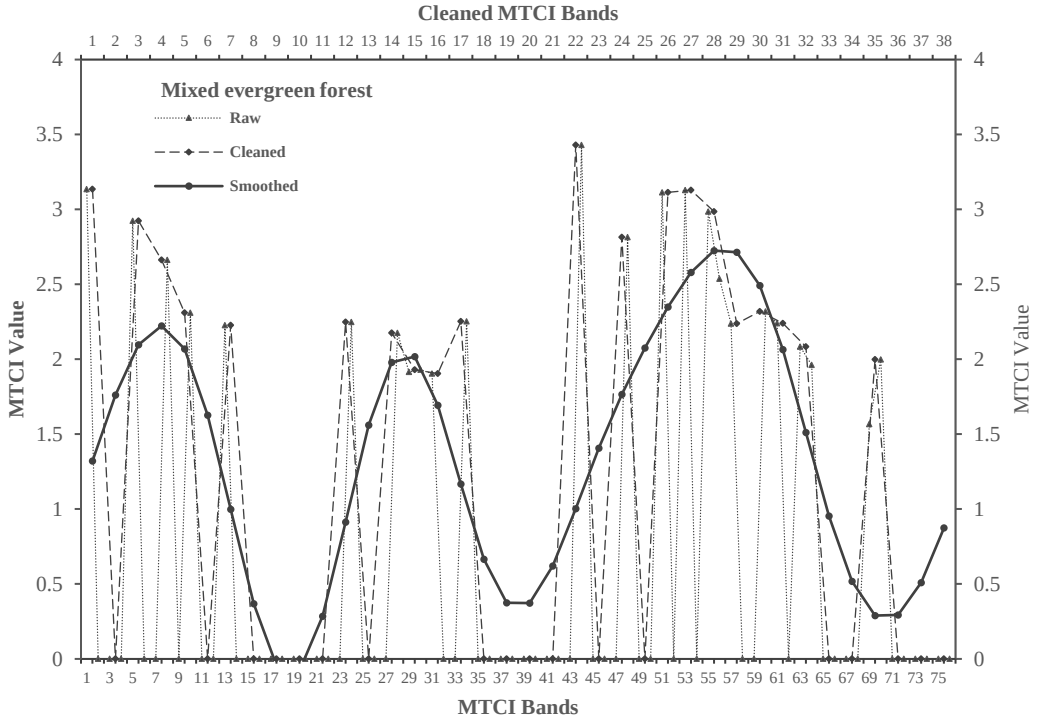
Cleaned MTCI Bands
Mixed evergreen forest
Raw
Cleaned
Smoothed
MTCI Value
MTCI Bands

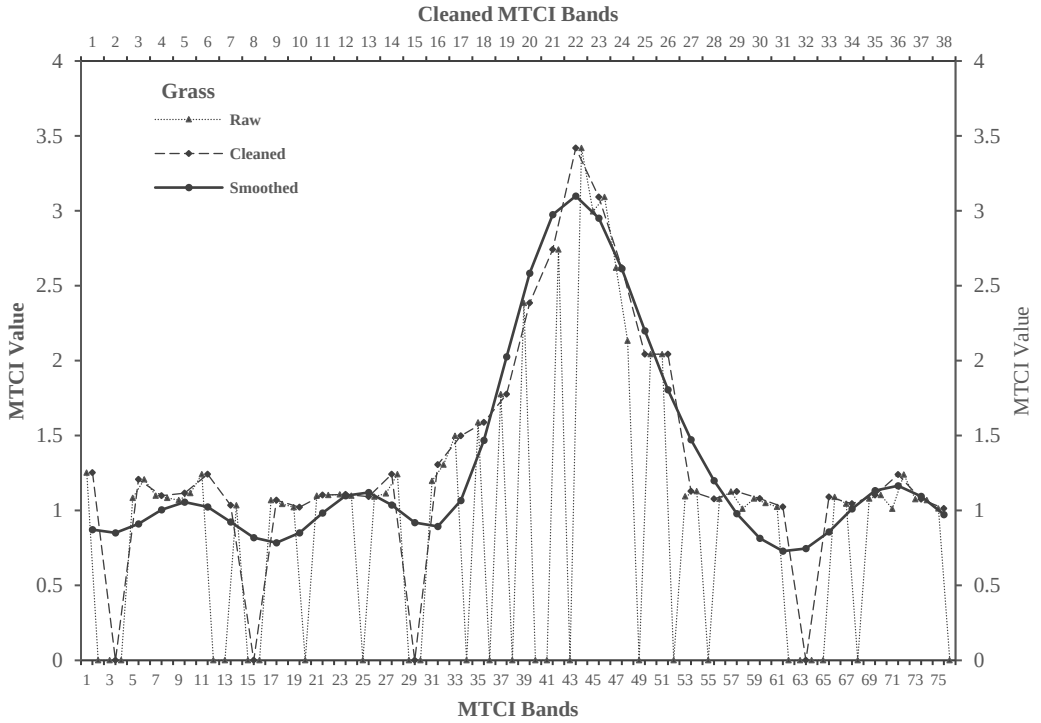
Cleaned MTCI Bands
Grass
Raw
Cleaned
Smoothed
MTCI Value
MTCI Bands

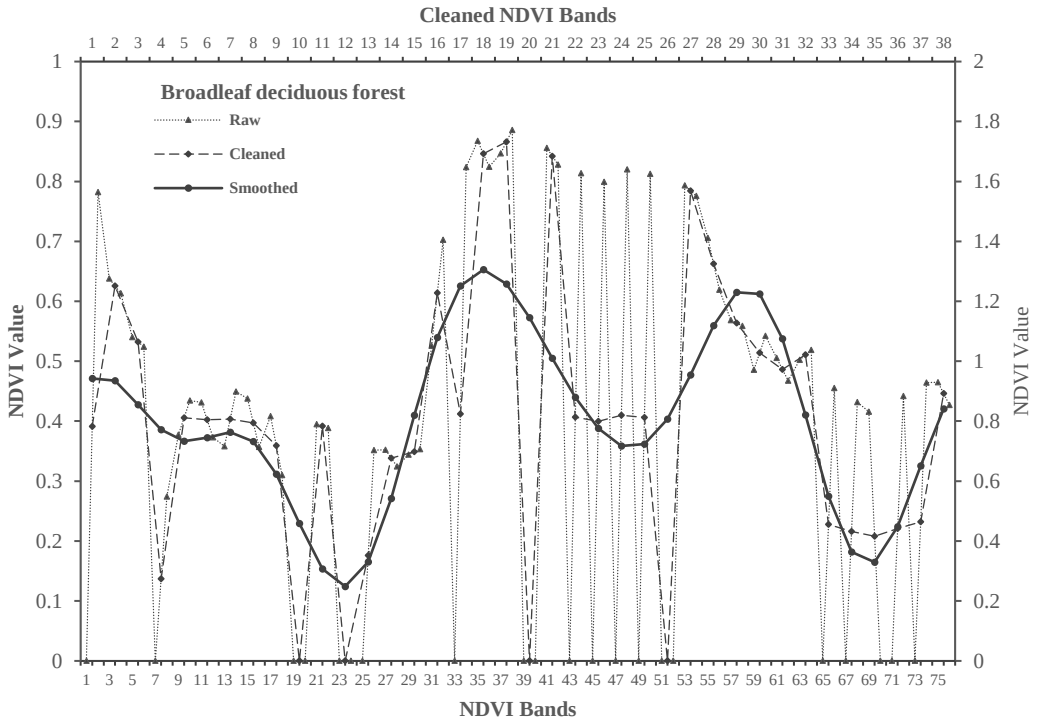
Cleaned NDVI Bands
Broadleaf deciduous forest
Raw
Cleaned
Smoothed
NDVI Value
NDVI Value
NDVI Bands

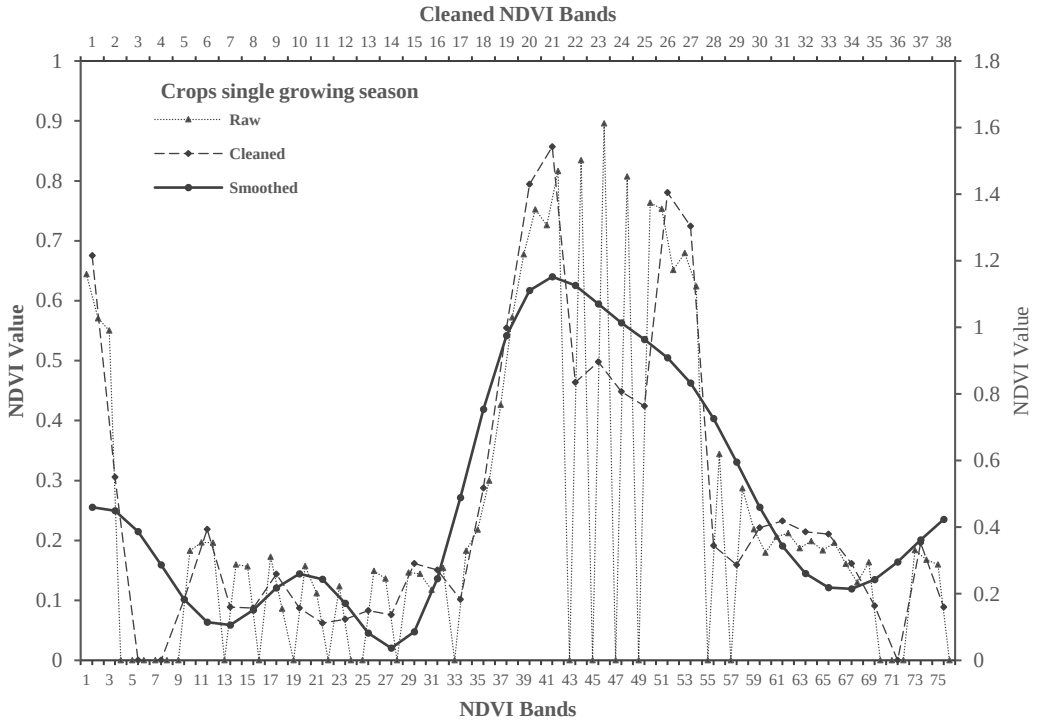
Cleaned NDVI Bands
Crops single growing season
Raw
Cleaned
Smoothed
NDVI Value
NDVI Value
NDVI Bands

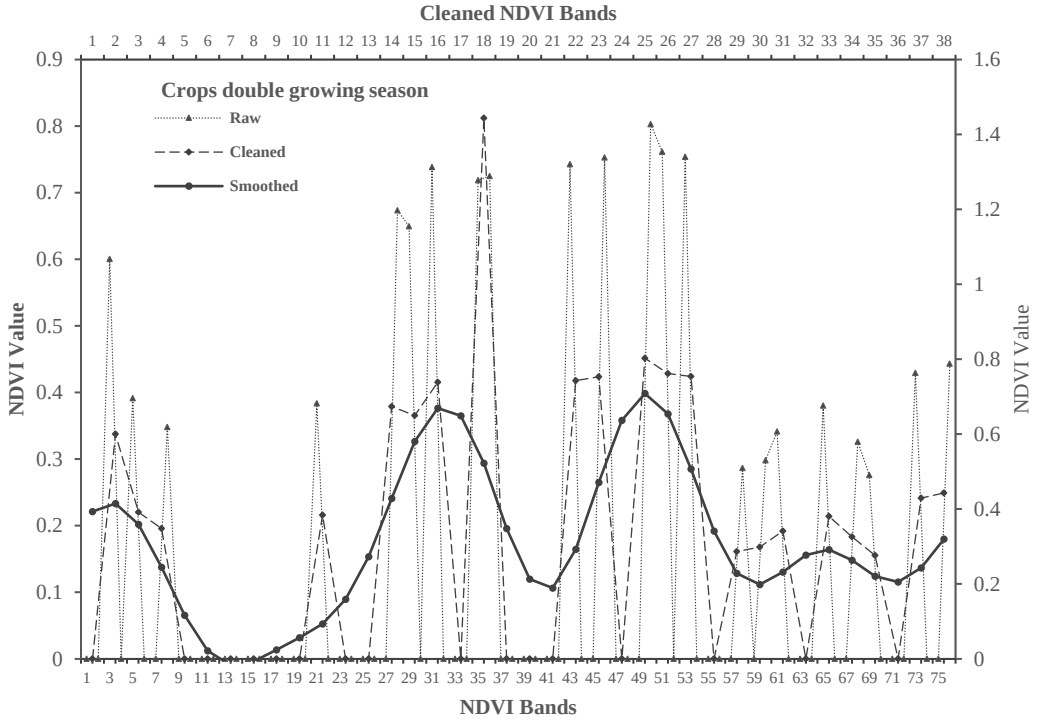
Cleaned NDVI Bands
Crops double growing season
Raw
Cleaned
Smoothed
NDVI Value
NDVI Value
NDVI Bands

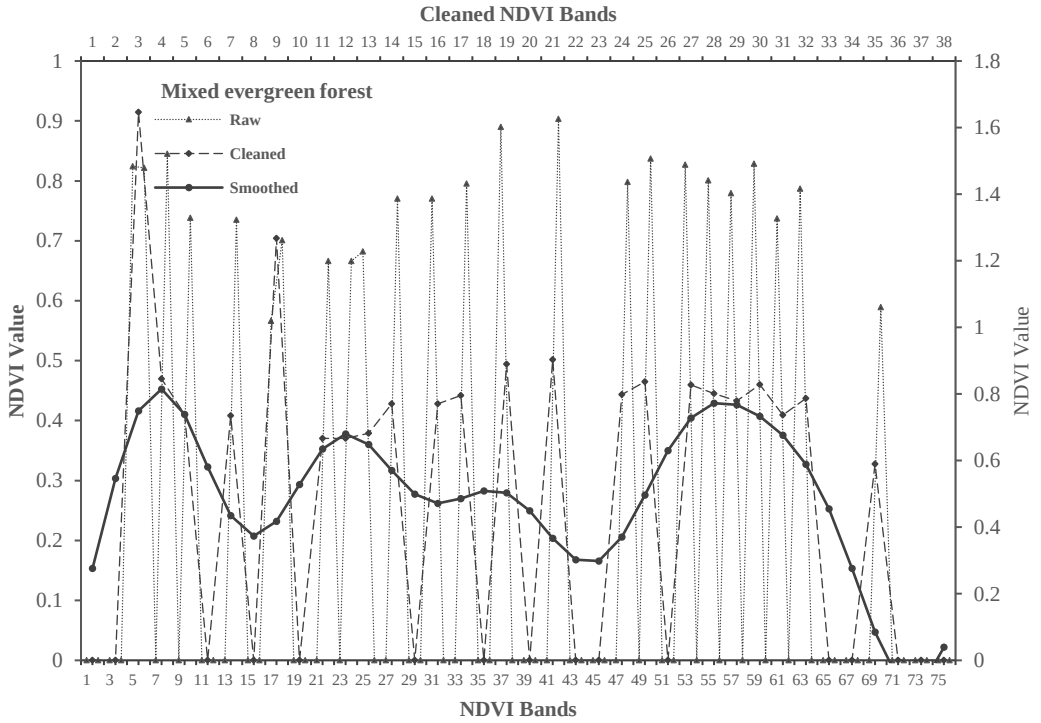
Cleaned NDVI Bands
Mixed evergreen forest
Raw
Cleaned
Smoothed
NDVI Value
NDVI Value
NDVI Bands

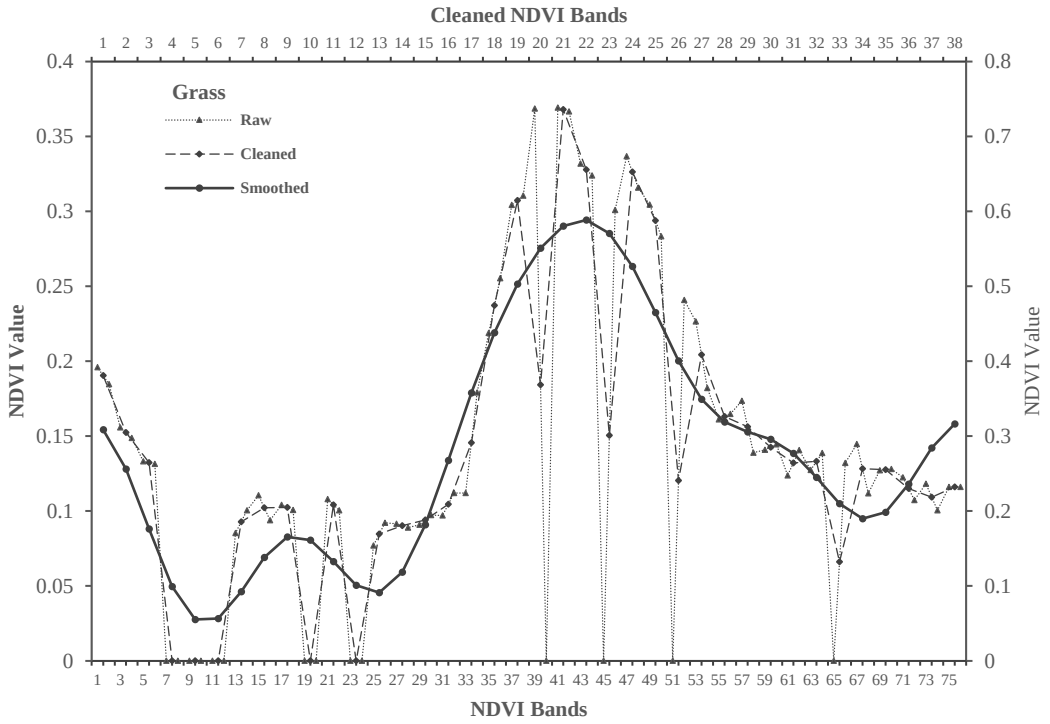

Figure 6 Data cleaning and smoothing examples for four major land cover types: broadleaf deciduous forest, cropland (including single and double cropping), mixed evergreen forest, and grassland.

3.4.3 Estimating phenological metrics

There are several available methods to estimate phenological variables from smoothed time-series vegetation data. According to Reed et al. (1994), these methods generally fall into three categories: threshold-based methods, trend derivative methods, and inflection point methods. A threshold is defined or referred for each pixel to define phenology transition dates in threshold-based methods (Lloyd 1990); departure points are identified between temporal data and a derivative curve in trend derivative methods; maximum curvature occurrences are detected in plotted time-series vegetation data in the inflection point-based methods (Zhang et al. 2003). However, each method has its own advantages and disadvantages; the choice of technique, therefore, depends on the purpose of the study. In this chapter, the inflection point-based method was applied for the reason that it is easy to implement and able to discriminate multiple growing seasons for vegetation such as crops (Reed et al. 1994). The inflection point method was employed here to extract two key phenological metrics: Onset of Greenness (OG)

and End of Senescence (ES).

By taking an MTCI time-series data as an example (Figure **7**), OG can be detected at a valley point at the start of the season, and the ES can be detected also at a valley point where is a decaying end in a phenology season. Also, the rate of green-up and senescence can be derived (not calculated in this chapter). It can also be clearly seen that it is easy to extract the phenological metrics if the phenology season is in a simple and smooth sinusoidal pattern. However, the ecosystem exhibits more complex patterns, sometimes because of multi-growth seasons or local climatic fluctuation. Therefore, OG and ES must be defined for each year independently rather than empirically. In fact, the ecosystem can be complex and diverse especially in a vast country such as China, since its territory crosses and stretches about 50° longitude and latitude. Hence, many of the ecosystems' phenological cycles may span across years. As a result, this can lead to the absence of OG or ES data in one single year of vegetation data.

The second growing season was not considered have as the major double cropping area is the east coastal provinces, which were not covered by MERIS 300 m data. Some areas in mid-east China also had a double cropping system. However, due to the poor coverage of MERIS 300 m data, the second growing season could not always be detected correctly. Therefore, only one growing season was considered in this study.

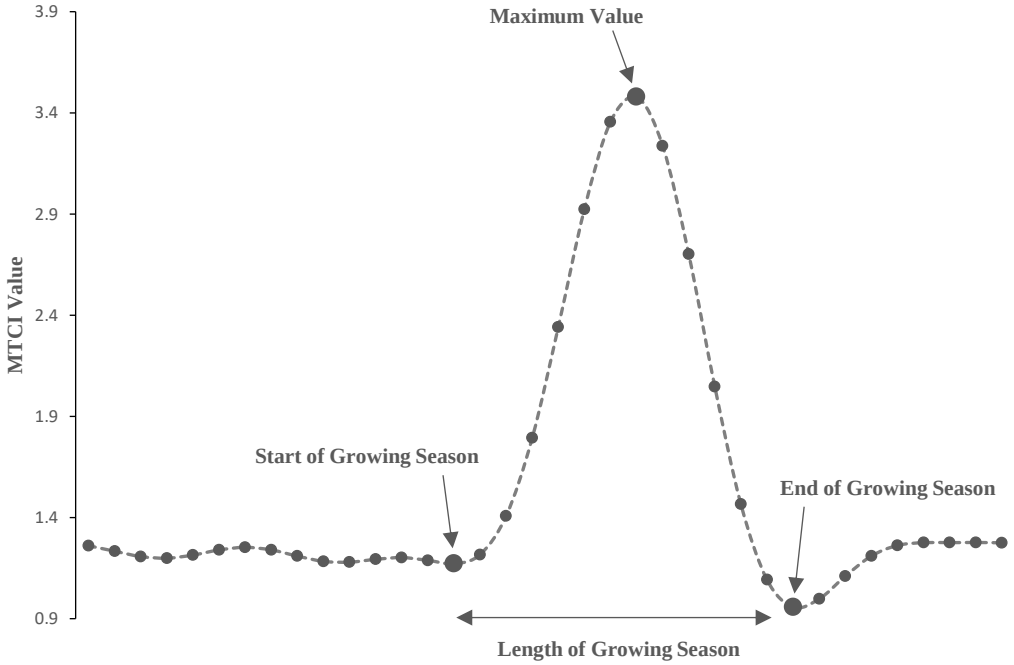

Figure 7 Phenological metrics extraction example.

The inflection point method for extracting phenological metrics (i.e., the OG and ES), starts from the dominant peaks and searches both forwards and backwards, checking the derivative at the same time. When the derivative changes from positive to negative or from negative to positive, it may indicate a valley point which might be assigned as OG or ES. However, because of local climatic fluctuations or stabilization or multi-growth seasons of vegetation types, the valley point may be located at a different place rather than the ideal theoretical place, resulting in a fluctuation to be determined as a growing cycle. To deal with this, the algorithm sets a rule that the difference between the maximum value and valley value is greater than one fifth of the maximum vegetation time-series signal value, for the valley point to be accepted as a phenological variable until a definite valley point is detected.

3.4.4 Comparison of phenological patterns and metrics

Time-series profiles of different vegetation types in different vegetation-climate zones were presented to test the performance of the MTCI and NDVI in characterising the variation of vegetation growing season. Furthermore, the OG and

ES derived from the MTCI and NDVI were calculated by $D = M_{NDVI} - M_{MTCI}$, where M_{NDVI} is OG(ES) derived from NDVI, and M_{MTCI} is OG(ES) derived from MTCI. Therefore, when *D* is positive that means the OG(ES) extracted from NDVI is delayed more than that extracted from MTCI.

3.5 Results

3.5.1 Comparison between MTCI and NDVI patterns

Figure **8** presents the profiles of the average value of MTCI and NDVI for the vegetation growing season in different vegetation-climate zones from Oct 2009 to Mar 2011. Comparing the broad MTCI and NDVI phenological patterns, it can be observed that the valley points of the OG and ES are clearly represented, except when then NDVI depicts the mixed evergreen forest in the subtropical evergreen broadleaf forest zone. It is also worth noting that the NDVI has two peaks around its maximum value, it is because of the missing values in the raw data that cause the fluctuations (e.g. the broadleaf deciduous forest and mixed evergreen forest).

For broadleaf deciduous vegetation, in both the subtropical and temperate zones, it can be noticed that the NDVI time-series shows two peaks, while the MTCI only one peak. For mixed evergreen vegetation (including broadleaf evergreen forest and needle leaf evergreen forest), a clear growing pattern was revealed by the MTCI while the NDVI failed in the subtropical evergreen broadleaf forest vegetation-climate zone, which has a higher annual temperature and less clear seasonality. The MTCI time-series produced a smooth growing pattern in the warm temperate deciduous broadleaf forest, and the NDVI showed more dramatic fluctuations than the MTCI, the NDVI had a flatter peak with fluctuation while the MTCI had a clear peak. For grassland, both the MTCI and the NDVI in the vegetation-climate zones of temperate steppe, subtropical evergreen broadleaf forest, Qinghai-Tibet Plateau alpine vegetation, and temperate desert, describe the growing patterns very clearly. And similarly, however, it can be noticed that the MTCI had an early OG and ES, and shorter lengths of growing season than the NDVI. For cropland, the NDVI was more able to depict double cropping seasons, and had a similar ability with the MTCI when there was only one growing season.

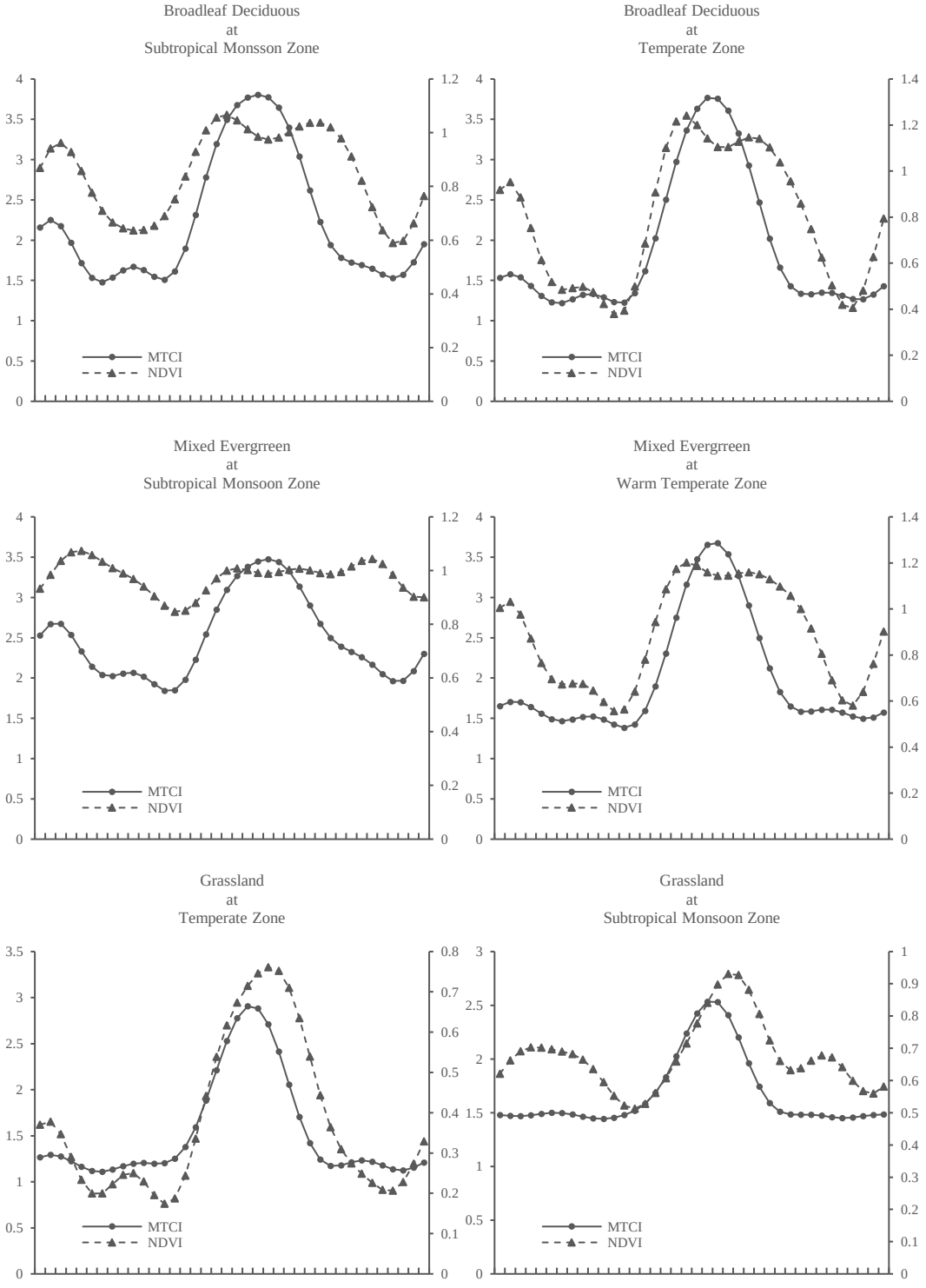
Broadleaf Deciduous
at
Subtropical Monsson Zone
MTCI
NDVI
Broadleaf Deciduous
at
Temperate Zone
MTCI
NDVI
Mixed Evergrreen
at
Subtropical Monsoon Zone
MTCI
NDVI
Mixed Evergrreen
at
Warm Temperate Zone
MTCI
NDVI
Grassland
at
Temperate Zone
MTCI
NDVI
Grassland
at
Subtropical Monsoon Zone
MTCI
NDVI

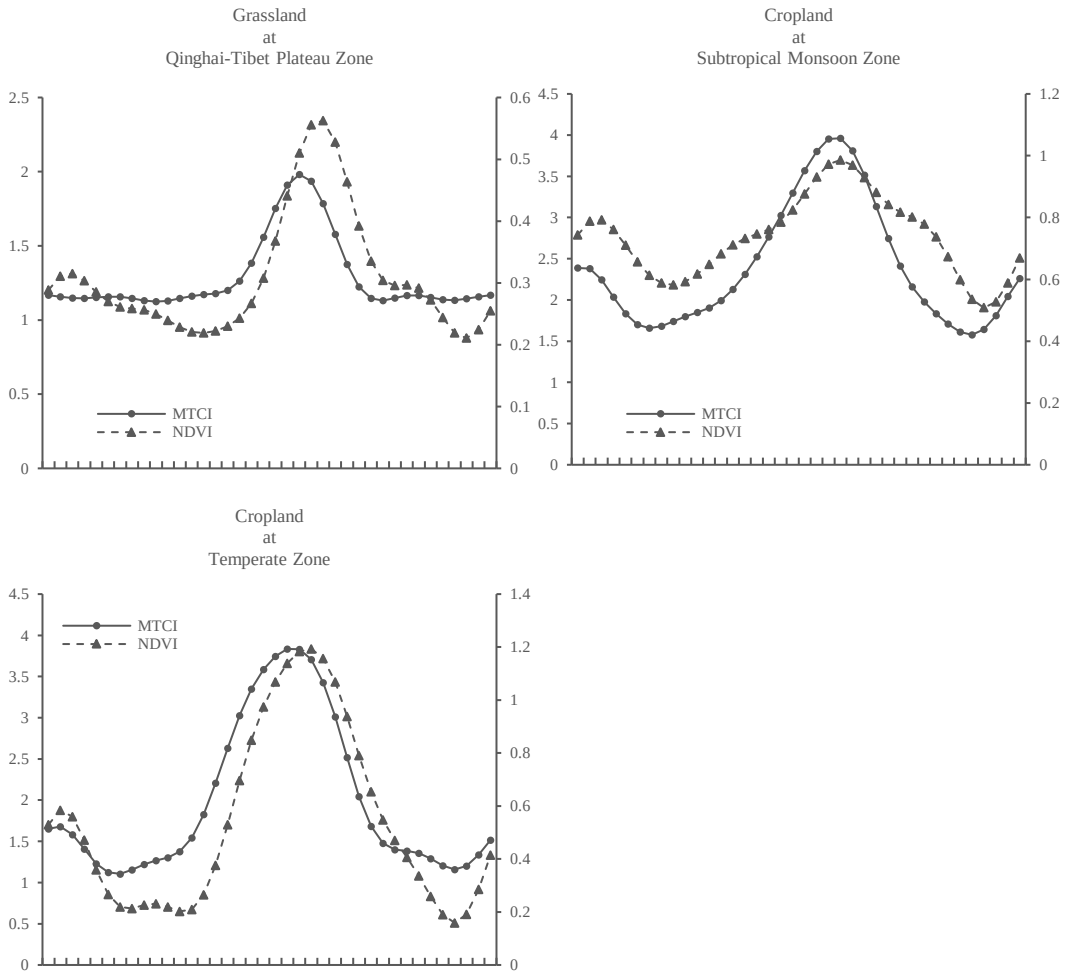

Figure 8 Growing patterns of NDVI and MTCI for broadleaf deciduous, cropland, grassland, mixed evergreen land covers in different climate zones, left y axis is the MTCI value, and the right axis is the NDVI value.

3.5.2 Comparison between phenological metrics extracted from MTCI and NDVI

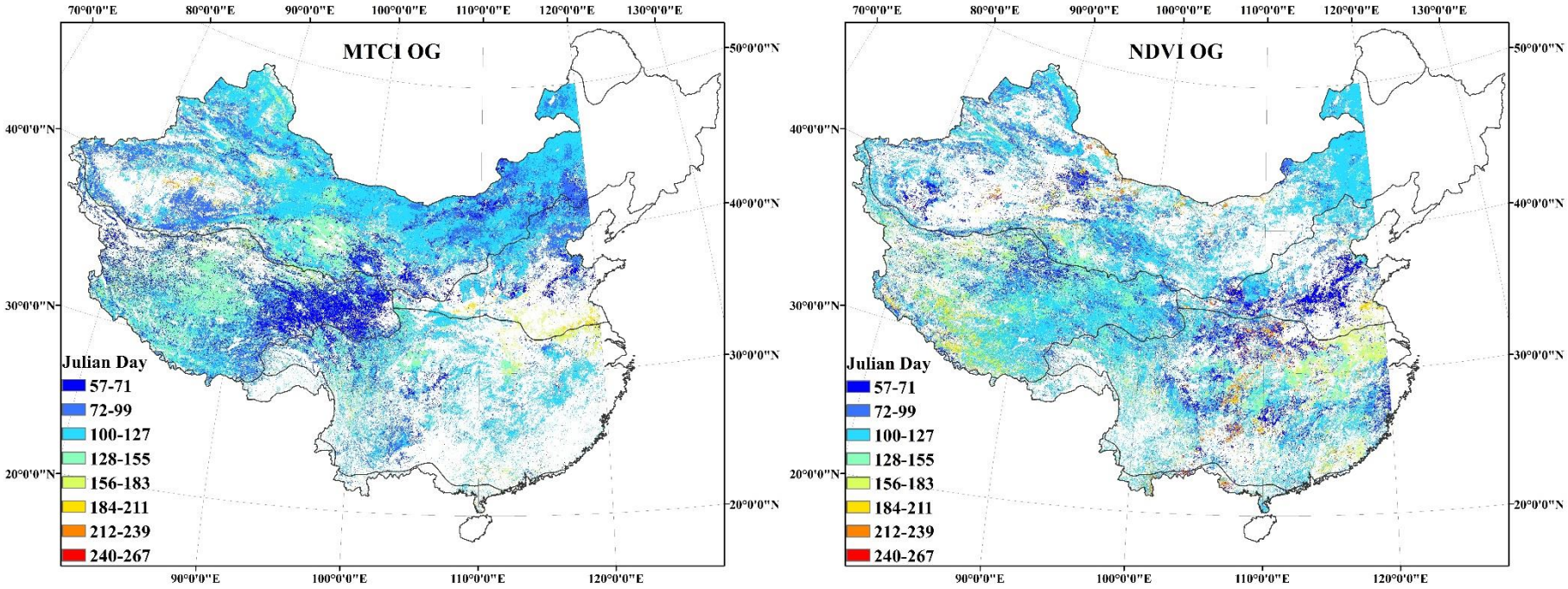

Figure 9 Distributions of OG for MTCI and NDVI for the year 2010.

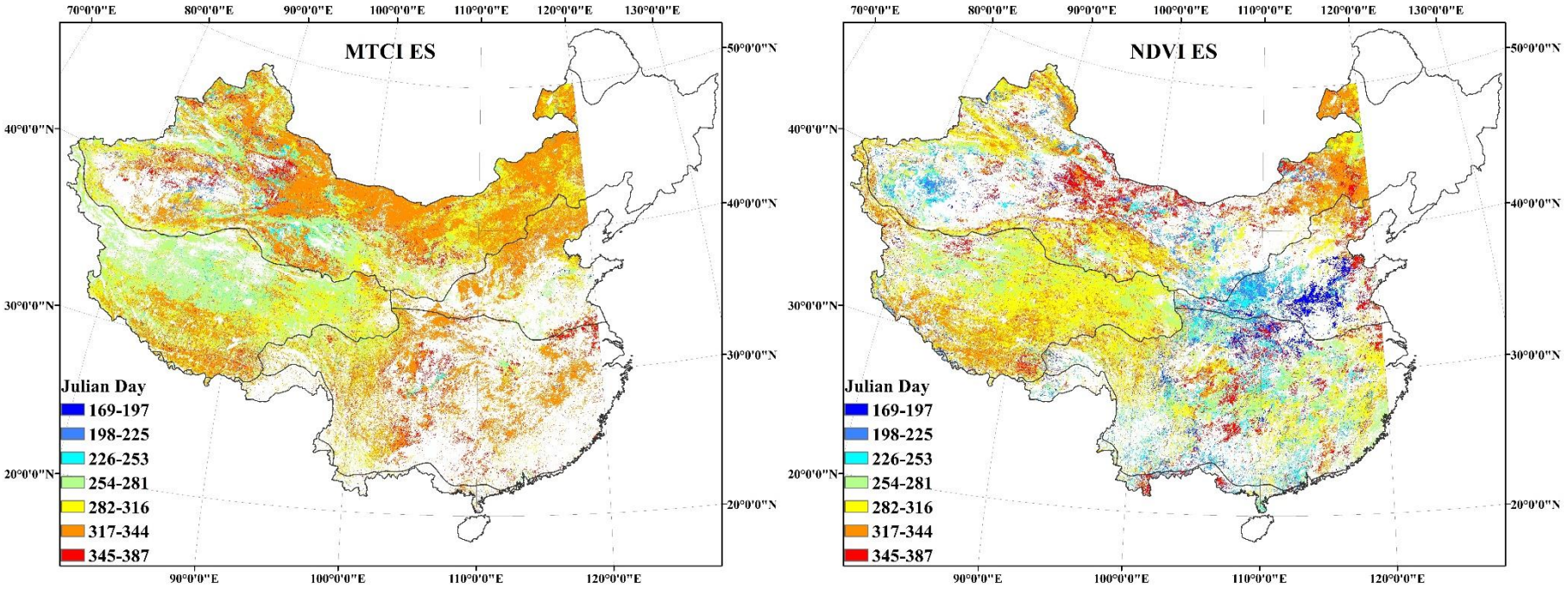

Figure 10 Distributions of ES for MTCI and NDVI for the year 2010.

Figures **9** and **10** show the distribution of OG and ES of the year 2010 derived from the MTCI and the NDVI of the first growing season, using the inflection point method. In general, the NDVI showed more variation regionally than the MTCI. The OG started earlier for the MTCI than the NDVI, especially in regions which have a cold and snow-covered winter. The spatial patterns of ES generally correspond with the latitudinal gradient. Overall, ES became earlier from south to north. Except for the middle-east part of the study area with a large area of cropland, the NDVI detected earlier OG and ES than the MTCI. In the northern part dominated by grassland, later OG and ES were detected by the NDVI.

	Zone Name	OG (Days)			ES (Days)		
		MTCI	NDVI	D	MTCI	NDVI	D
Broadleaf Deciduous	warm_temperate_deciduous_broadleaf_forest	137.71	144.66	6.95	355.56	332.42	-23.14
	subtropical_evergreen_broadlleaf_forest	146.84	130.99	-15.85	359.47	308.57	-50.90
	tropical_monsoon_rain_forest	139.76	144.34	4.58	349.80	321.19	-28.61
	temperate_steppe	152.05	160.46	8.42	345.51	349.45	3.94
	temperate_desert	147.97	172.20	24.24	340.50	354.39	13.89
	qinghai_tibet_plateau_alpine_vegetation	129.66	131.63	1.97	338.20	341.25	3.05
Cropland	warm_temperate_deciduous_broadleaf_forest	116.30	118.97	2.67	340.30	330.71	-9.59
	subtropical_evergreen_broadlleaf_forest	123.14	123.31	0.16	364.42	332.55	-31.87
	tropical_monsoon_rain_forest	110.86	131.86	20.99	364.80	314.93	-49.87
	temperate_steppe	136.16	144.22	8.06	344.03	355.31	11.28
	temperate_desert	132.38	143.96	11.59	348.19	349.39	1.21
	qinghai_tibet_plateau_alpine_vegetation	141.14	155.08	13.93	334.60	346.43	11.83
Grassland	warm_temperate_deciduous_broadleaf_forest	131.08	144.65	13.57	351.37	355.01	3.64
	subtropical_evergreen_broadlleaf_forest	139.26	144.13	4.87	345.31	346.46	1.14
	tropical_monsoon_rain_forest	135.41	135.35	-0.06	345.55	341.86	-3.69
	temperate_steppe	143.88	147.36	3.48	344.97	359.19	14.23
	temperate_desert	137.12	151.93	14.80	342.65	352.24	9.59
	qinghai_tibet_plateau_alpine_vegetation	148.78	161.34	12.55	339.13	347.06	7.93
Mixed Evergreen	warm_temperate_deciduous_broadleaf_forest	150.30	139.97	-10.34	351.65	331.68	-19.98
	subtropical_evergreen_broadlleaf_forest	156.78	135.96	-20.81	355.67	328.98	-26.69
	tropical_monsoon_rain_forest	145.79	137.05	-8.74	349.41	313.89	-35.52
	temperate_steppe	157.35	148.26	-9.09	342.93	354.97	12.03
	temperate_desert	154.55	137.03	-17.52	342.52	357.83	15.31
	qinghai_tibet_plateau_alpine_vegetation	153.08	136.32	-16.75	340.28	353.29	13.00

Table 3 Differences between the onset of greenness and end of senescence for different vegetation types extracted from MTCI and NDVI time-series for the year 2010.

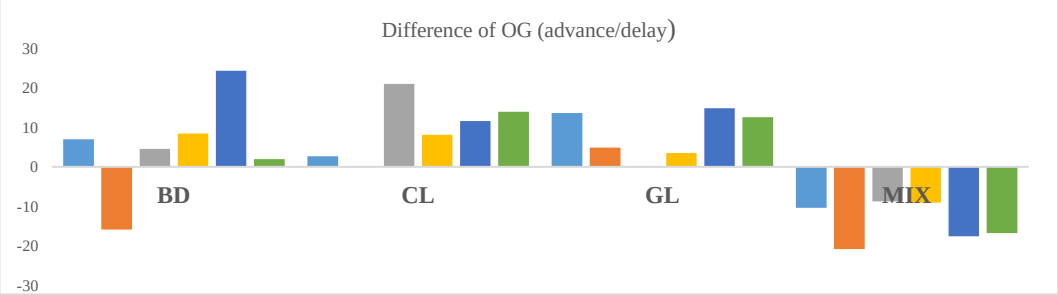

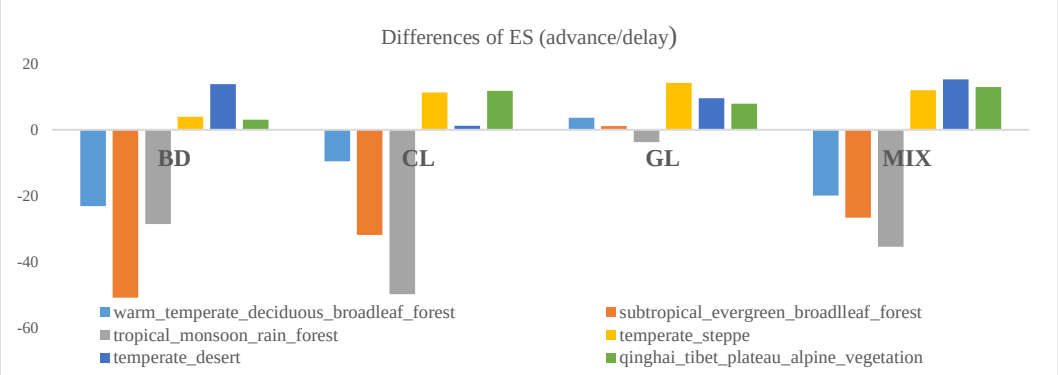

Figure 11 Plots of the differences between MTCI and NDVI of phenological metrics in the year 2010 for vegetation types of BD (broadleaf deciduous), CL (cropland), GL (grassland), and MIX (mixed evergreen), in different vegetation-climate zones. A positive value means NDVI delayed, in contrast, a negative value means NDVI advanced.

Table **3** and Figure **11** present the phenological differences between the MTCI and the NDVI in different vegetation-climate regions of the year 2010. OG and ES extracted from the NDVI and MTCI were different for vegetation types in most vegetation-climate zones. Generally, in the subtropical evergreen broadleaf forest and tropical monsoon rainforest zones, the NDVI and MTCI showed the largest differences for broadleaf deciduous, mixed evergreen, and grassland vegetation types. For broadleaf deciduous and cropland, the NDVI showed a shortened growing length (delayed in OG and advanced in ES), while for the other vegetation types in the remaining zones OG and ES showed the same shifting trend and more consistent than that in other zones resulting in a similar length of growing season.

The reasons for the variation between OG and ES extracted from MERIS NDVI and MTCI could be attributed to: (i) NDVI and MTCI are theoretically calculated based on different spectral bands. The NDVI is based on the red (560 nm) and near-infrared (NIR) (865 nm), band 8 and band 13 in normal MERIS band settings and MTCI is calculated from band 8 (681.25 nm), band 9 (708.75 nm), and band 10 (753.75 nm). The MTCI is calculated from narrower bands (band width 7.5 nm to 10 nm) than the NDVI (band width 10 nm to 20 nm), which could lead to a higher sensitivity to the minor changes (small reflectance variations) during vegetation growing season (Jensen et al. 2007); (ii) the Maximum Value Composite (MVC) technique dissolved some neighbouring data, which might give rise to some advances or delays when extracting phenological metrics.

3.6 Discussion

Several studies were undertaken to characterise vegetation phenology by remote sensing techniques in China (Chen et al. 2005b; Guo et al. 2013; He et al. 2015a; Le et al. 2014; Li et al. 2011a; Pan et al. 2012; Piao et al. 2006a; Wu et al. 2009; Wu et al. 2008). These studies highlighted variation in key phenological events such as start of season, end of season and length of season, at local or regional scales within China. Most of these studies used single vegetation indices such as NDVI from different data source like SPOT-VGT, MODIS, and AVHRR, focused on specific single or multi vegetation types at spatial and temporal resolutions from fine to coarse. Although relatively small regional studies are helpful to understand the impact on vegetation of climate changes, it is still far from enough to provide information for building bio-geochemical models at country to global scales. In addition, few studies employed the MTCI to investigate vegetation phenology in China. It is, therefore, necessary to apply the MTCI in extracting vegetation phenological metrics to compare with existing studies which were mainly based on NDVI.

This chapter employed the MTCI and MERIS NDVI to produce smoothed phenological patterns for the year 2010 for investigating the ability of phenology to describe and extract two key phenological metrics (OG and ES) for the purpose of making a comparison. Compared to the NDVI, the MTCI is more suitable for determining phenological events in situations with a high chlorophyll content such as mixed evergreen vegetation in the subtropical zone. The MTCI resulted in smoother and more conspicuous phenological profiles which made it easier to identify the OG and ES dates than the NDVI. In contrast, the NDVI is more sensitive to green biomass and will respond to the aggregated changes through seasons. The reason for this phenomenon could be attributed to saturation: when the vegetation cover has a high saturation in a large biomass ecosystem or during peaks of the growing season, the use of NDVI as a tool for phenological monitoring will be limited (Zarco-Tejada et al. 2001). On the contrary, the MTCI is based on the relationship between chlorophyll content and red-edge position, which has a large correlation with biomass (Dash et al. 2009a; Mutanga and Skidmore 2004). In addition, the NDVI had more fluctuations occurring during the growing season,

while the MTCI did not. Dash et al. (2010b) mentioned the same problem that some studies adopted NDVI suffered from unexplained variation in a smooth curve, it could because of image misalignment, sensor miscalibration, and a changing atmosphere including changing coverage of cloud, water, snow or shadow.

Because of poor data quality of the MERIS 300 m data, and to select the comparative quantity of pixels for comparison, the Maximum Value Composite (MVC) technique was employed to reduce the amount of missing data. However, replacing missing data with neighbouring ones might change the phenology patterns and timing of the onset and senescence of growing season. Therefore, it added potential sources of the uncertainty.

In summary, the MTCI captured the key phenological events in a similar fashion to the much more commonly used NDVI. If remote sensing data at finer spatial and temporal resolutions were available in the future, with other methods employed to derive the phenological event date, this would be advantageous. Additionally, since local climates will affect phenological events such as drought, cold and hot (Hwang et al. 2011), it is imperative to correlate phenological metrics extracted from remote sensing data with related time-series weather data, for studying the impacts of climate change.

3.7 Conclusion

Phenological metrics such as OG and ES are important for understanding the response of the vegetation system to climatic change (Tamstorf et al. 2007). Numerous studies have been undertaken to measure phenological metrics extracted from remote sensing data. However, few studies focused on the MTCI. In this chapter, a comparative analysis of phenological metrics extracted from MERIS NDVI and MTCI was undertaken for four vegetation types locating at different regions over mainland China for the year 2010.

Generally, MTCI captured an earlier OG than NDVI in western China and Inner Mongolia, dominated by grassland. In central China where there was mainly broadleaf deciduous forest, MTCI represented a later OG than NDVI. In southern China, dominated by broadleaf and needle leaf mixed evergreen vegetation, MTCI

captured less detail than NDVI but NDVI had more variation than MTCI. For the major agricultural area located in mid-east China, NDVI reflected more detail than MTCI. However, this ability cannot always be on the same level when applying the MTCI to different vegetation types at different locations. In conclusion, the MTCI is more suitable for mixed vegetation species land cover types while the NDVI is more efficient for dealing with low saturation biomass. Nonetheless the differences between MTCI-derived phenological profiles and those from the NDVI, introduced uncertainties as large as the climatic perturbations induced. At last, because lacking ground reference data for validating the accuracy of the MTCI and NDVI in extracting key phenological metrics, this chapter only compared the results of both indices and showed the differences and strong points for each index.

The use of remote sensing data in phenological studies is increasingly recognised. Time-series remote sensing data provide a mechanism to move from plant-specific to regional scale studies of phenology. However, it is still necessary to apply readily available MTCI data along with understanding the physical processes and computational approaches which determine the index values and how they vary from those obtained from other vegetation indices.

4.Land Surface Phenology over Mainland China

4.1 Background

Vegetation phenological metrics are significant indicators for biological life stages, driven by environmental factors, and are considered to be sensitive and accurate parameters for indicating climate change (Piao et al. 2006a). Recently, there has been an increasing interest in phenology, primarily due to changes in the timing of different phenological phases in plants and animals, connected to climate change (Richardson et al. 2013a; Ruml and Vulić 2005). Phenological variation can affect terrestrial ecosystems and human societies. For instance, changes in phenology may alter global carbon, water, and nitrogen cycles; affect crop production by unexpected frost damage; and also change the duration of pollination seasons as well as seasonal disease distribution (Piao et al. 2006a). Moreover, phenology can contribute to various scientific disciplines from biodiversity, agriculture, and forestry to human health. For example, phenology studies provide significantly valuable data for land-use planning, crop zonation, agricultural, forestry and domestic pest species control, conservational species protection and pollen release information, and their relations to human health (Ruml and Vulić 2005).

Most previous studies on vegetation phenology in China adopted conventional ground observation, within conservation or forestry regions for specific species, to study the phenological variation caused by climate changes. However, such approaches are limited by the number of *in situ* observation sites and, therefore, it is very hard to obtain information vegetation response to climate change at the biome scale. Moreover, in China, phenological stations and conventional phenological data are comparatively scarce (Chen and Pan 2002). Satellite remote sensing provides a powerful technique with which to observation vegetation phenology changes at a large scale in a long-term period, particularly by vegetation index satellite sensor imagery (White et al. 2005; White et al. 1997; Zhang et al. 2003).

During the last three decades, remote sensing satellite sensors data have been used at both regional and global geographic scales for monitoring the activity of vegetation. In particular, the Normalised Difference Vegetation Index (NDVI) has been widely used to measure phenological variation and thereby, analyse the

response from ecosystems to climate changes. However, because China has a vast territory and diverse terrestrial vegetation and climate conditions, most remote sensing studies in China on phenology were focused on natural vegetation types such as woodland, broadleaf forest, coniferous forest, shrublands, and grassland and mostly at a regional scale (Cai et al. 2012; Chen et al. 2000; Ding et al. 2013; Le et al. 2014; Meng et al. 2009; Pan et al. 2012; Pan et al. 2014; Piao et al. 2006a; Wu et al. 2010; Xin et al. 2002; You et al. 2013).

In the last few years, many studies focused on China adopted NDVI datasets derived from National Oceanic and Atmospheric Administration (NOAA)/advanced very high-resolution radiometer (AVHRR), TERRA/moderate resolution imaging spectrometer (MODIS), and SPOT/VEGETATION, to quantify annual vegetation phenological variation and its changing trend across China (Pan et al. 2012; Piao et al. 2006a; Wei et al. 2012; Wu et al. 2010; Wu et al. 2008; You et al. 2013). In this chapter, the Medium Resolution Imaging Spectrometer (MERIS) Terrestrial Chlorophyll Index (MTCI) was adopted rather than the NDVI to assess its potential for observing the inter-annual variation of vegetation phenology over China mainland. MTCI is directly related to canopy chlorophyll content, which is a function of chlorophyll concentration and leaf area index (LAI) (Dash and Curran 2004). ESA's Sentinel-3 mission aims to provide data continuity from Envisat's launch in 2002. The Sentinel-3 payload includes the Ocean and Land Colour Instrument (OLCI), and the level 2 land product OLCI Terrestrial Chlorophyll Index (OTCI) is based on the MTCI.

4.2 Study area

In this chapter, mainland China was investigated. China occupies a vast territory with a diverse climate, varied topography and great variety of flora. Mainland China extends over 5,000 kilometers from west to east (73°E to 135°E); it spans from a distance of 5,450 kilometres from north to south (53°N to 4°N). The varied climates span across frigid, temperate, subtropical, and tropical zones from north to south, and the distribution of climate regions determine China's vegetation patterns. Within China's territory, about one-third of the landmass is mountainous, with plateaus and high mountains dominating the west, while lower lands and plains lace

the eastern region.

4.3 Data

Three data sources were used: (i) 8-day and 10-day temporal composite of MTCI with 4.6 km spatial resolution (ii) ESA's 2009 global land cover map and (iii) ground observation data, collected from previous published research used for validation.

4.3.1 MTCI Data

MTCI data for 2002 – 2012 with a spatial resolution of 4.6 km and temporal resolutions of 8-day (2002 – 2007) and 10-day (2008 – 2012) were obtained from the NERC Earth Observation Data Centre (NEODC), to make time-series MTCI datasets of 18 months from 2003 to 2011 to detect all possible growing seasons. For 2002 and 2012, three months data each year were employed.

4.3.2 ESA's land cover map

ESA's 2009 global land cover map was used (Figure **12**). The map was produced using 12 months of data from Envisat's Medium Resolution Imaging Spectrometer at a spatial resolution of 300m. The map projection is WGS1984 and the classification uses the UN Food and Agriculture Organisation's (FAO) Land Cover Classification System (LCCS). ESA's 2009 global land cover map was used to locate major vegetation types within China for investigation in the later analysis.

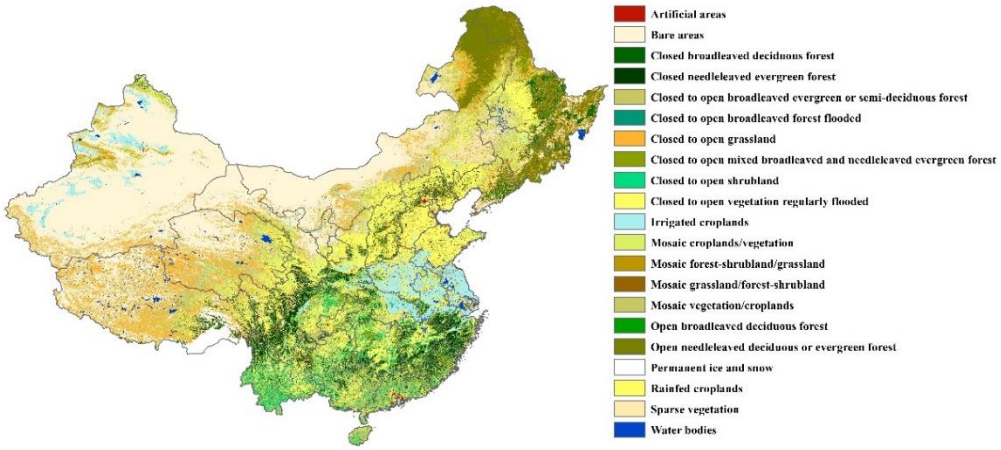

Figure 12 Land cover map of mainland China derived from ESA's 2009 Global Land Cover map (http://esamultimedia.esa.int/images/EarthObservation/globcover).

4.3.3 Ground observation data

Because of a lack of freely available first-hand ground observation data from the Chinese Phenological Observation Network (CPON), an inter-comparison of satellite derived phenological variables was undertaken based on data reported from previous studies (Chang et al. 2012; Chen et al. 2005b; Chen et al. 2000; Liu et al. 2011; Luo et al. 2007; Xiao et al. 2013; Zheng et al. 2006), the information of the ground data are in table **4**.

4.3.4 Gridded phenology dataset of *Fraxinus Chinensis*

The gridded dataset of spring phenology of *Fraxinus Chinensis* in China from 2003 to 2007 (Figure **13**) was used for validation with the onset of greenness extracted from MTCI data for the broadleaved forest, and the gridded data had a spatial resolution of 1°×1°. The dataset was acquired from the Institute of Geographic Science and Natural Resources Research, Chinese Academy of Sciences. It was established by adopting UniChill phenology model (Chuine 2000), with phenology records from the Chinese Phenological Observation Network at 12 stations located in eastern China (23°-45°N) and climatic data from the China Meteorological Data Service Centre (CMDC) at corresponding stations as input data. The dataset was validated with ground observation records. The results showed the $r^2 = 0.873$ ($p < 0.0001$), and RMSE was 6.1 days.

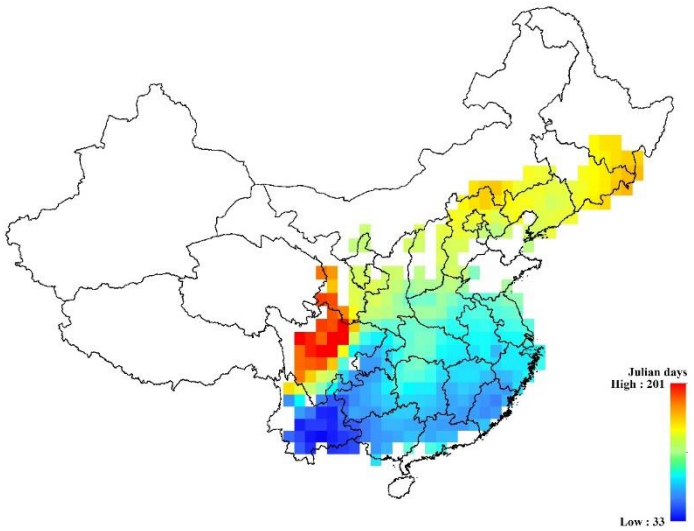

Figure 13 Distribution and average date for spring phenology of *Fraxinus Chinensis* in China from 2003 to 2007, with a gridded resolution of 1°×1°.

4.4 Method

To determine and extract the phenological variables of vegetation throughout China for nine years, three steps presented in the flowchart in Figure **14** were needed: at first, the raw MTCI data was pre-processed to acquire high-quality 18-month MTCI time-series for all pixels from 2003 to 2011; after that, phenological variables including Onset of greenness (OG), end of senescence (ES), and length of growing season (LGS) were extracted for each year. At last, the gridded phenology data and ground observation data collected from literatures were used to compare with extracted variables for an inter-comparison.

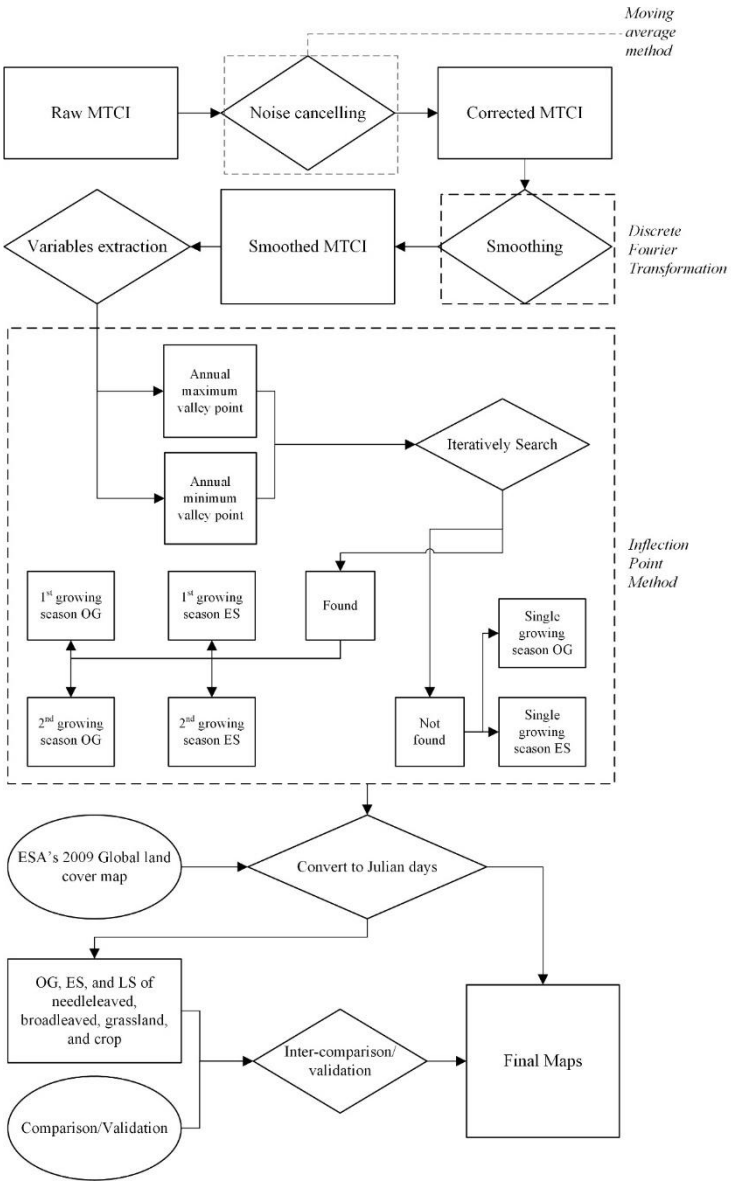

Figure 14 Flowchart showing data processing, phenology extraction, and validation processes.

4.4.1 Data pre-processing

The noise in the annual time-series is mainly due to cloud cover, atmospheric effects, and snow cover (Zhang et al. 2012b). A moving average function was applied to remove the missing data or erroneous values (MTCI=0) (valid MTCI values are from 1 to 6), by replacing incorrect data points with the mean of the neighbouring data points. To further reduce noise, the discrete Fourier transform (DFT) was used to smooth the time-series data. In this research, six harmonics are utilised to generate a smoothed time-series, as shown in Figure **15**.

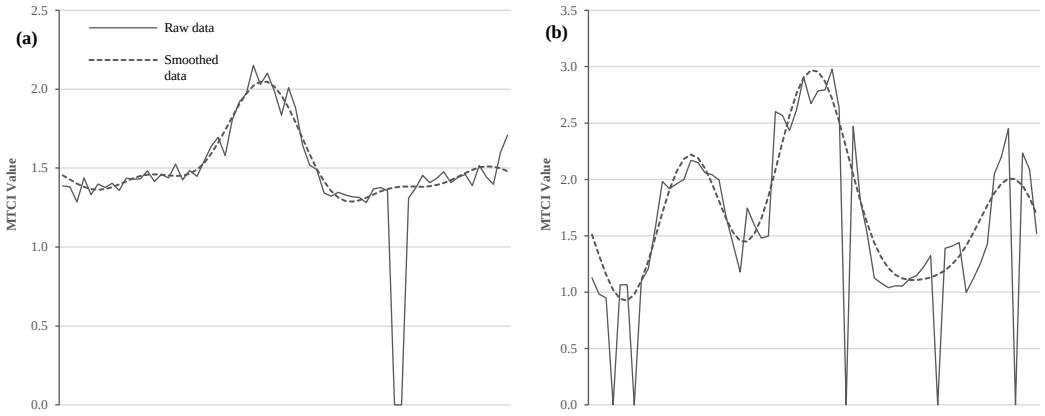

Figure 15 18-month time-series MTCI raw and smoothed data: (a) single growing season; (b) double growing seasons.

4.4.2 Phenological variables extraction

The inflection point method was adopted to extract phenological variables. The inflection point method for extracting phenological variables starts from the dominant peaks and checks the derivative both forwards and backwards at the same time. When the derivative changes from positive to negative or from negative to positive, a valley point might be assigned as OG or ES. However, because of local climatic variation or multi growth seasons, the valley point may not be located at the ideal theoretical place but somewhere has a larger value. To deal with this, a threshold of one-fifth of the maximum vegetation time-series signal value was applied for the valley point to be accepted as a phenological variable, until a definite valley point is detected (Dash et al. 2010b).

After the phenological variables were extracted, the mean values for OG, ES, and LGS were calculated for each pixel for the nine years (2003 – 2011), and phenology

maps of mainland China were produced as 9 year averages to present the general pattern of phenology over mainland China in the last decade.

To study the phenological variation within and across major vegetation types, the ESA's 2009 land cover map of the China sub-continent was resampled from the original 300 m to 4.6 km spatial resolution, by using the majority method, to match the MTCI data. After that, major vegetation types in mainland China were masked out: needle-leaved, broadleaved, shrub/grassland, and crop regions (Figure **16**).

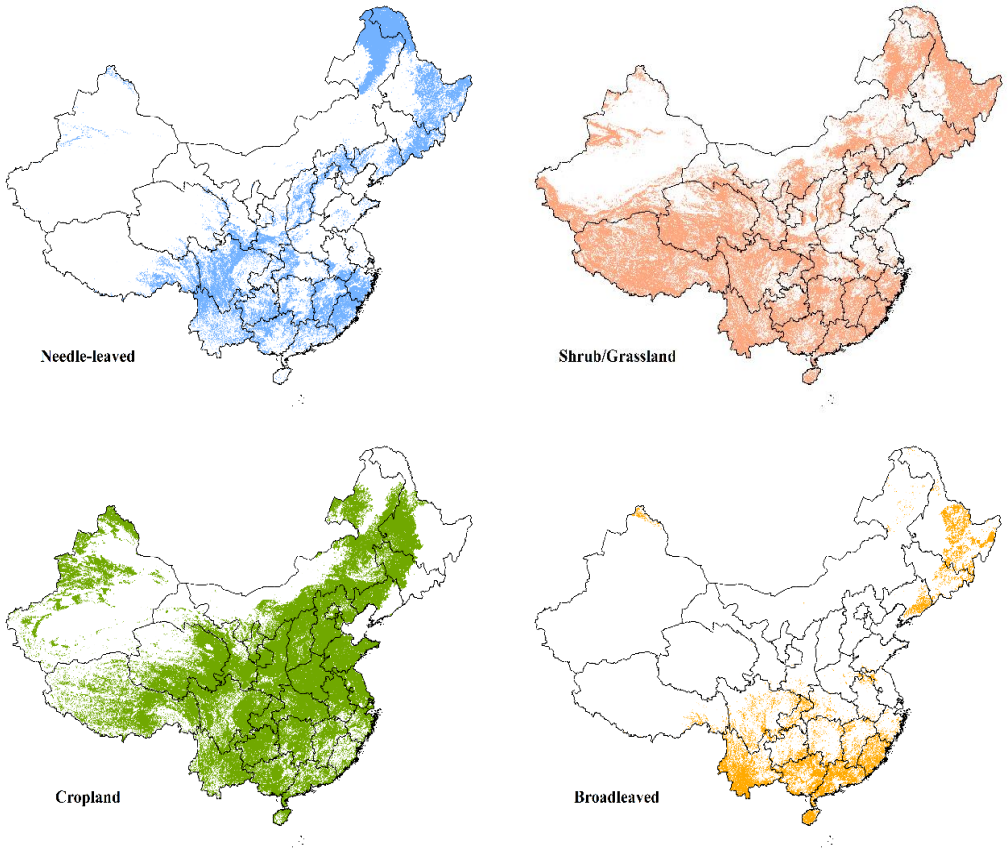

Figure 16 Major vegetation types masked out from land cover map: Needle leaf (including close/open needle leaf evergreen/deciduous forest), shrub/grassland (including close to open shrub and grassland), cropland (including irrigated and rain-fed cultivated and managed cropland), and broadleaf (including close/open broadleaf evergreen, deciduous/semi-deciduous forests).

4.4.3 Statistical analysis

Statistical analyses were done including: (1) average timing of OG, ES, and LGS were calculated to show the general distribution of vegetation phenology in mainland China. (2) Standard deviation of OG and ES were calculated for two

growing seasons, to show the variations of phenological variables during 2003 to 2011. (3) Average timing of OG and ES (the first growing season) of four major land cover types (needle-leaved forest, broadleaved forest, crop, and shrub/grass) were calculated to examine the effect of the latitude. (4) Inter-annual changes of phenological variables within mainland China were investigated, to represent the changes of the major vegetation types at country scale.

4.4.4 Comparison and validation

An inter-comparison was performed with ground observation data reported from previous studies in China (Chang et al. 2012; Chen et al. 2005b; Chen et al. 2000; Liu et al. 2011; Luo et al. 2007; Xiao et al. 2013; Zheng et al. 2006). A table was created to show the similarities and differences between ground observation dates from other works and the onset of greenness and end of senescence dates retrieved from single pixels of the MTCI data. As the spatial resolution of the MTCI is relatively coarse (4.6 km), therefore, the nearest pixels or the pixels cover the observation stations were selected on investigation. In addition, stations had been checked to make sure not locating in urban areas.

The gridded dataset of spring phenology of *Fraxinus Chinensis* in China from 2003 to 2007 was used for validation with the OG extracted from MTCI data for the broadleaved forest. Statistical analysis was done to evaluate the consistency and accuracy.

4.5 Results

4.5.1 Spatial distribution patterns of OG and ES over mainland China from 2003 to 2011.

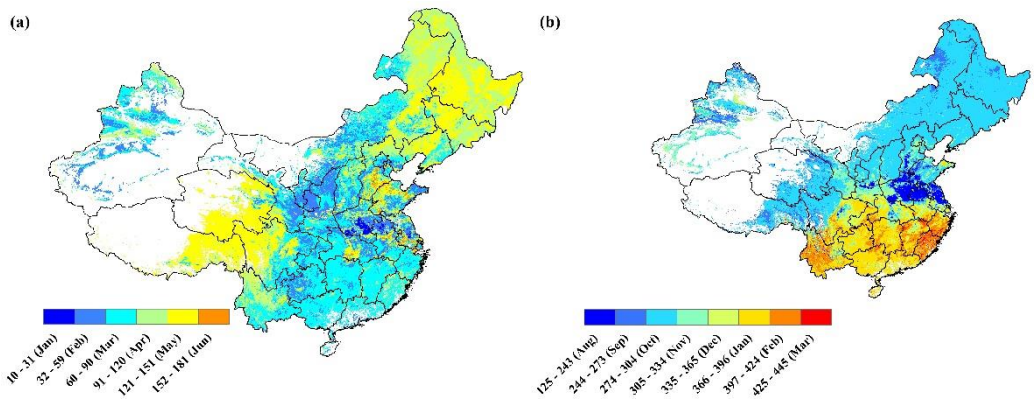

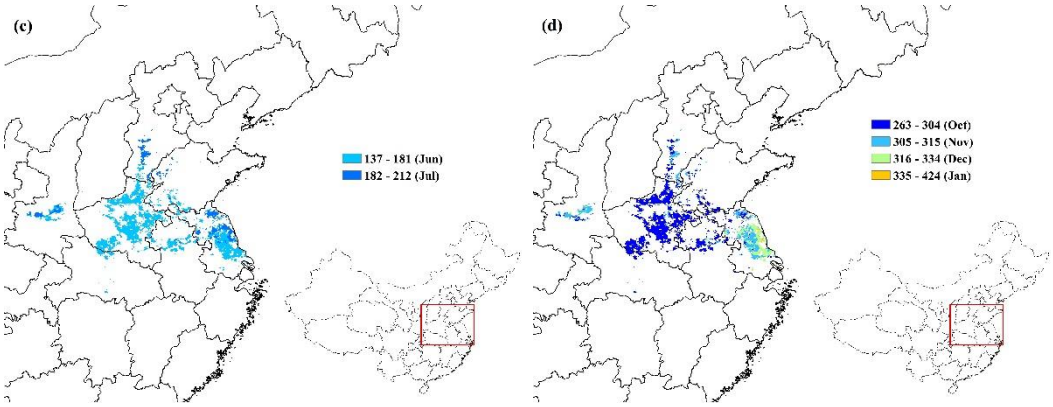

Figure 17 The distribution map for mainland China's average timing of OG and ES from 2003 to 2011: (a) mean OG of the 1st growing season; (b) mean ES of the 1st growing season; (c) mean OG of the 2nd growing season; (d) mean ES of 2nd growing season. The colour legend is the number of Julian days.

The spatial distribution of the 9-year averages of three key phenological variables (OG, ES, and LGS) of two growing seasons over mainland China are represented in Figures **17** and **18**. Some tropical regions in Southern China, for example, Hainan Province, have a triple cropping scheme. However, due to the coarse resolution and a relatively small area. Therefore, only a few values could be retrieved which were not necessarily representative and hence the triple cropping regions were not considered in this chapter.

For the first growing season it can be seen from Figure **17a** that the mean date of OG varied significantly over mainland China, and generally, the OG in northeast (April to May) and middle-west (May) China was later than most of the other parts of mainland China, which were dominated by rain fed crops. In mid-east China some parts also had a later OG (May to June), which is also an agricultural area. In southern China, there was less cropping area because most regions are mountainous and hilly, with a sub-tropical climate. Therefore, the OG was earlier than cropping regions (March to April). It also can be noticed that regions had the earliest OG (January to February) mostly scattered from central to east China and in Chongqing and Guizhou Province, most of which were grasslands and shrubs in the central region, and winter crops in the east.

Figure **17b** shows the pattern of the ES of the first growing season, it can be seen clearly that northern China experiences an earlier senescence than southern China while southeast China had the earliest ES where there is a major double cropping

region (Shanghai, Jiangsu, Anhui, Zhejiang, Hunan and Hubei Provinces). However, comparing with the OG in southern China, the corresponding ES was towards the end of the year or the beginning of next year (from December to March next year). This indicates that southern China has no clear phenological pattern or the phenological variables are hard to detect. This might be because the land cover in southern China is dominated by deciduous broadleaved forest. However, due to the mountainous landscape, needle-leaved forest exists at high altitude and especially is widely distributed on the plateau (Yunnan and Guizhou Provinces). In addition, the needle-leaved forest is also widely distributed in east coastal Provinces with low altitude, where there is more plantation.

The second growing season was mainly detected in mid-east China (Figures **17c** and **17d**), dominated by double cropping paddy rice agricultural regions in Henan, Hebei, Shandong, Jiangsu, and Anhui Provinces. It can be inferred that the second growing season was about five to six months long (from October to February next year). Within these regions, the start of greenness for the second crop was detected very late in the year (from June to July). It was also observed that most of these regions have an OG date in June, except most parts in Hebei Province, some parts in Shandong Province and northern Jiangsu Province which have a later OG date in June. Finally, for most of the area that had an early OG, the ES was also detected earlier (October), except for southern Jiangsu Province where the OG was early (June) but had a late ES (December to January next year). Moreover, in northern Jiangsu Province, the OG was in July but the ES varied from December to next February. This might because of the different crop types grown in these areas.

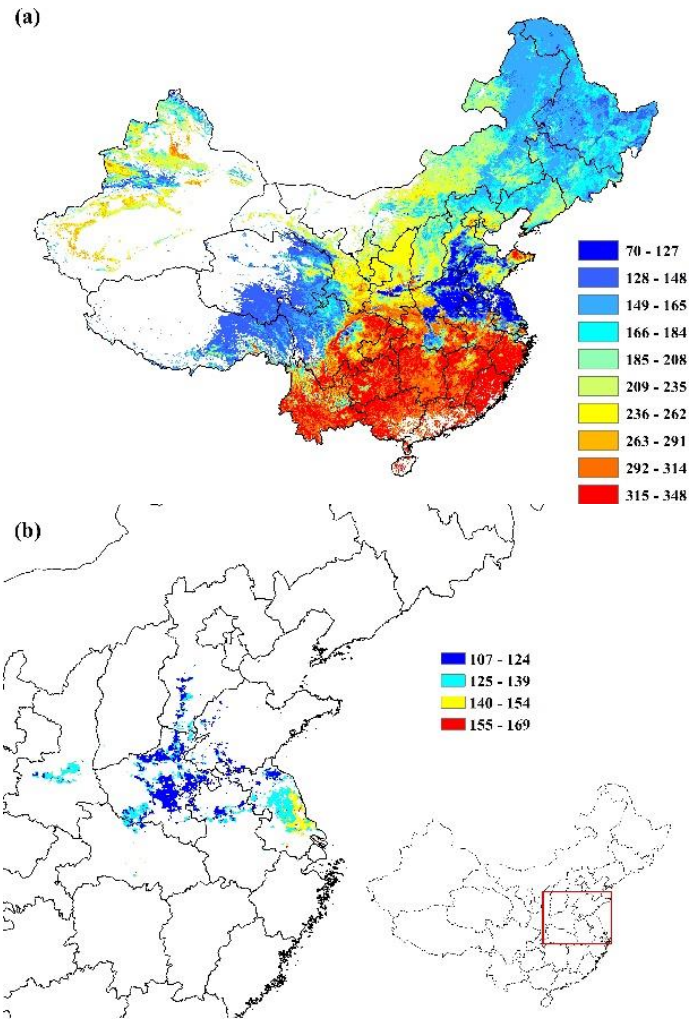

Figure 18 The distribution map of average LGS for mainland China from 2003 to 2011: (a) mean length of the 1st growing season; (b) mean length of 2nd growing season (double cropping area). The colour legend is the number of Julian days.

Figure **18** suggests the broad patterns of the mean length of the first and second growing seasons. Figure **18a** shows that the vegetation in the mid-east double cropping agricultural region had the shortest 1st LGS, while northeast and southwest China had a moderate LGS. Southern China had the longest LGS almost lasting the whole year, indicating low variations of vegetation phenology in southern China, because the evergreen vegetation did not have obvious seasonality in humid tropics and subtropics (Cong et al. 2013; Piao et al. 2006a). Figure **18b** showed double cropping agricultural areas had a growing length of about four to four and half months (107 to 138 days), except in Jiangsu Province where it lasts up to five and half months. This might be the result of different crops being grown in Jiangsu Province.

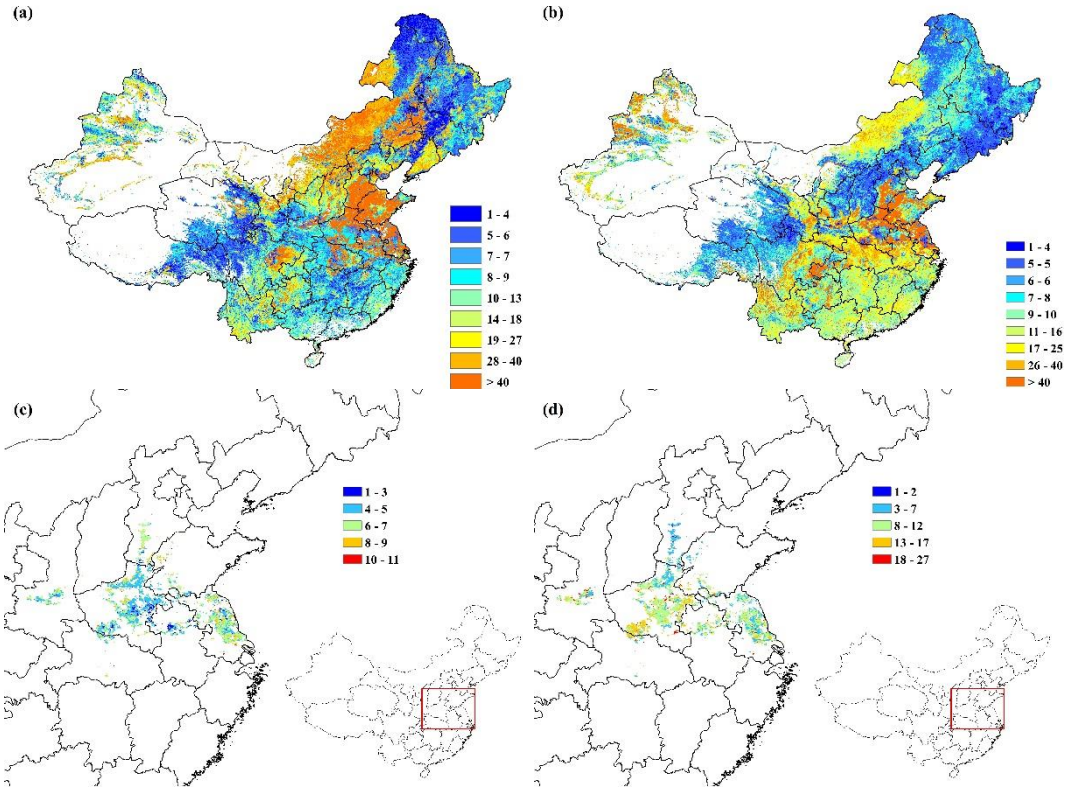

Figure 19 The variation (standard variation) for mainland China from 2003 to 2011: (a) variation of OG of 1st growing season; (b) variation of ES of 1st growing season; (c) variation of OG of 2nd growing season (double cropping area); (d) variation of ES of 2nd growing season (double cropping area). The colour legend is the number of Julian days.

Figure **19** sets out the mean variation in OG and ES over mainland China from 2003 to 2011. Figure **19a** shows the mean variation in OG is limited in southern, southwest and northeast China of the first growing season. In northeast China, the standard deviation of OG was less than 8 days for most of the area, although there were some locations with a standard deviation of about 16-30 days, mainly dominated by broadleaved deciduous forest. The reason for this can be attributed to the different OG dates among diverse agricultural areas and broadleaved forests. In southern China, where there is a lack of clear seasonality, small variations were found as expected (8 to 15 days). A large standard deviation, more than 40 days, was found in Inner Mongolia, where the major land cover classes were shrub and grass. Except for the major agricultural region in mid-east China with a high standard deviation more than 40 days, there was also another notable area with a standard deviation more than 40 days in Sichuan Province, southwest China. For these agricultural areas mixed vegetation types and a changing farming plan might be the cause of high variation. Compared to the OG, Figure **19b** showed that the

notably large deviation of more than 40 days of the first growing season in the main agricultural region in mid-east China and Sichuan Province. Mixed vegetation in southern China and grassland in west Inner Mongolia had standard deviations of about 11-30 days. From northeast China to southwest plateau, a low standard deviation of 4-6 days was found.

Figures **19c** and **19d** represents the variation of the second growing season in the major double cropping region. The standard deviation was less than 8 days for the OG, and less than 15 days for the ES. The reason for the smaller deviation for the second growing season in the agricultural region maybe because limited types of crops were planted compared to the first growing season.

4.5.2 Spatial and annual variation of OG and ES in mainland China from 2003 to 2011.

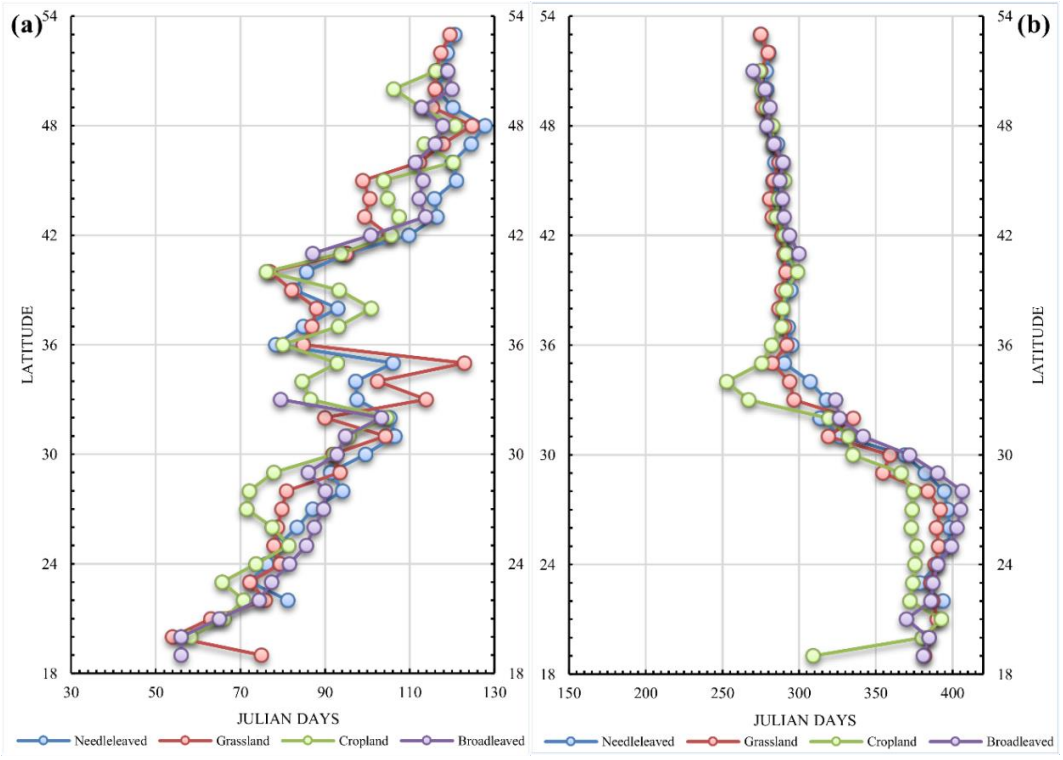

Figure 20 Changes in the average timing of onset of greenness (OG) (a) and end of senescence (ES) (b) of four major land cover types of the first growing seasons during 2003-2011 along the latitude of mainland China.

Four vegetation types (needle-leaved forest, shrub/grassland, cropland, and broad-leaved) were selected as major vegetation types to be investigated to quantify the effect of latitude in this chapter. As the double cropping region covers a relatively

small area, the second growing season in mid-east China was not examined.

The dependence of the four major vegetation types on latitude across mainland China are shown for both OG and ES are in Figure **20**. It can be seen that from south to north, the OG gradually delayed and the ES gradually advanced, which reflects the latitudinal differences of climate. Broadly, the ES for the four major vegetation types was more like each other than for the OG.

It is notable that around the middle latitude (32°N to 34°N) there were obvious drifts for the OG and ES of grassland/shrub as well as slight changes of other vegetation types. This might be because this latitude zone stretched across four different climatic zones (sub-tropical zone, warm temperate zone, Qinghai-Tibet Plateau vertical temperature zone, and mid-temperature zone). In addition, within this latitude zone, landscapes varied from east to west, including plain, basin, plateau, and meadow, leading to local climate differences. Moreover, comparatively single-species for some pixels and misclassification in the land cover map may result in these significant fluctuations.

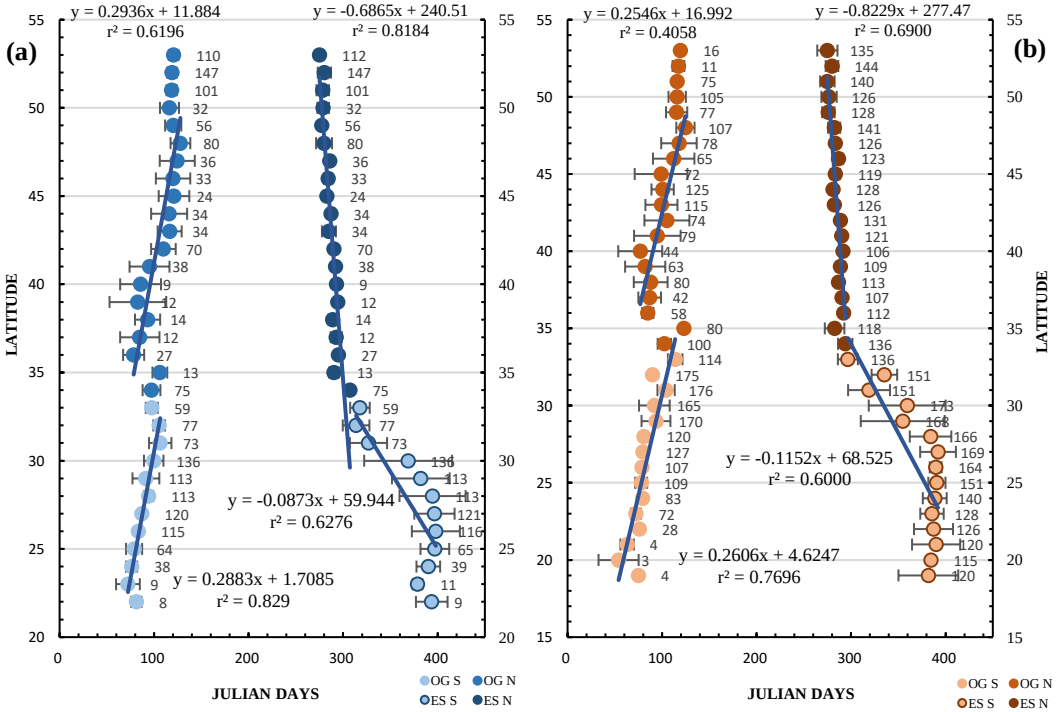

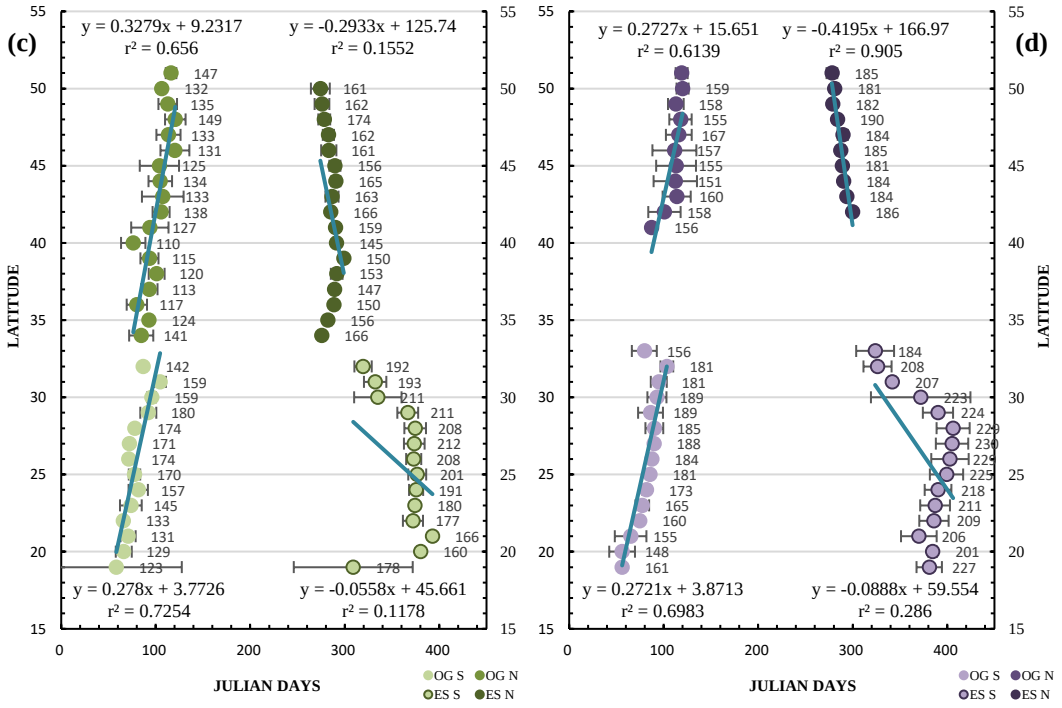

Figure 21 Changes in the average timing onset of greenness (OG) and end of senescence (ES) of the 1st growing season for (a) needle-leaved forest, (b) shrub/grassland, (c) cropland, and (d) broadleaved forest, along with the latitude during the year 2003 to 2011.

In Figure **21**, the distribution of the average timing of OG and ES for the first growing season of each major vegetation type is plotted. For the OG of major vegetation types, it is generally more latitudinally correlated in south China than in north China, while it is the reverse for the ES. In north China, crops (Figure **21c**) had a large positive correlation with latitude (r^2=0.7254), this can be attributed to limited crop types and unified management at large scales than in the south. Needle-leaved forest (Figure **21a**) and broadleaved forest (Figure **21d**) had smaller positive correlations with latitude (r^2=0.6196 for needle-leaved forest and r^2=0.6139 for broadleaved forest), while shrub/grassland (Figure **21b**) had the smallest positive correlation with latitude (r^2=0.4058). In south China, needle-leaved forest had the largest positive correlation with latitude (r^2=0.8293), shrub/grassland and crops had a smaller correlation (r^2=0.7696 for shrub/grassland and r^2=0.7254 for crops), and broadleaved forest had the smallest correlation (r^2=0.6983). This indicates that the OG delayed at higher latitudes. However, the magnitude of this delay was highly linked with vegetation types and their distribution as well as the local climate.

Comparing with the OG, the ES was more related with latitude in north China while less pronounced in the south. This could be because of various mixed vegetation

types in south China, and the ES itself was a much more complex phenomenon than the OG, which is highly relevant to plant species and light conditions. However, for needle-leaved forest (r^2=0.8184 at north and r^2=0.6276 at south) and shrub/grassland (r^2=0.6906 at north and r^2=0.6000 at south), the ES were more related with latitude than for crops (r^2=0.1552 at north and r^2=0.2746 at south) and broad-leaved forest (r^2=0.6591 at north and r^2=0.1178 at north). This might be because croplands are much more manufactured and broadleaved forest had an uneven distribution in south China.

4.5.3 Inter-annual changes of phenological variables within mainland China.

Figure **22** exhibits the inter-annual phenological change characteristics at the country scale, for the five major land cover types. Overall, the timing of OG for all the land cover types in mainland China advanced and the timing of the ES delayed from 2003 to 2011. The largest advance of the OG occurred in the broadleaved forest (2.2 days year^{-1}), and the longest delay of the ES occurred in the mixed evergreen forest (4.3 days year^{-1}). The smallest advance of the OG occurred in the needle-leaved forest (1.0 day year^{-1}), and the shortest delay of the ES occurred in the broad-leaved deciduous forest (1.3 days year^{-1}). The mean OG over mainland China from 2003 to 2011 of broadleaf deciduous forest (r^2=0.44), crops (r^2=0.47 and 0.47), needle leaf deciduous forest (r^2=0.34), and grassland (r^2=0.45) had significant advances over 9 years. With an annual advance of 2.2 days yr^{-1}, delay of 1.3 days yr^{-1} for broadleaf deciduous forest. 1.8 days yr^{-1} advance and 2.0 days yr^{-1} delay for crops in the first growing season and 1.61 days yr^{-1} advance and 2.5 days yr^{-1} delay in the second growing season. 1.0-day yr^{-1} advance and 2.1 days yr^{-1} delay for needle leaf deciduous forest. Moreover, 1.5 days yr^{-1} advance and 1.1 days yr^{-1} delay for grassland. The mixed evergreen and needle leaf deciduous forest did not show a clear trend. The variation in crop phenology was influenced by many factors including climate, farming schemes, fertilisers, agricultural management, and so on (Meng et al. 2009; Wu et al. 2008; Xin et al. 2002). Therefore, the OG and ES, especially the second growing season, could be influenced significantly.

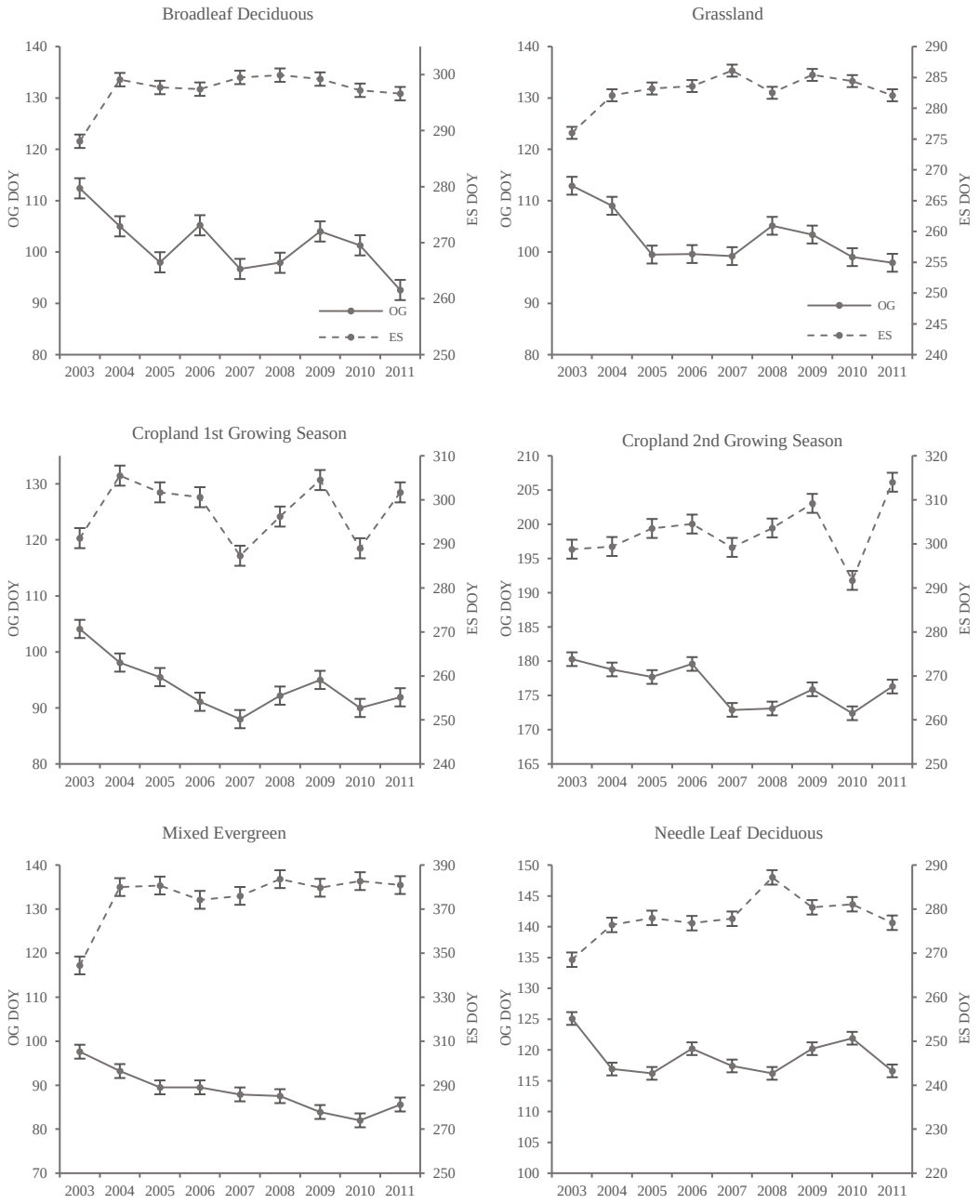

Figure 22 Changes in the average day of different land cover types in mainland China, during 2003 to 2011. Error bars show the standard error.

4.5.4 Inter-comparison with the literature

An inter-comparison between ground observation dates from other phenology studies about China and satellite-retrieved phenological variables from above analysis is provided in Table **4**.

Chen et al. (2000) analysed statistically 50-70 types of species in deciduous broad-leaved and coniferous mixed forests at Mudanjiang, deciduous broad-leaved forests

at Beijing, and Luoyang station during 1983 to 1990. Deciduous forests at Beijing and Luoyang station had a slight difference between ground observation onset of greenness and satellite-retrieved dates. The satellite retrieved ES date was 44 days late at Beijing station. At Mudanjiang station, the satellite retrieved OG date was 25 days later than the ground observation date. This can be attributed to the mixed species forests at this station, where dominant species were not clarified.

Chen et al. (2005b) observed the dominant vegetation types at seven stations located from 32°N to the northern border (53°31'N) including conifer forest in the cold temperate zone, deciduous broad-leaved and coniferous mixed forest and steppe in the middle temperate zone, deciduous broadleaved forest in the warm temperate zone, and various inter-zonal crops from 1982 to 1993. However, Xi'an station was excluded, as it was in an urban area. For the OG at Gaixian, Beijing and Luoyang stations the remotely sensed data were earlier than ground observed data, while at Harbin and Xingtai stations were later. At Mudanjiang station, it had a similar day for both remotely sensed and ground observed OG. The satellite-retrieved dates of ES at these stations were all later than ground observed dates while Beijing station had the latest end of senescence date about two months later. Zheng et al. (2006) selected 16 stations from North to South China. Two species were observed at each station and different phenophases were examined over the period from 1980 to 1989. First bloom dates were compared with the MTCI retrieved dates. At Shengyang, Liaocheng and Luoyang station shared similar OG dates, while the values differed at most of the stations which were located at lower latitudes less than 34°N in South China. This might be because in South China vegetation types are usually mixed and a few species were selected which could not represent local dominant species.

Luo et al. (2007) analysed the phenological dataset from 1962 to 1992 for three woody plant species, including *Prunus davidiana* (Carr.) Franch, *Hibiscus syriacus* L., and *Cercis Chinensis* Bunge, which were all common ornamental plants in the Beijing Metropolis. All three species are broadleaved and winter deciduous. P. *davidiana* and C. *chinensis* are both small trees that blossom in spring with OG dates of day 67 and 88, whilst H. *syriacus* is an ornamental shrub that blossoms most of the summer had an OG date of day 102 that was later than the satellite retrieved OG date of day 67. However, all these three species had similar ES dates

(318 for P. *davidiana*, 312 for H. *syriacus,* and 312 for C. *chinensis*) with a satellite-retrieved date of day 358.

Liu et al. (2011) selected 40 woody plant species of 13 families' trees and shrubs as sample plants in the plot constituting 75% of total woody plant species, at Meihuashan National Nature Reserve, Fujian Province, southeast China, in 2006 throughout the entire growing season from early March to mid-June. Shrubs and trees had OG dates of day 37 and 47, while the satellite-retrieved date was day 55.

Reference	Location	Species	Sample Points/Sources	Study Period	OG from LR (DoY)	Derived OG (DoY)	ES from LR (DoY)	Derived ES (DoY)
Chen et al., 2000.	Mudanjiang (44°26'N, 129°40'E, 300m)	Deciduous broad-leaved and coniferous mixed forests	50-70 kinds of trees and shrub for each station	1983-1988	98	**123**	286	**287**
	Beijing (40°01'N, 116°20'E, 50m)	Deciduous broad-leaved forest			75	**67**	314	**358**
	Luoyang (34°40'N, 112°25'E, 155m)	Deciduous broad-leaved forest			61	**66**	320	**311**
Chen et al., 2005.	Harbin (45°45'N, 126°40'E, 146m)	Conifer forest in the cold temperate zone, deciduous broad-leaved and coniferous mixed forest, and steppe in the middle temperate zone, deciduous broad-leaved forest in the warm temperate zone, and various interzonal crops.	Phenological data acquired from Chinese Yearbooks of Animal and Plant	1982-1993	127	**177**	269	**299**
	Mudanjiang (44°26'N, 129°40'E, 300m)				124	**123**	268	**287**
	Gaixian (40°26'N, 122°20'E, 45m)				112	**64**	287	**327**
	Beijing (40°01'N, 116°20'E, 50m)				105	**67**	298	**358**
	Xingtai (37°04'N, 114°30'E, 77m)				103	**154**	292	**311**
	Luoyang (34°40'N, 112°25'E, 155m)				100	**66**	295	**311**
Zheng et al., 2006.	Shengyang (42°05'N, 123°00'E, 50m)	Salix babylonica L.	Phenophase records of two species at each station	1980-1989	104	**133**	/	
	Liaocheng (36°28'N, 115°58'E, 31-32m)	Salix matsudana Koidz.			84	**85**	/	
	Luoyang (34°40'N, 112°25'E, 155m)	Salix babylonica L.			75	**66**	/	
	Yangzhou (32°25'N, 119°25'E, 8m)	Salix babylonica L.			82	**39**	/	
	Yinxian (29°52'N, 121°30'E, 5m)	Salix babylonica L.			73	**54**	/	
	Changde (28°40'N, 110°20'E, 43.9m)	Melia azedarach L.			100	**79**	/	
	Guiyang (26°25'N, 106°40'E, 1095m)	Firmiana simplex W.F.Wight			98	**47**	/	
	Guilin (25°11'N, 110°12'E, 155m)	Melia azedarach L.			90	**65**	/	
	Ganzhou (25°52'N, 115°00'E, 110m)	Melia azedarach L.			73	**60**	/	
Luo, 2007.	Beijing (40°01'N, 116°20'E, 50m)	Prums davidiana	a permanently marked group of more than 10	1962-1992	67	**67**	318	**358**
		Hibiscus syriacus			102		312	
		Cercis chinensis	…...more than 20		88		312	
Liu et al., 2011	Meihuashan National Nature Reserve (25°25´N, 116°50´E, 1200m)	40 woody plant species	For each species at least 8 individuals were located and five random branches with tips on the outer edge of the plant crown were selected	March to June, 2006	47	**55**	/	
Chang et al., 2012	Minqin Desert Botanical Garden (102°59'E, 38°34'N, 1378m)	22 species	3-5 individuals observed for each species	1974-2009	85	**70**	300	**304**
Xiao, 2013	North China Plain (Hebei, Henan, Shandong, and Shanxi Provinces.)	winter wheat	Phenological data acquired from Chinese Meteorological Administration (CMA)	1981-2009	54	**50**	/	

Table 4 An inter-comparison between ground observation dates and satellite-retrieved phenological variables in this study.

Chang et al. (2012) carried out phenological observations in the Minqin Desert Botanical Garden for 22 species (8 trees or small trees, 10 shrubs and semi-shrubs, and 4 herbs) from 1974 to 2009 with complete observation data. All observed vegetation had been divided into two groups, xerophytes, and mesophytes. The mean OG date of mesophytes was day 85 and day 97 for xerophytes, while the remotely sensed data for this location was day 70; the mean ES date of mesophytes was day 300 and day 303 for xerophytes, while the remotely sensed date was day 304.

Xiao et al. (2013) observed winter wheat in the NCP (North China Plain) including Hebei, Henan, Shandong, and Shanxi Provinces, and also Beijing and Tianjin Municipalities. Within the NCP, 36 stations were selected and investigated over the period 1981 to 2009. A vast region was observed, and therefore, 10 pixels of each Province were selected to calculate a mean onset of greenness date. This was day 50 while the observed date was day 54, which were very close to each other.

In summary, from Table **4**, it can be seen that the mixed vegetation type did not have a clear trend when comparing the last decade satellite-retrieved phenological dates with previous ground observation dates, in South China. Winter wheat, under human management, had a similar onset of greenness date since 1981 to 2011 in the North China Plain.

4.5.5 Validation with the gridded dataset of spring phenology *Fraxinus Chinensis* in China from 2003 to 2007.

By using the gridded data of *Fraxinus Chinensis* as a reference, which is a kind of broadleaf species, the relationship between extracted OG and reference data was plotted. Figure **23** shows that the OG for broadleaf deciduous extracted from MTCI from 2003 to 2007 correlated well with *Fraxinus Chinensis* gridded data (correlation coefficients r^2 of 0.7276, 0.7542, 0.8199, 0.7223, and 0.7493 for the year 2003, 2004, 2005, 2006, and 2007, respectively). The results demonstrate the whole phenology extraction process and methodology had the ability to monitor vegetation phenology at large scale with the MTCI dataset.

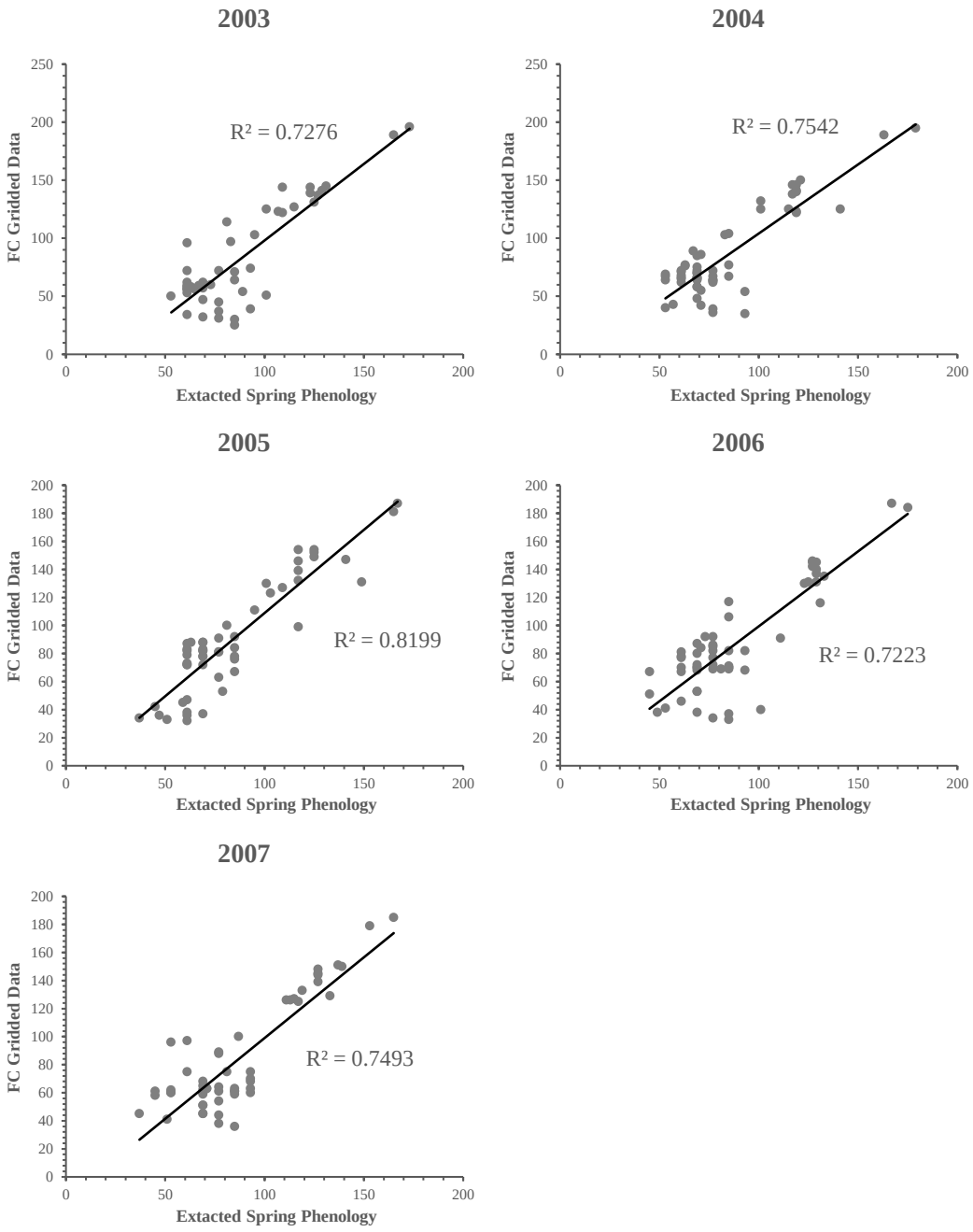

Figure 23 Validation between the *Fraxinus Chinensis* gridded data of spring phenology and the extracted spring phenology from MTCI dataset.

4.6 Discussion

Although many ground-based phenological observations were carried out across mainland China for different vegetation types or crops, ground observations are usually limited to single or a few species at the local scale, and sometimes can be discontinued due to weather or human factors. Remote sensing can measure the phenology from regional to global scales with even a daily repeat at different spatial

resolutions from metres to kilometres (Bradley et al. 1994). Therefore, in the last decade, remote sensing measurements for phenology have been used widely. A few studies have so far employed various remote sensing data to analyse plant phenology in China. Those studies mainly focused on the variation in major phenological variables over a short or long period and the response from vegetation to changing climatic conditions. However, due to China's complex climatic, geographical, and environmental conditions, most previous studies focused on single species (Ding et al. 2013; Le et al. 2014; Meng et al. 2009; Pan et al. 2012; Pan et al. 2014; Ren et al. 2008; Wu et al. 2010; Wu et al. 2008; Xin et al. 2002; You et al. 2013) and the regional scale (Cai et al. 2012; Chen et al. 2005b; Chen and Pan 2002; Dai et al. 2011; Lee et al. 2001; Li et al. 2011a; Piao et al. 2006a; Wang and Tao 2014; Xu and Liu 2007), by using NDVI.

This chapter provides an innovative attempt to use the time-series MTCI remote sensing data to present the phenological variation of vegetation during the last decade over whole mainland China. Mean and standard deviation maps of three key phenological variables (OG, ES, and LGS) over mainland China were produced. The results exhibited large standard deviation of OG in Inner Mongolia, dominated by grass, which was consistent with the findings from Cong et al. (2012), suggesting the grassland's OG is strongly connected with regional environment. However, the standard deviation of ES in the region was smaller. This can be attributed to regional climatic variation. Large standard deviation values of OG and ES of first growing season were also detected in the double-cropping agricultural region in mid-eastern China, which is affected by human management. In south China which is humid and temperate with mixed vegetation types, the standard deviation of both OG and ES were moderate. This might be because although vegetation types were complex in this area the temperature and precipitation were sustained and abundant. In northeast China and Qinghai-Tibet Plateau, the smallest standard deviation for both OG and ES were found. This can be a reason of relatively homogeneous vegetation covers in both areas.

The methodology presented in this study has some desirable properties. It processes each pixel individually for the time-series remotely sensed data, without any thresholds or empirical constants, therefore, it can be applied on a large scale.

Moreover, it can capture multiple growing seasons within a full growing cycle, which is common for crops and plants in tropical zones. The inflection points at the beginning and end of the growing period were assumed to be the timing of OG and ES by applied algorithm. However, it is common for time-series of remotely sensed data to have unexpected curves after smoothing, due to missing data, cloud, and other atmospheric contamination including dust, ozone or aerosols (Julien and Sobrino 2010). Therefore, the inflection point method may cause inaccuracy. It is also important to note that the spatial resolution of 4.6 km MTCI data were used. Therefore, sometimes satellite-retrieved phenological variables were less accurate in representing dominant vegetation types within each single pixel, comparing to ground observation results. In addition, climatic reasons were not considered in this chapter. As China has different climatic zones from south to north and increasing elevation from east to west, climatic conditions are complex. Further, altitude factors were not considered in this study. However, elevation was demonstrated to have distinct effects on vegetation. For example, the alpine grassland produced significant differentiation at different elevation and natural zones in the Qinghai-Tibetan Plateau, as reported by Ding et al. (2013). The ES shows a significant pattern with elevation changes in eastern China, as concluded by Han and Xie (2014).

The OG for most of the vegetation followed a latitudinal pattern with earlier OG at lower latitude (Figure **20** and **21**), while the ES has a later date at lower latitude. However, more fluctuations shown for the OG, especially around 35°N, whereas it shows more consistencies for the ES. It is also worth notifying the ES was earlier at higher latitudes and around 28°N to 30°N the ES starts showing more variants, where is close to the boundary between subtropical zone and warm temperate zone. The phenomenon indicates the plants phenology are controlled by complex zonal and regional factors. Wu et al. (2016) examined the vegetation phenology at north China and also found it showed high spatial heterogeneity for all land surface metrics, which were highly depended on the climate, the plant functional type and even soil characteristics.

Although China has a phenological observation network established in the early 1960s (Lu et al. 2006), the ground observation data were not obtained which could

be utilised to undertake validation with remote sensing results from this study. Therefore, the one-to-one relation could not be established which may demonstrate the accuracy of our satellite retrieved phenological variables. However, the overall results detected from the MTCI data set in this chapter broadly match with the ground observation results reported from previous studies, although there are still many differences especially for stations located in South China, where has vast mixed vegetation types. Generally, an advancing OG and a delaying ES was found.

4.7 Conclusion

Based on the MTCI 8-day and 10-day time-series data, with a spatial resolution of 4.6 km, key phenological variables were extracted from 2003 to 2011 by using the inflection point method. The discrete Fourier transform method was used to smooth the signal while keeping the main phenological patterns. Four major vegetation types were obtained from ESA's 2009 land cover map, to investigate spatial variation on phenology with latitude. The results showed the phenological metrics had strong regional characteristics irrespective of vegetation types. The OG was more related with latitude than the ES, and generally, in north China vegetation had weaker links with latitude than in south China for the OG. The opposite was the case for the ES. However, in the study, the situation could be more complex if the elevation was considered. Further, the timing of OG for all the vegetation types in mainland China advanced from 1.0 to 2.2 days $year^{-1}$ and the timing of the ES delayed from 1.3 to 4.3 days $year^{-1}$, during 2003 to 2011.

As the MTCI is more sensitive to chlorophyll with fewer effects from other disturbances, investigation on the relationship between phenology and climate will help us understand how vegetation response to climate changes, and thereby, more precise predictions of future phenology variations and global carbon cycle modelling are available (Piao et al. 2006a). Due to the lack of corresponding ground observation data, this work still has further potential for accurate validation.

5.Drivers of Phenology Variation in Mainland China

5.1 Background

It has been found that the vegetation-growing season has been extending in the northern high latitudes (Chuanfu et al. 2012; Menzel and Fabian 1999; Myneni et al. 1997; Yu et al. 2017; Zhang et al. 2012b). As a result of the noteworthy advancing start of the growing season, and to a less extent by the delay of vegetation senescence (Linderholm 2006). Shifts of vegetation phenology can profoundly affect terrestrial ecosystems and human societies, for example, by altering the global carbon, water, and nitrogen cycles, surface albedo and roughness, pollination season, crop production and disease distribution (Menzel 2002; Peng et al. 2013; Peñuelas and Filella 2001; Piao et al. 2006a; Richardson et al. 2013a; Walther et al. 2002). Therefore, it is crucial to understand the relationship between vegetation phenology and climate (e.g. temperature and precipitation drivers). Water is critical for vegetation growth. Therefore, the amount and timing of precipitation play a vital role in plant phenology changes. Temperature also is a significant factor in the vegetation green-up stage. The temperature difference between winter and spring results in a start of growing season, and sufficient winter chilling is essential for plants to release bud dormancy, initiate growth and flowering in spring (Pagter et al. 2015; Saure 1985; Wang et al. 2017c). Insufficient chilling during winters usually leads to serious consequences such as reduction of flower quality, abscission of flower buds, protraction of the flowering process, and a reduced fruit set; in sub-tropical and tropical areas it results in prolonged dormancy which can cause poor blooming, strong apical dominance, unsynchronised growth patterns, and low yields (Melke 2015). In cold and temperate regions, accumulated temperature which is also known as thermal time (i.e. the sum of daily mean temperature above a certain threshold value during a plant life cycle) is also important for plant green-up because plants need store a certain amount of heat to break the dormancy and trigger spring leaf onset (Piao et al. 2015). In summary, warm springs after cold winters (a large temperature difference), tend to bring about early initiation of the plant growing season.

Many studies have been conducted in China investigating the relationship between vegetation phenology and climatic factors. However, most of the studies were focused on limited locations or regions, even specific plants. For instance, Chen

and Pan (2002) used AVHRR NDVI data from 1982 to 1993 to investigate the response of the growing season of local plant communities to climate change at three sample stations in eastern China. The results showed that the mean air temperature and Growing Degree Days (GDDs) above 5°C during the late winter and spring, and precipitation in autumn, were the most important controls on the OG and ES. Piao et al. (2006b) used AVHRR NDVI data from 1982 to 1999, and concurrent mean precipitation and temperature data to investigate the possible impact of recent climate changes on growing season duration on the temperate vegetation of China. The results suggested that an earlier OG and later ES were observed. The OG was most significantly related with the mean temperature during the preceding 2-3 months. A warming in the early spring by 1°C could cause an earlier OG of 7.5 days, whereas the same increase of mean temperature during autumn could lead to a delay of 3.8 days of ES. Dai et al. (2011) used GIMMS NDVI data to analyse the spatial-temporal variation of vegetation cover and the driving factors in northwest China during 1982 to 2006. The results indicated that in the area natural vegetation change was mainly influenced by climate change, while planting vegetation was affected by human activities. It also showed that in the last 25 years in the area temperature rose significantly by an average rate of 0.67°C per decade and precipitation increased by an average rate of 8.15 mm per decade. A positive relation was detected between vegetation cover, temperature, and annual precipitation changes. Guo et al. (2015) evaluated the temperature response of apricot bloom at five climatically contrasting sites in China, to test the effects of increasing temperature in spring and autumn/winter on advancing spring phases. The results showed warmer spring temperatures lead to an earlier apricot bloom in cold areas, and chilling temperatures were the main driver of bloom, implying a warm autumn/winter caused delayed spring phases.

The MERIS Terrestrial Chlorophyll Index (MTCI) 4.6 km 8-day and 10-day interval dataset and gridded (0.5°×0.5°) monthly climate records were used to investigate the connections and relationships between climatic factors and dates of regional vegetation phenology over the whole mainland China from 2003 to 2011, to find the main drivers for each region at the country level.

5.2 Study area

In this chapter, mainland China was divided into eight vegetation-climate zones for later analysis of how vegetation responds to climate change. Mainland China extends over 3,200 miles from west to east (73°E to 135°E); it spans 3,400 miles from north to south (53°N to 4°N). China probably has the most diverse climates and landscapes in the world. The country spans across frigid, temperate, subtropical, and tropical zones from north to south, and within the territory, about one third of it is mountainous. Plateaus and high mountains dominate the west, while lower lands and plains lace the eastern region. Generally, the altitude increases from -150 m at east China to around 1500 m in mid China, and up to around 5000 m in west China (Tibet) (Figure **24**). The temperature decreases along this direction (around 25°C to -10°C) (Figure **28**), while the precipitation decreases from southeast to northwest (from 2000 mm $year^{-1}$ to less than 50 mm $year^{-1}$) (Figure **28**). The huge differences in elevation, temperature, and precipitation from east to west, and from south to north, result in diverse vegetation land covers and various kinds of landscapes.

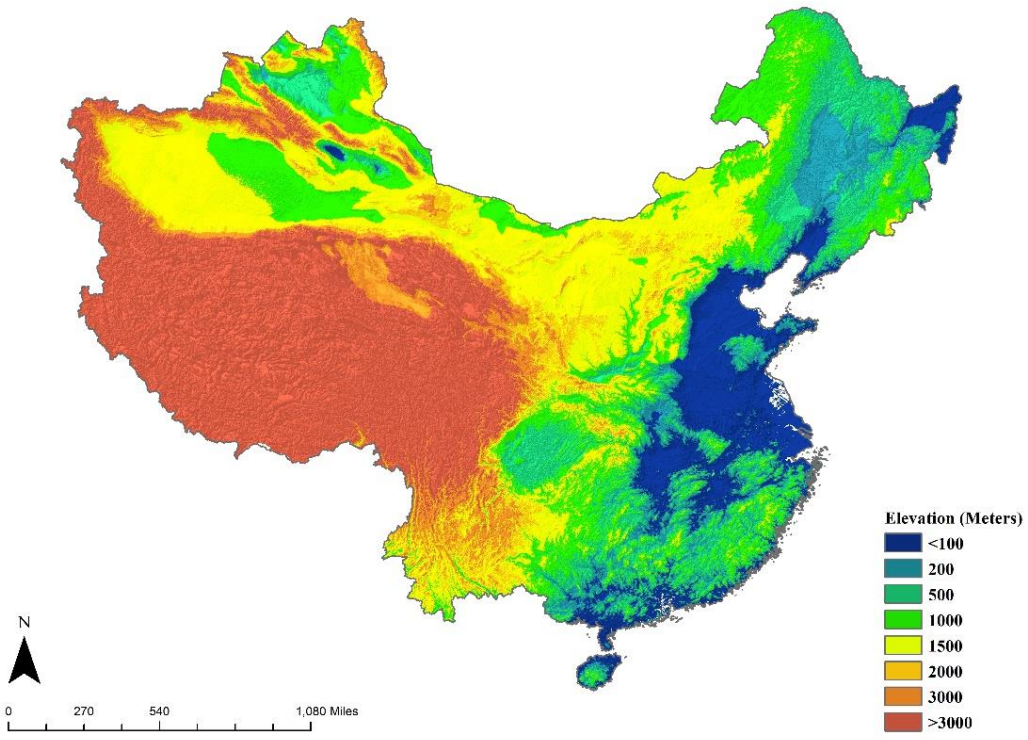

Figure 24 Elevation map of mainland China.

5.3 Data

Four data sources were used in this study: (i) OG and ES phenology maps derived from 8-day and 10-day temporal composites of MTCI with 4.6 km spatial resolution (produced in Chapter 4); (ii) ESA's 2009 global land cover map (downloaded from http://maps.elie.ucl.ac.be/CCI); (iii) China's climatic monthly data including precipitation (mm) and average temperature (°C) from 2003 to 2011 (obtained from China Meteorological Data Service Centre (CMDC) (http://data.cma.cn/en); (iv) climate zone map of mainland China (Figure **25**).

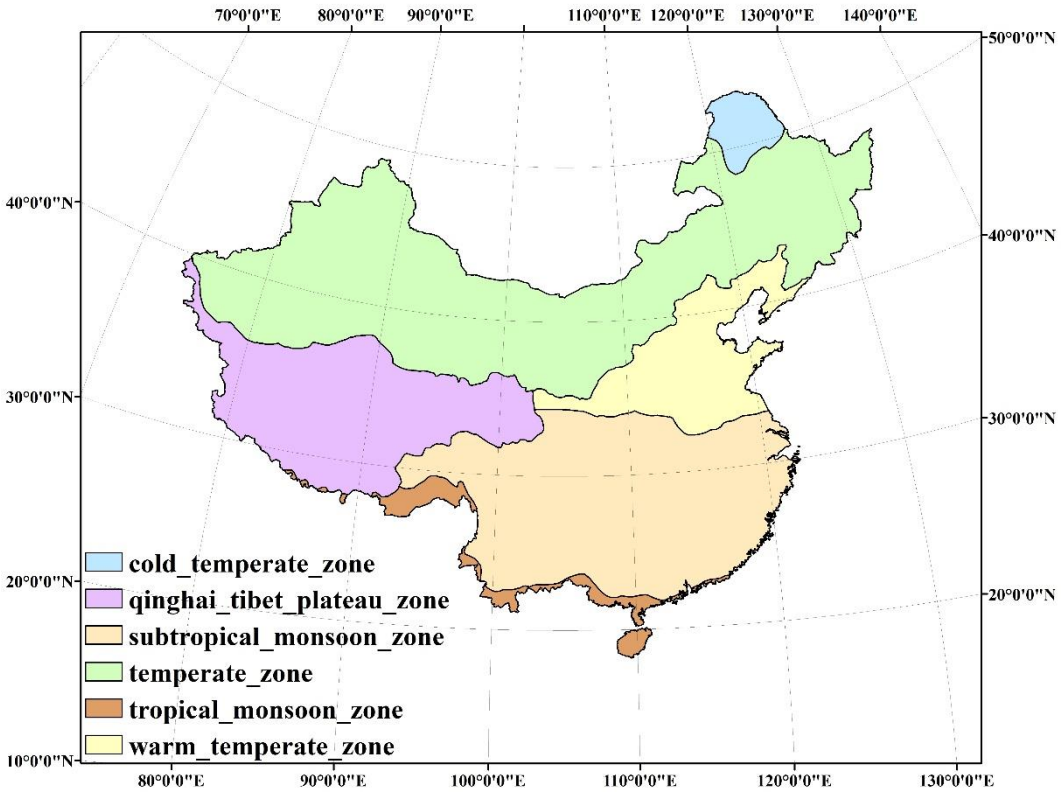

Figure 25 Climate zone map of mainland China.

5.3.1 Remote sensing data

Based on the extracted phenological variables in the last chapter, the onset of greenness (OG) and end of senescence (ES) of each year from 2003 to 2011 were prepared for later statistical analysis. Figure **26** shows the average Julian days OG and ES distribution during the year 2003 to 2011 across mainland China.

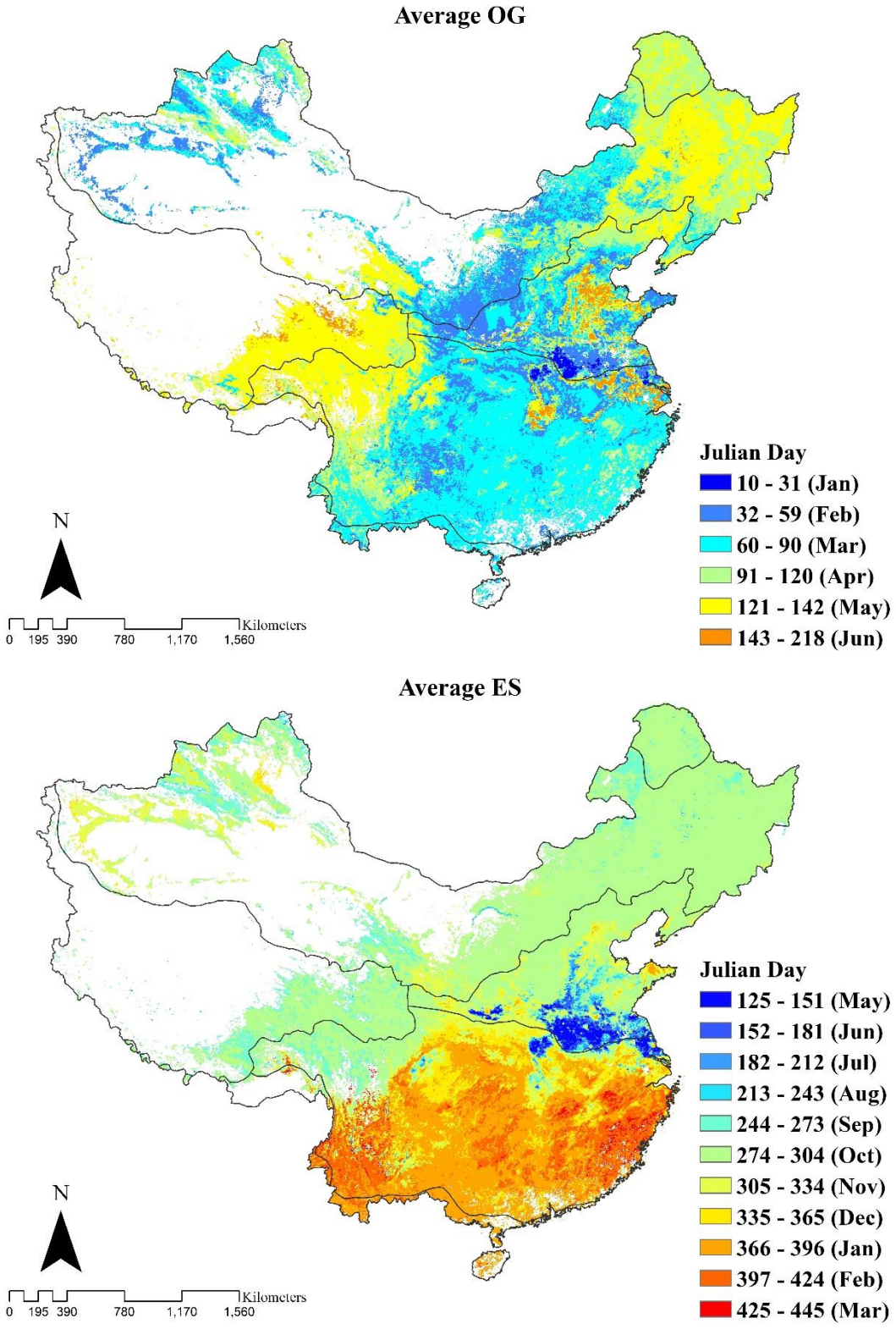

Figure 26 Average onset and senescence time of vegetation growing season map of mainland China, derived from 4.6 km MTCI dataset.

5.3.2 Land cover map

ESA's global land cover map of 2009 was used. The original resolution was 300 m,

and it had been resampled to meet the same resolution with MTCI data, which was 4.6 km. The land cover map of mainland China was clipped, and values were reclassified in order to select five major vegetation types including broadleaf deciduous (*BD*), cropland (*CL*), grassland (*GL*), mixed evergreen (*Mix*), needle leaf deciduous (*ND*), in mainland China (Figure **27)**.

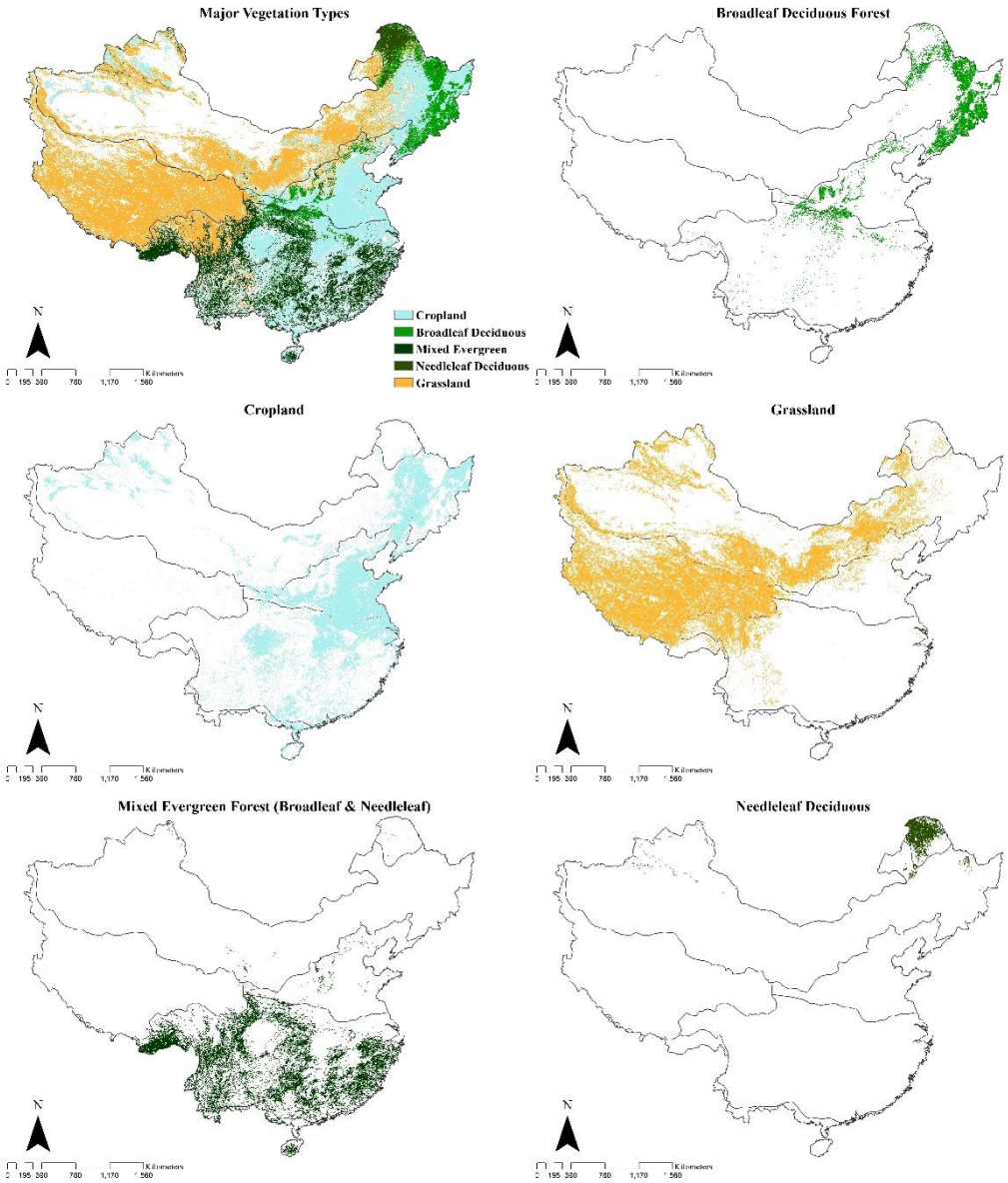

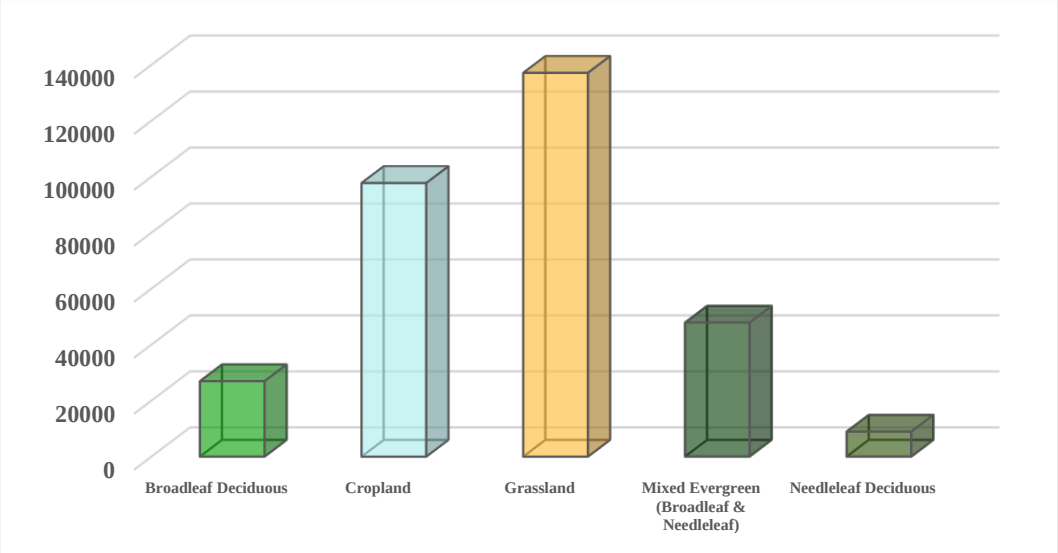

Figure 27 Five major selected vegetation types (broadleaf deciduous, cropland, grassland, mixed evergreen, and needle leaf deciduous) and their distribution in mainland China. The plot represents the number of pixels for different vegetation types.

5.3.3 Climatic data

Two climatic factors – temperature and precipitation – that greatly influence plant growth and geographic distribution were taken into consideration. Surface temperature and precipitation monthly gridded data (0.5°×0.5°) in ASCII format from 2003 to 2011 were downloaded from http://www.cma.gov.cn/ and then transformed into projected raster data. Both datasets were generated by the National Meteorological Information Centre, based on records from 2472 national meteorological stations, and spatially interpolated by using the Thin Plate Spline (TPS) method with a DEM extracted and resampled to 0.5°×0.5° from Global 30 Arc-Second Elevation (GTOPO30) (0.05°×0.05°). Figure **28** shows the average annual temperature and accumulative precipitation during the study period.

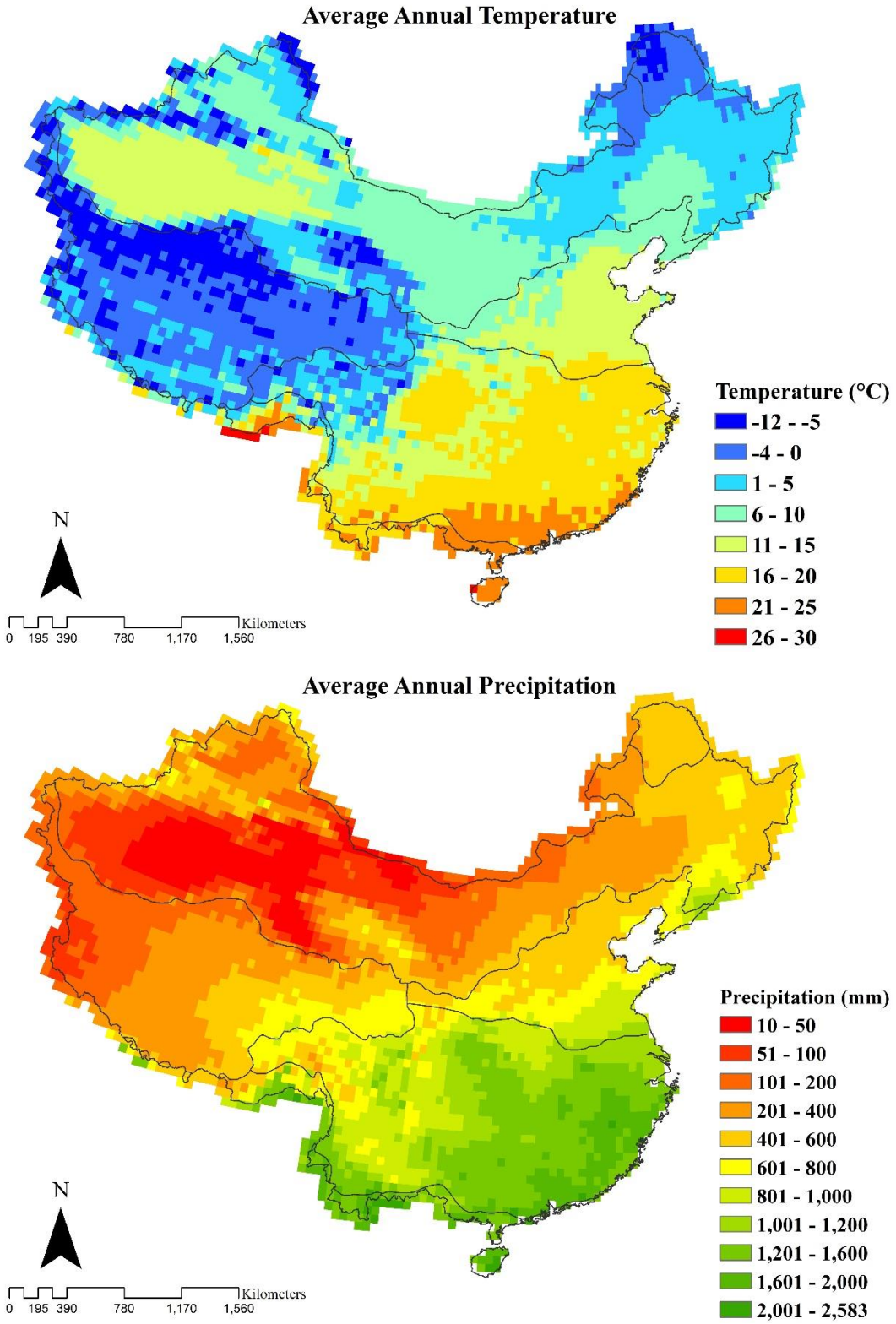

Figure 28 Maps showing annual average temperature and annual average precipitation in mainland China.

5.4 Method

Two phenological variables were extracted from the MERIS Terrestrial Chlorophyll Index (MTCI) dataset, OG and ES, and their relationships with meteorological parameters (temperature and precipitation) were investigated. Mainland China was divided into six climate zones (cold temperate zone (*CT*), temperate zone (*Tm*), warm temperate zone (*WT*), subtropical monsoon zone (*StM*), tropical monsoon rain forest (*TrM*), and Qinghai-Tibet Plateau zone (*QTP*)). The correlations between vegetation and climatic parameters were shown for each zone.

5.4.1 Remote sensing data preparation

Before extracting phenological metrics (OG and ES), procedures were needed to be undertaken for cleaning the missing values within the time-series, which were commonly caused by cloud cover, atmospheric effect, and snow cover (Zhang et al. 2012b). There were many methods for data filling. A moving average function was applied to remove missing values with a mean neighbourhood of two values (windows size = 3). After that, the Fourier transformation was utilised to smooth the cleaned time-series data, with a parameter of six harmonics.

5.4.2 Phenological metrics extraction

Many methods were available for extracting phenological metrics through time-series remote sensing data. Generally, there are two main approaches to finding the dates of growing onset and senescence from time-series data. One sets a threshold for a vegetation index such as NDVI, to identify the initiation of photosynthesis of leaves in spring (Chen et al. 2000; Fischer 1994; Lloyd 1990; White et al. 1997). Another approach is monitoring the derivative variation of time-series, to find the great change period to mark the growing seasons (Ahl et al. 2006; He et al. 2015b; Li et al. 2011a; Piao et al. 2006b; Zhang et al. 2003). The inflection point method was used to monitor the maxima and minima curvature rate changes that can possibly exhibit the timing of a growing season (Zhang et al. 2004).

5.4.3 Statistical analysis

Correlation analysis is commonly used to analyse the relationship between inter-

annual vegetation phenological changes and climatic factors. The correlation coefficient (Pearson), referred to as *r*, is a value between -1 to 1, where 1 is a total positive relationship, 0 is no linear correlation, and -1 is a negative relationship. After phenology extraction, climatic data and phenological dates during 2003 to 2011 over mainland China were analysed to find quantitative relationships. Along with the phenological variables (OG and ES) retrieved from 9-year MTCI imagery, in spatial and temporal respects, remotely sensed phenological variables will be related to meteorological factors. The correlation coefficients (*r*) were calculated for phenological season month (*m*) (the month OG or ES happened), sum of preseason month to phenological season month (*pm1*), and sum of two month before preseason month to phenological season month (*pm2*), to investigate the relationships between phenological metrics and accumulative climatic effects.

To explore possible driving factors of the lengthened growing season of major vegetation types distributed in eight climate-vegetation zones, the dominant vegetation in zones was summarized according to the land cover maps, shown in Table 6.

	Broadleaf Deciduous	*Cropland*	*Grassland*	*Mixed Evergreen*	*Needleleaf Deciduous*
1.cold temperate zone (CT)					
2.temperate zone (Tm)					
3.warm temperate zone (WT)					
4.subtropical monsoon zone (StM)					
5.tropical monsoon zone (TrM)					
6.qinghai tibet plateau zone (QTP)					

Table 5 Major vegetation distributions in climate zones.

5.5 Results

To analyse the variation of vegetation phenology with climatic factors, including temperature and precipitation, correlations were established between changing vegetation phenology and climatic factors in the corresponding months, at both the country level and vegetation-climate regional level. Furthermore, as plant phenological events are cumulative, the results of climatic effects over the certain period ahead of the timing of phenological dates were analysed (Piao et al. 2006b; Yu et al. 2003). Therefore, 'pre-season' climatic factors were taken into consideration by investigating two months climatic changes before OG and ES.

5.5.1 Vegetation phenology variation in mainland China

Table **6** lists the average onset and senescence dates by vegetation with corresponding average monthly precipitation and temperature in the phenological months from 2003 to 2011. Broadleaf deciduous forest, grassland, and cropland showed early OG in April, with the temperature around 8°C and precipitation around 38 mm. ES occurred from mid-to-late October when precipitation was less than 30 mm and temperature lower than 8°C. The OG of needle leaf deciduous forest varied from late April to early May with higher average precipitation of 47 mm and temperature of 9.4°C, and the ES occurred around late September to early October. Mixed evergreen forest did not show any seasonality with a full growing period around the whole year.

		2003		2004		2005		2006		2007		2008		2009		2010		2011		Average Monthly Precipitation (mm)	Average Monthly Tempareature (°C)
Broadleaf deciduous	OG	112.4	Late Apr	105.0	Mid Apr	98.0	Early Apr	105.2	Mid Apr	96.7	Early Apr	97.9	Early Apr	104.0	Mid Apr	101.3	Mid Apr	92.6	Early Apr	**38.5**	**8.4**
	ES	288.1	Mid Oct	299.1	Late Oct	297.7	Late Oct	297.4	Late Oct	299.5	Late Oct	297.4	Late Oct	299.2	Late Oct	297.2	Late Oct	296.6	Late Oct	**29.7**	**7.8**
Cropland	OG1st	104.1	Early Apr	98.1	Early Apr	95.5	Early Apr	91.1	Late Mar	88.0	Early Apr	92.2	Early Apr	95.0	Early Apr	90.0	Late Mar	91.9	Late Mar	**37.5**	**7.6**
	ES1st	291.3	Late Oct	305.5	Late Oct	301.7	Late Oct	300.6	Late Oct	287.3	Mid Oct	296.2	Late Oct	304.5	Late Oct	289.0	Mid Oct	301.7	Late Oct	**26.9**	**7.1**
	OG2nd	180.3	Late Jun	178.8	Late Jun	177.7	Late Jun	179.6	Late Jun	172.9	Late Jun	173.1	Late Jun	175.9	Late Jun	172.4	Late Jun	176.3	Late Jun	**94.7**	**18**
	ES2nd	298.8	Late Oct	299.4	Late Oct	303.5	Late Oct	304.5	Late Oct	299.2	Late Oct	303.6	Late Oct	309.2	Early Nov	291.7	Late Oct	314.0	Mid Nov	**26.5**	**6.2**
Grassland	OG	112.9	Late Apr	109.0	Mid Apr	99.5	Early Apr	99.6	Early Apr	99.2	Early Apr	105.1	Mid Apr	103.4	Mid Apr	99.0	Early Apr	97.9	Early Apr	**38.5**	**8.4**
	ES	276.0	Early Oct	282.1	Mid Oct	283.7	Mid Oct	283.2	Mid Oct	282.1	Mid Oct	284.4	Mid Oct	285.5	Mid Oct	282.5	Mid Oct	286.1	Mid Oct	**29.7**	**7.8**
Mixed evergreen	OG	97.6	Early Apr	93.2	Early Apr	89.5	Late Mar	89.5	Late Mar	87.9	Late Mar	87.5	Late Mar	83.9	Late Mar	82.0	Late Mar	85.6	Late Mar	**28.7**	**4.6**
	ES	344.4	Late Dec	380.1	Mid Jan	380.7	Mid Jan	374.2	Early Jan	376.0	Early Jan	383.6	Mid Jan	379.7	Mid Jan	382.7	Mid Jan	380.9	Mid Jan	**10.5**	**-8**
Needle leaf deciduous	OG	125.1	Early may	116.9	Late Apr	116.2	Late Apr	120.2	Late Apr	117.4	Late Apr	116.2	Late Apr	120.2	Late Apr	121.9	Late Apr	116.6	Late Apr	**47**	**9.4**
	ES	268.5	Late Sep	276.4	Early Oct	278.0	Early Oct	276.8	Early Oct	277.8	Early Oct	287.2	Mid Oct	280.4	Early Oct	281.1	Early Oct	276.9	Early Oct	**32.9**	**8.5**

Table 6 Average parameters of the OG and ES by vegetation type over mainland China from 2003 to 2011, with corresponding average monthly precipitation and temperature in the phenological months.

5.5.2 Phenology variation in relation to precipitation and temperature in the climate zones

Figure **29** (*a-l*) shows the CCs between OG and ES and two climatic factors in different regions. It can be seen that generally the OG had a great number of positive correlations with precipitation and temperature than negative correlations, suggesting that the increase in temperature or precipitation results in advancing OG. Conversely, the ES was more negatively related to precipitation and temperature.

The cold temperate zone (*CT*), the most northern region in China. For the OG, the large correlations were negative (*r* ranged from -0.703 to -0.376 for BD and from -0.715 to -0.376 for ND). It can be clearly noticed that there were declines in correlations for accumulative precipitation with the OG for both vegetation in the last two months before the seasonal month (*r* ranged from -0.571 to -0.290 for BD and from -0.666 to -0.376 for ND). For the ES, it was found that the relationships between BD and ND and two climatic factors during the three months were high positively consistent (*r* ranged from 0.723 to 0.843 for broadleaf deciduous and from 0.766 to 0.886 for needle leaf deciduous). This suggests that a sufficient store of precipitation before the seasonal month was critical for the spring phenology stage in this region. Therefore, in northern China, temperature contributed more to the OG and ES than precipitation in *CT*, and both of precipitation and temperature were the main causes of an earlier OG for the crops. However, for the grass and broadleaf forest, it did not show any clear relationships with precipitation and temperature. For the ES, both precipitation and temperature were highly positive related with all three vegetation types.

In the temperate zone (*Tm*), for the OG, the CL was high negatively correlated with two climatic factors, while the BD and GL were less affected. It might be because the needle leaf deciduous vegetation itself was less influenced by the severe growing environment (Fu et al. 2012). For the ES, the CL was more related with accumulative precipitation and temperature (*r* ranged from 0.589 to 0.657 for precipitation and from 0.570 to 0.690 for temperature). The BD was also strongly related with the two climatic factors during all three months. Thus

In the warm temperate zone (*WT*), which has sufficient rainfall all year round, the temperature determined the OG for the CL after the crops had stored sufficient water since the month before preseason months (*pm2*=0.267). The BD showed a similar reaction of being influenced by temperature after storing enough water since the preseason months. Therefore, it can be said that the summer temperature was the main factor driving the delay in the OG for the CL and BD in this region, and precipitation was partly responsible for the variation in triggering the OG. For the ES, both climatic factors influenced the BD greatly in this region, compared to the CL. It can be concluded in central China, temperature was the main driver of earlier OG for broadleaf forest and crops in the *WT*, while precipitation had a weaker impact on them. For the ES, both precipitation and temperature cause an earlier date for the BD, whereas the crops were positively correlated with the temperature during the three months.

In the subtropical monsoon zone (*StM*) and tropical monsoon (*TrM*) zone, there were four major vegetation covers. The temperature had more impact on the OG, while the precipitation was relatively more important for vegetation dormancy, as the higher absolute value of *r* for all vegetation could be found. In southern China, in *StM* and *TrM* zones, the situation was more complex than other regions. Generally, temperature determined the OG while temperature contributed to the ES mostly with precipitation partly contributing. Among the vegetations in *StM* zone, the ND was controlled by temperature, while the other vegetations were heavily influenced by precipitation. For the ES, grass and mixed forest showed positive correlation with both precipitation and temperature as expected, but the broadleaf forest and crops showed the opposite.

In the Qinghai-Tibet Plateau zone (*QTP*), the land cover is dominated by grass. It can be seen that the OG in the *QTP* was influenced by both precipitation and temperature negatively, and in the seasonal month, they had the most significant effect on the OG. The ES in this region was mainly affected by precipitation started in the preseason month (*pm1*=0.214). The accumulative temperature from two months before seasonal month had a higher positive impact on the OG (pm2=0.140), and negative impact in the seasonal month (*m*=-0.095).

In summary, the results showed that generally, the relationship between OG and climatic factors was negative, while the relationship between ES and climatic factors was positive. In north China including cold temperate and temperate zones, temperature was the main driver for the earlier OG and both of the two factors were responsible for the later ES. In central China the main driver is not clear for the green-up onset but both precipitation and temperature were the drivers for later ES in the warm temperate zone. In south China, precipitation was the main driver for the earlier OG in subtropical zone, while it is not clear for the ES. In tropical zone, both precipitation and temperature impact on the timing of green-up and senescence. In Qinghai-Tibet Plateau, the precipitation was the main driver for both shifting OG and ES of grass, while temperature influenced less.

(e) OG in WT

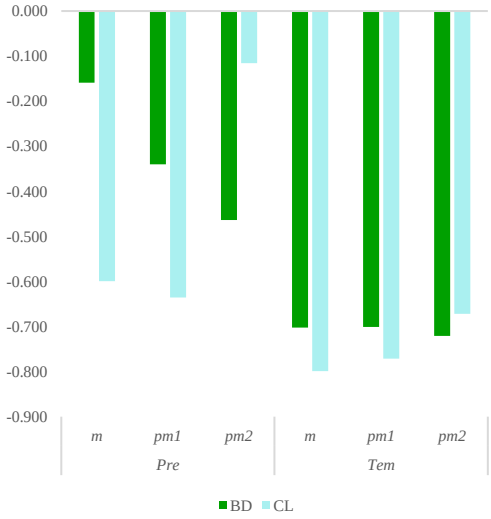

(f) ES in WT

(g) OG in StM

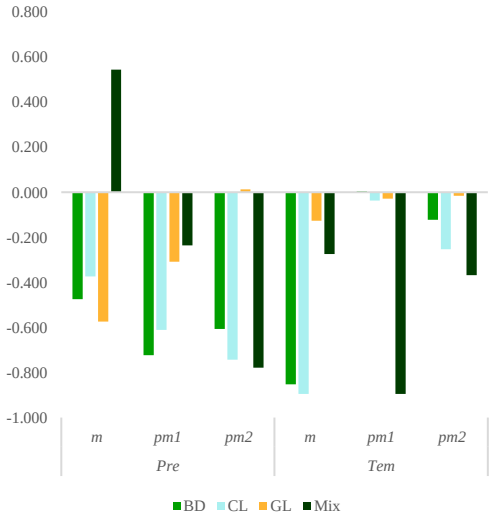

(h) ES in StM

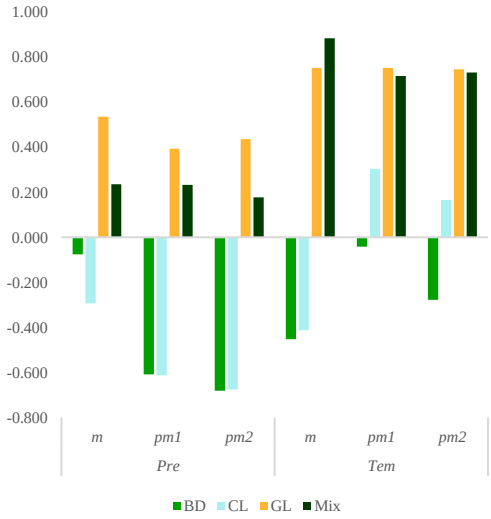

(i) OG in TrM

(j) ES in TrM

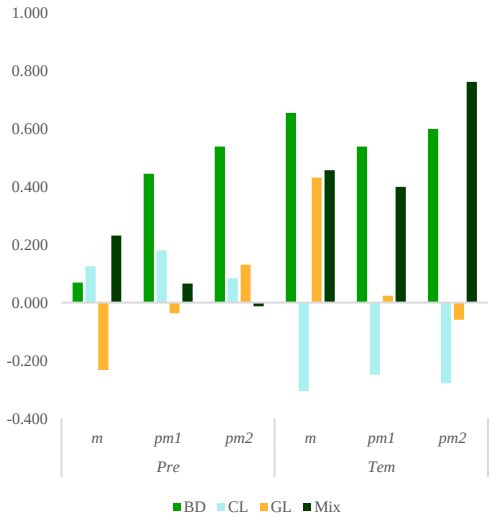

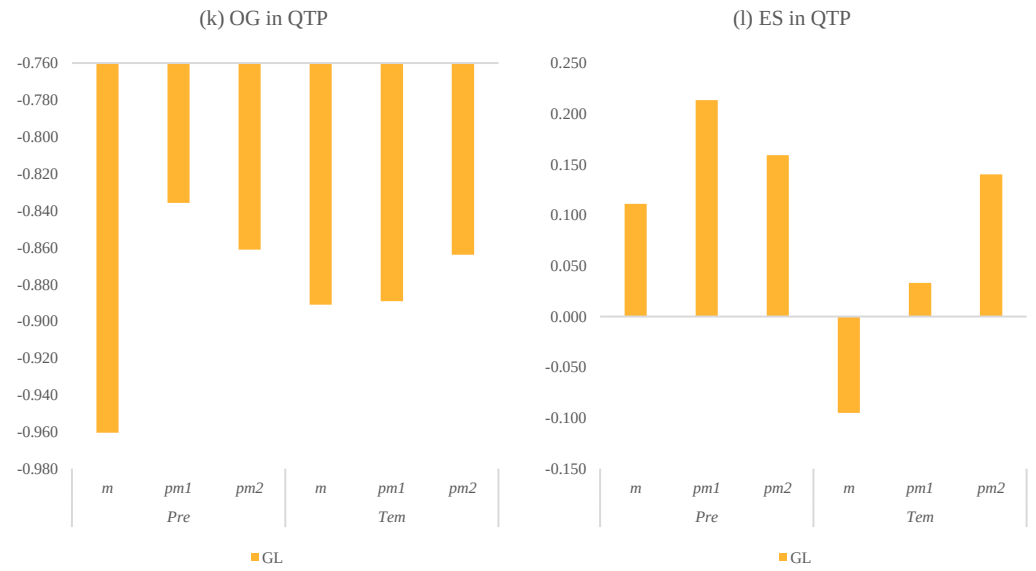

Figure 29 Correlation coefficient between OG(ES) and precipitation(temperature) in season month (*m*), preseason month to season month (*pm1*), and one month before preseason month to season month (*pm2*). For different vegetation types, include broadleaf deciduous forest (*BD*), cropland (*CL*), grassland (*GL*), mixed evergreen forest (*Mix*), and needle leaf deciduous forest (*ND*). In climate zones, include cold temperate zone (*CT*), temperate zone (*Tm*), warm temperate zone (*WT*), subtropical monsoon zone (*StM*), tropical monsoon zone (*TrM*), and Qinghai-Tibet Plateau zone (*QTP*).

5.6 Discussion

Many studies have suggested that climate change has caused variation in vegetation phenology. In this study the major climatic factors affecting the vegetation phenology were summarised, and temperature was suggested to be a more correlated climatic factor rather than precipitation in north and central China, although precipitation was significant in preseason months occasionally. In most cases the OG of crops was affected by climate but the ES were more influenced by human activities (Dai et al. 2011). Warmer winters and springs may advance the OG of major vegetation in most regions in mainland China. Leaf development of most plants is sensitive to temperature (Polgar and Primack 2011) and needs a certain amount of winter chilling (Saure 1985) followed by adequate thermal time to trigger leaf unfolding (Hänninen and Kramer 2007). In addition, winter and spring precipitation could allow the well-developed root system to store sufficient water earlier in the growing season to advance the growth (Li et al. 2011a). Large negative correlations between the OG and precipitation and temperature of major vegetation including BD and ND in the cold temperate zone were found (Figure

29a), showing a warmer winter tend to advance the OG in northeast China. The same situation was found in other temperate zones for major vegetation. Except for the BD in the temperate zone showed most correlations were positive (Figure **29c**), further investigation on understanding chilling and thermal requirement mechanism in BD is still needed.

Increases in summer and autumn temperature and precipitation possibly delay the ES of most vegetation types. Most major vegetation in main regions showed positive correlations with climatic factors, except BD in the warm temperate and subtropical zones. Warming tends to accelerate the photosynthetic process (Shi et al. 2014), and at same time slow down chlorophyll degradation in autumn (Liu et al. 2016b). Warmer nights also tend to protect vegetation from frost damage (Hoffmann et al. 2010). On the other hand, increase in summer day time temperature may also cause more evapotranspiration and soil moisture stress (Wang et al. 2017c), and then an earlier ES will take place because of the poor water supply such as grass in Figure **32**.

Few studies have focused on the southern part of China, as it has no obvious seasonality (Piao et al. 2006b). It can be indicated from our results that in south China, temperature and precipitation might not be sufficient factors to explain the change of vegetation phenology. It can be also highly related to other factors such as solar radiation as well.

Additionally, it is important to be aware that the phenological dates of OG and ES were determined by remote sensing data. Although effective corrections have been done, missing values and errors caused by clouds, aerosols, etc. still exist in MTCI data (Tang et al. 2015). Therefore, the OG and ES could be possibly under or overestimated, leading to differences comparing with other studies.

The trends in vegetation phenology were investigated at national scale rather than regional scale, as China is a large country. The only simple relationship was investigated between regional vegetation phenology and climate parameters including precipitation and temperature, to find the major drivers of phenology changes. Further, the research was based on a vegetation-climate region map rather than pixel level. Therefore, factors such as effects of latitude, solar radiation

changes, land use and land cover changes, that influencing vegetation phenology in many ways (Tang et al. 2015), were not taken into account in this study.

5.7 Conclusion

In this chapter, based on the 4.6 km MTCI time-series data, the phenological metrics OG and ES of vegetation were extracted, and the phenological trends in different vegetation types were estimated during 2003 to 2011. Moreover, with concurrent monthly precipitation and temperature gridded dataset, the relationships between phenological metrics and climate parameters were investigated. The results showed that the OG and ES in different regions had main climatic driving factors and they varied from regions and vegetation types. In cold temperate zone and temperate zone, temperature was the main driver for the earlier OG and both precipitation and temperature were driving the ES to be late. In warm temperate zone the OG was not driven specifically by climatic factor but both precipitation and temperature were the drivers for later ES. In subtropical zone, precipitation was the main driver for the earlier OG but the ES had no clear driver. In tropical zone, both precipitation and temperature advanced the timing of green-up and senescence. In Qinghai-Tibet Plateau zone, the precipitation was the main driver for both shifting OG and ES of grass, while less influenced by temperature. Among the vegetation that were investigated, broadleaf forest was more influenced by temperature to the OG in north China (*CT*, *Tm* and *WT*) and precipitation to the ES in south China (*StM* and *TrM*). Grass phenology was mainly controlled by temperature both *Tm* and *QTP,* and precipitation played an important role in *QTP* for the ES. The mixed forest was mostly driven by temperature but the precipitation in seasonal month had a great correlation with the OG. Crops were greatly affected by temperature in central China (*WT*) while affected by precipitation in southern China (*StM* and *TrM*). Further studies with more specific quantitative analysis will be helpful for understanding the relationship between vegetation growth and climate variables.

6.Mapping Paddy Rice Planting Area through Time-series Analysis of MERIS Terrestrial Chlorophyll Index and MODIS Vegetation Index Data

6.1 Background

Rice is the second largest, but the most important staple food in the world, it feeds more than half the population on the planet. In 2016, paddy rice fields accounted for more than 10% of global cropland area, and the fields have increased about 3.4% in 2017 compared to 2010, according to FAOSTAT. More than 90% of the rice is grown and consumed in Asia where 60% of the world population live (Khush 2005a). China is the world's largest rice producer and consumer, rice makes up almost half of the country's total grain output, and it plays a very important role in the China's economy and food security. However, in recent years, with the urbanisation, natural degradation and hazards, challenges have emerged for growing demands of rice, due to an increasing population (Zhang et al. 2018a).

Paddy rice plays an important role in water use, climate change, and disease transmission. Firstly, rice is the most water-intensive staple grain. Approximately 95% of global rice is cultivated on flooded lands (Belder et al. 2004). In Asia, agricultural water consumption accounts for about 84% of total water withdrawal, with major emphasis on flooded rice irrigation (Loucks et al. 2005). Therefore, the high water demands of irrigation have an important impact on water quality. Secondly, paddy rice fields have been recognised as one of the most significant sources of greenhouse emissions, particularly methane (CH_4), while they provide essential food for billions of people in the world (Li et al. 2004). CH_4 is the second important greenhouse gas following CO_2, with the capacity as 28 times as CO_2 (Dong and Xiao 2016). Lastly, paddy rice is correlated to the transmission of disease such as highly pathogenic avian influenza A (H5N1) virus, because paddy fields are common breeding sites for free-range ducks (Gilbert et al. 2008). In sum, map rice at fine spatial resolution is critical for food production and security, water resource management, environmental sustainability, disease control and governmental decision-making.

The traditional way of paddy rice areas monitoring requires massive ground survey and statistical analyses, which is time consuming, labour intensive, and less accurate (Zhang et al. 2018b). Remote sensing has been used widely as an efficient tool for monitoring crops for the past decades, providing timely spatial and temporal

information on crop distribution area and their growing conditions. Unsupervised (Fang 1998; Okamoto 1999) and supervised classification such as the maximum likelihood classifier (MLC) were used widely for paddy rice classification in early studies, mainly with Landsat data (Fang et al. 1998; Kurosu et al. 1997; McCLOY et al. 1987; Parihar 1992; Tennakoon et al. 1992). Since 2000, new classification approaches were developed such as the Neural Network (NN) (Chen and McNairn 2006; Kussul et al. 2017; Lu et al. 2017; Zhang et al. 2018a), the Support Vector Machine (SVM) (Dou et al. 2017; Hu et al. 2017; Li et al. 2014; Tan et al. 2007; Zhang et al. 2009), and Random Forest (RF) (Kontgis et al. 2015; Son et al. 2018), with MODIS, Landsat 8, Sentinel and other data sources. Although these new methods (e.g., NN, SVM, RF) have improved the accuracies compared to the early classification methods (e.g., MLC), however, they still rely on: (i) the amount of training samples, which normally ranges from hundreds to thousands depending on the size of study area, results in high labour intensity and time-consuming; (ii) sample acquisition time window, which can be affected by different farming schemes, especially at large scales; (iii) spatial resolution of remotely sensed data, which can overestimate the paddy fields area due to sub-pixel vegetation. Therefore, an alternative way for identifying rice paddies is based on the phenological characteristics of paddy rice.

A unique physical characteristic of paddy rice is that during the transplanting period paddy fields are a mixture of open water and rice seedlings. According to Xiao et al. (2006), pixels within the flooding area can be tracked using vegetation indices which are sensitive to changes in the land surface water content and the growing canopy. In this chapter, the MERIS Terrestrial Chlorophyll Index (MTCI), Enhanced Vegetation Index (EVI), and Land Surface Water Index (LSWI) are used to detect the changes of paddy fields during the transplanting period.

EVI is constructed to overcome the shortage of NDVI, it takes all the advantages of MODIS. It is calculated similarly to the NDVI, but includes the blue band to correct distortions in the reflected light caused by particles in the air as well as the ground cover below the vegetation (Matsushita et al. 2007). In addition, the EVI does not saturate as easily as the NDVI, when processing high biomass situations (Li et al. 2010).

The LSWI was also known as normalised difference water index (NDWI), was first proposed by Gao (1996), and uses a shortwave infrared (SWIR) band centered at 1240nm for the purpose of estimating vegetation liquid water from remote sensing data. The SWIR band based indices have been widely adopted in identifying flooding period during the rice growing cycle. Xiao et al. (2002) used the near-infrared and middle-infrared bands to generate $NDWI_{VGT}$ by SPOT-VGT data to test the ability of detecting flooding and rice transplanting across the landscape. Chen et al. (2005a) tested both SWIR bands at 1640 nm and 2130 nm to calculate NDWI for estimating the vegetation water contents of corn and soybean. Xiao et al. (2006; 2005) adopted the same principle of NDWI but named as LSWI, centred at 1640 nm to identify water properties during the flooding and transplanting period of paddy rice farming, by applying the conditions of $LSWI + threshold \geq NDVI$ or $LSWI + threshold \geq EVI$. Sun et al. (2009) based on Xiao's method, set ranges for NDVI and EVI in order to detect early and late rice all over China. Ying et al. (2015) tested NDVI, NDWI or LSWI at different SWIR bands (1240 nm, 1640 nm, and 2130 nm) for estimating Vegetation Water Content (VWC), according to historical studies on VWC. The results show that $NDWI_{1640}$ and NDVI have greater accuracy for VWC estimation, while $NDWI_{1240}$ lacks supportive literature. Due to the unique flooding period in paddy fields during the transplanting period, soil moisture becomes an important fact for consideration. Moreover, according to Parinussa et al. (2011), the retrieval error of soil moisture value is generally larger at higher microwave frequencies. Therefore, $LSWI_{1640}$ were adopted to detect paddy rice fields in this chapter.

The objective of this study was to test the ability of MTCI to detect flooding paddy fields with EVI and $LSWI_{1640}$ in northeast China, and analyse the tempo-spatial distribution of rice in the three provinces from 2007 to 2011.

6.2 Study area

Northeast China extends from 118°50′5′′E to 134°46′26′′E in longitude, and from 38°43′15′′N to 55°33′39′′N in latitude, covers an area of 7.9×10^5 km^2 with about 30% arable land (Shi et al. 2013). The arable land comprises three provinces of Heilongjiang, Jilin, and Liaoning, and is one of the most significant agricultural

production bases in China for soybeans, maize, and japonica rice. Soybean production in northeast China accounts for over 40% of the national total production; japonica rice takes up 30-50% of the national total, and maize output was more than 30% in entire China in 2015 (National Bureau of Statistics of China, http://stats.gov.cn/). Altitude in northeast China is mostly less than 600 m, annual precipitation varies from 480 mm in the west to 900 mm along the east coast; the annual temperature ranges from 1°C to 7 °C, and the cumulative temperature is lower than 3000°C, with a frost-free period of 100 – 180 days through a year. Japonica rice in northeast China enjoys the reputation of being high yield and higher quality, because it is cultivated as a single-season crop, planted in major alluvial plains with a flat topography, abundant precipitation, and fertile soils (Shi et al. 2013; Zhang et al. 2015b).

6.3Data

6.3.1 Remote sensing data

Medium Resolution Imaging Spectrometer (MERIS) Data

The MERIS Terrestrial Chlorophyll Index (MTCI) dataset used in this study was obtained from the Envisat MERIS sensor. The 1 km reduced spatial resolution and 10-day cloud free composites were downloaded from the UK Natural Environment Research Council Earth Observation Data Centre (NERC NEODC; http://www.ceda.ac.uk/). It is believed that MERIS was the most radiometrically accurate imaging spectrometer in space (Curran and Steele 2005). The MTCI data were composited from standard level 2 reduced resolution MERIS products by an arithmetic mean and a flux conversion resampling method (Dash and Curran 2007).

Moderate Resolution Imaging Spectroradiometer (MODIS) Data

The National Aeronautics and Space Administration (NASA) provides a range of MODIS products which are processed with standard correction algorithms for free download. The MODIS sensor on-board the NASA EOS Terra/Aqua satellite has 36 bands, amongst which bands 1 to 7 are designed for vegetation and Earth surface studies: Band 1 (red: 620-670nm), Band 2 (NIR1: 841-876nm), Band 3 (blue: 459-479nm), Band 4 (green: 545-565nm), Band 5 (NIR2: 1230-1250nm), Band 6

(SWIR1: 1628-1652nm), and Band 7 (SWIR2: 2105-2155nm). The MODIS products are available from daily to yearly with different spatial resolutions and various composite products. 8-day, 500 m surface reflectance data (MOD09A1) were acquired from the Land Processes Distributed Active Archive Centre (LPDAAC) (https://lpdaac.usgs.gov/). The MOD09A1 dataset has quality control flags to reduce the effects of clouds, cloud shadows and so on. It includes two quality assessment (QA) datasets at pixel and band levels, which were used to remove cloud contaminated pixels, before compositing indices. MODIS data are organised in a tile system with the Sinusoidal (SIN) projection grid, and each tile covers an area of 1200 km by 1200 km, which is about 10° latitude by 10° longitude. To cover northeast China, five tiles (h25v03, h26v03, h26v04, h27v04, h27v05) of MOD09A1 data were used to calculate indices including EVI and $LSWI_{1640}$ from 2007 to 2009.

GlobeLand30 land cover map

In 2010, China launched a global land cover (GLC) mapping project, and the 30 m GLC data product (GlobeLand30) with 10 classes for years 2000 and 2010 were produced in 2014 (Chen et al. 2015). GlobeLand30 datasets are freely available from http://www.globallandcover.com/GLC30, with ten classes namely: water bodies, wetland, artificial surfaces, cultivated land, permanent snow/ice, forest, shrubland, grassland, bareland, and tundra. GlobeLand 30 employed a pixel-object-knowledge-based (POK-based) classification approach, because in experiment four common classifiers (Maximum Likelihood Classifier (MLC), J4.8 Decision Tree Classifier (DT), Random Forest Classifier (RF), and Support Vector Machine (SVM)) were tested and it was found that the overall classification accuracy (OCA) was at 64.9%, produced by SVM, which was less satisfying (Gong et al. 2013). In this chapter, the cultivated land map was extracted and resampled by the majority method (a 4 by 4 filter finds the pixel values that are occupying more than 50% cells within it and output the majority as the new 4 by 4 cells) to match the resolution of 1 km (Figure **30**), for the purpose of discriminating flooded forest, shrubland, wetland, and other water bodies from paddy rice fields.

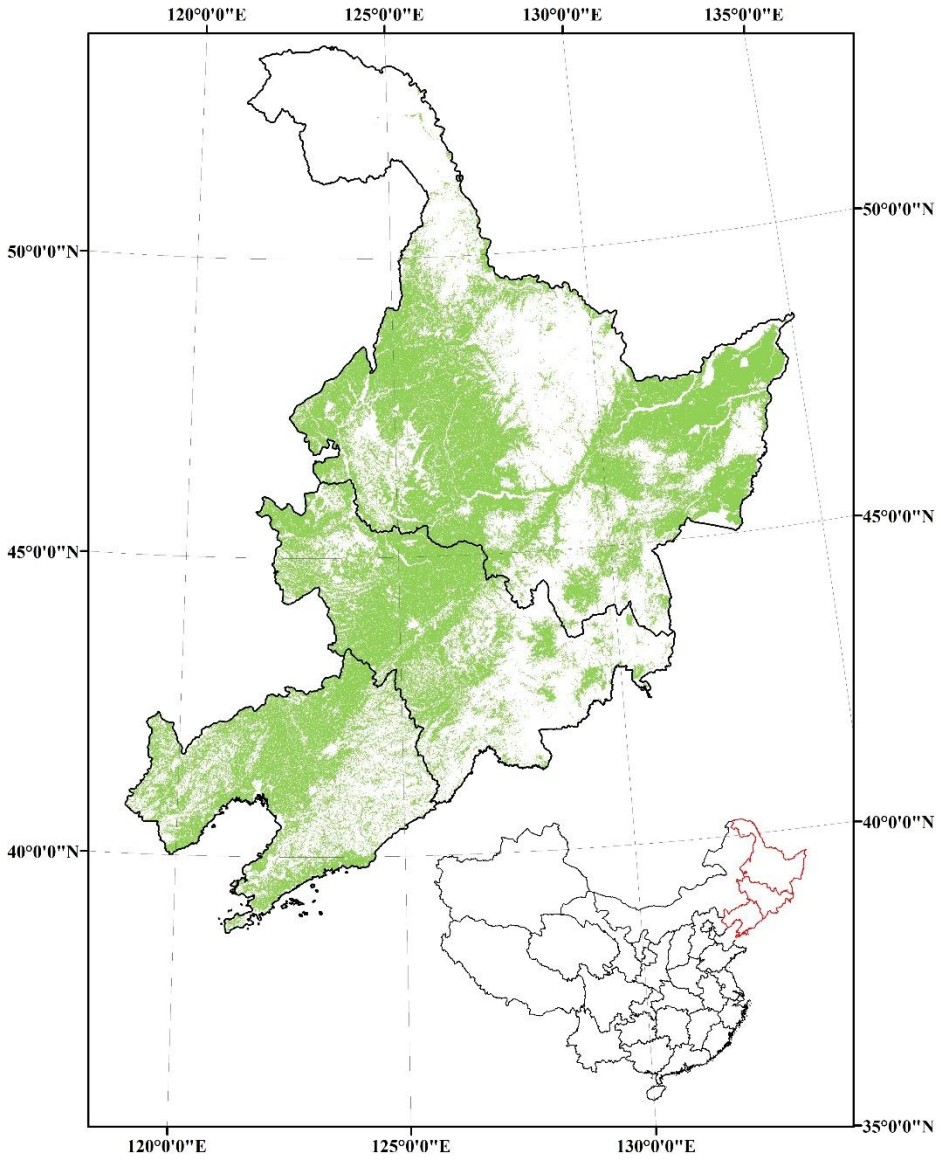

Figure 30 Cultivated land map extracted from GlobeLand30 of Northeast China.

6.3.2 Census data

Agricultural census data of sowing area were derived from the statistical yearbooks of Heilongjiang, Jilin, and Liaoning Provinces from 2007 to 2011, to evaluate the rice maps. In China, the administrative levels from large to small are provincial level, prefectural level, county level, township level, and the smallest is village level. The statistical yearbooks are published officially by provincial governments, gathering from the statistics done by governments from prefectural level to county

level. In the yearbooks, for Heilongjiang and Liaoning Provinces, only prefectural level data were available, while for Jilin Province, both prefectural level and county level data were available. In summary, there were 36 prefectures in northeast China, including 13 in Heilongjiang Province, 9 in Jilin Province, and 14 in Liaoning Province; and there are 50 counties in Jilin Province (Figure **35**).

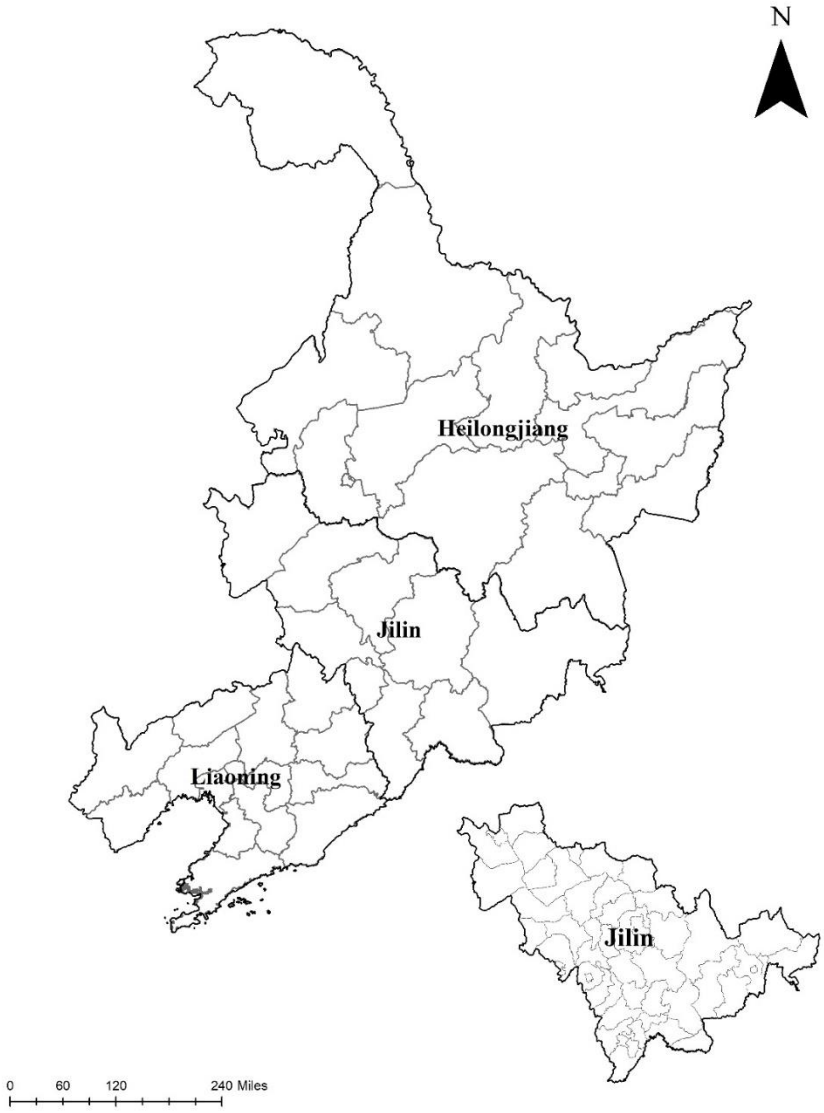

Figure 31 Northeast China administrative regions map.

6.3.3 The National Land Cover Dataset (NLCD)

The National Land Cover Dataset (NLCD) for China was developed by the Chinese Academy of Sciences in the late 1980s, and updated in 1995, 2000, 2005, and 2010 (Liu et al. 2014). The dataset was generated through human-computer interactive

interpolation of Landsat Thematic Mapper ™ and Enhanced Thematic Mapper (ETM+) images, with supplemental data from the Chinese Huanjing-1 satellite (HJ-1). Six major land cover categories (cropland, woodland, grassland, water body, built-up land, and unused land) and 25 subclasses were contained in the dataset, with specific classes of "paddy cropland" (mainly used for planting paddy rice) and "dry cropland" (for upland crops). The acquired 2010 NLCD dataset was in 1 km spatial resolution, and in northeast China, there was a total area of 4.6×10^4 km^2 of paddy cropland in the three provinces (Figure **32**). The "paddy cropland" class in the NLCD 2010 dataset was extracted for comparing with the rice maps derived from MTCI and MODIS data.

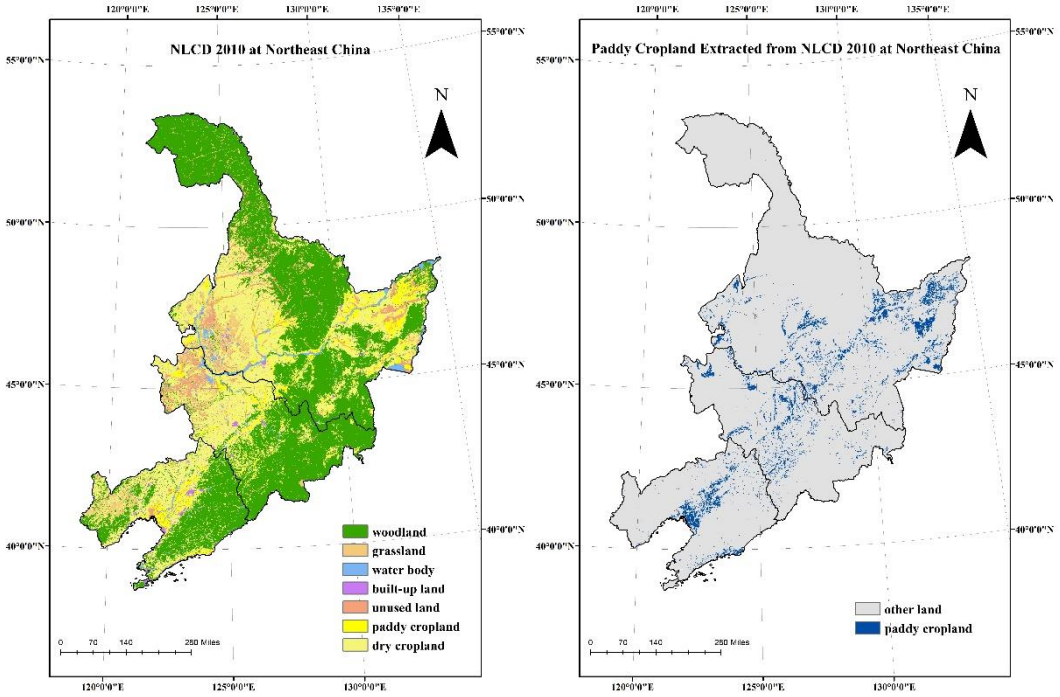

Figure 32 The National Land Cover Dataset (NLCD) 2010 in northeast China in the three provinces and the derived paddy cropland distribution.

Province	Paddy Cropland Area (km^2)	Percentage
Heilongjiang	26060	55.65
Jilin	11102	23.71
Liaoning	9667	20.64
Total	46828	

Table 7 Summary of paddy cropland area in three northeast China provinces and percentage, calculated from NLCD 2010.

6.4 Method

Figure **33** shows a flowchart that describes the complete processing chain. There were two main steps for identifying paddy rice in northeast China: (1) data preparation. Two vegetation indices (EVI and LSWI) were calculated from MODIS 500 m data, after the raw MOD09A1 MODIS surface reflectance data tiles were mosaicked and re-projected. To use the MTCI data and MODIS data together, all vegetation indices data were processed into the same bands and data value range; (2) conduct a vegetation indices analysis based on the characteristic that the paddy fields are flooded during transplanting period, to identify paddy rice fields in the three provinces, in northeast China.

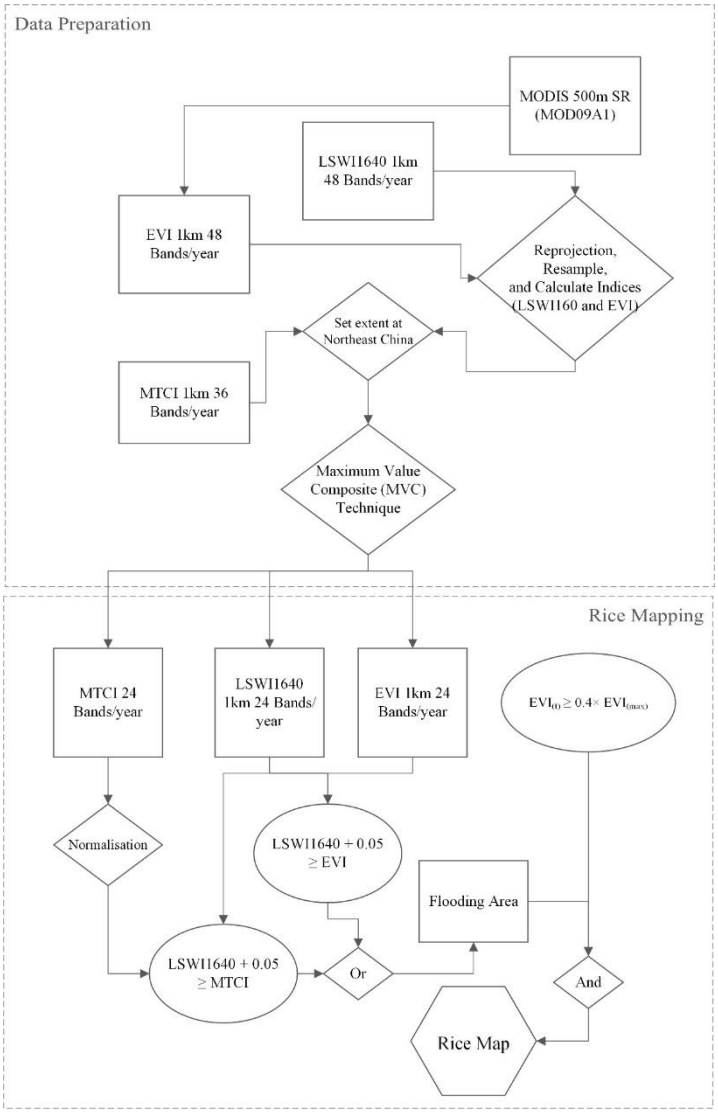

Figure 33 Workflow for mapping paddy rice distribution in northeast China using MODIS and MTCI data.

6.4.1 Remote sensing data pre-processing

Based on Xiao et al.'s researches (2006; 2002; 2005) many studies had been conducted. MODIS surface reflectance data or Landsat high resolution data were used and the same principle with more or less modifications or improvements were adopted, such as additional condition, different threshold, and different LSWI ($LSWI_{2130}$) (Jin et al. 2015; Qiu et al. 2015; Shi et al. 2013; Sun et al. 2009; Zhang et al. 2015a; Zhou et al. 2016). It is the first time to use the MERIS Terrestrial Chlorophyll Index (MTCI) instead of the Normalised Difference Vegetation Index (NDVI), because MTCI has proved abilities of detecting vegetation growing phenology and an advance in high biomass situation, where the NDVI saturates (Dash et al. 2010b). Moreover, the MTCI also has another advantage for detecting paddy rice growing. Before transplanting the soil needs to be prepared by plowing, overturning, flooding, and levelling (Jin et al. 2015), at this phase there is barely green covers on the rice fields. Therefore, the MTCI value is extremely low or equal to zero, which is the biggest difference from the NDVI. After that, from transplanting phase, the MTCI signal shows a similar pattern with the NDVI (Figure **34**). However, the MTCI 1km dataset have a 10-day temporal resolution; while MODIS surface reflectance data have an 8-day interval. To replace MODIS NDVI with MERIS MTCI, then it was very necessary to resample their temporal resolution into a same number of bands through one year. The Maximum Value Composite (MVC) method was applied to capture the max value for every two bands and finally, both MERIS and MODIS dataset were converted to 24 bands a year. Meanwhile, the raw data were cleaned by replacing the missing values with the larger ones with a window of two valid values. After that, another fact needed to be considered which was the value range of the MTCI is from 0 to 6 (values usually range from 1 to 4 for rice), while values of EVI and LSWI are within 0 to 1. Therefore, the easiest way to solve the problem was to apply a normalisation for the MTCI data in each pixel within a time-series by using the following equation:

$$x_{new} = \frac{x - x_{min}}{x_{max} - x_{min}} \quad (10)$$

Where x is the value of one date within the time-series of MTCI, x_{min}, x_{max} is the minimum value and maximum value of a set of time-series data, in another word

they are the minimum and maximum values for one MTCI pixel of the year.

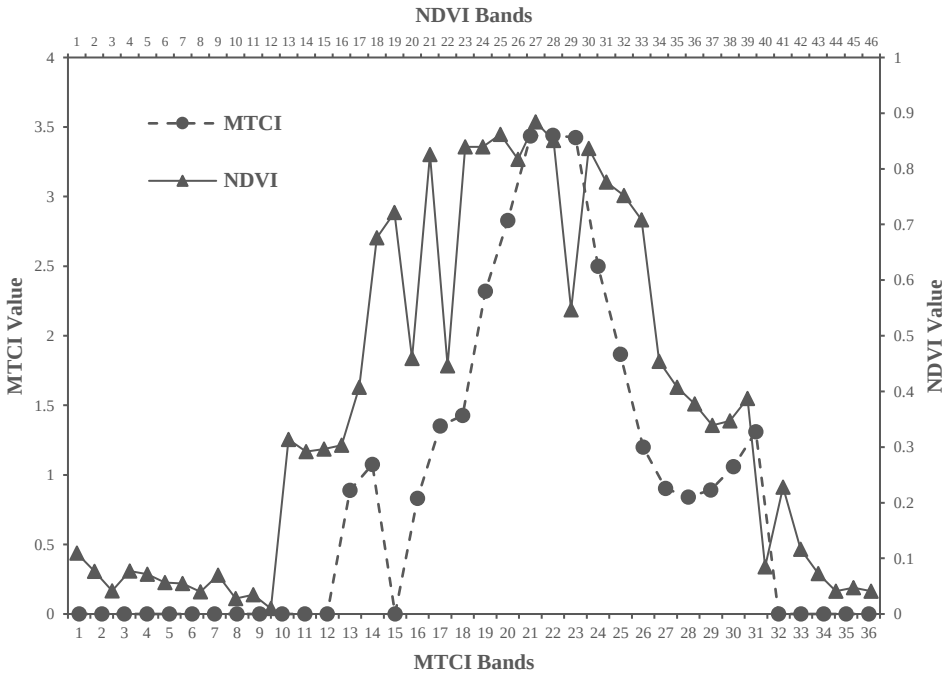

Figure 34 An example of 8-day MODIS NDVI (46 bands) and 10-day MTCI (36 bands). NDVI valid values ranging from 0 to 1 and MTCI valid values ranging from 1 to 6 (zeros from the beginning of the year till transplanting include snow cover and land preparation period).

Replacing NDVI with MTCI in phenology based multi indices method; Figure **35** shows the result of the temporal conversion for one sample point of paddy rice. It can be seen from the line plots that after applying the Maximum Value Composite (MVC) technique, 24 bands time-series can clearly represent the changes, i.e. the start and end of the season, and retains the similar patterns from the original data, which is significant for keeping the accuracy from original data. The different place is that the 24-band has a smoother profile with less fluctuation between values. However, the timing of inflection points within the growing season stay around the similar dates, which correctly represent the development of paddy rice growth.

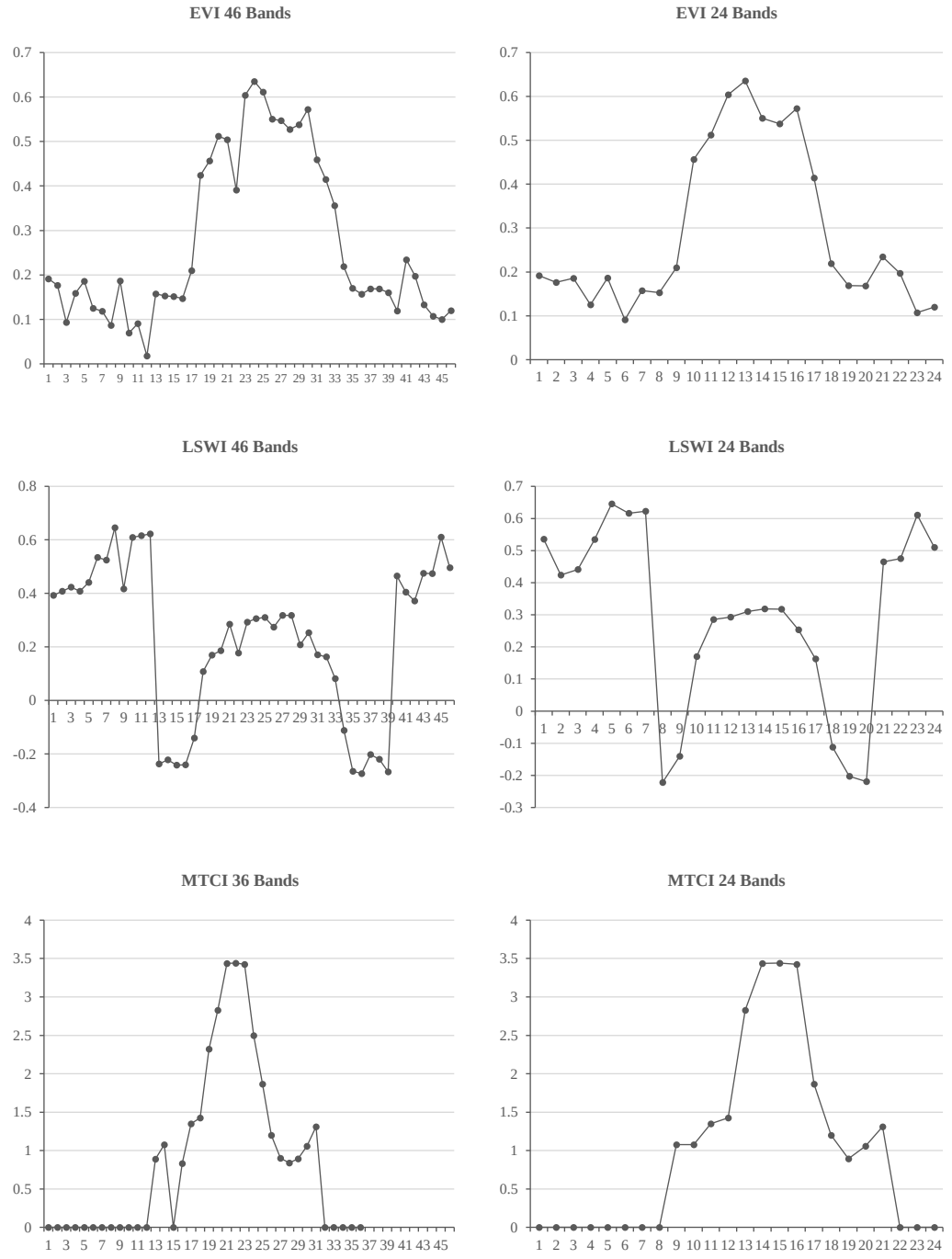

Figure 35 Temporal resolution conversion by Maximum Value Composite (MVC) technique. The left three are original 8-day MODIS (46 bands/year) and 10-day MTCI data (36 bands/year), the right three are converted time-series data with 24 bands/year for both MODIS and MTCI.

In order to be integrated with EVI and LSWI, MTCI values were normalised into the range of 0 to 1, Figure **36** shows the plots for the average values from 56 sample fields of paddy rice in Sanjiang Plain in 2011. It can be indicated from the plots that after applying the normalisation, 24 bands time-series MTCI still stayed in its shape

and all the significant break points remained. Therefore, the normalisation process was feasible and necessary.

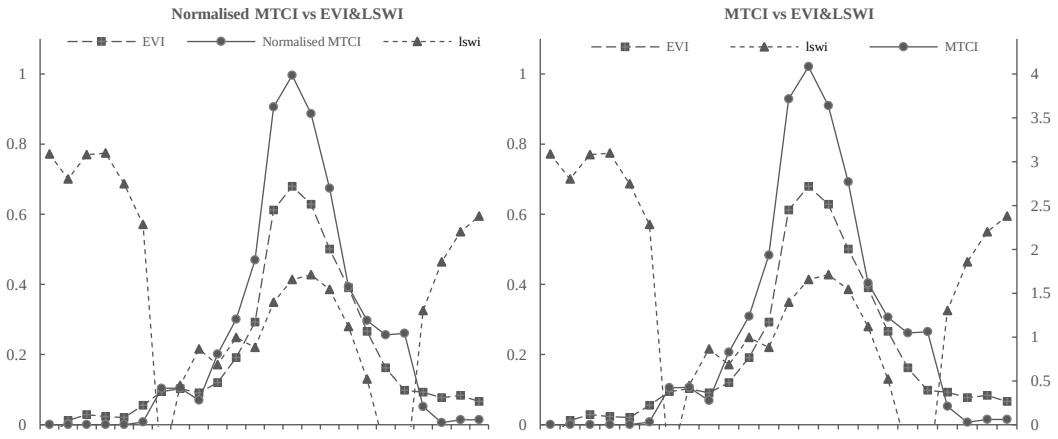

Figure 36 Normalised MTCI and original MTCI together with EVI and LSWI to show paddy rice growth pattern from 56 sample fields in Sanjiang Plain in 2011.

6.4.2 Algorithms for identifying paddy rice fields

Figure **37** shows the cropping calendar for northeast China and Figure **38** shows the average changes of three VIs within one-year period, from 56 sample points in Sanjiang Plain. Starting from February the LSWI value shows a dramatic decrease until late March, which is because of the snow melting during the spring; after that, the LSWI rapidly increased for about 4 months during the growing period. In late to early June rice seedlings are transplanted to flooded paddies with a water depth of 2 to 15 cm until about one week before harvest. During the transplanting period the paddy fields are mostly dominated by water, hence within the period LSWI values are usually larger than NDVI and MTCI values, shown in Figure **38**, framed part. From mid-June to early July, rice grows rapidly during the vegetation growing phase (tillering and stem elongation), and the canopies may cover most of the paddy fields about 50 to 60 days after transplanting (2006; Xiao et al. 2005). During this period, NDVI and MTCI values are increasing rapidly and larger than LSWI values. In late July, the vegetation-to-water ratio reaches its maximum and then remains stable or slightly decreases during the ripening period (NDVI, MTCI, and LSWI values reach their maximums), which is the last stage of rice growth prior to harvesting. The moisture in both the paddy fields and leaf and stem start to decreases in ripening stage, and the number of green leaves decreases as well.

Therefore, the suitable timing for identifying paddy fields should be in the early flooding period before the fields are fully covered by the canopies.

April			May			June			July			August			September			October	
Early	Mid	Late	Early	Mid	Late	Early	Mid	Late	Early	Mid	Late	Early	Mid	Late	Early	Mid	Late	Early	Mid
		Transplanting				Growing			Reproductive			Ripening					Harvest		

Figure 37 Rice cropping calendar in northeast China area.

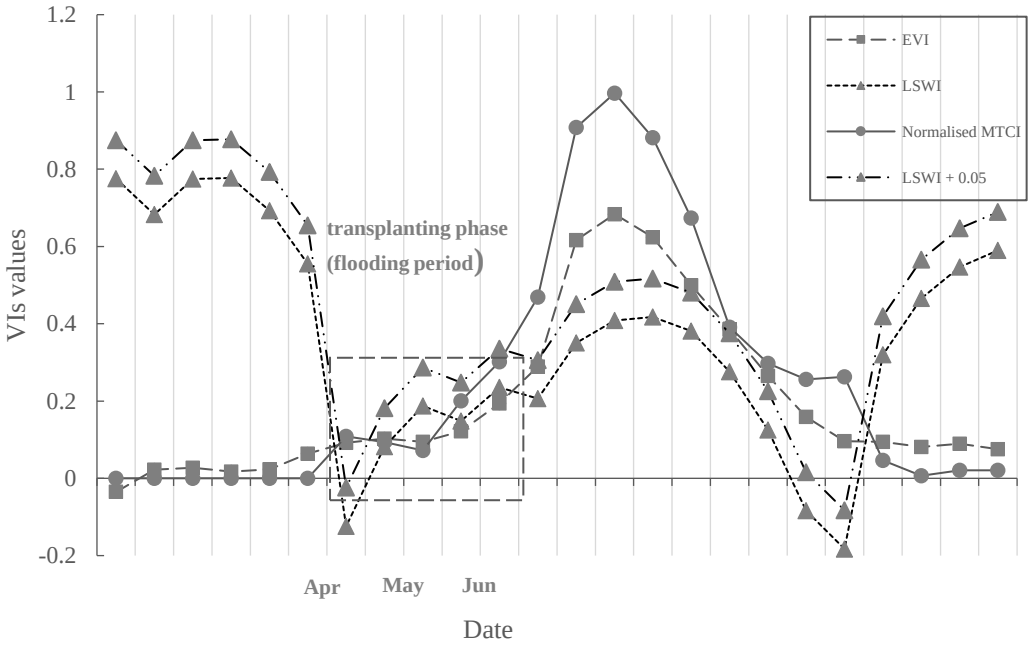

Figure 38 An average seasonal dynamic of normalised MERIS Terrestrial Chlorophyll Index (MTCI), the Enhanced Vegetation Index (EVI), and the Land Surface Water Index (LSWI) at 96 sample GPS points in three provinces, northeast China.

Step **1** With the purpose of detecting significant water content changes during the transplanting period in paddy rice fields with MODIS surface reflectance data, two spectral indices namely, EVI and $LSWI_{1640}$ were calculated using the following equations:

$$\boldsymbol{EVI = 2.5 \times \frac{NIR-Red}{NIR+6\times Red-7.5\times Blue+1} = 2.5 \times \frac{Band2-Band1}{Band2+6\times Band1-7.5\times Band3+1}} \quad (11)$$

$$\boldsymbol{LSWI_{1640} = \frac{NIR-SWIR_{1640}}{NIR+SWIR_{1640}} = \frac{Band2-Band6}{Band2+Band6}} \quad (12)$$

Step **2** Simple conditions were used for identifying paddy fields in the studies of Xiao et al. (2006; 2005), which were based on the situation that water content in the paddy fields is much higher than the vegetation coverage at the earlier stage of rice transplanting ($LSWI \geq EVI\ or\ NDVI$), and to reconcile the differences in planting schedules (commonly one to two weeks), LSWI was slightly relaxed with a value of 0.05 (LSWI can reach around 0.2 from zero within two months from late April to early June, during the transplanting period, therefore, average LSWI value is 0.05 for two weeks):

$$\boldsymbol{LSWI_{1640} + 0.05 \geq EVI} \ \textbf{Or} \ \boldsymbol{LSWI_{1640} + 0.05 \geq NDVI} \quad (13)$$

According to Sun et al. (2009), within two to four 8-day MODIS composites significant differences can be captured by optical sensors. Xiao et al. (2006; 2005) and Wang et al. (2015) indicated that the EVI value of a true rice pixel reaches over half of the maximum EVI value within five 8-day MODIS composites (40 days) following the date of flooding and transplanting. Therefore, EVI value reaches its maximum value within five 8-day composites after transplanting was used as additional condition for identifying paddy rice:

$$\boldsymbol{EVI_t > 0.5 \times EVI_{max}} \quad (14)$$

In this study, the same principles were adopted with a slight change of the EVI condition and the replacement of MODIS NDVI by MTCI. Because of the comparison between the 8-day MODIS and 10-day MERIS data, the time-series data were transformed from 46 bands to 24 bands through a year. Therefore, the corresponding date of the growing period could be slightly advanced, hence a lower threshold was applied (0.4):

$$\boldsymbol{LSWI_{1640} + 0.05 \geq EVI} \ \text{Or} \ \boldsymbol{LSWI_{1640} + 0.05 \geq MTCI} \quad (15)$$

$$\boldsymbol{EVI_t > 0.4 \times EVI_{max}} \quad (16)$$

Step **3** To prevent unexpected interference from wetlands, seasonal flooding area and so on, GlobeLand30 land cover map was used to exclude the non-agricultural area in northeast China. The method could not be applied to double or triple cropping system areas. However, in northeast China, there is only one growing season through the year.

6.5 Results

6.5.1 Temporal-spatial distribution of paddy rice in northeast China from remote sensing derived rice map

Figure **40** shows the paddy rice maps derived from MTCI and MODIS data from 2007 to 2011. Paddy rice fields are distributed across three provinces, and the paddy fields were distributed mainly at two major alluvial plains: Sanjiang Plain, locates in northeastern Heilongjiang, where is developed by three major rivers of Heilongjiang River, Songhua River, and Ussuri River; and Liaohe Plain locates in the central part of Liaoning Province, where the Liao River flows through. Most paddy rice fields locate at where has an elevation of less than 200 m, except some fields found in the mountainous region in Jilin Province with an elevation around 600 m. Also, it can be noticed that Heilongjiang Province had the largest area of paddy rice fields.

The planting area of paddy rice increased each year according to the official statistical yearbook. The inter-annual variation of MTCI and MODIS derived paddy rice fields area generally was consistent with the agricultural census data with a slightly larger count of planting area, except for the year 2009, shown in Figure **39**. According to the State of the Climate in 2009: Special Supplement to the "Bulletin of the American Meteorological Society" (Vol.91, No.6, June 2010), the year 2009 was the fourth driest year since 1951 and the driest year since 1987. Severe drought happened in China in 2009. From April to May Heilongjiang Province suffered severe spring drought impact, while severe summer and autumn drought took place in Liaoning and Jilin Provinces from late June to early November. Hence, the map derived from remotely sensed data correctly reflected the paddy cropland during drought. However, the official agricultural record of the year 2009 was about sowing area, which was not capable of reflecting the drought.

The overall increase of paddy rice field area in northeast China, derived from remote sensing data and census data, were 117200 km^2 and 121625 km^2 from 2007 to 2011, respectively. It can be observed from Figure **40** that most of the increase of planting area occurred at the east of Heilongjiang Province where the Sanjiang Plain is, characterised by enhanced agricultural irrigated infrastructure and high

mechanisation. The slopes of remote sensing derived data and agricultural census data were 2774 km^2 $year^{-1}$ and 2989 km^2 $year^{-1}$ respectively, that is almost 3000 km^2 $year^{-1}$. To sum up, the results demonstrated that through time remotely sensed data processing for paddy rice field detection could be used as a valid monitoring tool for detecting the paddy rice planting area and evaluating the variation between years at large scales with low cost and high efficiency.

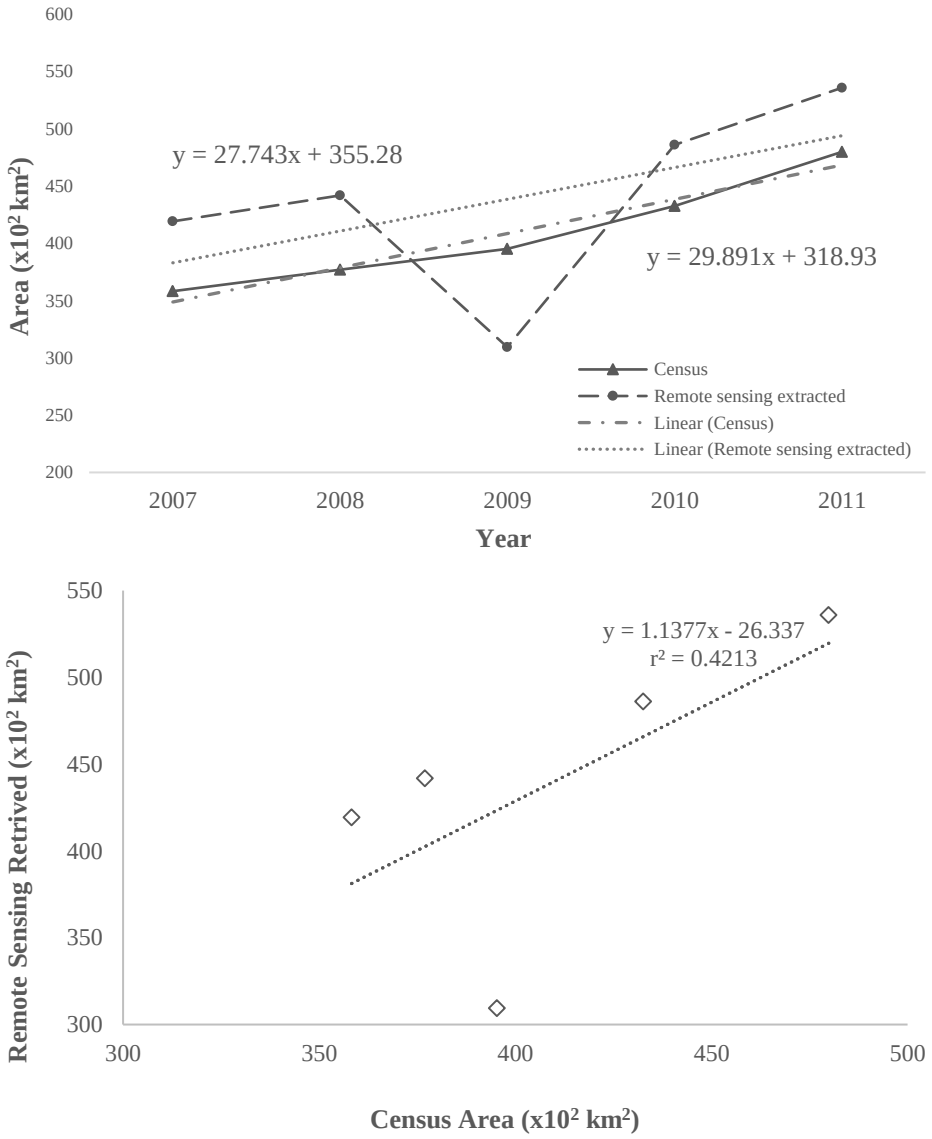

Figure 39 Above plot is the inter-annual variation of the paddy rice growing area derived from MTCI and MODIS data and agricultural census data of sowing area in northeast China three provinces. Below is the comparison between the paddy rice growing area derived from MTCI and MODIS data, and agricultural census data of sowing area during the year 2007 to 2011.

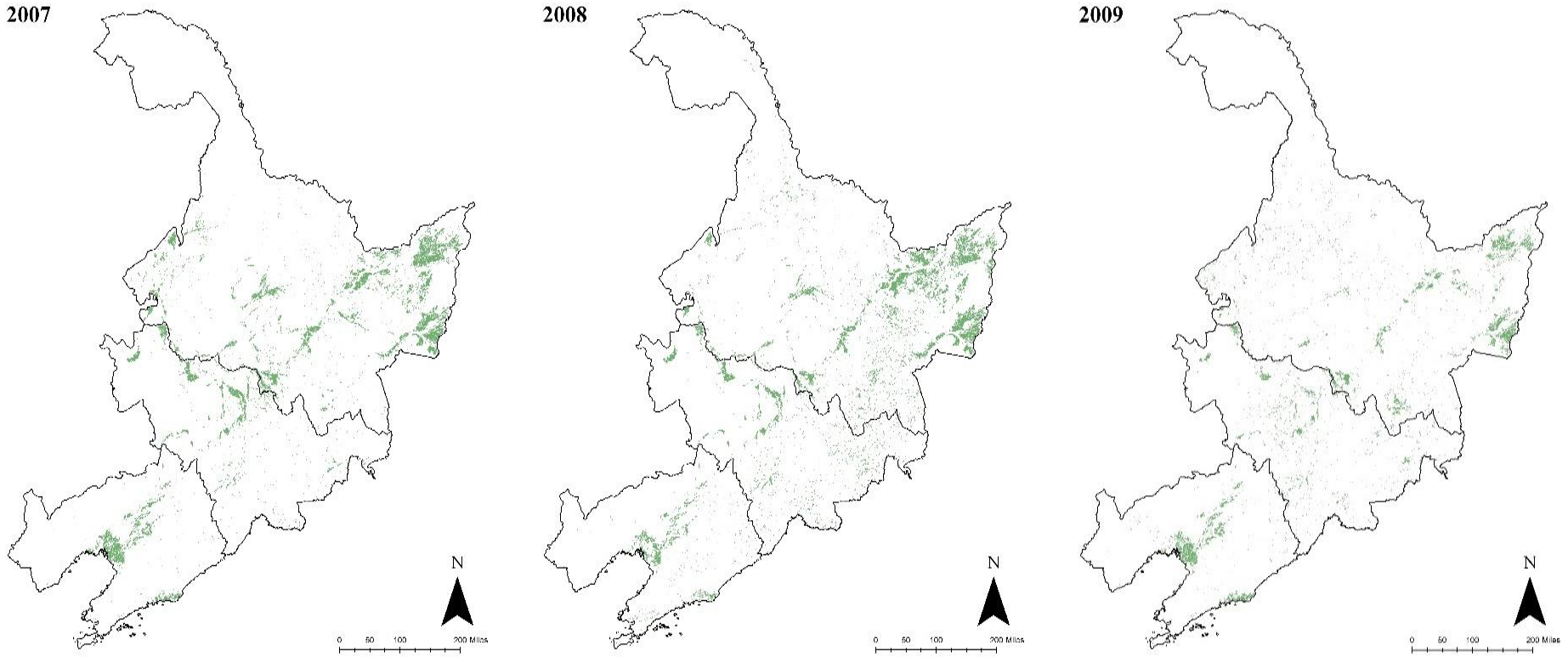
2007
N
0 50 100 200 Miles
2008
N
0 50 100 200 Miles
2009
N
0 50 100 200 Miles

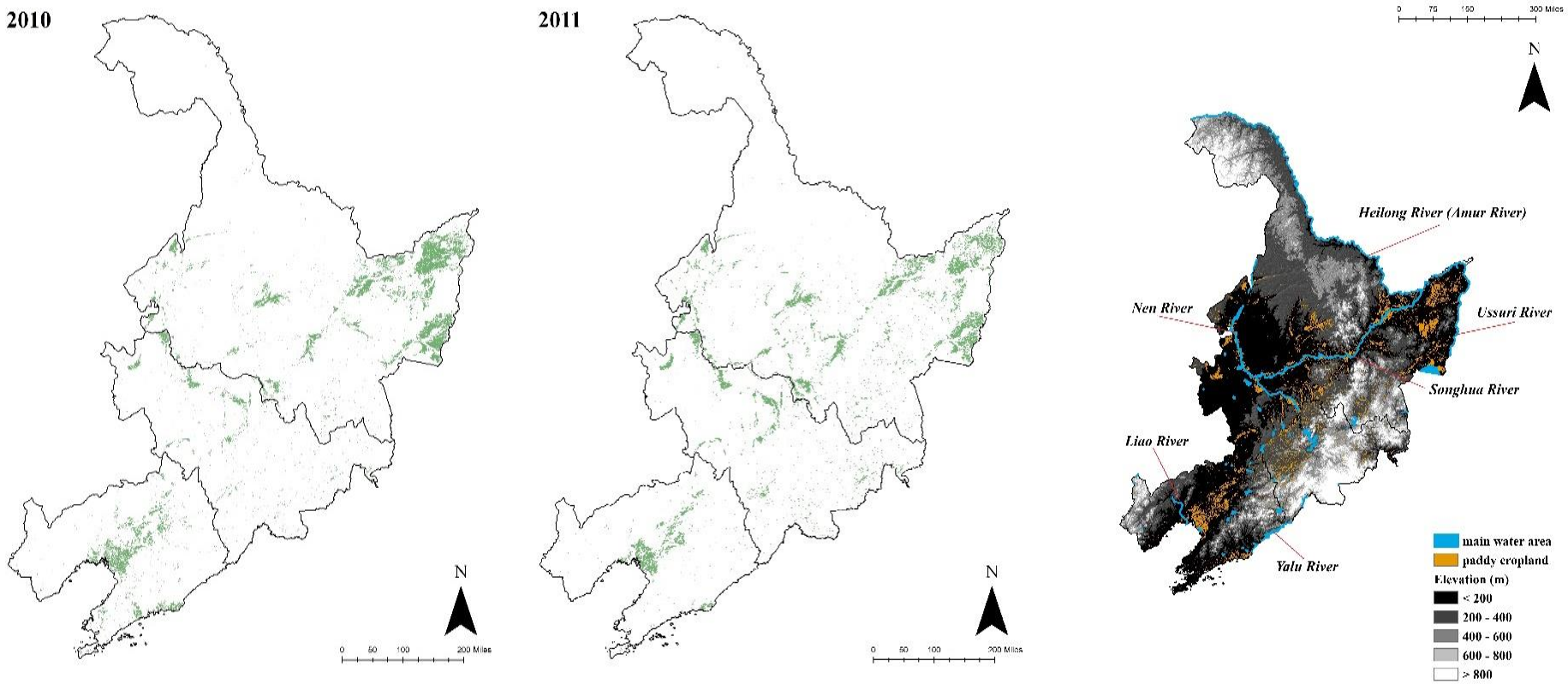

Figure 40 Spatial distribution of paddy rice in northeast China derived from MTCI and MODIS data from 2003 to 2011 and the main river areas along with paddy cropland extracted from NLCD 2010.

6.5.2 Comparison between the paddy rice maps derived from MTCI and MODIS data and the NLCD 2010 data.

The rice map for 2010 for comparison with the NLCD 2010 data. In general, there are several marked differences at the provincial level shown in Table **8**: the rice maps derived from the MTCI and MODIS data detected similar areas of paddy rice fields in Heilongjiang Province (5.21% vs 5.89%) and in Liaoning Province (6.01% vs 6.61%), but less paddy rice fields in Jilin Province (2.49% vs 5.64%), compared with the NLCD 2010 dataset. However, in Heilongjiang Province, it can be seen from Figure **40** that more paddy rice fields were identified, mainly located at Sanjiang Plain from remote sensing derived rice maps compared with the NLCD 2010. By correlating with Google Earth for inspection, most of them were correct. While the NLCD 2010 had more scattered fields located at other places; In Jilin Province, the inconsistencies with the NLCD 2010 were identified mainly located in mountainous areas with an elevation around 600 m, which can be attributed to smaller scale farming than in the plains with low elevation, leading to an underestimation by remote sensing data with a larger spatial resolution, 1 km in this case, while the NLCD 2010 was based on 30m fine-resolution Landsat and HJ-1 data.

Provinces	Rice_Results	Total Counts_Results	%_Results	Rice_NLCD	Total Counts_NLCD	%_NLCD
Heilongjiang	35533	681976	5.21	40146	681718	5.89
Jilin	6668	267583	2.49	15088	267508	5.64
Liaoning	11813	196686	6.01	12986	196331	6.61
Total	54014	1146245	4.71	68220	1145557	5.96

Table 8 Summary of paddy rice field pixels distribution and percentage within the areas, both datasets were in same spatial resolution.

At prefectural level, a comparison between the MTCI and MODIS data derived rice map of 2010 and the NLCD 2010 extracted rice map was conducted, the result was shown in Figure **41**. The counts of paddy rice field pixels were calculated by zonal statistics for the 36 prefectures in northeast China. The result demonstrated MTCI and MODIS data derived rice map had a large correlation with the NLCD 2010 dataset, with r^2=0.8148 and *RMSE*=464 (n=36).

At county level in Jilin Province, for the 50 counties under 8 prefectural units, the same zonal statistics were conducted. It can be seen from Figure **41** that the MTCI and MODIS derived rice map had a moderate linear correlation with the NLCD 2010, with r^2=0.6324 and *RMSE*=108 (*n*=50).

The distribution of paddy rice derived from MTCI and MODIS data, validating with NLCD 2010 dataset, implied the combined conditions method for mapping paddy rice fields at northeast China performed accurately, based on the large linear correlations with the NLCD 2010 dataset at both the prefectural and county levels, given the coarse spatial resolution of 1 km relative to the size of the paddy rice fields.

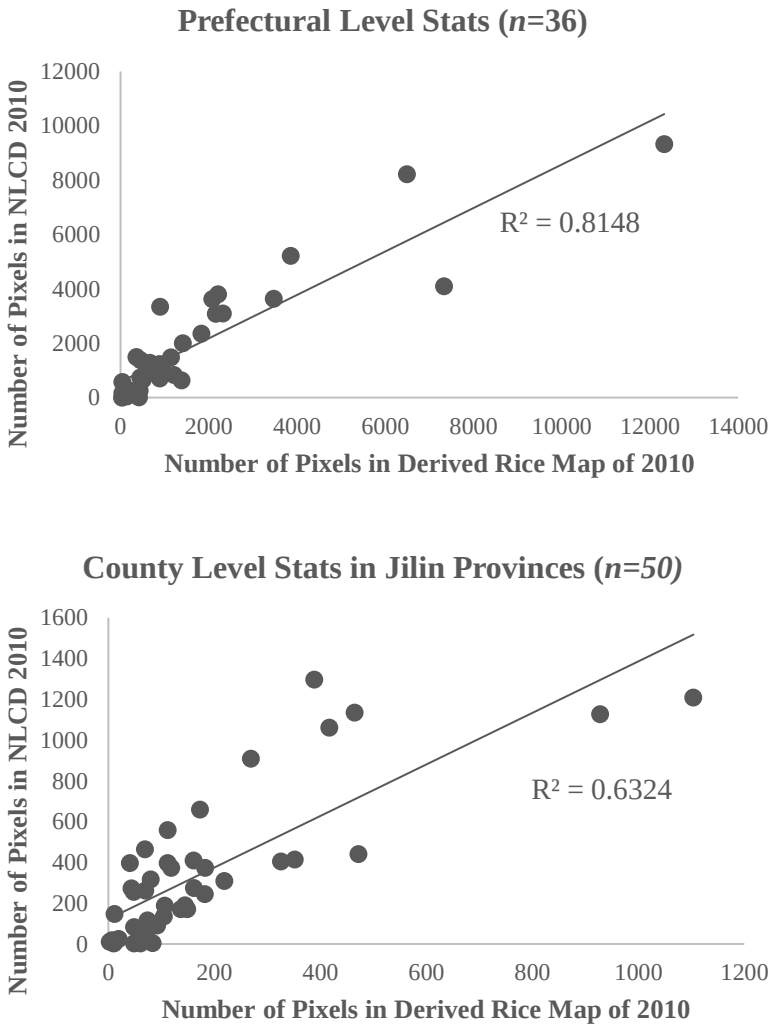

Figure 41 Prefectural and county level quantitative comparison of pixels identified as paddy rice fields in northeast China and Jilin Province respectively.

6.5.3 Validation of remote sensing derived rice planting area with census data.

The MTCI and MODIS derived paddy rice map of 2010 was compared with census data acquired from National Bureau of Statistics of China (NBSC), at both prefectural levels for all three provinces in northeast China, and at the county level for Jilin Province. In Figure **42**, the results exhibited a linear correlation between remote sensing derived paddy rice field area and census records with r^2=0.5524, *RMSE*=628 km^2 (*n*=36); and at the county level, it returned the r^2=0.5134, and *RMSE*=119 km^2 (*n*=50). Comparing with the consistency between the NLCD 2010 data and census records, it showed a slightly more accurate result than the MTCI and MODIS derived rice map.

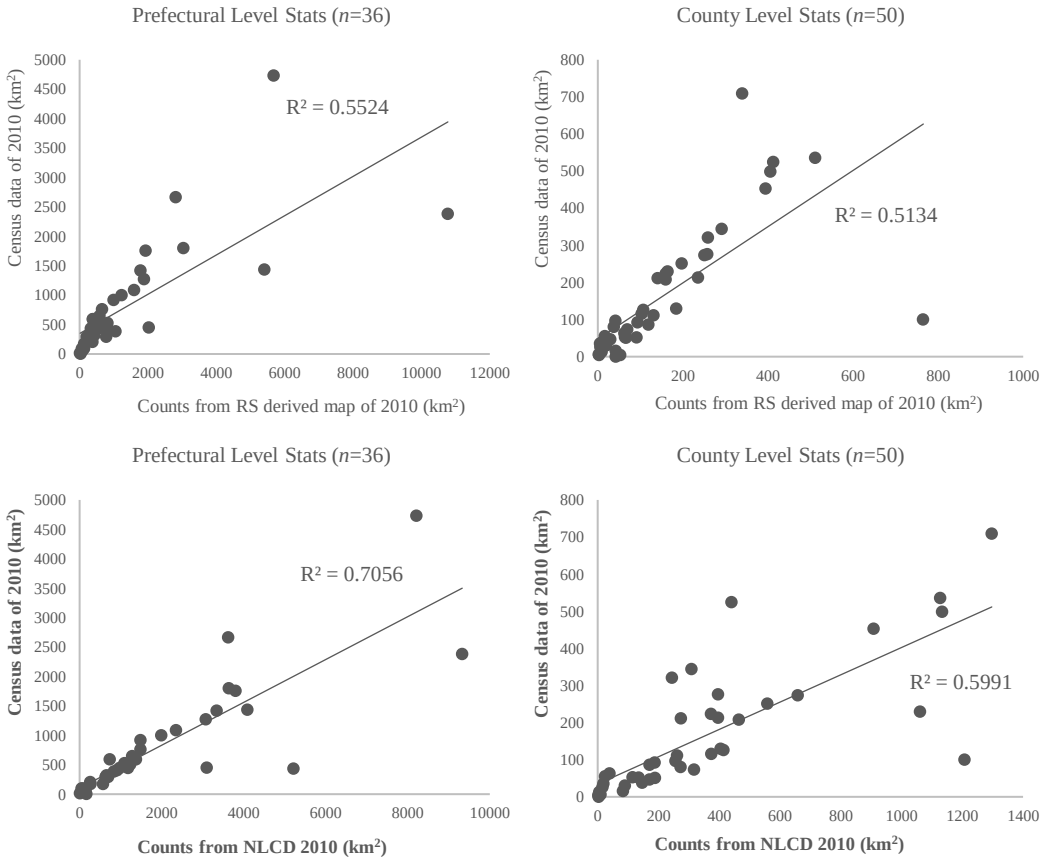

Figure 42 Prefectural and county level quantitative comparison of the area of paddy rice fields in Jilin Province.

6.6 Discussion

A number of studies were conducted based on machine learning techniques

including support vector machine classifier classification (SVM), the random forest (RF), and other clustering analysis (Hao et al. 2016; Hu et al. 2017; Zhang et al. 2017; Zhang et al. 2008; Zhong et al. 2016). However, these machine learning methods are limited to the quantity and quality of sample points, which can be time-consuming and high cost (Černá and Chytrý 2005; Kussul et al. 2017; Zhang et al. 2008), while the vegetation indices profiles analysis overcomes the disadvantages.

In this study based on the physical feature of paddy rice, a vegetation index profiles analysis was employed to identify paddy rice fields at a large scale. This method takes advantages of the flooding paddy fields and open canopy characteristics during rice transplanting period (Jin et al. 2015; Shi et al. 2013; Xiao et al. 2006), by analysing the different behaviours of three indices including MTCI, EVI, and LSWI, to separate paddy rice fields from other croplands with no flooding period. Rice maps derived from MTCI and MODIS data showed good consistency with both the NLCD 2010 and the census data from three provinces statistical yearbooks. However, several factors can affect the process of identifying paddy rice by analysing vegetation indices profiles. The first factor is the use of MTCI instead of MODIS NDVI comparing to other similar studies. The mixing use of indices derived from different satellite sensors introduces the problem of handling different spatial and temporal resolutions. For resampling the temporal resolution to the same time interval, the MVC technique was applied. However, from the before and after profiles comparison, it can be noticed that some details were lost, although the inflection points and general patterns were kept. It has a possibility that the rice distribution is overestimated or underestimated. The second factor is related to MTCI and MODIS datasets. The MODIS 8-day dataset was generated by selecting the value for each pixel from all the acquisitions within the 8-day composite period, with the minimum blue band value, in another word, the clearest atmosphere condition with least cloud coverage (LPDAAC, USGS); while the MTCI is generated by calculating the mean value for each pixel within every time interval (Dash et al. 2007). The compositing method could mean that some observations are omitted which can affect the identification of flooding paddy fields during the transplanting period. Although MODIS daily data are available and free to obtain, the problem with data redundancy and a higher rate of cloud contamination must

be considered (Williamson et al. 2012). The 5-day Sentinel-2 dataset is also worth considering, which has a shorter revisit cycle than MERIS and MODIS. But the Sentinel-2 satellites were launched in 2015, which means a lack of data for long-term observations and studies at the moment. The third factor is the spatial resolution of the dataset. MTCI has a spatial resolution of 1 km, therefore, 500 m spatial resolution MODIS derived vegetation indices need to be resampled, as well as the GlobLand30 land cover map (30 m). Moreover, in China most farmers do not have much land (1 km is probably covered too much for farmland) (Chen et al. 2011), both of which could result in overestimating or underestimating. Thus, finer spatial and temporal resolution input data may be much more suitable and helpful for mapping paddy rice in China. The Sentinel-2 satellites (Sentinel-2A and Sentinel-2B) carry a single multi-spectral instrument (MSI) with 13 spectral channels in the visible/near-infrared (VNIR) and shortwave infrared spectral range (SWIR) (Figure **43**), and the data are free for download from https://sentinel.esa.int/. Therefore, the algorithm in this chapter can be fully applied to Sentinel-2 data. With time, the increasing amount of Sentinel data can be applied to more situations.

Spatial Resolution	**Band Number**	**Bands**	**S2A**	**S2B**
(m)			**Central Wavelength (nm)**	**Central Wavelength (nm)**
10	2	Blue	496.6	492.1
	3	Green	560	559
	4	Red	664.5	665
	8	Red Edge	835.1	833
20	5	Red Edge	703.9	703.8
	6	Red Edge	740.2	739.1
	7	NIR	782.5	779.7
	8a	Narrow NIR	864.8	864
	11	SWIR	1613.7	1610.4
	12	SWIR	2202.4	2185.7
60	1	Coastal aerosol	443.9	442.3
	9	Water vapour	945	943.2
	10	SWIR	1373.5	1376.9

Figure 43 Wavelengths and bandwidths of the three spatial resolutions of the multi-spectral instrument (MSI). (https://sentinel.esa.int/web/sentinel/missions/sentinel-2/instrument-payload/resolution-and-swath)

The last factor is the that vegetation indices analysis method, which was originally proposed by Xiao et al. (2005), contains only three vegetation indices. Bringing in additional variables could increase the accuracy of rice mapping. For example, Zhang et al. (2015a) and Zhou et al. (2016) adopted the same condition of LSWI and EVI for detecting flooding area, and also utilised night temperature data from the MODIS land surface temperature product to set rules for detecting the flooding and transplanting period, based on the fact that a stable temperature is needed for the occurrence of rice transplanting. In addition to all the above factors, slope was not taken into consideration, which might lead to underestimation of paddy rice area in mountainous regions.

Although there are some uncertainties in the processing of paddy rice identification, still, MTCI and MODIS indices are reasonable choices for the advantages of coverage, moderate time interval, and availability, to monitor paddy rice distribution over a long period. Moreover, the MTCI has a strength of clearly marking the growing season in the cold region such as northeast China which has snow cover in the winter (MTCI≤0).

6.7 Conclusion

Monitoring paddy rice distribution is important for studies of yield prediction, food security assessment, water resource management, and methane emission assessment (Jin et al. 2015). Using remote sensing data to monitor the spatial extent of paddy rice planting area at large scale is low cost and efficient. This chapter demonstrated the ability to use phenology profiles derived from different indices in regional scale paddy rice identification and tested the performance of MTCI in detecting rice phenological spectral features. Future studies should adopt finer temporal and spatial resolution satellite sensors data to extract phenology profiles, such as Sentinel-2, which can calculate MTCI, EVI, and LSWI together. Further, additional variables and conditions can be added for rice field identification when applying the methodology in the multi-cropping area such as southern China.

7.Use of Phenological Variables to Forecast Rice Yield

7.1 Background

Paddy rice is one of the most important and widely grown crops in China. The total rice production in 2016 reached 207.1 million tonnes, and it accounts for 36.6% of the total grain production in China (565.4 million tonnes), according to China statistical yearbook of 2017. As China's huge population keeps growing, China has to meet the food demand by improving 14% of the rice production by 2030, reported by Cheng et al. (2007).

Timely and accurate estimation of rice crop yield prior to harvest is crucial, especially in the regions with uncertain climatic characteristics. Well forecasted crop yield will help farming planners and decision makers to plan harvest, storage, and prepare for food import or export in case of any shortfall or surplus (Huang et al. 2013). Therefore, paddy rice yield estimation is important for the food security of China. There are many conventional methods for estimating crop yield, which can be divided into two categories: empirical-statistical models and crop growth models (Jørgensen 1994). Empirical-statistical models usually adopted effective environmental factors such as temperature, solar radiation, and precipitation, to relate with annual crop yield records by an empirical equation, to estimate the coefficient for each factor. With the coefficients, crop yield can be forecasted. Crop growth models are normally based on the physiological processes between crops and environment, to estimate biomass production by simulating daily crop growth.

These conventional methods for predicting crop yield are based on a collection of ground or experimental data, which is time-consuming, labour-intensive, and sometimes the data become available when it is too late (Huang et al. 2013; Huang et al. 2012). Precision farming is practised in most countries in the world. However, conventional methods cannot be applied to all crop types simultaneously.

Remote sensing has been used widely for agricultural monitoring since the 1980s based on Landsat images (Tenkorang and Lowenberg-DeBoer 2008), it provides an opportunity of overcoming both spatial and temporal scaling challenges in forecasting crop yield. Therefore, satellite sensors data have been recognised as valuable resources for yield forecast. Vegetation Indices (VIs), the most common one in use being the NDVI, have been used widely in predicting crop yield, for its

close relationship to the vegetation vigour (Xue and Su 2017). A number of methods have been developed to incorporate spectral information into yield forecast, the most common approach is to develop the direct empirical relationship between the variables of vegetation indices measures and the crop yield records, using regression models. Ren et al. (2008) used 250 m MODIS-NDVI data to estimate the winter wheat in Jining, Shandong Province, China. A linear regression model was established between the accumulation of NDVI and the production of winter wheat by using a stepwise regression method at county level, and the results showed relative errors from -4.62% to 5.40% comparing the predicted yield with actual yield. Huang et al. (2013) tested 28 NDVI variables in generating a regression model with official statistical data of rice yield, by using an AVHRR NDVI dataset from 1981 to 2006. The results showed that different NDVI variables performed differently in effectiveness depending on the region, with an overall relative error of approximately 5.82%. Wang et al. (2014b) calculated five vegetation indices including Enhanced Vegetation Index (EVI), Normalised Difference Vegetation Index (NDVI), Normalised Difference Water Index (NDWI), Land Surface Water Index (LSWI), and Wide Dynamic Range Vegetation Index (WDRVI) from MODIS data to develop linear regression models with corn yield data in northeast China. LSWI showed the largest correlation with crop yield and the results demonstrated a feasible and helpful way of forecasting crop yield by phenology-tuned spectral indices. Furthermore, a range of studies found different NDVI variables and crop yields had a strong linkage at the pixel level (Huang et al. 2013). For example, original NDVI values (Labus et al. 2002; Ren et al. 2008), cumulative NDVI values during a certain period (usually through the consecutive month of the growing season or over selected critical dates) (Labus et al. 2002; Rojas 2007; Wall et al. 2008), maximum NDVI value (Benedetti and Rossini 1993; Doraiswamy and Cook 1995; Tucker et al. 1980), average NDVI values (Boken and Shaykewich 2002; Esquerdo et al. 2011; S. Mkhabela et al. 2005), and standard deviation in NDVI (Boken and Shaykewich 2002). In summary, the use of NDVI variables is in accordance with the crop conditions during the growing period, such as heading (peak phenological phase of growth) and ripening (after mid- growing season).

The red-edge position (REP) in the vegetative spectra has been applied in estimating variation of chlorophyll content during plant growing period (Almond

2009; Dash et al. 2009a; Filella and Penuelas 1994; Liu et al. 2004; Ullah et al. 2012; Zhang and Liu 2014). Many techniques such as curve fitting, determination of a derivative spectrum, Lagrangian interpolation, and linear interpolation, were employed to estimate chlorophyll content (Dash and Curran 2004). However, these techniques were designed for hyperspectral data with continuous spectral data rather than discontinuous multispectral data (Dash and Curran 2004; Zhang and Liu 2014). The Medium Resolution Imaging Spectrometer (MERIS) Terrestrial Chlorophyll Index (MTCI) was designed by Dash and Curran (2004) for the purpose of easy calculation based on standard MERIS band settings and high sensitivity to a wide range of chlorophyll contents.

In this chapter, the MERIS Terrestrial Chlorophyll Index (MTCI) was used to replace the common Normalised Difference Vegetation Index (NDVI) to evaluate the potential of estimating crop yield in the three provinces in northeast China, based on the rice maps produced in the last chapter.

7.2 Study area

The study was carried out in northeast China, mainly located in the cool temperate zone and partially located in the semi-arid zone, with an annual temperature of -3~11°C. It has a markedly continental climate with an average rainfall of 400~900 mm, concentrated during July to September, making this region the typical rain-fed farming area in China. Northeast China has many big rivers including Amur River, Songhua River, Ussuri River, Liao River, and Yalu River (Amnok River), forming alluvial plains including Songnen Plain, Liaohe Plain, and Sanjiang Plain. Accordingly, the flat topography, abundant precipitation, and fertile soils, resulting in a high production of japonica rice, account for more than 40% of the national output (Zhou et al. 2017).

7.3 Materials and method

7.3.1 Data

In this chapter, the MERIS Terrestrial Chlorophyll Index (MTCI) with 1 km spatial resolution and 10-day temporal resolution (level-3 product) was used to construct time-series data from 2007 to 2010. In addition, the NDVI was used in the study

for comparison with the MTCI. The NDVI was developed by Rouse et al. (1974), and it has been used widely for more than 40 years all over the world. NDVI is based on the difference between the leaf absorption in the red band because of chlorophyll, and the reflectance in the infrared band caused by leaf cellular structure (Zhang and Liu 2014). 8-day 500 m MODIS surface reflectance data (MOD09A1) from 2007 to 2011 were used in this chapter. Five tiles (h25v03, h26v03, h26v04, h27v04, h27v05) for covering northeast China were selected, and each tile covers an area of 1200 km × 1200 km with a sinusoidal projection. The data were downloaded from NASA's Land Processes Distributed Active Archive Centre (LPDAAC) (https://lpdaac.usgs.gov/data_access), and then the raw data were reprojected and NDVI data were calculated with band 1 (645nm) and band 2 (858nm) of the MODIS standard band settings in the meantime according to the following equation:

$$\boldsymbol{NDVI} = \frac{\boldsymbol{NIR-Red}}{\boldsymbol{NIR+Red}} = \frac{\boldsymbol{Band2-Band1}}{\boldsymbol{Band2+Band1}} \quad (17)$$

The contaminated pixels, which were generated by clouds and atmospheric noises, were removed by utilising the quality assurance (QA) band in the MOD09A1 data.

To establish a relationship between vegetation indices and yield records, it was necessary to identify areas of paddy rice fields. Therefore, rice distribution maps of three provinces in northeast China for 2007 to 2011 (Figure **44**), which were generated in the last chapter by a method of combined conditions of vegetation indices including MTCI, MODIS EVI, and MODIS $LSWI_{1640}$, were used in this chapter to mask out non-paddy rice area in northeast China.

Yield records from the statistical yearbook for three provinces in northeast China of 2007 to 2014 were acquired from National Bureau of Statistics of China (NBSC) (http://www.stats.gov.cn/). The NBSC is the agency in China for collecting and publishing statistical information based on sub-province sample surveys. For northeast China, prefectural level statistical data were acquired for Heilongjiang, Jilin, and Liaoning Provinces, with a total number of thirty-six prefectures, among them, thirteen in Heilongjiang Province, 9 in Jilin Province, and fourteen in Liaoning Province.

7.3.2 Remote sensing data smoothing

In this chapter, to eliminate noise and fluctuations during rice growth, time-series of MTCI and MODIS NDVI data were cleaned at first, by using a window size of three pixels and the moving average method, for removing missing data and errors, caused by cloud contamination and atmospheric variability (Ren et al. 2008). Then, the discrete Fourier transformation (DFT) method was used to smooth the time-series data, for representing the growing profiles of rice accurately.

7.3.3 Phenological variables extracted from time-series remote sensing data

It has been demonstrated that crop production or yield is highly related to VI changes because crops are strongly affected by various conditions during each growing stage (Doraiswamy and Cook 1995; Fontana 2005; Huang et al. 2013; Jing-feng et al. 2002; Ren et al. 2008). Therefore, crop phenological variables can be used for estimating crop yield. Furthermore, crop phenology varies spatially and temporally, therefore, it is not optimal to only use a fixed date within the growing period to estimate crop yield (Bolton and Friedl 2013).

In this study, four phenological variables including maximum value, summation before the peak, summation after the peak, and summation of growth were taken into consideration in the correlation between phenological variables and rice yield. The maximum value was equal to the peak value of a smoothed time-series remote sensing data, MTCI and MODIS NDVI in this case. Summation before peak was computed by summing up the values before peak point to peak point. Summation after peak was computed by summing up the values from peak point to the fourth point after peak, and the summation over growing period was the summation of before and after peak summation. In this study we choose the fourth point before and after the peak point. In other words, 40 days before and after heading stage (which has the maximus MTCI value during the growing period). In northeast China, it is usually in the booting stage for paddy rice around 40 days before the heading stage (during which it is the fastest growing period of paddy rice, and rice plants need large amount of nutrients during this period, making this stage is critically associated with rice yield); and it is grain filling and maturation period

including flowering stage, milky and doughy stage (ripening phase/filling stage) around 40 days after heading stage. Therefore, from boosting to heading and from heading to maturity, the two important growing periods were represented by phenological variables for examining the accuracy in estimating rice yield. According to the location of summation at rice growing profile versus peak point, variables were named as, taking MTCI as an example, $MTCI_{peak}$, $MTCI_{left}$, $MTCI_{right}$, and $MTCI_{whole}$, as shown in Figure **44**.

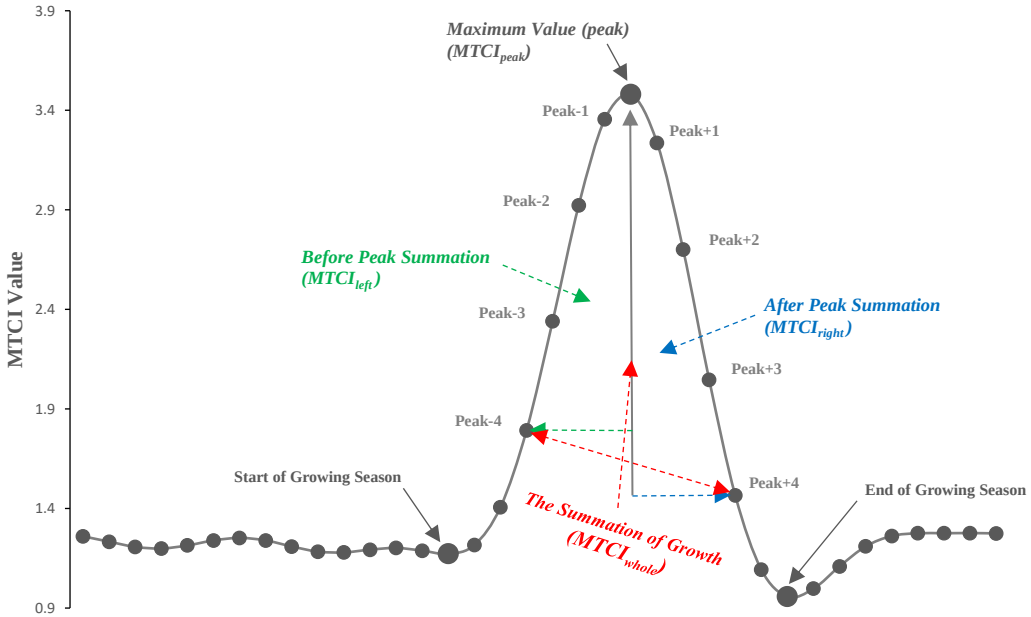

Figure 44 Phenological variables extracted from time-series remote sensing data for correlation analysis.

7.3.4 Regression model development

Crop yield is greatly affected by various conditions during each crop growth stage, such as the development of agricultural technologies, fertilizer applications, and improved management, in the form of changing VI values. Therefore, a linear relationship between phenological variables extracted from VI time-series data and crop yield can be expected as:

$$\hat{\boldsymbol{Y}} = \boldsymbol{a} + \boldsymbol{bV} \quad (18)$$

Where $\hat{Y}$ is the estimated prefectural level yield, and V is the mean of four phenological variables of training years, extracted from smoothed time-series data. To estimate the models using prefectural level yield records, it was necessary to aggregate remote sensing data to prefectural level for all average phenological variables, based on the 5 years processed remote sensing time-series data from 2007 to 2011.

7.3.5 Model validation

Validating model performance is essential. The MTCI data were unavailable after April 2012, and 1 km MTCI data were only available for 2007 to 2011. Therefore, as a final test, the established model accuracy was assessed by using a leave-one-year-out-approach (Mkhabela et al. 2011; Schut et al. 2009), in which the model is iteratively trained on four years of data and used to predict yield as well as total production in the held-out year. The root mean square error (RMSE) was calculated between actual and predicted yield for the held-out year as follows:

$$\boldsymbol{RMSE} = \sqrt{\frac{\mathbf{1}}{\boldsymbol{n}}\sum_{\boldsymbol{i}=\mathbf{1}}^{\boldsymbol{n}}(\widehat{\boldsymbol{Y}}_{\boldsymbol{\iota}} - \boldsymbol{Y}_{\boldsymbol{i}})^{\mathbf{2}}} \quad (19)$$

Where n is the number of prefectures ($n=36$ in this case), $\widehat{Y}_{\iota}$ is the predicted yield at prefectural level, and Y_i is the actual yield at prefectural level.

Furthermore, the MODIS NDVI from 2007 to 2011 were used as input data to generate the linear models, and an inter-comparison between MTCI and MODIS NDVI was conducted. In summary, the processes were shown in a flowchart of Figure **45**.

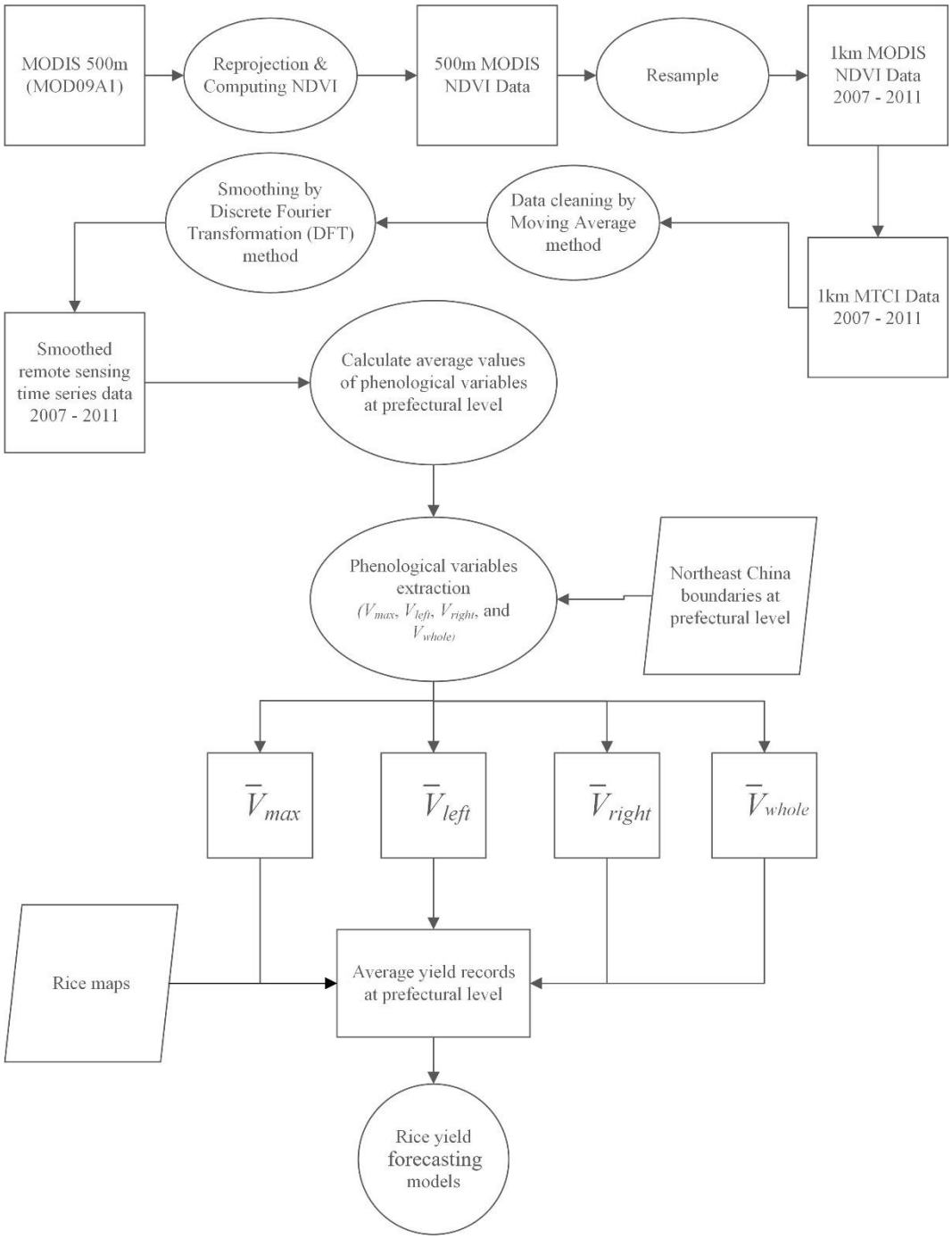

Figure 45 A flow chart of the processes for establishing rice yield estimation models.

7.4 Results and Discussion

7.4.1 Yield estimation model

Figure **46** presents the multi-year average coefficients of determination (r^2) for four variables derived from linear regression models using MTCI and MODIS NDVI time-series data, for forecasting paddy rice yield for all study years. Figure **47**

exhibited the relationship and models between each phenological variable of MTCI and MODIS NDVI and yield, all of which were at prefectural level with n=35 (Daxinganling Province did not have any records as it had very few paddy rice fields). Each model contains variables using the data from 2007 to 2011. The MTCI and MODIS NDVI values were used as the independent variables, and the yield was used as the dependent variable. The coefficients of determination ranged from 0.6162 to 0.6869 for MTCI, and from 0.6079 to 0.6777 for MODIS NDVI.

Overall, both MTCI and MODIS NDVI variables produced acceptable coefficients of determination, with MTCI producing a slightly larger coefficient of determination than MODIS NDVI. It can be clearly seen that the maximum value had the largest coefficient of determination between paddy rice yield and the maximum values of MTCI and MODIS NDVI during all the study years, with an average coefficient of determination of 0.6869 and 0.6777 for MTCI and MODIS NDVI, respectively. It was agreed with the studies reporting that the grain filling stage was more related with rice yield (Marti et al. 2007; Mkhabela et al. 2011; Mkhabela et al. 2005), and specifically, the rice yield was mostly determined by crop conditions during the heading (i.e. peak phenological phase of growth) (Huang et al. 2013). Also, it can be noticed that the V_{right} (average r^2=0.6721 for MTCI and r^2=0.6538 for NDVI) had a generally larger coefficient of determination than V_{left} (average r^2=0.6676 for MTCI and r^2=0.6524 for NDVI). In 2009, the northeast China suffered from drought, both MTCI and MODIS NDVI had relatively low coefficients of determination. Because grain yield was critically subjected to the conditions during the flowering and grain filling periods, and water stress may result in reduced yield and production during these growing stages (Labus et al. 2002). In addition, V_{whole} (average r^2=0.6162 for MTCI and r^2=0.6079 for NDVI) had the smallest value of the coefficient of determination than other variables. The maturing stage of paddy rice showed a significant correlation with rice yield, end of tillering/before heading stage could affect the yield, and summation of middle part of growing stage had the least determination with the rice yield. This might be because the longer the period considered, the more potential factors could have effects on the final rice production or yield, and it was reported that grain yield was influenced mostly by crop conditions during the heading phase (Mkhabela et al. 2011; Salazar et al. 2007). Therefore, the results indicated that the paddy rice yield

in northeast China can be forecasted during mid- to late- August, when the paddy rice experiences the filling/milky phase, by the phenological variables extracted from VIs.

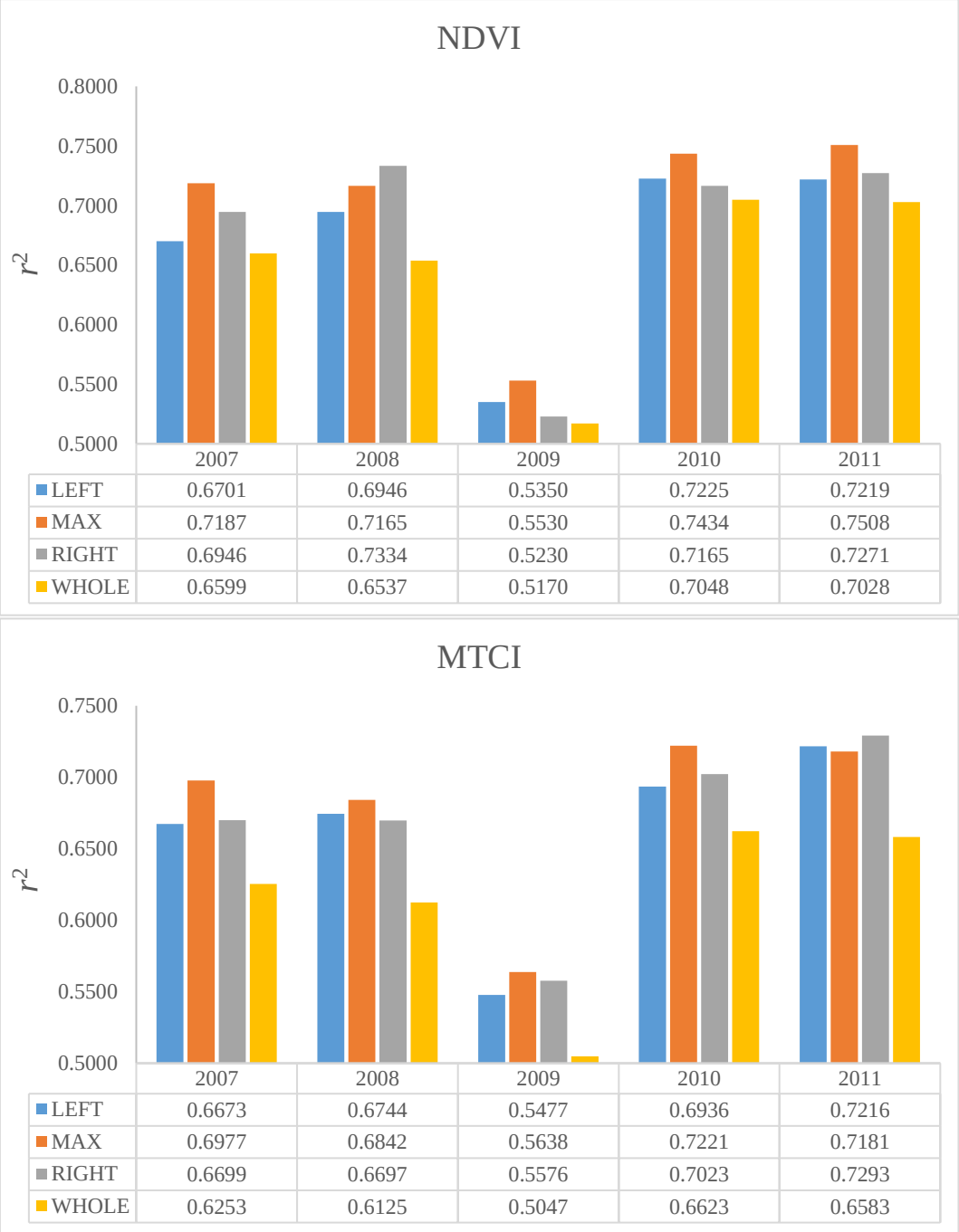

Figure 46 The coefficients of determination for phenological variables of MTCI and MODIS NDVI, including V_{max}, V_{left}, V_{right}, and V_{whole}.

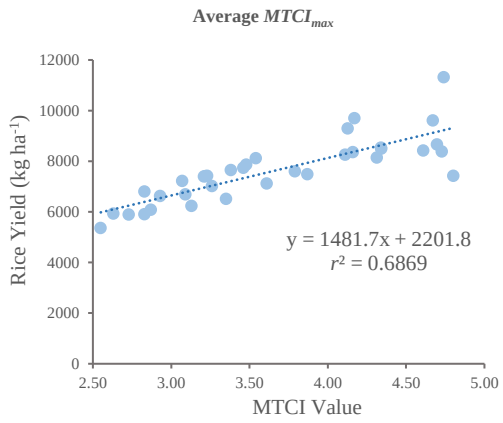
Average $MTCI_{max}$
Rice Yield (kg ha⁻¹)
MTCI Value
y = 1481.7x + 2201.8
r² = 0.6869

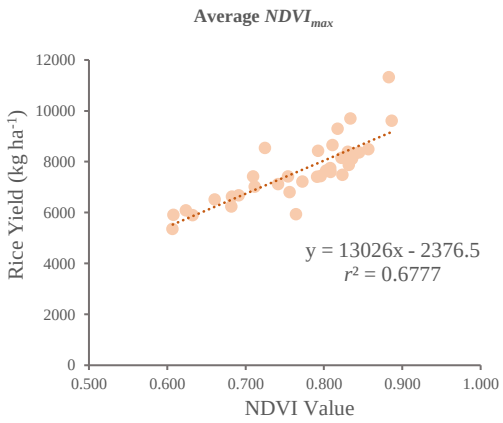
Average $NDVI_{max}$
Rice Yield (kg ha⁻¹)
NDVI Value
y = 13026x - 2376.5
r² = 0.6777

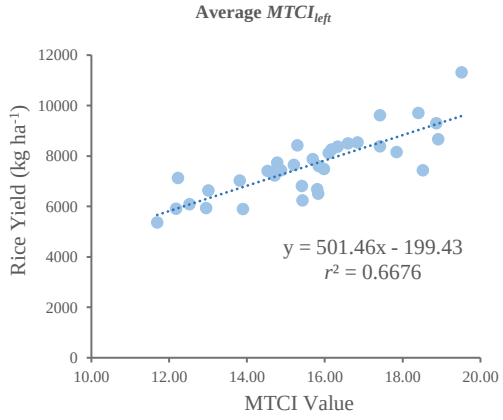
Average $MTCI_{left}$
Rice Yield (kg ha⁻¹)
MTCI Value
y = 501.46x - 199.43
r² = 0.6676

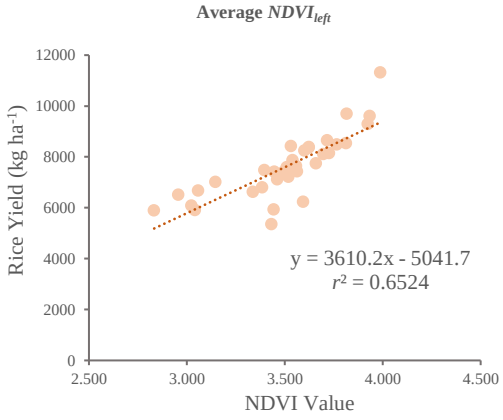
Average $NDVI_{left}$
Rice Yield (kg ha⁻¹)
NDVI Value
y = 3610.2x - 5041.7
r² = 0.6524

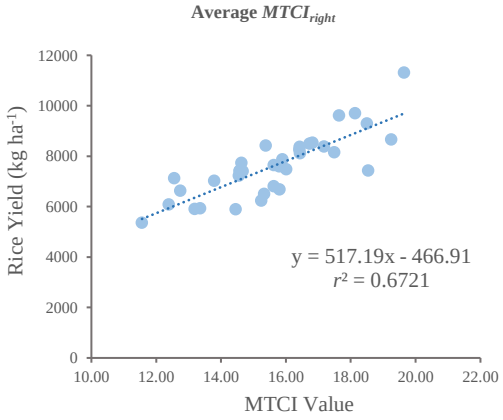
Average $MTCI_{right}$
Rice Yield (kg ha⁻¹)
MTCI Value
y = 517.19x - 466.91
r² = 0.6721

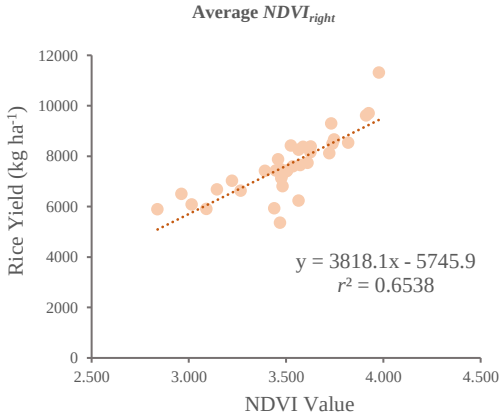
Average $NDVI_{right}$
Rice Yield (kg ha⁻¹)
NDVI Value
y = 3818.1x - 5745.9
r² = 0.6538

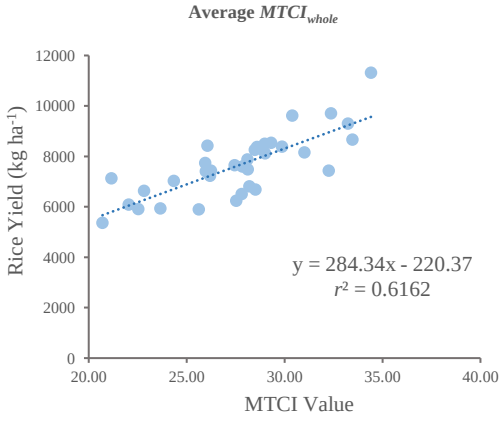
Average $MTCI_{whole}$
Rice Yield (kg ha⁻¹)
MTCI Value
y = 284.34x - 220.37
r² = 0.6162

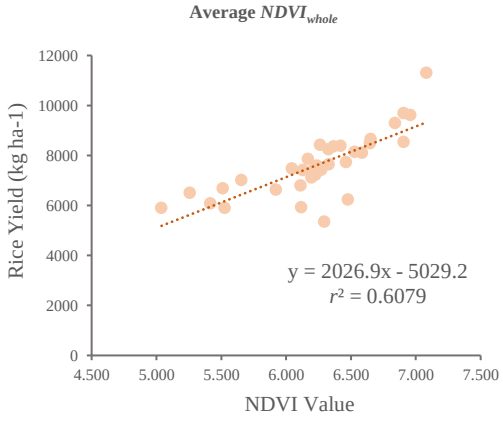
Average $NDVI_{whole}$
Rice Yield (kg ha-1)
NDVI Value
y = 2026.9x - 5029.2
r² = 0.6079

Figure 47 Relationships between the average rice yield and the average of four variables. The x-axis is values of MTCI and MODIS NDVI values; the Y-axis is yield records (kg ha^{-1}), n=35.

7.4.2 Yield forecast model validation

Four phenological variables were used to fit the models to forecast rice yield in northeast China. The MTCI and MODIS NDVI were used in the processes, both of which worked. Therefore, the validation was concentrated on the MTCI by using the leave-one-year-out method to estimate rice yield for each from 2007 to 2011.

Table **9** shows the models, coefficients of determination (r^2), and the root mean square errors (RMSE) based on the leave-one-year-out method. The results suggest that $MTCI_{max}$ has a larger r^2 value than other variables (r^2 = 0.624~0.689), whereas for $MTCI_{left}$ is generally smaller (r^2 = 0.458~0.596). $MTCI_{right}$ (r^2 = 0.542~0.619) and $MTCI_{whole}$ (r^2 = 0.517~0.617) perform equally well for predicting rice yield in northeast China. In addition, it can be noticed that the models established by using four years when the year 2009 was held out, produced the smallest r^2 compared to other held-out-years. This might be because of the drought in 2009. Overall the RMSE (expressed in units of percentage relative to the mean yield) ranges from 9.8% to 14.5%. Among them, $MTCI_{max}$ has the RMSE ranges from 9.8% to 12.9%, which is lower than other variables (10.6%~14.5% for $MTCI_{left}$, 10.6%~13.5% for $MTCI_{right}$, and 10.4%~13.4% for $MTCI_{whole}$). The differences between predicted and actual yield shows a smaller range, compared to those recorded by Ren et al. (2008) (reported the differences ranging from -4.6% to 5.4%), Bolton and Friedl (2013) (reported the differences ranging from 5% to 15%), and Wang et al. (2014b) (reported the differences ranged from 7.3% to 16.9%), however, multiple indices were used in their studies to correlate with grain yield.

Figure **48** showed the forecasted rice production at prefectural level (n=35), calculated from estimated yield and identified paddy fields in the previous study, for 2007 to 2011, against official statistical records within the same period. It can be seen from the figure that the data are linearly related, the r^2 ranges from 0.5373 to 0.7466. The largest coefficient of determination was obtained for $MTCI_{whole}$ of 2011, and the least was 0.5373 for $MTCI_{whole}$ of 2009. Still, it can be noticed that in 2009 the estimated production was less linearly related with historical records,

which might be because of the drought in 2009.

Table 9 Linear regression models for forecasting rice yield established from MTCI variables and rice yield records at the prefectural level from every four years except one held-out year. The numbers in the bracket are percent RMSE, expressed in units of percentage relative to the mean.

	$MTCI_{max}$			$MTCI_{left}$			$MTCI_{right}$			$MTCI_{whole}$		
Held-out-year	**Model**	r^2	***RMSE(kg/ha)(%)***	**Model**	r^2	***RMSE(kg/ha)(%)***	**Model**	r^2	***RMSE(kg/ha)(%)***	**Model**	r^2	***RMSE(kg/ha)(%)***
2007	y = 0.6526x + 2604.7	0.647	742.07 (9.8)	y = 0.6057x + 2955.4	0.585	805.28 (10.6)	y = 0.6273x + 2829.3	0.600	814.12 (10.8)	y = 0.6508x + 2669.9	0.583	790.11 (10.4)
2008	y = 0.5429x + 3608.2	0.659	781.46 (10)	y = 0.495x + 3929.3	0.466	949.27 (12.2)	y = 0.5661x + 3369.7	0.595	826.95 (10.6)	y = 0.5059x + 3820.5	0.517	919.48 (11.8)
2009	y = 0.6965x + 2341.1	0.624	975.07 (12.9)	y = 0.6409x + 2729.8	0.458	1125.55 (14)	y = 0.643x + 2587.4	0.542	997.25 (13.2)	y = 0.6433x + 2585.3	0.549	1012.231 (13.4)
2010	y = 0.7607x + 1906.4	0.689	805.17 (10.9)	y = 0.7114x + 2285	0.546	1008.97 (13.7)	y = 0.6998x + 2325	0.548	994.5 (13.5)	y = 0.7037x + 2322.5	0.557	985.33 (13.4)
2011	y = 0.5979x + 3464.7	0.683	888.99 (11.5)	y = 0.6137x + 3333.9	0.596	1059.32 (14.5)	y = 0.6546x + 2917.2	0.619	1005.37 (13)	y = 0.6107x + 3294.3	0.617	996.05 (12.9)

Figure 48 Comparison between estimated rice production at prefectural level (n=35) and official statistical records from 2007 to 2011, for four phenological variables of MTCI: $MTCI_{max}$ (a-e), $MTCI_{left}$ (f-j), $MTCI_{right}$ (k-o), and $MTCI_{whole}$ (p-t).

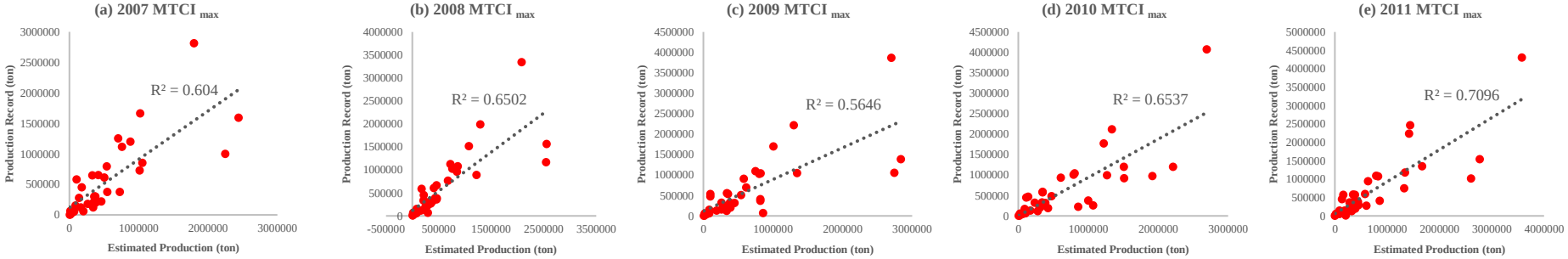

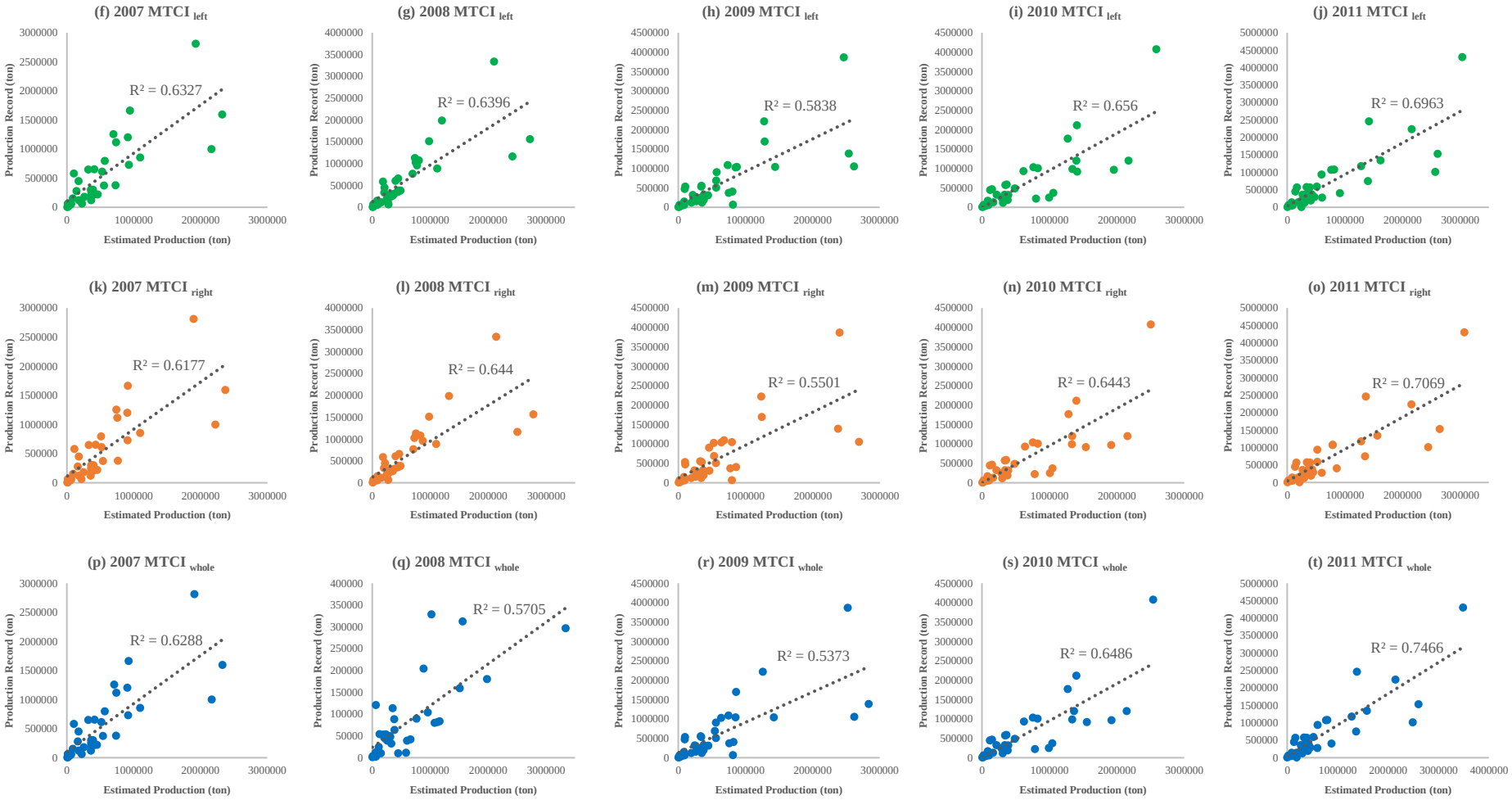
(f) 2007 MTCI left
R² = 0.6327
(g) 2008 MTCI left
R² = 0.6396
(h) 2009 MTCI left
R² = 0.5838
(i) 2010 MTCI left
R² = 0.656
(j) 2011 MTCI left
R² = 0.6963
(k) 2007 MTCI right
R² = 0.6177
(l) 2008 MTCI right
R² = 0.644
(m) 2009 MTCI right
R² = 0.5501
(n) 2010 MTCI right
R² = 0.6443
(o) 2011 MTCI right
R² = 0.7069
(p) 2007 MTCI whole
R² = 0.6288
(q) 2008 MTCI whole
R² = 0.5705
(r) 2009 MTCI whole
R² = 0.5373
(s) 2010 MTCI whole
R² = 0.6486
(t) 2011 MTCI whole
R² = 0.7466
Production Record (ton)
Estimated Production (ton)

7.5 Discussion

The MTCI was used to extract four paddy rice phenological variables during the growing period, for establishing relationships with yield records in this chapter. MODIS NDVI was also adopted as an input into the same procedure, as a comparative indicator. The results indicated that the rice yield was mostly related with the maximum VIs at the prefectural level, compared to other variables standing for different rice growing stages.

MTCI showed a slightly greater accuracy than MODIS NDVI in establishing the relationship with rice yield. More generally, the results from this study imply that the remotely sensed information is useful and efficient for providing rice yield forecasting before harvest around the mid of the growing season when coupled with historical yield records. Among the phenological variables that were investigated, the maximum values of both MTCI and NDVI showed the better performance in estimating rice yield than other variables. The maximum value normally appears during the heading stage (Wang et al. 2014a), it can be attributed to the heading stage is the end of rice reproductive phase, following by flowering stage which is the beginning of the ripening phase. Therefore, the health of rice plants after experiencing the vegetative phase can be reflected by VIs at the heading stage, which is highly correlated with the final yield. Lopresti et al. (2015) found the best correlation between NDVI and wheat yield coincided with the period of highest LAI, during the heading stage, using MODIS-NDVI, which is similar with the results of Ren et al. (2008). Qader et al. (2018) found that winter wheat and barley production were highly and linearly correlated with the maximum value of both MODIS NDVI and EVI at the governorate level in Iraq. However, it is not a general case for the maximum value to be most correlated with grain yield. Esquerdo et al. (2011) found that the whole productive cycle was the most significantly correlated with soybean yield among five phenological parameters investigated. Nuarsa et al. (2011) found the summation of NDVI during rice growing period showed the strongest exponential relationship with rice yield, among three growth variables. This might be because of the different climatic factors.

The method worked in northeast China, which has only one growing season, with

a larger farmland per farmer and higher rate of mechanisation than elsewhere in China. In south China, mountainous landscape and higher elevation resulted in smaller scale farming with more labour intensive activities (Xiao et al. 2005), With the performance of MTCI data used in the last chapter for mapping paddy rice, fewer rice fields were detected in middle Jilin Province which is mountainous with smaller scale farmlands. The same situation would happen in estimating rice yield. Moreover, the validation was somewhat limited by the inadequate data sources in the study. Because the MTCI 1 km data were only available for 2007 to April 2012, no future data were used as input for validating the rice yield model with a cross comparison with yield records.

The coarse spatial resolution of 1 km used in this study is less sensitive than finer resolutions in handling paddy rice fields in China. Moreover, the less accurate rice distribution maps used in this study affected the result to some extent. In addition, since the Envisat was not in operation since 2012, there were no data available from then. Hence validation like cross-comparison with following years could not be conducted. Furthermore, the approaches for establishing linear models between VIs and yield used in this study considered a limited number of variables, which might result in less comprehensive conclusions.

7.6 Conclusion

This chapter focused on testing the performance of the MTCI in forecasting rice yield, and has shown the potential for using the MTCI variable in large area crop yield and production forecasting. The results of this analysis suggest the MTCI can be applied in yield forecasting area as a replacement of the NDVI, and the maximum value of MTCI has a better correlation with rice yield than other phenological variables. In the light of the MERIS data is not available after February 2012, the most suitable sensor for compositing free MTCI dataset is the Multispectral Instrument (MSI) on-board sentinel-2 and Ocean and Land Colour Instrument (OLCI) on-board Sentinel-3, new indices can be developed and applied with better spatial and temporal resolutions.

8.Discussion

This chapter will conduct a comprehensive discussion based on each chapter around the main topic of this thesis: test the performance of MERIS Terrestrial Chlorophyll Index (MTCI) in analysing phenology dynamics and in specific applications, for example, agricultural ones.

8.1 In phenology studies

The outcomes of Chapter 3 and 4 in conjunction highlight the importance of using vegetation indices derived from remotely sensed data for long-term vegetation phenology observation, and reveal the convenience in depicting vegetation phenology at a large scale. Furthermore, in Chapter 5, the metrics were associated with climatic data including precipitation and temperature.

The MTCI was developed based on the relationship between chlorophyll absorption and the increase in the wavelength (spectral) range 650-700 nm, and the red-edge position (REP) is the point of maximum change in reflectance. The MTCI benefits from the MERIS sensor which has well-placed spectral sampling at visible and near-infrared (NIR) wavelengths coupled with narrow bands, making it theoretically accurate in vegetation monitoring (Boyd et al. 2011), and less influenced by atmospheric effects as well as soil background (Dash et al. 2009b), compared to red and near-infrared based broad-band indices such as the NDVI. One key point need to be addressed that the relationship between REP and chlorophyll content is asymptotic, hence REP is not an accurate indicator at high chlorophyll contents (Dash and Curran 2007).

Since the REP is strongly linked with the content of chlorophyll, the pigment for foliar photosynthesis, the MTCI can be used as an indicator for onset of productivity and senescence before canopies change in structure (Boyd et al. 2011). In Chapter 3 the results showed that the MTCI performed very well in high chlorophyll content situations, for instance, mixed evergreen vegetation in the subtropical region, where there is a high average annual temperature and high biomass all year around: the MTCI exhibited a more legible pattern than NDVI. In addition, the close relationship between REP and chlorophyll is particularly advantageous in demonstrating the changes in the chlorophyll concentration in plants that occur because of rising temperatures, but may not result in biomass change. Therefore, in most cases, the MTCI has an earlier decline for autumnal senescence than the NDVI

and sometimes more rapid increase during the onset of vegetation growth, during which both chlorophyll content and leaf area grow quickly, reflected in Figure **8**.

All the features of MTCI provide the opportunity for monitoring vegetation phenology. With a moderate temporal resolution of 8-days and 10-days, and relatively coarse spatial resolution of 4.6 km but is suitable for large scales, in Chapter 7, 9 years phenology maps for mainland China were produced for the first time. Although it has been suggested by Piao et al. (2006a) that there is no obvious seasonality in the humid tropical and subtropical areas in China (approximately south of 30°N), because NDVI presents aberrant seasonal fluctuations related to non-vegetation weather impact, the MTCI still managed to delineate the growing patterns. Comparison with ground observation data that collected from the literature and the gridded dataset of spring phenology of *Fraxinus Chinensis* in China from 2003 to 2007, produced satisfying results. However, as mentioned in Chapter 4, dimensional factors were not taken into consideration (e.g. slope and elevation), which affect the vegetation distribution and consequently cause variation in growth environment (e.g. temperature, solar radiation, soil condition and so on), all of which finally were reflected in local-to-regional differences in phenology and the phenomenon has been particularly marked around the "Three Gradient Terrains" of mainland China where elevation and slope increase sharply from east to west.

Many time-series smoothing methods can be used for reducing noise and extracting vegetation phenological variables from stacked remote sensing images, but there is still no conclusion in favour of one over the others. They can be generally divided into two categories according to their functionalities. One category contains methods that can capture short-term phenological variation precisely during the growing season, by employing statistical filters, e.g. the best index slope extraction (BISE) (Viovy et al. 1992), running median (Velleman 1980), the repeated moving-window median filter (Filipova-Racheva and Hall-Beyer 2000), Fourier analysis (Menenti et al. 1993; Olsson and Eklundh 1994); anther category includes methods employing mathematical functions that are applicable for all situations such as part of the growing season, one season, and multi seasons. For example, the double logistic function (DL) (Beck et al. 2006), the Asymmetric Gaussian function (A-G) (Jonsson and Eklundh 2002), and so on.

The Fourier transformation method has been used through all the smoothing process

in this thesis. It has an advantage over other methods that there is only one parameter that needs to be decided, i.e. how many harmonics are needed to input. It has been tested and demonstrated by (Jakubauskas et al. 2001; Jakubauskas et al. 2002) that the first two harmonics were capable of representing only annual and semi-annual cycles; the first four harmonics were able to represent single growing season very well. Dash et al. (2009a) used six harmonics to extract phenology in agricultural areas in India where usually there are up to three growing seasons for crops. Given China has a complex vegetation land cover and multiple climatic zones, six harmonics were used in this thesis to generate a smoothed time-series.

Based on the produced 9 years phenology maps, in Chapter 5, coupling with vegetation regionalisation map and climate data, regional climate change over mainland China was analysed. As the effects from climate acting on vegetative events is a process of accumulation, phenological stages such as OG or ES are not only determined by the climatic factors of the month, but also influenced from months before. For example, in cold and temperate regions, plants require a certain amount of heat accumulated through winter to trigger spring leaf onset and also a continuous decrease in temperature is also a significant precondition for plants dormancy (Piao et al. 2015). In Chapter 5, three months including the seasonal month were considered, limiting its own conclusiveness regarding the impact over longer times ahead of the phenological events.

8.2 In agricultural applications

Crop analysis is generally separated into two categories. One is focused on measuring crop area or agricultural land area; another is centred upon monitoring crop growth/health, and estimating crop yield. In Chapter 6 and 7, the MTCI was utilised in agriculture for mapping paddy rice distribution and estimating rice yield at northeast China.

Conventional crops classification techniques broadly include two approaches, unsupervised classification and supervised classification. Unsupervised classification in essence is a clustering analysis that groups pixels into different categories according to the similarity in the spectral values; supervised classification is based on selected training samples of representative crop types, associating with appropriate spectral bands of certain remotely sensed data,

different crops can be identified accordingly, usually by using machine learning techniques such as support vector machine classifier (SVM), random forest (RF), and other clustering analysis in supervised classification. They are efficient but rely heavily on the quantity and quality of the sample fields, which make supervised classification cannot be suitable for places that are prohibited or limited due to regional conflict, political regime, or short of surveyors (Moody et al. 2017).

In Chapter 6, 5-year time-series MTCI data were combined with MODIS 500 m surface reflectance data for mapping paddy rice by analysing the growing profiles of MTCI, MODIS LSWI and MODIS EVI, in terms of paddy rice growing calendar in the region. Comparing to conventional statistical classification methods, this phenological profile-based method was more accurate. Phenological metrics such as OG and ES have the advantage of bearing a physiological significance (Zhong et al. 2016), while conventional statistical methods are more relying on specific datasets which contain more uncertainties.

Comparing with other studies that adopted the same principle of combing several VIs derived from MODIS and Landsat in reflecting rice growing profiles in Northeast China (Dong et al. 2016; Jin et al. 2015; Qin et al. 2015; Shi et al. 2013; Zhang et al. 2015a), the MTCI showed good performance in depicting paddy rice growing seasons after flooding period, during which there was only water in the paddies. And the final identified paddy rice area had an agreement with NCLD 2010 dataset as well as the multi-year official statistical records.

There are still some limitations in the whole procedure, and using MTCI instead of NDVI to integrate with EVI and LSWI, there were some inherent differences. At first, MTCI is an index developed from narrow bands which are continuous in red edge position, while NDVI is derived from separated broad bands. Studies comparing between narrow-band and broad-band vegetation indices have been made on estimating biophysical parameters showing in most cases narrow-band indices perform more accurately than broad-band ones (Hansen and Schjoerring 2003; Thenkabail et al. 2000; Ullah et al. 2012). This can be attributed to broad-band indices such as NDVI using average spectral information over broad band widths (e.g. MODIS Band 1 red: 620-670nm, Band 2 NIR1: 841-876nm), leading to a loss of some information available in narrow bands. Furthermore, it was reported by Huete (1988) that red and NIR based indices were influenced by soil

background at low vegetation cover. However, when dealing with specific agricultural situations such as mapping rice fields and predicting yield, spatial and temporal resolution always affects the results. 1 km spatial resolution of MTCI can be somewhat coarse for small farmlands not only in mountainous areas such as in Jilin Province mentioned in Chapter 6, but also terrace fields in hilly areas, scattered farms around big cities, and less developed rural areas.

The method proposed by Xiao et al. (2006; 2002; 2005) had an advantage of adopting free remote sensing images of MODIS dataset, overcoming the problem of the discordance in planting schedule, and on the basis of the flooding physical features at the early stage of paddy rice growing cycle, it also avoids the high cost and inefficient fieldwork for collecting field data for input in any statistical method. However, for the purpose of integrating MTCI with MODIS EVI and LSWI, MTCI original temporal resolution and data values were transferred and normalised to match with the other two. The temporal transformation was carried out to adjust MTCI, EVI, and LSWI into a bi-week interval. Although it is sensible for observing rice growth by the MVC method picking the largest value of every two bands, according to the regional rice calendar (Figure **37**), major events happen in early, mid, and late months from April to October (preparation to harvest) in northeast China, the temporal transformation dissolved some details and generally made the patters of all indices exhibited more continuous than original ones, which might result in slight overestimation.

The normalisation of MTCI time-series data might magnify the growth pattern to some extent (i.e. earlier OG, later ES, and higher peak value). The valid MTCI value usually is from 0 to 6 and normally rice reaches around 3.5 to 4.0 (other crops or vegetation may have a lower or higher values), but after normalisation the peak value reached nearly to 1. This might also give a side effect that underestimates the area where LSWI was greater than MTCI during the flooding/transplanting period. What is more, the GLC30 land cover map was used in Chapter 6 to mask out non-agricultural area which was produced with a pixel-object-knowledge-based (POK-based) classification approach, a pixel and object-based method with human knowledge interactive verification (Guo et al. 2007); while more complex conditions by other indices were used in other studies focused on mapping rice. But no studies have been done to compare the accuracy between land cover based and

indices conditions-based methods.

In Chapter 7, based on the results of mapped paddy rice distribution in northeast China, the phenology-based method was utilised to investigate the correlation between four phenological variables and rice yield. The results were satisfying compared to official yield and production records. But some comments need to be made about the methodology. Many studies have explored the feasibility and accuracy of estimating models between phenological variables/metrics and crop yield (Bolton and Friedl 2013; Labus et al. 2002; Ren et al. 2008; Rojas 2007; Wall et al. 2008; Wang et al. 2014b), various kinds of phenological variables/metrics calculated from the original values of vegetation indices such as NDVI were tested including accumulation, summation, standard deviation, average, maximum and so on. In most cases, the maximum value of VIs shows the largest correlation with crop yield. In Chapter 7, only four phenological variables were considered including three summation of MTCI values at different rice growing stages, plus the maximum MTCI value. This can be a limitation which narrows the complexity and scope. Also, it needs to be mentioned that drought had a great influence on the phenology-based methodology in both mapping paddy fields and yield prediction. In Chapters 6 and 7, it was found that both mapped paddy rice fields and predicted yield had the smallest correlation with statistical records in 2009, when a severe drought took place in China.

This thesis tested the MTCI products in various scenarios, and satisfying results were produced. However, the Envisat's mission was formally stopped on 9 May 2012, with the MERIS sensor onboard, hence the MTCI data were not available any more. In the past last several years and onwards, an increasing amount of free remotely sensed data have started becoming available including optical and synthetic aperture radar (SAR) with fine spatial resolution (10-30 m), such as Sentinel-1 A/B and Sentinel 2A within the European Copernicus programme; and Landsat-8 within the Landsat Programme, co-managed by U.S. Geological Survey (USGS) and the National Aeronautics and Space Administration (NASA), launched during 2013-2016 period. In addition, the Sentinel-3B satellite will be launched on 25th April 2018, to work in conjunction with the Sentinel-3A which was launched on 16th Feb 2016. These datasets are all freely available, giving unprecedented opportunities for a wide range of remote sensing applications in the environment

and agriculture domains, benefiting from fine temporal and spatial resolution. Furthermore, the terrestrial chlorophyll index can be continued, due to the on-board Multi-Spectral Instrument (MSI) (Sentinel-2) and Ocean and Land Colour Instrument (OLCI) (Sentinel-3), both of which have narrow spectral bands covering the vegetation red-edge position.

9.Conclusions and Future Work

This thesis primarily focused on the application of the MERIS Terrestrial Chlorophyll Index (MTCI). At first, the MTCI was compared with MERIS NDVI to test the ability of MTCI in determining key vegetation phenological metrics. After that, the MTCI was used in practical applications from the national scale to regional scale, specifically in mapping vegetation phenology across the whole of mainland China, examining phenology variations correlated with climatic factors, and application in agriculture including mapping paddy rice and estimating rice yield. This chapter draws the main conclusions from the works presented in Chapters 3 to Chapter 6, with a specific view of assessing the objectives of the research stated in Chapter 1.

9.1 Thesis summary

The thesis has tested the potential use of the MTCI in practical applications as a refinement for NDVI. The significant novel contribution of the research is the use of MERIS MTCI at large and regional scales in mainland China, which probably has the most complex physical diversity in the world. MERIS MTCI at 300 m, 1 km, and 4.6 km spatial resolution were all tested in the research, and the results were generally positive and satisfying.

The Ph.D. objectives have been achieved:

1. **To investigate the performance of using the MTCI to monitor vegetation phenology at large and regional scales for different vegetation types.**

   In Chapter 3, 18 months 300 m full resolution MERIS surface reflectance data were used to compute MTCI and MERIS NDVI, for comparison in determining the phenological timing of different vegetation types including broadleaf deciduous, cropland, grassland, and mixed evergreen (broadleaf and needle leaf) in six major vegetation-climate zones of mainland China including warm temperate deciduous broadleaf forest, subtropical evergreen broadleaf forest, tropical monsoon rain forest, temperate steppe, temperate desert, and Qinghai-Tibet plateau alpine vegetation. Two key phenological metrics OG and ES were extracted from both the MTCI and NDVI time-series data with a full temporal coverage of 2010.

The results implied that the both the MTCI and the NDVI captured the plant phenology patterns very well for different vegetation types. However, unlike the NDVI, the MTCI is more sensitive to large values of chlorophyll content. The NDVI is more sensitive to green biomass and will respond to the aggregated change in seasonal.

2. **To estimate vegetation phenology over a 9 years period across mainland China by using the MTCI data.**

   In Chapter 4, 9 years reduced spatial resolution at 4.6km of the MTCI data were used to map the vegetation phenology across mainland China, and the variation in vegetation phenology was demonstrated. The results were validated with phenology data from the literature and a gridded phenology dataset of *Fraxinus Chinensis* from 2003 to 2007. Moreover, the general trends of vegetation phenology were investigated along longitude, and generally showed good consistencies. However, a high standard deviation of vegetation phenology was found in the double-cropping agricultural region at mid-eastern China, where affected by human management, and South China where is humid and temperate with mixed vegetation types.

3. **To investigate vegetation phenological variation at the regional scale and the drivers of this variation.**

   In Chapter 5, based on the phenology maps produced in Chapter 4, coupling with long-term gridded temperature and precipitation data and climate regionalisation map of mainland China, the quantitative analysis was conducted for determining the main regional drivers of phenology. The results showed in north China, the temperature was the main driver for the earlier OG, while in the south precipitation played a prominent role in advancing the OG. For the ES, both precipitation and temperature influenced partially. In Qinghai-Tibet Plateau, the precipitation was the main driver for both shifting OG and ES of grass, while less influenced by temperature. Among the vegetations that were examined, the broadleaf forest had the strongest correlation with climatic factors; the needle leaf forest was also greatly influenced by climate in cold temperate zone; the grass was highly affected by climate, while the mixed forest and crops were at moderate level.

4. **To evaluate the potential of using phenological information derived**

from MTCI in specific application such as agricultural mapping and crop yield estimating.

In Chapter 6 and 7, the reduced resolution MTCI data of 1 km were used in agricultural applications of mapping paddy rice fields and predict rice yield, in northeast China, combined with MODIS 500 m data. The results confirmed the ability and feasibility of the use of MTCI for an agricultural purpose.

By adopting a combined conditions method, the paddy rice field distribution was mapped based on vegetation indices including MTCI, MODIS EVI, and MODIS $LSWI_{1640}$. NLCD 2010 data and census data from China statistics yearbook for validation. The results showed good consistencies between produced paddy rice maps and NLCD 2010 data and census data, at both the prefectural and county level in northeast China. However, fewer paddy rice fields were detected in the mountainous area with higher altitude around 600 m to 800 m. Based on the census data of paddy rice yield and the produced paddy rice field maps from 2007 to 2011, simple linear models were established between four phenological variables extracted from MTCI time-series and yield records. A leave-on-year-out-approach was used to validate the yield prediction model. The results showed rice yield was most related with the maximum values of the MTCI and the NDVI at the prefectural level compared to other phenological variables derived from VIs, and the established models produced reasonable coefficients of determination and relative errors between forecasted yield and production with statistical records from the official yearbook.

9.2 Strengths and weaknesses

This research tested the 300 m, 1 km, and 4.6 km MTCI data in vegetation phenology determination and related applications in various situations, thus, the strengths and weaknesses of the research need to be examined.

The strengths of this research are that:

- The results were produced using relatively simple methods including moving average data cleaning method, discrete Fourier transformation

(DFT) time-series data smoothing method, and inflection point method for extracting key phenological variables, to process remote sensing time-series data, for the purpose of applying in complex circumstances (i.e. mainland China with high fault-tolerance performances).

- Unlike most of the previous studies conducted in China, which were normally concentrated on some parts of China, in this research, the whole of mainland China and all the subdivisions based on vegetation types and climate were taken into consideration when analysing the variation of phenology.
- Integrated the MTCI with MODIS derived vegetation indices in mapping paddy rice fields at northeast China, by employing a sophisticated approach, and then the produced map and MTCI phenological variables were used to forecasted rice yield.
- The MTCI has a generic advantage when applied in cold temperate climate region, where snow cover exists during the winter before spring, with MTCI values are equal to zero. It is also the same with the situation that there is a farmland preparation period before the crop growing season, (i.e. paddy rice).

The weaknesses of this research are that:

- The quality of 300 m MERIS surface reflectance data was inadequate enough. Therefore an extra process was carried out to improve the proportion of valid data. To some extent, this step may cause an advance or delay when extracting phenological metrics. And it was the same situation in converting MTCI and MODIS data into the same temporal interval.
- Lack of ground reference data for validating the phenological variables extracted from the MTCI dataset. In Chapter 3, the only comparison between MERIS NDVI and MTCI was conducted, no reference data were used for validating the accuracy of 300 m MERIS NDVI and MTCI in determining key phenological metrics. And when using 4.6 km MTCI data in measuring OG and ES for mainland China, still, no reference data were introduced for validating.

- The spatial and temporal resolution of 1 km MTCI for the agricultural application could be coarse to a certain extent. For example, when mapping the paddy fields in Jilin Province, the results showed less mapped fields than NLCD 2010, which was produced based on 30 m Landsat TM and ETM and HJ-1 satellite sensors data. And when establishing linear models between VIs and rice yield, the coefficients of determination were less than 0.7, which indicates only moderate strength compared with other studies. The reason could be attributed to the 1 km spatial resolution, which might be too large for small sale farms, located in the mountainous area with a higher elevation than the plain area.

9.3 Future work

The studies documented in this thesis have presented the use of the MERIS Terrestrial Chlorophyll Index (MTCI) in estimating plant chlorophyll content in describing vegetation phenology. The research demonstrated the advantage and sensitivity of the MTCI as a tool in determining key vegetation phenological variables and exhibited the potential to be used in a range of agricultural applications such as mapping paddy rice area and forecasting yield at a large scale. The research also returned satisfying results in terms of the performance from the MTCI, providing the foundation for broad application prospects.

9.3.1 Extending to other sensors

One of the major issues with the algorithm implemented in this research is that the MERIS Chlorophyll Terrestrial Index (MTCI) is calculated based on the red-edge position (REP) wavelength located in the red and near-infrared bands of Envisat MERIS, use of which is commonly designed for hyperspectral data with continuous narrow wavelength of spectral bands rather wide spectral wavelength, discontinuous multispectral data (Zhang and Liu 2014). The Multispectral Imager (MSI) onboard the Sentinel-2 satellites, which were launched in 2015, also has the red edge bands for computing a new index based on the same principle of the MTCI, with a finer spatial resolution of 30 m. Dong et al. (2015b) conducted studies testing the performance of 28 chlorophyll-related vegetation indices in estimating crop

FPAR (the Fraction of Absorbed Photosynthetically Active Radiation) by using Sentinel-2 data, and the MTCI was also included. The results showed a coefficient of determination of 0.86 and 0.10 of RMSE, more accurate than NDVI. Therefore, with time the remotely sensed data sources will increase with no doubt, as well as for such chlorophyll content based vegetation indices like the MTCI. Further, the indices can be widely used into agricultural applications in crops acreage mapping, health monitoring and yield forecasting, not only for paddy rice, but also for other crops such as wheat, soybeans, and so on. Moreover, the indices can also be applied for carbon related studies (Harris and Dash 2010, 2011) and land cover classification (Dash et al. 2007).

9.3.2 Methods improvements

Although the algorithm for processing remote sensing data and phenological variables extraction, generated satisfying results, still there are several potential areas for improvement. Firstly, for pre-processing the remote sensing data, the simple moving average method was used. Although it is quick, simple, and suitable for most occasions, for specific applications its performance has not been validated and compared with other common methods. For example, as far as known, the moving average method is good at cleaning remote sensing data of the same species as calculating the average values will eliminate the characteristics of vegetation growth reflected on data curves, to some extent. Therefore, additional research can be conducted.

Secondly, the discrete Fourier transformation (DFT) was used for smoothing data and the inflection point method was used to determine the phenological metrics. Although the DFT is simple to use with a minimal input variable, model-based methods are sometimes more accurate (Dash et al. 2010b). Moreover, the phenology extraction method needs to be assessed. Methods such as the threshold method can be applied for agricultural use coupling with experimental or ground observation data to determine the rice growing season more accurately, while in this research it was based on the empirical cropping calendar.

In the end, for mapping paddy rice and estimating yield, widely accepted methods were adopted for testing the MTCI in agricultural use, rather than developing new

methods. However, more factors can be introduced into the agricultural applications. For example, when mapping rice, land surface temperature (LST), the 2 band EVI, and $LSWI_{2130}$, can be considered for additional conditions when identifying flooding areas (Jin et al. 2015; Shi et al. 2013; Sun et al. 2009; Zhang et al. 2015a); and for estimating rice yield, LSWI, gross primary productivity (GPP), NDVI, and EVI can be included with the MTCI for establishing yield prediction models; and the MTCI also can be tested for use as input to rice growth models (Zhang and Liu 2014).

9.4 Conclusion

In this thesis, the MERIS Terrestrial Chlorophyll Index (MTCI) was employed with 300 m, 1 km, and 4.6 km spatial resolution and 8-day, 10-day intervals, for testing its potential ability in phenology observation at large scales and phenology based agricultural applications. The use of MTCI in China at both national and regional scales was the most novel contribution to the research. It can be foreseen with the development of satellite and spectral technologies, the MTCI and its derivations have a broad prospect in the applications of many fields.

List of References

Adamsen, F.G., Pinter, P.J., Barnes, E.M., LaMorte, R.L., Wall, G.W., Leavitt, S.W., & Kimball, B.A. (1999). Measuring Wheat Senescence with a Digital Camera. *Crop Sci., 39*, 719-724

Ahl, D.E., Gower, S.T., Burrows, S.N., Shabanov, N.V., Myneni, R.B., & Knyazikhin, Y. (2006). Monitoring spring canopy phenology of a deciduous broadleaf forest using MODIS. *Remote Sensing of Environment, 104*, 88-95

Ahmad, I., Saeed, U., Fahad, M., Ullah, A., Habib ur Rahman, M., Ahmad, A., & Judge, J.J.J.o.t.I.S.o.R.S. (2018). Yield Forecasting of Spring Maize Using Remote Sensing and Crop Modeling in Faisalabad-Punjab Pakistan, *46*, 1701-1711

Ahrends, H.E., Brügger, R., Stöckli, R., Schenk, J., Michna, P., Jeanneret, F., Wanner, H., & Eugster, W. (2008). Quantitative phenological observations of a mixed beech forest in northern Switzerland with digital photography. *Journal of Geophysical Research: Biogeosciences, 113*, G04004

Alcamo, J., & Olesen, J.E. (2012). *Life in Europe Under Climate Change*. Wiley

Almond, S. (2009). Validation and application of the MERIS Terrestrial Chlorophyll Index. In, *Conservation Science*: Bournemouth University

Aono, Y., & Kazui, K. (2008). Phenological data series of cherry tree flowering in Kyoto, Japan, and its application to reconstruction of springtime temperatures since the 9th century. *International Journal of Climatology, 28*, 905-914

Atkinson, P.M., Jeganathan, C., Dash, J., & Atzberger, C. (2012). Inter-comparison of four models for smoothing satellite sensor time-series data to estimate vegetation phenology. *Remote Sensing of Environment, 123*, 400-417

Atzberger, C., & Eilers, P.H.C. (2011). A time series for monitoring vegetation activity and phenology at 10-daily time steps covering large parts of South America. *International Journal of Digital Earth, 4*, 365-386

Baldocchi, D.D., Black, T.A., Curtis, P.S., Falge, E., Fuentes, J.D., Granier, A., Gu, L., Knohl, A., Pilegaard, K., Schmid, H.P., Valentini, R., Wilson, K., Wofsy, S., Xu, L., & Yamamoto, S. (2005). Predicting the onset of net carbon uptake by deciduous forests with soil temperature and climate data: a synthesis of FLUXNET data. *International Journal of Biometeorology, 49*, 377-387

Bastiaanssen, W.G.M., & Ali, S. (2003). A new crop yield forecasting model based on satellite measurements applied across the Indus Basin, Pakistan. *Agriculture, Ecosystems & Environment, 94*, 321-340

Battey, N.H. (2000). Aspects of seasonality. *Oxford Journals, 51*, 1769-1780

Beck, P.S.A., Atzberger, C., Høgda, K.A., Johansen, B., & Skidmore, A.K. (2006). Improved monitoring of vegetation dynamics at very high latitudes: A new method using MODIS NDVI. *Remote Sensing of Environment, 100*, 321-334

Belder, P., Bouman, B.A.M., Cabangon, R., Guoan, L., Quilang, E.J.P., Yuanhua, L., Spiertz, J.H.J., & Tuong, T.P. (2004). Effect of water-saving irrigation on rice yield and

water use in typical lowland conditions in Asia. *Agricultural Water Management, 65*, 193-210

Benedetti, R., & Rossini, P. (1993). On the use of NDVI profiles as a tool for agricultural statistics: The case study of wheat yield estimate and forecast in Emilia Romagna. *Remote Sensing of Environment, 45*, 311-326

Bertin, R., I. (2008). Plant Phenlogy and Distribution in Relation to Recent Cliamte Change. *Journal of the Torrey Botanical Society, 135*, 126-146

Bhandari, S., Phinn, S., & Gill, T. (2012). Preparing Landsat Image Time Series (LITS) for Monitoring Changes in Vegetation Phenology in Queensland, Australia. *Remote sensing, 4*, 1856

Boken, V.K., & Shaykewich, C.F. (2002). Improving an operational wheat yield model using phenological phase-based Normalized Difference Vegetation Index. *International Journal of Remote Sensing, 23*, 4155-4168

Bolton, D.K., & Friedl, M.A. (2013). Forecasting crop yield using remotely sensed vegetation indices and crop phenology metrics. *Agricultural and Forest Meteorology, 173*, 74-84

Booth, D.T., Cox, S., & Berryman, R. (2006). Point Sampling Digital Imagery with 'Samplepoint'. *Environmental Monitoring and Assessment, 123*, 97-108

Botta, A., Viovy, N., Ciais, P., Friedlingstein, P., & Monfray, P. (2000). A global prognostic scheme of leaf onset using satellite data. *Global Change Biology, 6*, 709-725

Bouvet, A., & Le Toan, T. (2011). Use of ENVISAT/ASAR wide-swath data for timely rice fields mapping in the Mekong River Delta. *Remote Sensing of Environment, 115*, 1090-1101

Boyd, D.S., Almond, S., Dash, J., Curran, P.J., & Hill, R.A. (2011). Phenology of vegetation in Southern England from Envisat MERIS terrestrial chlorophyll index (MTCI) data. *International Journal of Remote Sensing, 32*, 8421-8447

Bradley, C., Reed, Jesslyn, F., Brown, Darrel, V., Thomas, R., Loveland, James, W., Merchant, & Donald, O., Ohlen (1994). Measuring phenological variability from satellite imagery. *Journal of Vegetation Science, 5*, 703-714

Bridhikitti, A., & Overcamp, T.J. (2012). Estimation of Southeast Asian rice paddy areas with different ecosystems from moderate-resolution satellite imagery. *Agriculture, Ecosystems & Environment, 146*, 113-120

Brisson, N., Gary, C., Justes, E., Roche, R., Mary, B., Ripoche, D., Zimmer, D., Sierra, J., Bertuzzi, P., Burger, P., Bussière, F., Cabidoche, Y.M., Cellier, P., Debaeke, P., Gaudillère, J.P., Hénault, C., Maraux, F., Seguin, B., & Sinoquet, H. (2003). An overview of the crop model stics. *European Journal of Agronomy, 18*, 309-332

Brown, L.A., Dash, J., Ogutu, B.O., & Richardson, A.D. (2017). On the relationship between continuous measures of canopy greenness derived using near-surface remote sensing and satellite-derived vegetation products. *Agricultural and Forest Meteorology, 247*, 280-292

Cai, H., Zhang, S., & Yang, X. (2012). Forest Dynamics and Their Phenological Response to Climate Warming in the Khingan Mountains, Northeastern China. *International Journal of Environmental Research and Public Health, 9*, 3943-3953

Cammalleri, C., Anderson, M.C., Gao, F., Hain, C.R., & Kustas, W.P. (2013). A data fusion approach for mapping daily evapotranspiration at field scale. *Water Resources Research, 49*, 4672-4686

Černá, L., & Chytrý, M. (2005). Supervised classification of plant communities with artificial neural networks, *16*, 407-414

Chang, Z., Zhu, S., Han, F., & Zhong, S. (2012). Differences in response of desert plants of different ecotypes to climate warming; a case study in Minqin, Northwest China. *Journal of Arid Land, 3*, 140-150

Chen, C., & McNairn, H. (2006). A neural network integrated approach for rice crop monitoring. *International Journal of Remote Sensing, 27*, 1367-1393

Chen, D., Huang, J., & Jackson, T.J. (2005a). Vegetation water content estimation for corn and soybeans using spectral indices derived from MODIS near- and short-wave infrared bands. *Remote Sensing of Environment, 98*, 225-236

Chen, J., Chen, J., Liao, A., Cao, X., Chen, L., Chen, X., He, C., Han, G., Peng, S., Lu, M., Zhang, W., Tong, X., & Mills, J. (2015). Global land cover mapping at 30m resolution: A POK-based operational approach. *ISPRS Journal of Photogrammetry and Remote Sensing, 103*, 7-27

Chen, J., Huang, J., & Hu, J. (2011). Mapping rice planting areas in southern China using the China Environment Satellite data. *Mathematical and Computer Modelling, 54*, 1037-1043

Chen, J., Jönsson, P., Tamura, M., Gu, Z., Matsushita, B., & Eklundh, L. (2004). A simple method for reconstructing a high-quality NDVI time-series data set based on the Savitzky–Golay filter. *Remote Sensing of Environment, 91*, 332-344

Chen, X., Hu, B., & Yu, R. (2005b). Spatial and temporal variation of phenological growing season and climate change impacts in temperate eastern China. *Global Change Biology, 11*, 1118-1130

Chen, X., & Pan, W. (2002). Relationships among phenological growing season, time-integrated normalized difference vegetation index and climate forcing in the temperate region of eastern China. *International Journal of Climatology, 22*, 1781-1792

Chen, X., Tan, Z., & Schwartz, M.D. (2000). Determining the grow season of land vegetation on the basis of plant phenology and satellite data in Northern China. *International Journal of Biometeorol, 44*, 97-101

Cheng, S.-H., Zhuang, J.-Y., Fan, Y.-Y., Du, J.-H., & Cao, L.-Y. (2007). Progress in Research and Development on Hybrid Rice: A Super-domesticate in China. *Annals of Botany, 100*, 959-966

Chuanfu, X., Jing, L., & Qinhuo, L. (2012). Monitoring vegetation phenology in China using time-series MODIS LAI data. In, *Geoscience and Remote Sensing Symposium (IGARSS), 2012 IEEE International* (pp. 48-51)

Chuine, I. (2000). A Unified Model for Budburst of Trees. *Journal of Theoretical Biology, 207*, 337-347

Churkina, G., Schimel, D., Braswell, B.H., & Xiao, X. (2005). Spatial analysis of growing season length control over net ecosystem exchange. *Global Change Biology, 11*, 1777-1787

Clauss, K., Yan, H., & Kuenzer, C. (2016). Mapping Paddy Rice in China in 2002, 2005, 2010 and 2014 with MODIS Time Series, *8*, 434

Clevers, J.G.P.W., De Jong, S.M., Epema, G.F., Van Der Meer, F.D., Bakker, W.H., Skidmore, A.K., & Scholte, K.H. (2002). Derivation of the red edge index using the MERIS standard band setting. *International Journal of Remote Sensing, 23*, 3169-3184

Cong, N., Piao, S., Chen, A., Wang, X., Lin, X., Chen, S., Han, S., Zhou, G., & Zhang, X. (2012). Spring vegetation green-up date in China inferred from SPOT NDVI data: A multiple model analysis. *Agricultural and Forest Meteorology, 165*, 104-113

Cong, N., Wang, T., Nan, H., Ma, Y., Wang, X., Myneni, R.B., & Piao, S. (2013). Changes in satellite-derived spring vegetation green-up date and its linkage to climate in China from 1982 to 2010: a multimethod analysis. *Global Change Biology, 19*, 881-891

Crimmins, M., & Crimmins, T. (2008). Monitoring Plant Phenology Using Digital Repeat Photography. *Environmental Management, 41*, 949-958

Cui, M., Xue, S., & Huang, Y. (2010). Land Cover Classification Base on Fourier Analysis. In, *2010 Fourth International Conference on Genetic and Evolutionary Computing* (pp. 390-393)

Curran, P.J., Dungan, J.L., & Gholz, H.L. (1990). Exploring the relationship between reflectance red edge and chlorophyll content in slash pine. *Tree Physiology, 7*, 33-48

Curran, P.J., & Steele, C.M. (2005). MERIS: the re‐branding of an ocean sensor. *International Journal of Remote Sensing, 26*, 1781-1798

Dai, S., Zhang, B., Wang, H., Wang, Y., Guo, L., Wang, X., & Li, D. (2011). Vegetation cover change and the driving factors over Northwest China. *Journal of Arid Land, 3*, 25-33

Darwin, R., & Kennedy, D. (2000). Economic effects of CO2 fertilization of crops: transforming changes in yield into changes in supply. *Environmental Modeling & Assessment, 5*, 157-168

Das, K.D., Mishra, K.K., & Kalra, N. (1993). Assessing growth and yield of wheat using remotely-sensed canopy temperature and spectral indices *International Journal of Remote Sensing, 14*, 3081-3092

Dash, J., Curran, P., & Foody, G. (2009a). Remote sensing of terrestrial chlorophyll content. *Global Climatology and Ecodynamics* (pp. 77-105): Springer Berlin Heidelberg

Dash, J., & Curran, P.J. (2004). The MERIS terrestrial chlorophyll index. *Remote sensing, 25*, 5403-5413

Dash, J., & Curran, P.J. (2007). Evaluation of the MERIS terrestrial chlorophyll index (MTCI). *Advances in Space Research, 39*, 100-104

Dash, J., Curran, P.J., & Foody, G.M. (2009b). Remote sensing of terrestrial chlorophyll content. *Global Climatology and Ecodynamics: Anthropogenic Changes to Planet Earth* (pp. 77-105). Berlin, Heidelberg: Springer Berlin Heidelberg

Dash, J., Curran, P.J., Tallis, M.J., Llewellyn, G.M., Taylor, G., & Snoeij, P. (2010a). Validating the MERIS Terrestrial Chlorophyll Index (MTCI) with ground chlorophyll content data at MERIS spatial resolution. *International Journal of Remote Sensing, 31*, 5513-5532

Dash, J., Jeganathan, C., & Atkinson, P.M. (2010b). The use of MERIS Terrestrial Chlorophyll Index to study spatio-temporal variation in vegetation phenology over India. *Remote Sensing of Environment, 114*, 1388-1402

Dash, J., Mathur, A., Foody, G.M., Curran, P.J., Chipman, J.W., & Lillesand, T.M. (2007). Land cover classification using multi‐temporal MERIS vegetation indices. *International Journal of Remote Sensing, 28*, 1137-1159

Dawson, T.P. (2000). The potential for estimating chlorophyll content from a vegetation canopy using the Medium Resolution Imaging Spectrometer (MERIS). *International Journal of Remote Sensing, 21*, 2043-2051

Dawson, T.P., & Curran, P.J. (1998). Technical note A new technique for interpolating the reflectance red edge position. *International Journal of Remote Sensing, 19*, 2133-2139

de Beurs, K.M., & Henebry, G.M. (2010). Spatio-Temporal Statistical Methods for Modelling Land Surface Phenology. In I.L. Hudson, & M.R. Keatley (Eds.), *Phenological Research: Methods for Environmental and Climate Change Analysis* (pp. 177-208). Dordrecht: Springer Netherlands

de Wit, A., Boogaard, H., Fumagalli, D., Janssen, S., Knapen, R., van Kraalingen, D., Supit, I., van der Wijngaart, R., & van Diepen, K. (2019). 25 years of the WOFOST cropping systems model. *Agricultural Systems, 168*, 154-167

Delbart, N., Picard, G., Le toan, T., Kergoat, L., Quegan, S., Woodward, I., Dye, D., & Fedotova, V. (2008). Spring phenology in boreal Eurasia over a nearly century time scale, *14*, 603-614

Delegido, J., Verrelst, J., Alonso, L., & Moreno, J. (2011). Evaluation of Sentinel-2 red-edge bands for empirical estimation of green LAI and chlorophyll content. *Sensors (Basel, Switzerland), 11*, 7063-7081

Demarée, G.R., & Rutishauser, T. (2009). Origins of the Word "Phenology", *90*, 291-291

Dempewolf, J., Adusei, B., Becker-Reshef, I., Hansen, M., Potapov, P., Khan, A., & Barker, B. (2014). Wheat Yield Forecasting for Punjab Province from Vegetation Index Time Series and Historic Crop Statistics, *6*, 9653

Ding, M., Zhang, Y., Sun, X., Liu, L., Wang, Z., & Bai, W. (2013). Spatiotemporal variation in alpine grassland phenology in the Qinghai-Tibetan Plateau from 1999 to 2009. *Chinese Science Bulletin, 58*, 396-405

Dong, J., & Xiao, X. (2016). Evolution of regional to global paddy rice mapping methods: A review. *ISPRS Journal of Photogrammetry and Remote Sensing, 119*, 214-227

Dong, J., Xiao, X., Kou, W., Qin, Y., Zhang, G., Li, L., Jin, C., Zhou, Y., Wang, J., Biradar, C., Liu, J., & Moore, B. (2015a). Tracking the dynamics of paddy rice planting area in 1986–2010 through time series Landsat images and phenology-based algorithms. *Remote Sensing of Environment, 160*, 99-113

Dong, J., Xiao, X., Menarguez, M.A., Zhang, G., Qin, Y., Thau, D., Biradar, C., & Moore, B. (2016). Mapping paddy rice planting area in northeastern Asia with Landsat 8 images, phenology-based algorithm and Google Earth Engine. *Remote Sensing of Environment, 185*, 142-154

Dong, T., Meng, J.-h., Shang, J., Liu, J., & Wu, B. (2015b). *Evaluation of Chlorophyll-Related Vegetation Indices Using Simulated Sentinel-2 Data for Estimation of Crop Fraction of Absorbed Photosynthetically Active Radiation*.

Donnelly, A., & Yu, R. (2017). The rise of phenology with climate change: an evaluation of IJB publications. *International Journal of Biometeorology, 61*, 29-50

Doraiswamy, P.C., & Cook, P.W. (1995). Spring Wheat Yield Assessment Using NOAA AVHRR Data. *Canadian Journal of Remote Sensing, 21*, 43-51

Dou, Y., Wang, J., Song, P., Zhang, D., Huang, J., Wang, L., Dou, Y., Wang, J., Song, P., Zhang, D., Huang, J., Dou, Y., Wang, J., Song, P., Zhang, D., & Huang, J. (2017). Paddy rice field mapping using GF-1 images with SVM method. In, *2017 6th International Conference on Agro-Geoinformatics* (pp. 1-5)

Droogers, P., & International Water Management, I. (2002). *Global irrigated area mapping : overview and recommendations*. Colombo, Sri Lanka: International Water Management Institute

Du, J., Yan, P., & Dong, Y. (2010). Phenological response of *Nitraria tangutorum* to climate change in Minqin County, Gansu Province, northwest China. *International Journal of Biometeorology, 54*, 583-593

Du, X., Song, F., Wang, H., Huanxuezhang, Meng, J., Li, Q., Liu, J., Ding, L., & Lu, Y. (2014). Soybean yield estimation using HJ-1 CCD data in Northeast China. In, *2014 The Third International Conference on Agro-Geoinformatics* (pp. 1-4)

Dube, P.A., Perry, L.P., & Vittum, M.T. (1984). Instructions for phenological observations: lilac and honeysuckle. *Bulletin/Vermont Agricultural Experiment Station (USA)*

Duchemin, B.t., Goubier, J., & Courrier, G. (1999). Monitoring Phenological Key Stages and Cycle Duration of Temperate Deciduous Forest Ecosystems with NOAA/AVHRR Data. *Remote Sensing of Environment, 67*, 68-82

Esquerdo, J.C.D.M., Zullo Júnior, J., & Antunes, J.F.G. (2011). Use of NDVI/AVHRR time-series profiles for soybean crop monitoring in Brazil. *International Journal of Remote Sensing, 32*, 3711-3727

Eyshi Rezaei, E., Gaiser, T., Siebert, S., Sultan, B., & Ewert, F. (2014). Combined impacts of climate and nutrient fertilization on yields of pearl millet in Niger. *European Journal of Agronomy, 55*, 77-88

Fan, L., Gao, Y., Brück, H., & Bernhofer, C. (2009). Investigating the relationship between NDVI and LAI in semi-arid grassland in Inner Mongolia using in-situ measurements. *Theoretical and Applied Climatology, 95*, 151-156

Fang, H. (1998). Rice crop area estimation of an administrative division in China using remote sensing data. *International Journal of Remote Sensing, 19*, 3411-3419

Fang, H., Wu, B., Liu, H., & Huang, X. (1998). Using NOAA AVHRR and Landsat TM to estimate rice area year-by-year. *International Journal of Remote Sensing, 19*, 521-525

Fang, J., Song, Y., Liu, H., & Piao, S. (2002). Vegetation-Climate Relationship and Its Application in the Division of Vegetation Zone in China. *Acta Botanica Sinica, 44*, 1105-1122

Fenner, M. (1998). The phenology of growth and reproduction in plants. *Perspectives in Plant Ecology, Evolution and Systematics, 1*, 78-91

Filella, I., & Penuelas, J. (1994). The red edge position and shape as indicators of plant chlorophyll content, biomass and hydric status. *International Journal of Remote Sensing, 15*, 1459-1470

Filipova-Racheva, D., & Hall-Beyer, M. (2000). Smoothing of NDVI time series curves for monitoring of vegetation changes in time. *Ecological Monitoring and Assessment Network National Science Meeting*, 17-22

Fischer, A. (1994). A model for the seasonal variations of vegetation indices in coarse resolution data and its inversion to extract crop parameters. *Remote Sensing of Environment, 48*, 220-230

Fischer, G., Shah, M., N. Tubiello, F., & van Velhuizen, H. (2005). Socio-economic and climate change impacts on agriculture: an integrated assessment, 1990–2080. *Philosophical Transactions of the Royal Society B: Biological Sciences, 360*, 2067-2083

Fischer, G., Shah, M.M., & van Velthuizen, H.T. (2002). Climate Change and Agricultural Vulnerability. In: IIASA, Laxenburg, Austria

Fisher, J.I., & Mustard, J.F. (2007). Cross-scalar satellite phenology from ground, Landsat, and MODIS data. *Remote Sensing of Environment, 109*, 261-273

Fisher, J.I., Mustard, J.F., & Vadeboncoeur, M.A. (2006). Green leaf phenology at Landsat resolution: Scaling from the field to the satellite. *Remote Sensing of Environment, 100*, 265-279

Fontana, D. (2005). *Assessing the relationship between shire winter crop yield and multi-temporal MODIS NDVI and EVI images*.

Fu, Y.H., Campioli, M., Deckmyn, G., & Janssens, I.A. (2012). The Impact of Winter and Spring Temperatures on Temperate Tree Budburst Dates: Results from an Experimental Climate Manipulation. *PLoS ONE, 7*, e47324

Ganjurjav, H., Gao, Q., Schwartz, M.W., Zhu, W., Liang, Y., Li, Y., Wan, Y., Cao, X., Williamson, M.A., Jiangcun, W., Guo, H., & Lin, E. (2016). Complex responses of spring vegetation growth to climate in a moisture-limited alpine meadow. *Scientific Reports, 6*, 23356

Gao, B. (1996). NDWI—A normalized difference water index for remote sensing of vegetation liquid water from space. *Remote Sensing of Environment, 58*, 257-266

Gao, X., Xu, Y., Zhao, Z., Pal, J.S., & Giorgi, F. (2006). On the role of resolution and topography in the simulation of East Asia precipitation. *Theoretical and Applied Climatology, 86*, 173-185

Geng, L., Ma, M., Wang, X., Yu, W., Jia, S., & Wang, H. (2014). Comparison of Eight Techniques for Reconstructing Multi-Satellite Sensor Time-Series NDVI Data Sets in the Heihe River Basin, China. *Remote sensing, 6*, 2024

Gilbert, M., Xiao, X., Pfeiffer, D.U., Epprecht, M., Boles, S., Czarnecki, C., Chaitaweesub, P., Kalpravidh, W., Minh, P.Q., Otte, M.J., Martin, V., & Slingenbergh, J. (2008). Mapping H5N1 highly pathogenic avian influenza risk in Southeast Asia. *Proceedings of the National Academy of Sciences of the United States of America, 105*, 4769-4774

Gitelson, A.A., & Merzlyak, M.N. (1998). Remote sensing of chlorophyll concentration in higher plant leaves. *Advances in Space Research, 22*, 689-692

Gong, P., Wang, J., Yu, L., Zhao, Y., Zhao, Y., Liang, L., Niu, Z., Huang, X., Fu, H., Liu, S., Li, C., Li, X., Fu, W., Liu, C., Xu, Y., Wang, X., Cheng, Q., Hu, L., Yao, W., Zhang, H., Zhu, P., Zhao, Z., Zhang, H., Zheng, Y., Ji, L., Zhang, Y., Chen, H., Yan, A., Guo, J., Yu, L., Wang, L., Liu, X., Shi, T., Zhu, M., Chen, Y., Yang, G., Tang, P., Xu, B., Giri, C., Clinton, N., Zhu, Z., Chen, J., & Chen, J. (2013). Finer resolution observation and monitoring of global land cover: first mapping results with Landsat TM and ETM+ data. *International Journal of Remote Sensing, 34*, 2607-2654

Graham, E.A., Hamilton, M.P., Mishler, B.D., Rundel, P.W., & Hansen, M.H. (2006). Use of a networked digital camerato estimate net CO2 uptake of a desiccation-tolerant moss. *Int J Plant Sci, 167*, 751-758

Graham, E.A., Yuen, E.M., Robertson, G.F., Kaiser, W.J., Hamilton, M.P., & Rundel, P.W. (2009). Budburst and leaf area expansion measured with a novel mobile camera system and simple color thresholding. *Environmental and Experimental Botany, 65*, 238-244

Gu, J., Li, X., Huang, C., & Okin, G.S. (2009). A simplified data assimilation method for reconstructing time-series MODIS NDVI data. *Advances in Space Research, 44*, 501-509

Günter, S., Stimm, B., Cabrera, M., Diaz, L., Maria,, Lojan, M., Ordonez, E., Richter, M., & Weber, M. (2008). Tree phenology in montane forests of southern Ecuador can be explained by precipitation, radiation and photoperiodic control. *Journal of Tropical Ecology, 24*, 247-258

Guo, L., Dai, J., Ranjitkar, S., Xu, J., & Luedeling, E. (2013). Response of chestnut phenology in China to climate variation and change. *Agricultural and Forest Meteorology, 180*, 164-172

Guo, L., Dai, J., Wang, M., Xu, J., & Luedeling, E. (2015). Responses of spring phenology in temperate zone trees to climate warming: A case study of apricot flowering in China. *Agricultural and Forest Meteorology, 201*, 1-7

Guo, Q., Kelly, M., Gong, P., & Liu, D. (2007). An Object-Based Classification Approach in Mapping Tree Mortality Using High Spatial Resolution Imagery. *GIScience & Remote Sensing, 44*, 24-47

Haggerty, B.P.a.M., Susan J. (2008). Phenology Hand Book. In. Santa Barbara: University of California

Han, G., & Xie, H. (2014). A study on land surface phenology in eastern China based on SPOT/VGT datasets. *IOP Conference Series: Earth and Environmental Science, 17*, 012002

Hänninen, H., & Kramer, K. (2007). A framework for modelling the annual cycle of trees in boreal and temperate regions. *Silva Fennica, 41*, 167-205

Hansen, P.M., & Schjoerring, J.K. (2003). Reflectance measurement of canopy biomass and nitrogen status in wheat crops using normalized difference vegetation indices and partial least squares regression. *Remote Sensing of Environment, 86*, 542-553

Hao, P., Wang, L., Zhan, Y., Niu, Z., & Wu, M. (2016). Using historical NDVI time series to classify crops at 30m spatial resolution: A case in Southeast Kansas. In, *2016 IEEE International Geoscience and Remote Sensing Symposium (IGARSS)* (pp. 6316-6319)

Harris, A., & Dash, J. (2010). The potential of the MERIS Terrestrial Chlorophyll Index for carbon flux estimation. *Remote Sensing of Environment, 114*, 1856-1862

Harris, A., & Dash, J. (2011). A new approach for estimating northern peatland gross primary productivity using a satellite-sensor-derived chlorophyll index. *Journal of Geophysical Research: Biogeosciences, 116*, n/a-n/a

Hastings, D.A., & Emery, W.J. (1992). The advanced very high resolution radiometer (AVHRR) - A brief reference guide. *Photogrammetric Engineering and Remote Sensing, 58*, 1183-1188

He, L., Asseng, S., Zhao, G., Wu, D., Yang, X., Zhuang, W., Jin, N., & Yu, Q. (2015a). Impacts of recent climate warming, cultivar changes, and crop management on winter wheat phenology across the Loess Plateau of China. *Agricultural and Forest Meteorology, 200*, 135-143

He, Y., Bo, Y., de Jong, R., Li, A., Zhu, Y., & Cheng, J. (2015b). Comparison of vegetation phenological metrics extracted from GIMMS NDVIg and MERIS MTCI data sets over China. *International Journal of Remote Sensing, 36*, 300-317

Helman, D. (2018). Land surface phenology: What do we really 'see' from space? *Science of The Total Environment, 618*, 665-673

Hoffmann, A.A., Camac, J.S., Williams, R.J., Papst, W., Jarrad, F.C., & Wahren, C.H. (2010). Phenological changes in six Australian subalpine plants in response to experimental warming and year‐to‐year variation. *Journal of Ecology, 98*, 927-937

Hollister, R.D., Webber, P.J., & Bay, C. (2005). Plant Response To Temperature In Northern Alaska: Implications For Predicting Vegetation Change, *86*, 1562-1570

Homolová, L., Malenovský, Z., Clevers, J.G.P.W., García-Santos, G., & Schaepman, M.E. (2013). Review of optical-based remote sensing for plant trait mapping. *Ecological Complexity, 15*, 1-16

Horler, D.N.H., Dockray, M., & Barber, J. (1983). The red edge of plant leaf reflectance. *International Journal of Remote Sensing, 4*, 273-288

Hu, C., & Campbell, J. (2014). Oceanic Chlorophyll-a Content. In J.M. Hanes (Ed.), *Biophysical Applications of Satellite Remote Sensing* (pp. 171-203). Berlin, Heidelberg: Springer Berlin Heidelberg

Hu, Q., Wu, W.-b., Song, Q., Lu, M., Chen, D., Yu, Q.-y., & Tang, H.-j. (2017). How do temporal and spectral features matter in crop classification in Heilongjiang Province, China? *Journal of Integrative Agriculture, 16*, 324-336

Huang, J., Wang, X., Li, X., Tian, H., & Pan, Z. (2013). Remotely Sensed Rice Yield Prediction Using Multi-Temporal NDVI Data Derived from NOAA's-AVHRR. *PLoS ONE, 8*, e70816

Huang, L., Yang, Q., Liang, D., Dong, Y., Xu, X., & Huang, W. (2012). The Estimation of Winter Wheat Yield Based on MODIS Remote Sensing Data. In D. Li, & Y. Chen (Eds.), *Computer and Computing Technologies in Agriculture V* (pp. 496-503): Springer Berlin Heidelberg

Huete, A., Didan, K., Miura, T., Rodriguez, E.P., Gao, X., & Ferreira, L.G. (2002). Overview of the radiometric and biophysical performance of the MODIS vegetation indices. *Remote Sensing of Environment, 83*, 195-213

Huete, A.R. (1988). A soil-adjusted vegetation index (SAVI). *Remote Sensing of Environment, 25*, 295-309

Huete, A.R., Liu, H.Q., Batchily, K., & van Leeuwen, W. (1997). A comparison of vegetation indices over a global set of TM images for EOS-MODIS. *Remote Sensing of Environment, 59*, 440-451

Huh, O.K. (1991). Limitations and capabilities of the NOAA satellite advanced very high resolution radiometer (AVHRR) for remote sensing of the Earth's surface. *Preventive Veterinary Medicine, 11*, 167-183

Hwang, T., Song, C., Vose, J.M., & Band, L.E. (2011). Topography-mediated controls on local vegetation phenology estimated from MODIS vegetation index. *Landscape Ecology, 26*, 541-556

Jackson, T.J., Chen, D., Cosh, M., Li, F., Anderson, M., Walthall, C., Doriaswamy, P., & Hunt, E.R. (2004). Vegetation water content mapping using Landsat data derived normalized difference water index for corn and soybeans. *Remote Sensing of Environment, 92*, 475-482

Jago, R.A., Cutler, M.E.J., & Curran, P.J. (1999). Estimating Canopy Chlorophyll Concentration from Field and Airborne Spectra. *Remote Sensing of Environment, 68*, 217-224

Jakubauskas, M.E., Legates, D.R., & Kastens, J.H. (2001). Harmonic analysis of time-series AVHRR NDVI data. *Photogrammetric Engineering and Remote Sensing, 67*, 461-470

Jakubauskas, M.E., Legates, D.R., & Kastens, J.H. (2002). Crop identification using harmonic analysis of time-series AVHRR NDVI data. *Computers and Electronics in Agriculture, 37*, 127-139

Jeganathan, C., Dash, J., & Atkinson, P.M. (2010). Mapping the phenology of natural vegetation in India using a remote sensing-derived chlorophyll index. *International Journal of Remote Sensing, 31*, 5777-5796

Jensen, R., Mausel, P., Dias, N., Gonser, R., Yang, C., Everitt, J., & Fletcher, R. (2007). Spectral analysis of coastal vegetation and land cover using AISA+ hyperspectral data. *Geocarto International, 22*, 17-28

Jiang, Z., Huete, A.R., Didan, K., & Miura, T. (2008). Development of a two-band enhanced vegetation index without a blue band. *Remote Sensing of Environment, 112*, 3833-3845

Jin, C., Xiao, X., Dong, J., Qin, Y., & Wang, Z. (2015). Mapping paddy rice distribution using multi-temporal Landsat imagery in the Sanjiang Plain, northeast China. *Frontiers of Earth Science*, 1-14

Jing-feng, H., Shu-chuan, T., Abou-Ismail, O., & Ren-chao, W. (2002). Rice yield estimation using remote sensing and simulation model. *Journal of Zhejiang University Science, 3*, 461-466

Jones, M., Kimball, J., Small, E., & Larson, K. (2014). Comparing land surface phenology derived from satellite and GPS network microwave remote sensing. *International Journal of Biometeorology, 58*, 1305-1315

Jonsson, P., & Eklundh, L. (2002). Seasonality extraction by function fitting to time-series of satellite sensor data. *IEEE Transactions on Geoscience and Remote Sensing, 40*, 1824-1832

Jørgensen, S.E. (1994). Models as instruments for combination of ecological theory and environmental practice. *Ecological Modelling, 75-76*, 5-20

Julien, Y., & Sobrino, J.A. (2010). Comparison of cloud-reconstruction methods for time series of composite NDVI data. *Remote Sensing of Environment, 114*, 618-625

Justice, C.O., Vermote, E., Townshend, J.R.G., DeFries, R., Roy, D.P., Hall, D.K., Salomonson, V.V., Privette, J.L., Riggs, G., Strahler, A., Lucht, W., Myneni, R.B., Knyazikhin, Y., Running, S.W., Nemani, R.R., Zhengming, W., Huete, A.R., Van Leeuwen, W., Wolfe, R.E., Giglio, L., Muller, J.P., Lewis, P., & Barnsley, M.J. (1998). The Moderate Resolution Imaging Spectroradiometer (MODIS): land remote sensing for global change research. *Geoscience and Remote Sensing, IEEE Transactions on, 36*, 1228-1249

Kaptué Tchuenté, A.T., De Jong, S.M., Roujean, J.-L., Favier, C., & Mering, C. (2011). Ecosystem mapping at the African continent scale using a hybrid clustering approach based on 1-km resolution multi-annual data from SPOT/VEGETATION. *Remote Sensing of Environment, 115*, 452-464

Kaufman, Y.J., & Tanre, D. (1992). Atmospherically resistant vegetation index (ARVI) for EOS-MODIS. *Geoscience and Remote Sensing, IEEE Transactions on, 30*, 261-270

Kawamura, K., Akiyama, T., Yokota, H.-o., Tsutsumi, M., Yasuda, T., Watanabe, O., & Wang, S. (2005). Comparing MODIS vegetation indices with AVHRR NDVI for monitoring the forage quantity and quality in Inner Mongolia grassland, China. *Grassland Science, 51*, 33-40

Kawamura, K., Ikeura, H., Phongchanmaixay, S., & Khanthavong, P. (2018). Canopy Hyperspectral Sensing of Paddy Fields at the Booting Stage and PLS Regression can Assess Grain Yield, *10*, 1249

Kawashima, S., & Nakatani, M. (1998). An algorithm for estimating chlorophyll content in leaves using a video camera. *Annals of Botany, 81*, 49-54

Keller, M., Schimel, D.S., Hargrove, W.W., & Hoffman, F.M. (2008). A continental strategy for the national ecological observatory network. *The Ecological Society of America*, 282-284

Khamala, E. (2017). *Review of the available remote sensing tools, products, methodologies and data to improve crop production forecasts*. Rome: Food and Agriculture Organization of the United Nations (FAO)

Khush, G.S. (2005a). What it will take to Feed 5.0 Billion Rice consumers in 2030. *Plant Molecular Biology, 59*, 1-6

Khush, G.S.J.P.M.B. (2005b). What it will take to Feed 5.0 Billion Rice consumers in 2030, *59*, 1-6

Khwarahm, N.R., Dash, J., Skjøth, C.A., Newnham, R.M., Adams-Groom, B., Head, K., Caulton, E., & Atkinson, P.M. (2017). Mapping the birch and grass pollen seasons in the UK using satellite sensor time-series. *Science of The Total Environment, 578*, 586-600

Kobayashi, H., & Dye, D.G. (2005). Atmospheric conditions for monitoring the long-term vegetation dynamics in the Amazon using normalized difference vegetation index. *Remote Sensing of Environment, 97*, 519-525

Koch, E., Bruns, E., Chmielewski, F.-M., Defila, C., Lipa, W., & Menzel, A. (2007). Guidelines for plant phenological observations. In

Kontgis, C., Schneider, A., & Ozdogan, M. (2015). Mapping rice paddy extent and intensification in the Vietnamese Mekong River Delta with dense time stacks of Landsat data. *Remote Sensing of Environment, 169*, 255-269

Kovalskyy, V., Roy, D.P., Zhang, X.Y., & Ju, J. (2012). The suitability of multi-temporal web-enabled Landsat data NDVI for phenological monitoring – a comparison with flux tower and MODIS NDVI. *Remote Sensing Letters, 3*, 325-334

Kurosu, T., Fujita, M., & Chiba, K. (1997). The identification of rice fields using multi-temporal ERS-1 C band SAR data *International Journal of Remote Sensing, 18*, 2953-2965

Kussul, N., Lavreniuk, M., Skakun, S., & Shelestov, A. (2017). Deep Learning Classification of Land Cover and Crop Types Using Remote Sensing Data. *IEEE Geoscience and Remote Sensing Letters, 14*, 778-782

Labus, M.P., Nielsen, G.A., Lawrence, R.L., Engel, R., & Long, D.S. (2002). Wheat yield estimates using multi-temporal NDVI satellite imagery. *International Journal of Remote Sensing, 23*, 4169-4180

Langley, S.K., Cheshire, H.M., & Humes, K.S. (2001). A comparison of single date and multitemporal satellite image classifications in a semi-arid grassland. *Journal of Arid Environments, 49*, 401-411

Lauscher, F. (1978). Neue Analysen ältester und neuerer phänologischer Reihen. *Archiv für Meteorologie, Geophysik und Bioklimatologie, Serie B, 26*, 373-385

Le, L., Mark, A.F., Qinchuan, X., Josh, G., Yaozhong, P., & Steve, F. (2014). Mapping crop cycles in China using MODIS-EVI time series. *Remote sensing, 6*, 2473-2493

Lee, R., Yu, F., Price, K.P., Ellis, J., & Shi, P. (2001). Evaluating vegetation phenological patterns in Inner Mongolia using NDVI time-series analysis. *Remote sensing, 23*, 2505-2512

Li, B.-L., Ti, C.-P., & Yan, X.-Y. (2017). Estimating rice paddy areas in China using multi-temporal cloud-free NDVI imagery based on change detection. *Pedosphere*

Li, C., Mosier, A., Wassmann, R., Cai, Z., Zheng, X., Huang, Y., Tsuruta, H., Boonjawat, J., & Lantin, R. (2004). Modeling greenhouse gas emissions from rice-based production systems: Sensitivity and upscaling. *Global Biogeochemical Cycles, 18*, n/a-n/a

Li, M., Wu, Z., Qin, L., & Meng, X. (2011a). Extracting vegetation phenology metrics in Changbai Mountains using an improved logistic model. *Chinese Geographical Science, 21*, 304-311

Li, P., Feng, Z., Jiang, L., Liu, Y., & Xiao, X.J.J.o.G.S. (2012). Changes in rice cropping systems in the Poyang Lake Region, China during 2004–2010, *22*, 653-668

Li, Q., Zhang, H., Du, X., Wen, N., & Tao, Q. (2014). *County-level rice area estimation in southern China using remote sensing data*. SPIE

Li, W.-g., Li, H., & Zhao, L.-h. (2011b). Estimating Rice Yield by HJ-1A Satellite Images. *Rice Science, 18*, 142-147

Li, Z., Li, X., Wei, D., Xu, X., & Wang, H. (2010). An assessment of correlation on MODIS-NDVI and EVI with natural vegetation coverage in Northern Hebei Province, China. *Procedia Environmental Sciences, 2*, 964-969

Liang, L. (2009). Landscape phenology of Wisconsin's temperate mixed forest. In: University of Wisconsin-Milwaukee

Lieth, H. (1974). *Phenology and Seasonality Modeling*. (1 ed.). Springer-Verlag Berlin Heidelberg

Linderholm, H.W. (2006). Growing season changes in the last century. *Agricultural and Forest Meteorology, 137*, 1-14

Liu, C., Sun, P., & Liu, S. (2016a). *A review of plant spectral reflectance response to water physiological changes*.

Liu, J., Kuang, W., Zhang, Z., Xu, X., Qin, Y., Ning, J., Zhou, W., Zhang, S., Li, R., Yan, C., Wu, S., Shi, X., Jiang, N., Yu, D., Pan, X., & Chi, W. (2014). Spatiotemporal characteristics, patterns, and causes of land-use changes in China since the late 1980s. *Journal of Geographical Sciences, 24*, 195-210

Liu, J., Liu, M., Tian, H., Zhuang, D., Zhang, Z., Zhang, W., Tang, X., & Deng, X. (2005). Spatial and temporal patterns of China's cropland during 1990–2000: An analysis based on Landsat TM data. *Remote Sensing of Environment, 98*, 442-456

Liu, L., Wang, J., Huang, W., Zhao, C., Zhang, B., & Tong, Q. (2004). Estimating winter wheat plant water content using red edge parameters. *International Journal of Remote Sensing, 25*, 3331-3342

Liu, Q., Fu, Y.H., Zeng, Z., Huang, M., Li, X., & Piao, S. (2016b). Temperature, precipitation, and insolation effects on autumn vegetation phenology in temperate China. *Global Change Biology, 22*, 644-655

Liu, Z., Li, K., Cai, Y., & Fang, Y. (2011). Correlations between leafing phenology and traits: woody species of evergreen broad-leaved forests in subtropical China. *Polish Journal of Ecology, 59*, 463-473

Lloyd, D. (1990). A phenological classification of terrestrial vegetation cover using shortwave vegetation index imagery. *International Journal of Remote Sensing, 11*, 2269-2279

Lobell, D.B. (2013). The use of satellite data for crop yield gap analysis. *Field Crops Research, 143*, 56-64

Lobell, D.B., Sibley, A., & Ivan Ortiz-Monasterio, J. (2012). Extreme heat effects on wheat senescence in India. *Nature Climate Change, 2*, 186

Lopresti, M.F., Di Bella, C.M., & Degioanni, A.J. (2015). Relationship between MODIS-NDVI data and wheat yield: A case study in Northern Buenos Aires province, Argentina. *Information Processing in Agriculture, 2*, 73-84

Loucks, D.P., Van Beek, E., Stedinger, J.R., Dijkman, J.P., & Villars, M.T. (2005). *Water resources systems planning and management: an introduction to methods, models and applications*. Paris: Unesco

Lovell, J.L., & Graetz, R.D. (2001). Filtering Pathfinder AVHRR Land NDVI data for Australia. *International Journal of Remote Sensing, 22*, 2649-2654

Loyarte, M.M.G., Menenti, M., & Diblasi, A.M. (2008). Modelling bioclimate by means of Fourier analysis of NOAA-AVHRR NDVI time series in Western Argentina. *International Journal of Climatology, 28*, 1175-1188

Lu, P., Yu, Q., Liu, J., & He, Q. (2006). Effects of changes in spring temperature on flowering dates of woody plants across China. *Botanical Studies, 47*, 153-161

Lu, X., Liu, R., Liu, J., & Liang, S. (2007). Removal of Noise by Wavelet Method to Generate High Quality Temporal Data of Terrestrial MODIS Products. *Photogrammetric Engineering & Remote Sensing, 73*, 1129-1139

Lu, Y., Yi, S., Zeng, N., Liu, Y., & Zhang, Y. (2017). Identification of rice diseases using deep convolutional neural networks. *Neurocomputing, 267*, 378-384

Luo, X., Chen, X., Wang, L., Xu, L., & Tian, Y. (2014). Modeling and predicting spring land surface phenology of the deciduous broadleaf forest in northern China. *Agricultural and Forest Meteorology, 198–199*, 33-41

Luo, Z., Sun, O., Ge, Q., Xu, W., & Zheng, J. (2007). Phenological responses of plants to climate change in an urban environment. *Ecological Research, 22*, 507-514

Ma, M., & Veroustraete, F. (2006). Reconstructing pathfinder AVHRR land NDVI time-series data for the Northwest of China. *Advances in Space Research, 37*, 835-840

Ma, T., & Zhou, C. (2012). Climate-associated changes in spring plant phenology in China. *International Journal of Biometeorology, 56*, 269-275

Maignan, F., Bréon, F.M., Bacour, C., Demarty, J., & Poirson, A. (2008). Interannual vegetation phenology estimates from global AVHRR measurements: Comparison with in situ data and applications. *Remote Sensing of Environment, 112*, 496-505

Mansaray, L.R., Huang, W., Zhang, D., Huang, J., & Li, J. (2017). Mapping Rice Fields in Urban Shanghai, Southeast China, Using Sentinel-1A and Landsat 8 Datasets, *9*, 257

Markon, C.J., Fleming, M.D., & Binnian, E.F. (1995). Characteristic of vegetation phenology over the Alaskan landscape using AVHRR time-series data. *Polar Record, 31*, 179-190

Marti, J., Bort, J., Slafer, G.A., & Araus, J.L. (2007). Can wheat yield be assessed by early measurements of Normalized Difference Vegetation Index? *Annals of Applied Biology, 150*, 253-257

Maselli, F., Conese, C., Petkov, L., & Gilabert, M.A. (1993). Environmental monitoring and crop forecasting in the Sahel through the use of NOAA NDVI data. A case study: Niger 1986–89. *International Journal of Remote Sensing, 14*, 3471-3487

Mašková, Z., Zemek, F., & Květ, J. (2008). Normalized difference vegetation index (NDVI) in the management of mountain meadows. *Boreal Environment Research, 13*, 417-432

Matsushita, B., Yang, W., Chen, J., Onda, Y., & Qiu, G. (2007). Sensitivity of the Enhanced Vegetation Index (EVI) and Normalized Difference Vegetation Index (NDVI) to Topographic Effects: A Case Study in High-Density Cypress Forest. *Sensors (Basel, Switzerland), 7*, 2636-2651

McCLOY, K.R., Smith, F.R., & Robinson, M.R. (1987). Monitoring rice areas using LANDSAT MSS data. *International Journal of Remote Sensing, 8*, 741-749

Melke, A. (2015). *The Physiology of Chilling Temperature Requirements for Dormancy Release and Bud-break in Temperate Fruit Trees Grown at Mild Winter Tropical Climate*.

Mendelsohn, R., Basist, A., Dinar, A., Kurukulasuriya, P., & Williams, C. (2007). What explains agricultural performance: climate normals or climate variance? *Climatic Change, 81*, 85-99

Menenti, M., Azzali, S., Verhoef, W., & van Swol, R. (1993). Mapping agroecological zones and time lag in vegetation growth by means of fourier analysis of time series of NDVI images. *Advances in Space Research, 13*, 233-237

Meng, J., Wu, B., Li, Q., Du, X., & Jia, K. (2009). Monitoring Crop Phenology with MERIS Data - A Case Study of Winter Wheat in North China Plain. *Progress In Electromagnetics Research Symposium*, 1125-1128

Menzel, A. (2000). Trends in phenological phases in Europe between 1951 and 1996. *International Journal of Biometeorology, 44*, 76-81

Menzel, A. (2002). Phenology: Its Importantce to the Global Change Community. *Climate Change, 54*, 379-385

Menzel, A., & Fabian, P. (1999). Growing season extended in Europe. *Nature, 397*, 659

Menzel, A., Sparks, T.h., Estrella, N., Koch, E., Aasa, A., Ahas, R., Alm-kübler, K., Bissolli, P., Braslavská, O.g., Briede, A., Chmielewski, F.m., Crepinsek, Z., Curnel, Y., Dahl, Å., Defila, C., Donnelly, A., Filella, Y., Jatczak, K., Måge, F., Mestre, A., Nordli, Ø., Peñuelas, J., Pirinen, P., Remišová, V., Scheifinger, H., Striz, M., Susnik, A., Van Vliet, A.j.H., Wielgolaski, F.-e., Zach, S., & Zust, A. (2006). European phenological response to climate change matches the warming pattern, *12*, 1969-1976

Miyaoka, K., Maki, M., Susaki, J., Homma, K., Noda, K., & Oki, K. (2013). Rice-Planted Area Mapping Using Small Sets of Multi-Temporal SAR Data. *IEEE Geoscience and Remote Sensing Letters, 10*, 1507-1511

Mkhabela, M.S., Bullock, P., Raj, S., Wang, S., & Yang, Y. (2011). Crop yield forecasting on the Canadian Prairies using MODIS NDVI data. *Agricultural and Forest Meteorology, 151*, 385-393

Mkhabela, M.S., Mkhabela, M.S., & Mashinini, N.N. (2005). Early maize yield forecasting in the four agro-ecological regions of Swaziland using NDVI data derived from NOAA's-AVHRR. *Agricultural and Forest Meteorology, 129*, 1-9

Moody, A., & Johnson, D.M. (2001). Land-Surface Phenologies from AVHRR Using the Discrete Fourier Transform. *Remote Sensing of Environment, 75*, 305-323

Moody, D.I., Brumby, S.P., Chartrand, R., Keisler, R., Longbotham, N., Mertes, C., Skillman, S.W., & Warren, M.S. (2017). Crop classification using temporal stacks of multispectral satellite imagery. In, *SPIE Defense + Security* (p. 12): SPIE

Moreno, Á., García-Haro, F., Martínez, B., & Gilabert, M. (2014). Noise Reduction and Gap Filling of fAPAR Time Series Using an Adapted Local Regression Filter. *Remote sensing, 6*, 8238

Mosleh, M.K., Hassan, Q.K., & Chowdhury, E.H. (2015). Application of remote sensors in mapping rice area and forecasting its production: a review. *Sensors (Basel, Switzerland), 15*, 769-791

Moulin, S., Kergoat, L., Viovy, N., & Dedieu, G. (1997). Global-Scale Assessment of Vegetation Phenology Using NOAA/AVHRR Satellite Measurements. *Journal of Climate, 10*, 1154-1170

Munden, R., Curran, P.J., & Catt, J.A. (1994). The relationship between red edge and chlorophyll concentration in the Broadbalk winter wheat experiment at Rothamsted. *International Journal of Remote Sensing, 15*, 705-709

Mutanga, O., & Skidmore, A.K. (2004). Narrow band vegetation indices overcome the saturation problem in biomass estimation. *International Journal of Remote Sensing, 25*, 3999-4014

Myneni, R.B., & Hall, F.G. (1995). The interpretation of spectral vegetation indexes. *Geoscience and Remote Sensing, IEEE Transactions on, 33*, 481-486

Myneni, R.B., Keeling, C.D., Tucker, C.J., Asrar, G., & Nemani, R.R. (1997). Increased plant growth in the northern high latitudes from 1981 to 1991. *Nature, 386*, 698

Nordberg, M.L., & Evertson, J. (2005). Vegetation index differencing and linear regression for change detection in a Swedish mountain range using Landsat TM® and ETM+® imagery. *Land Degradation & Development, 16*, 139-149

Nuarsa, I.W., Nishio, F., & Hongo, C. (2011). Relationship between Rice Spectral and Rice Yield Using Modis Data, *3*, 80-88

O'Connor, B., Dwyer, E., Cawkwell, F., & Eklundh, L. (2012). Spatio-temporal patterns in vegetation start of season across the island of Ireland using the MERIS Global Vegetation Index. *ISPRS Journal of Photogrammetry and Remote Sensing, 68*, 79-94

Okamoto, K. (1999). Estimation of rice-planted area in the tropical zone using a combination of optical and microwave satellite sensor data. *International Journal of Remote Sensing, 20*, 1045-1048

Olsson, L., & Eklundh, L. (1994). Fourier Series for analysis of temporal sequences of satellite sensor imagery. *International Journal of Remote Sensing, 15*, 3735-3741

Onojeghuo, A.O., Blackburn, G.A., Wang, Q., Atkinson, P.M., Kindred, D., & Miao, Y. (2018). Mapping paddy rice fields by applying machine learning algorithms to multi-temporal Sentinel-1A and Landsat data. *International Journal of Remote Sensing, 39*, 1042-1067

Ostberg, S., Schewe, J., Childers, K., & Frieler, K. (2018). Changes in crop yields and their variability at different levels of global warming. *Earth Syst. Dynam., 9*, 479-496

Pagter, M., Andersen, U.B., & Andersen, L. (2015). Winter warming delays dormancy release, advances budburst, alters carbohydrate metabolism and reduces yield in a temperate shrub. *AoB PLANTS, 7*, plv024-plv024

Pan, Y., Li, L., Zhang, J., Liang, S., Zhu, X., & Sulla-Menashe, D. (2012). Winter wheat area estimation from MODIS-EVI time series data using the Crop Proportion Phenology Index. *Remote Sensing of Environment, 119*, 232-242

Pan, Z., Huang, J., Zhou, Q., Wang, L., Cheng, Y., Zhang, H., Blackburn, G.A., Yan, J., & Liu, J. (2014). Mapping crop phenology using NDVI time-series derived from HJ-1 A/B data. *International Journal of Applied Earth Observation and Geoinformation, 34*, 188-197

Parihar, J.S. (1992). Role of middle infrared bands of Landsat thematic mapper in determining the classification accuracy of rice AU - PANIGRAHY, S. *International Journal of Remote Sensing, 13*, 2943-2949

Parinussa, R.M., Meesters, A.G.C.A., Liu, Y.Y., Dorigo, W., Wagner, W., & Jeu, R.A.M.d. (2011). Error Estimates for Near-Real-Time Satellite Soil Moisture as Derived From the Land Parameter Retrieval Model. *IEEE Geoscience and Remote Sensing Letters, 8*, 779-783

Peckham, S.D., Ahl, D.E., Serbin, S.P., & Gower, S.T. (2008). Fire-induced changes in green-up and leaf maturity of the Canadian boreal forest. *Remote Sensing of Environment, 112*, 3594-3603

Peng, S., Piao, S., Ciais, P., Myneni, R.B., Chen, A., Chevallier, F., Dolman, A.J., Janssens, I.A., Peñuelas, J., Zhang, G., Vicca, S., Wan, S., Wang, S., & Zeng, H. (2013). Asymmetric effects of daytime and night-time warming on Northern Hemisphere vegetation. *Nature, 501*, 88

Peñuelas, J., & Filella, I. (2001). Responses to a Warming World. *Science, 294*, 793-795

Peñuelas, J., Filella, I., & Comas, P. (2002). Changed plant and animal life cycles from 1952 to 2000 in the Mediterranean region. *Global Change Biology, 8*, 531-544

Peñuelas, J., Rutishauser, T., & Filella, I. (2009). Phenology Feedbacks on Climate Change. *Science, 324*, 887

Piao, S., Fang, J., Zhou, L., Ciais, P., & Zhu, B. (2006a). Variations in satellite-derived phenology in China's temperate vegetation. *Global Change Biology, 12*, 672-685

Piao, S., Fang, J., Zhou, L., Ciais, P., & Zhu, B. (2006b). Variations in satellite-derived phenology in China's temperate vegetation. *Global Change Biology, 12*, 672-685

Piao, S., Friedlingstein, P., Ciais, P., de Noblet-Ducoudré, N., Labat, D., & Zaehle, S. (2007). Changes in climate and land use have a larger direct impact than rising CO_2 on global river runoff trends. *Proceedings of the National Academy of Sciences, 104*, 15242-15247

Piao, S., Tan, J., Chen, A., Fu, Y.H., Ciais, P., Liu, Q., Janssens, I.A., Vicca, S., Zeng, Z., Jeong, S.-J., Li, Y., Myneni, R.B., Peng, S., Shen, M., & Peñuelas, J. (2015). Leaf onset in the northern hemisphere triggered by daytime temperature. *Nature Communications, 6*, 6911

Piekielek, N.B. (2012). Remote sensing grassland phenology in the greater yellowstone ecosystem: biophysical correlates, land use effects and patch dynamics. In, *Ecology and Evironmental Sciences* (p. 178): Montana State University

Pinzon, J., & Tucker, C. (2014). A Non-Stationary 1981–2012 AVHRR NDVI3g Time Series. *Remote sensing, 6*, 6929

Polgar, C.A., & Primack, R.B. (2011). Leaf-out phenology of temperate woody plants: from trees to ecosystems. *New Phytol, 191*, 926-941

Prasad, A.K., Chai, L., Singh, R.P., & Kafatos, M. (2006). Crop yield estimation model for Iowa using remote sensing and surface parameters. *International Journal of Applied Earth Observation and Geoinformation, 8*, 26-33

Purcell, L.C. (2000). Soybean canopy coverage and light interception measurements using digital imagery *Crop Sci., 40*, 834-837

Qader, S.H., Dash, J., & Atkinson, P.M. (2018). Forecasting wheat and barley crop production in arid and semi-arid regions using remotely sensed primary productivity and crop phenology: A case study in Iraq. *Science of The Total Environment, 613-614*, 250-262

Qin, Y., Xiao, X., Dong, J., Zhou, Y., Zhu, Z., Zhang, G., Du, G., Jin, C., Kou, W., Wang, J., & Li, X. (2015). Mapping paddy rice planting area in cold temperate climate region through analysis of time series Landsat 8 (OLI), Landsat 7 (ETM+) and MODIS imagery. *ISPRS Journal of Photogrammetry and Remote Sensing, 105*, 220-233

Qiu, B., Li, W., Tang, Z., Chen, C., & Qi, W. (2015). Mapping paddy rice areas based on vegetation phenology and surface moisture conditions. *Ecological Indicators, 56*, 79-86

Quarmby, N.A., Milnes, M., Hindle, T.L., & Silleos, N. (1993). The use of multi-temporal NDVI measurements from AVHRR data for crop yield estimation and prediction. *International Journal of Remote Sensing, 14*, 199-210

Rasmussen, M.S. (1992). Assessment of millet yields and production in northern Burkina Faso using integrated NDVI from the AVHRR. *International Journal of Remote Sensing, 13*, 3431-3442

Rasmussen, M.S. (1997). Operational yield forecast using AVHRR NDVI data: Reduction of environmental and inter-annual variability. *International Journal of Remote Sensing, 18*, 1059-1077

Rasmussen, M.S. (1998). Developing simple, operational, consistent NDVI-vegetation models by applying environmental and climatic information. Part II: Crop yield assessment. *International Journal of Remote Sensing, 19*, 119-139

Reed, B., Schwartz, M., & Xiao, X. (2009). Remote Sensing Phenology. In A. Noormets (Ed.), *Phenology of Ecosystem Processes* (pp. 231-246): Springer New York

Reed, B.C., Brown, J.F., VanderZee, D., Loveland, T.R., Merchant, J.W., & Ohlen, D.O. (1994). Measuring phenological variability from satellite imagery. *Journal of Vegetation Science, 5*, 703-714

Ren, J., Chen, Z., Zhou, Q., & Tang, H. (2008). Regional yield estimation for winter wheat with MODIS-NDVI data in Shandong, China. *International Journal of Applied Earth Observation and Geoinformation, 10*, 403-413

Reynolds, C.A., Yitayew, M., Slack, D.C., Hutchinson, C.F., Huete, A., & Petersen, M.S. (2000). Estimating crop yields and production by integrating the FAO Crop Specific Water Balance model with real-time satellite data and ground-based ancillary data. *International Journal of Remote Sensing, 21*, 3487-3508

Richardson, A.D., Braswell, B.H., Hollinger, D.Y., Jenkins, J.P., & Ollinger, S.V. (2009). Near-surface remote sensing of spatial and temporal variation in canopy phenology. *Ecological Applications, 19*, 1417-1428

Richardson, A.D., Jenkins, J.P., Braswell, B.H., Hollinger, D.Y., Ollinger, S.V., & Smith, M.-L. (2007). Use of digital webcam images to track spring green-up in a deciduous broadleaf forest. *Oecologia, 152*, 323-334

Richardson, A.D., Keenan, T.F., Migliavacca, M., Ryu, Y., Sonnentag, O., & Toomey, M. (2013a). Climate change, phenology, and phenological control of vegetation feedbacks to the climate system. *Agricultural and Forest Meteorology, 169*, 156-173

Richardson, A.D., Keenan, T.F., Migliavacca, M., Ryu, Y., Sonnentag, O., & Toomey, M. (2013b). Climate change, phenology, and phenological control of vegetation feedbacks to the climate system. *Agricultural and Forest Meteorology, 169*, 156-173

Ricotta, C., & Avena, G.C. (2000). The remote sensing approach in broad‐scale phenological studies. *Applied Vegetation Science, 3*, 117-122

Rocha, A.V., & Shaver, G.R. (2009). Advantages of a two band EVI calculated from solar and photosynthetically active radiation fluxes. *Agricultural and Forest Meteorology, 149*, 1560-1563

Roerink, G.J., Menenti, M., & Verhoef, W. (2000). Reconstructing cloudfree NDVI composites using Fourier analysis of time series. *International Journal of Remote Sensing, 21*, 1911-1917

Rojas, O. (2007). Operational maize yield model development and validation based on remote sensing and agro-meteorological data in Kenya. *Int. J. Remote Sens., 28*, 3775-3793

Rouse, J.W., Jr., Haas, R.H., Schell, J.A., & Deering, D.W. (1974). Monitoring vegetation systems in the Great Plains with ERTS. In, *3rd Earth Resource Technology Satellite (ERTS) Symposium* (pp. 48-62)

Ruml, M., & Vulić, T. (2005). Importance of phenology observations and predictions in agriculture. *Journal of Agriculture Science, 50*, 217-225

Rutishauser, T., Luterbacher, J., Jeanneret, F., Pfister, C., & Wanner, H. (2007). A phenology-based reconstruction of interannual changes in past spring seasons. *Journal of Geophysical Research: Biogeosciences, 112*, G04016

S. Mkhabela, M., S. Mkhabela, M., & N. Mashinini, N. (2005). *Early maize yield forecasting in the four agro-ecological regions of Swaziland using NDVI data derived from NOAA's-AVHRR*.

Saint, G. (1994). "Vegetation" onboard SPOT 4 mission specifications. In. Ispra, Italy

Salazar, L., Kogan, F., & Roytman, L. (2007). Use of remote sensing data for estimation of winter wheat yield in the United States. *International Journal of Remote Sensing, 28*, 3795-3811

Saure, M.C. (1985). Dormancy Release in Deciduous Fruit Trees. *Horticultural Reviews* (pp. 239-300): John Wiley & Sons, Inc.

Schlenker, W., & Roberts, M.J. (2009). Nonlinear temperature effects indicate severe damages to U.S. crop yields under climate change. *Proceedings of the National Academy of Sciences, 106*, 15594

Schmidt, M., Udelhoven, T., Röder, A., & Gill, T.K. (2012). Long term data fusion for a dense time series analysis with MODIS and Landsat imagery in an Australian Savanna. In (p. 19): SPIE

Schut, A.G.T., Stephens, D.J., Stovold, R.G.H., Adams, M., & Craig, R.L. (2009). Improved wheat yield and production forecasting with a moisture stress index, AVHRR and MODIS data. *Crop and Pasture Science, 60*, 60-70

Schwartz, M.D. (2013). *Phenology: An Integrative Environmental Science*. (2 ed.). Springer Netherlands

Schwartz, M.D., & Chen, X. (2002). Examing the onset of spring in China. *Climate research, Clim Res, 21*, 157-164

Schwartz, M.D., & Karl, T.R. (1990). Spring Phenology: Nature's Experiment to Detect the Effect of "Green-Up" on Surface Maximum Temperatures. *Monthly Weather Review, 118*, 883-890

Schwartz, M.D., & Reed, B.C. (1999). Surface phenology and satellite sensor-derived onset of greenness: An initial comparison *International Journal of Remote Sensing, 20*, 3451-3457

Sehgal, V.K., Jain, S., Aggarwal, P.K., & Jha, S. (2011). Deriving Crop Phenology Metrics and Their Trends Using Times Series NOAA-AVHRR NDVI Data. *Journal of the Indian Society of Remote Sensing, 39*, 373-381

Shao, Y., Fan, X., Liu, H., Xiao, J., Ross, S., Brisco, B., Brown, R., & Staples, G. (2001). Rice monitoring and production estimation using multitemporal RADARSAT. *Remote Sensing of Environment, 76*, 310-325

Shen, S., Yang, S., Li, B., Tan, B., Li, Z., & Le Toan, T. (2009). A scheme for regional rice yield estimation using ENVISAT ASAR data. *Science in China Series D: Earth Sciences, 52*, 1183-1194

Shi, C., Sun, G., Zhang, H., Xiao, B., Ze, B., Zhang, N., & Wu, N. (2014). Effects of Warming on Chlorophyll Degradation and Carbohydrate Accumulation of Alpine Herbaceous Species during Plant Senescence on the Tibetan Plateau. *PLoS ONE, 9*, e107874

Shi, J.-j., Huang, J.-f., & Zhang, F. (2013). Multi-year monitoring of paddy rice planting area in Northeast China using MODIS time series data. *Journal of Zhejiang University. Science. B, 14*, 934-946

Smetacek, V., & Nicol, S. (2005). Polar ocean ecosystems in a changing world. *Nature, 437*, 362

Smith, R., Adams, J., Stephens, D., & Hick, P. (1995). Forecasting wheat yield in a Mediterranean-type environment from the NOAA satellite. *Australian Journal of Agricultural Research, 46*, 113-125

Son, N.-T., Chen, C.-F., Chen, C.-R., & Minh, V.-Q. (2018). Assessment of Sentinel-1A data for rice crop classification using random forests and support vector machines. *Geocarto International, 33*, 587-601

Soudani, K., François, C., le Maire, G., Le Dantec, V., & Dufrêne, E. (2006). Comparative analysis of IKONOS, SPOT, and ETM+ data for leaf area index estimation in temperate coniferous and deciduous forest stands. *Remote Sensing of Environment, 102*, 161-175

Sparks, T., & Menzel, A. (2007). Plant phenology changes and climate change

Sparks, T.H., & Carey, P.D. (1995). The Responses of Species to Climate Over Two Centuries: An Analysis of the Marsham Phenological Record, 1736-1947. *Journal of Ecology, 83*, 321-329

Sparks, T.H., Huber, K., & Croxton, P.J. (2006). Plant development scores from fixed-date photographs: the influence of weather variables and recorder experience. *International Journal of Biometeorology, 50*, 275-279

Stöckle, C.O., Donatelli, M., & Nelson, R. (2003). CropSyst, a cropping systems simulation model. *European Journal of Agronomy, 18*, 289-307

Studer, S., Stöckli, R., Appenzeller, C., & Vidale, P.L. (2007). A comparative study of satellite and ground-based phenology. *International Journal of Biometeorology, 51*, 405-414

Suepa, T., Qi, J., Lawawirojwong, S., & Messina, J.P. (2016). Understanding spatio-temporal variation of vegetation phenology and rainfall seasonality in the monsoon Southeast Asia. *Environmental Research, 147*, 621-629

Sun, H.-s., Huang, J.-f., Huete, A., Peng, D.-l., & Zhang, F. (2009). Mapping paddy rice with multi-date moderate-resolution imaging spectroradiometer (MODIS) data in China. *Journal of Zhejiang University SCIENCE A, 10*, 1509-1522

Tadesse, G., Algieri, B., Kalkuhl, M., & von Braun, J. (2014). Drivers and triggers of international food price spikes and volatility. *Food Policy, 47*, 117-128

Tamstorf, M., Illeris, L., Hansen, B., & Wisz, M. (2007). Spectral measures and mixed models as valuable tools for investigating controls on land surface phenology in high arctic Greenland. *BMC Ecology, 7*, 1-16

Tan, C.P., Koay, J.Y., Lim, K.S., Ewe, H.T., & Chuah, H.T. (2007). Classification of multi-temporal SAR images for rice crops using combined entropy decomposition and support vector machine technique. *Progress In Electromagnetics Research, 71*, 19-39

Tang, H., Li, Z., Zhu, Z., Chen, B., Zhang, B., & Xin, X. (2015). Variability and climate change trend in vegetation phenology of recent decades in the Greater Khingan Mountain area, Northeastern China. *Remote sensing, 7*, 11914

Tao, F., Zhang, S., & Zhang, Z. (2012). Spatiotemporal changes of wheat phenology in China under the effects of temperature, day length and cultivar thermal characteristics. *European Journal of Agronomy, 43*, 201-212

Tenkorang, F., & Lowenberg-DeBoer, J. (2008). On-Farm Profitability of Remote Sensing in Agriculture. *Terrestrial Observation, 1*, 50-59

Tennakoon, S.B., Murty, V.V.N., & Eiumnoh, A. (1992). Estimation of cropped area and grain yield of rice using remote sensing data. *International Journal of Remote Sensing, 13*, 427-439

Tewes, A., Thonfeld, F., Schmidt, M., Oomen, R., Zhu, X., Dubovyk, O., Menz, G., & Schellberg, J. (2015). Using RapidEye and MODIS Data Fusion to Monitor Vegetation Dynamics in Semi-Arid Rangelands in South Africa. *Remote sensing, 7*, 6510

Thenkabail, P.S., Smith, R.B., & De Pauw, E. (2000). Hyperspectral Vegetation Indices and Their Relationships with Agricultural Crop Characteristics. *Remote Sensing of Environment, 71*, 158-182

Thornes, J.E. (2002). IPCC, 2001: Climate change 2001: impacts, adaptation and vulnerability, Contribution of Working Group II to the Third Assessment Report of the Intergovernmental Panel on Climate Change, edited by J. J. McCarthy, O. F. Canziani, N. A. Leary, D. J. Dokken and K. S. White (eds). Cambridge University Press, Cambridge, UK, and New York, USA, 2001. No. of pages: 1032. Price: £34.95, ISBN 0-521-01500-6 (paperback), ISBN 0-521-80768-9 (hardback). *International Journal of Climatology, 22*, 1285-1286

Toming, K., Kutser, T., Uiboupin, R., Arikas, A., Vahter, K., & Paavel, B. (2017). Mapping Water Quality Parameters with Sentinel-3 Ocean and Land Colour Instrument imagery in the Baltic Sea, *9*, 1070

Tucker, C.J., Holben, B.N., Elgin Jr, J.H., & McMurtrey Iii, J.E. (1980). Relationship of spectral data to grain yield variation. *Photogrammetric Engineering & Remote Sensing, 46*, 657-666

Tucker, C.J., Slayback, D.A., Pinzon, J.E., Los, S.O., Myneni, R.B., & Taylor, M.G. (2001). Higher northern latitude normalized difference vegetation index and growing season trends from 1982 to 1999. *International Journal of Biometeorology, 45*, 184-190

Ullah, S., Si, Y., Schlerf, M., Skidmore, A.K., Shafique, M., & Iqbal, I.A. (2012). Estimation of grassland biomass and nitrogen using MERIS data. *International Journal of Applied Earth Observation and Geoinformation, 19*, 196-204

Velleman, P.F. (1980). Definition and Comparison of Robust Nonlinear Data Smoothing Algorithms. *Journal of the American Statistical Association, 75*, 609-615

Vermote, E., & Kaufman, Y.J. (1995). Absolute calibration of AVHRR visible and near-infrared channels using ocean and cloud views. *International Journal of Remote Sensing, 16*, 2317-2340

Viña, A., Gitelson, A.A., Nguy-Robertson, A.L., & Peng, Y. (2011). Comparison of different vegetation indices for the remote assessment of green leaf area index of crops. *Remote Sensing of Environment, 115*, 3468-3478

Viovy, N., Arino, O., & Belward, A.S. (1992). The Best Index Slope Extraction (BISE): A method for reducing noise in NDVI time-series. *International Journal of Remote Sensing, 13*, 1585-1590

Vitasse, Y., François, C., Delpierre, N., Dufrêne, E., Kremer, A., Chuine, I., & Delzon, S. (2011). Assessing the effects of climate change on the phenology of European temperate trees. *Agricultural and Forest Meteorology, 151*, 969-980

Wall, L., Larocque, D., & Léger, P.M. (2008). The early explanatory power of NDVI in crop yield modelling. *International Journal of Remote Sensing, 29*, 2211-2225

Walther, G., Post, E., Convey, P., Menzel, A., Parmesan, C., Beebee, T., Fromentin, J., HOegh-Guildberg, O., & Birlein, F. (2002). Ecological responses to recent climate change. In, *Nature* (pp. 389-395)

Wang, C., Li, J., Liu, Q., Zhong, B., Wu, S., & Xia, C. (2017a). Analysis of Differences in Phenology Extracted from the Enhanced Vegetation Index and the Leaf Area Index. *Sensors, 17*, 1982

Wang, J., Xiao, X., Qin, Y., Dong, J., Zhang, G., Kou, W., Jin, C., Zhou, Y., & Zhang, Y. (2015). Mapping paddy rice planting area in wheat-rice double-cropped areas through integration of Landsat-8 OLI, MODIS, and PALSAR images. *Scientific Reports, 5*, 10088

Wang, L., Zhang, F.-c., Jing, Y.-s., Jiang, X.-d., Yang, S.-b., & Han, X.-m. (2014a). Multi-Temporal Detection of Rice Phenological Stages Using Canopy Spectrum. *Rice Science, 21*, 108-115

Wang, M., Tao, F.-l., & Shi, W.-j. (2014b). Corn Yield Forecasting in Northeast China Using Remotely Sensed Spectral Indices and Crop Phenology Metrics. *Journal of Integrative Agriculture, 13*, 1538-1545

Wang, M., & Tao, F. (2014). Comparison of three NDVI time-series fitting methods in crop phenology detection in Northeast China. *IOP Conference Series: Earth and Environmental Science, 17*, 012007

Wang, S., Xu, X., Shrestha, N., Zimmermann, N.E., Tang, Z., & Wang, Z. (2017b). Response of spatial vegetation distribution in China to climate changes since the Last Glacial Maximum (LGM). *PLoS ONE, 12*, e0175742

Wang, S., Yang, B., Yang, Q., Lu, L., Wang, X., & Peng, Y. (2016). Temporal Trends and Spatial Variability of Vegetation Phenology over the Northern Hemisphere during 1982-2012. *PLoS ONE, 11*, e0157134

Wang, X., Gao, Q., Wang, C., & Yu, M. (2017c). Spatiotemporal patterns of vegetation phenology change and relationships with climate in the two transects of East China. *Global Ecology and Conservation, 10*, 206-219

Wassmann, R., Papen, H., & Rennenberg, H. (1993). Methane emission from rice paddies and possible mitigation strategies. *Chemosphere, 26*, 201-217

Wei, H., Heilman, P., Qi, J., Nearing, A., Mark, Gu, Z., & Zhang, Y. (2012). Assessing phenological change in China from 1982 to 2006 using AVHRR imagery. *Front. Earth Sci, 6*, 227-236

Wei, W., Quanfang, W., Huaying, W., Yuanyuan, C., & Xinsheng, W. (2013). Yield estimation of semilate rice using remote sensing data in Honghu city, China. In, *Agro-Geoinformatics (Agro-Geoinformatics), 2013 Second International Conference on* (pp. 135-138)

Wheeler, T., & von Braun, J. (2013). Climate Change Impacts on Global Food Security, *341*, 508-513

White, M.A., De Beurs, K.M., Didan, K., Inouye, D.W., Richardson, A.D., Jensen, O.P., O'Keefe, J., Zhang, G., Nemani, R.R., Van Leeuwen, W.J.D., Brown, J.F., De Wit, A., Schaepman, M., Lin, X., Dettinger, M., Bailey, A.S., Kimball, J., Schwartz, M.D., Baldocchi, D.D., Lee, J.T., & Lauenroth, W.K. (2009). Intercomparison, interpretation, and assessment of spring phenology in North America estimated from remote sensing for 1982–2006. *Global Change Biology, 15*, 2335-2359

White, M.A., Hoffman, F., Hargrove, W.W., & Nemani, R.R. (2005). A global framework for monitoring phenological responses to climate change. *Geophysical Research Letters, 32*, L04705

White, M.A., & Nemani, R.R. (2006). Real-time monitoring and short-term forecasting of land surface phenology. *Remote Sensing of Environment, 104*, 43-49

White, M.A., Thornton, P.E., & Running, S.W. (1997). A continental phenology model for monitoring vegetation responses to interannual climatic variability. *Global Biogeochemical Cycles, 11*, 217-234

Wielgolaski, F.E. (1999). Starting dates and basic temperatures in phenological observations of plants. *International Journal of Biometeorology, 42*, 158-168

Wielgolaski, F.E. (2001). Phenological modifications in plants by various edaphic factors. *International Journal of Biometeorology, 45*, 196-202

Williamson, S.N., Hik, D.S., Gamon, J.A., Kavanaugh, J.L., & Koh, S. (2012). Evaluating Cloud Contamination in Clear-Sky MODIS Terra Daytime Land Surface Temperatures Using Ground-Based Meteorology Station Observations. *Journal of Climate, 26*, 1551-1560

Wu, C., Hou, X., Peng, D., Gonsamo, A., & Xu, S. (2016). Land surface phenology of China's temperate ecosystems over 1999–2013: Spatial–temporal patterns, interaction effects, covariation with climate and implications for productivity. *Agricultural and Forest Meteorology, 216*, 177-187

Wu, C., Niu, Z., Tang, Q., Huang, W., Rivard, B., & Feng, J. (2009). Remote estimation of gross primary production in wheat using chlorophyll-related vegetation indices. *Agricultural and Forest Meteorology, 149*, 1015-1021

Wu, W.-b., Yang, P., Tang, H.-j., Zhou, Q.-b., Chen, Z.-x., & Shibasaki, R. (2010). Characterizing Spatial Patterns of Phenology in Cropland of China Based on Remotely Sensed Data. *Agricultural Sciences in China, 9*, 101-112

Wu, W., Shibasaki, R., Yang, P., Zhou, Q., & Tang, H. (2008). Variations in cropland phenology in China from 1983 to 2002. *The International Archives of the Photogrammetry, Remote Sensing and Spatial Information Sciences, 37*, 1539-1544

Xiao, D., Tao, F., Liu, Y., Shi, W., Wang, M., Liu, F., Zhang, S., & Zhu, Z. (2013). Observed changes in winter wheat phenology in the North China Plain for 1981–2009. *International Journal of Biometeorology, 57*, 275-285

Xiao, X., Boles, S., Frolking, S., Li, C., Babu, J.Y., Salas, W., & Moore Iii, B. (2006). Mapping paddy rice agriculture in South and Southeast Asia using multi-temporal MODIS images. *Remote Sensing of Environment, 100*, 95-113

Xiao, X., Boles, S., Frolking, S., Salas, W., Moore, B., Li, C., He, L., & Zhao, R. (2002). Observation of flooding and rice transplanting of paddy rice fields at the site to landscape scales in China using VEGETATION sensor data. *International Journal of Remote Sensing, 23*, 3009-3022

Xiao, X., Boles, S., Liu, J., Zhuang, D., Frolking, S., Li, C., Salas, W., & Moore Iii, B. (2005). Mapping paddy rice agriculture in southern China using multi-temporal MODIS images. *Remote Sensing of Environment, 95*, 480-492

Xie, Y., Sha, Z., & Yu, M. (2008). Remote sensing imagery in vegetation mapping: a review. *Journal of Plant Ecology, 1*, 9-23

Xin, J., Yu, Z., van Leeuwen, L., & Driessen, P.M. (2002). Mapping crop key phenological stages in the North China Plain using NOAA time series images. *International Journal of Applied Earth Observation and Geoinformation, 4*, 109-117

Xu, W., & Liu, X. (2007). Response of Vegetation in the Qinghai-Tibet Plateau to Global Warming. *Chinese Geographical Science, 17*, 151-159

Xue, J., & Su, B. (2017). Significant Remote Sensing Vegetation Indices: A Review of Developments and Applications. *Journal of Sensors, 2017*, 17

Ying, G., Alessandra, M., & Dongryeol, R. (2015). Optical Sensing of Vegetation Water Content: A Sysnthesis Study. *IEEE Journal of Selected Topics in Applied Earth Observations and Remote Sensing, 8*, 1456-1464

You, X., Meng, J., Zhang, M., & Dong, T. (2013). Remote sensing based detection of crop phenology for agricultural zones in China using a new threshold method. *Remote sensing, 5*, 3190-3211

Yu, F., Price, K.P., Ellis, J., & Shi, P. (2003). Response of seasonal vegetation development to climatic variations in eastern central Asia. *Remote Sensing of Environment, 87*, 42-54

Yu, L., Liu, T., Bu, K., Yan, F., Yang, J., Chang, L., & Zhang, S. (2017). Monitoring the long term vegetation phenology change in Northeast China from 1982 to 2015. *Scientific Reports, 7*, 14770

Yu, X., Wang, Q., Yan, H., Wang, Y., Wen, K., Zhuang, D., & Wang, Q. (2014). Forest Phenology Dynamics and Its Responses to Meteorological Variations in Northeast China. *Advances in Meteorology, 2014*, 12

Zarco-Tejada, P.J., Miller, J.R., Noland, T.L., Mohammed, G.H., & Sampson, P.H. (2001). Scaling-up and model inversion methods with narrowband optical indices for chlorophyll content estimation in closed forest canopies with hyperspectral data. *Geoscience and Remote Sensing, IEEE Transactions on, 39*, 1491-1507

Zeng, H., Jia, G., & Epstein, H. (2011). Recent changes in phenology over the northern high latitudes detected from multi-satellite data. *Environmental Research Letters, 6*, 045508

Zhang, G., Song, Q., & Yang, D. (2006a). Phenology of *Ficus racemosa* in Xishuangbanna, Southwest China1. *Biotropica, 38*, 334-341

Zhang, G., Xiao, X., Dong, J., Kou, W., Jin, C., Qin, Y., Zhou, Y., Wang, J., Menarguez, M.A., & Biradar, C. (2015a). Mapping paddy rice planting areas through time series analysis of MODIS land surface temperature and vegetation index data. *ISPRS Journal of Photogrammetry and Remote Sensing, 106*, 157-171

Zhang, H., Chen, H., & Zhou, G. (2012a). The Model of Wheat Yield Forecast Based on MODIS-NDVI —— A Case Study of Xinjiang. In, *XXII ISPRS* (pp. 25-28). Melbourne, Australia

Zhang, H., Li, Q., Liu, J., Shang, J., Du, X., Zhao, L., Wang, N., & Dong, T. (2017). Crop classification and acreage estimation in North Korea using phenology features. *GIScience & Remote Sensing, 54*, 381-406

Zhang, J., Feng, L., Zou, H., & Liu, D.L. (2015b). Using ORYZA2000 to model cold rice yield response to climate change in the Heilongjiang province, China. *The Crop Journal, 3*, 317-327

Zhang, L., Turkington, R., & Tang, Y. (2010). Flowering and fruiting phenology of 24 plant species on the north slope of Mt. Qomolangma (Mt. Everest). *Journal of Mountain Science, 7*, 45-54

Zhang, M., Lin, H., Wang, G., Sun, H., & Fu, J. (2018a). Mapping Paddy Rice Using a Convolutional Neural Network (CNN) with Landsat 8 Datasets in the Dongting Lake Area, China, *10*, 1840

Zhang, S., & Liu, L. (2014). The potential of the MERIS Terrestrial Chlorophyll Index for crop yield prediction. *Remote Sensing Letters, 5*, 733-742

Zhang, X., Friedl, A.M., Schaaf, B.C., Strahler, H.A., Hodges, C.F.J., Gao, F., Reed, C.B., & Huete, A. (2003). Monitoring vegetation phenology using MODIS. *Remote Sensing of Environment, 84*, 471-475

Zhang, X., Friedl, M.A., & Schaaf, C.B. (2006b). Global vegetation phenology from Moderate Resolution Imaging Spectroradiometer (MODIS): Evaluation of global patterns and comparison with in situ measurements. *Journal of Geophysical Research: Biogeosciences, 111*, G04017

Zhang, X., Friedl, M.A., Schaaf, C.B., & Strahler, A.H. (2004). Climate controls on vegetation phenological patterns in northern mid- and high latitudes inferred from MODIS data. *Global Change Biology, 10*, 1133-1145

Zhang, X., Friedl, M.A., Tan, B., Goldberg, M.D., & Yu, Y. (2012b). Long-Term Detection of Global Vegetation Phenology from Satellite Instruments. In X. Dr. Zhang (Ed.), *Phenology and Climate Change* (pp. 297-320): InTech

Zhang, X., Sun, R., Zhang, B., & Tong, Q. (2008). *Land cover classification of the North China Plain using MODIS_EVI time series*.

Zhang, X., Wu, B., Ponce-Campos, G.E., Zhang, M., Chang, S., & Tian, F. (2018b). Mapping up-to-Date Paddy Rice Extent at 10 M Resolution in China through the Integration of Optical and Synthetic Aperture Radar Images, *10*, 1200

Zhang, Y., Wang, C., Wu, J., Qi, J., & Salas, W.A. (2009). Mapping paddy rice with multitemporal ALOS/PALSAR imagery in southeast China. *International Journal of Remote Sensing, 30*, 6301-6315

Zhao, J., Zhang, Y., Tan, Z., Song, Q., Liang, N., Yu, L., & Zhao, J. (2012). Using digital cameras for comparative phenological monitoring in an evergreen broad-leaved forest and a seasonal rain forest. *Ecological Informatics, 10*, 65-72

Zheng, J., Ge, Q., Hao, Z., & Wang, W.-C. (2006). Spring Phenophases in Recent Decades Over Eastern China and Its Possible Link to Climate Changes. *Climatic Change, 77*, 449-462

Zhong, L., Gong, P., & Biging, G.S. (2014). Efficient corn and soybean mapping with temporal extendability: A multi-year experiment using Landsat imagery. *Remote Sensing of Environment, 140*, 1-13

Zhong, L., Hu, L., Yu, L., Gong, P., & Biging, G.S. (2016). Automated mapping of soybean and corn using phenology. *ISPRS Journal of Photogrammetry and Remote Sensing, 119*, 151-164

Zhou, M., Wang, H., & Huo, Z. (2017). A new prediction model for grain yield in Northeast China based on spring North Atlantic Oscillation and late-winter Bering Sea ice cover. *Journal of Meteorological Research, 31*, 409-419

Zhou, Y., Xiao, X., Qin, Y., Dong, J., Zhang, G., Kou, W., Jin, C., Wang, J., & Li, X. (2016). Mapping paddy rice planting area in rice-wetland coexistent areas through analysis of Landsat 8 OLI and MODIS images. *International Journal of Applied Earth Observation and Geoinformation, 46*, 1-12

Zhu, K., & Wan, M. (1963). A productive science - Phenology. *Public Science (Chinese)*

Zhu, W., Pan, Y., He, H., Wang, L., Mou, M., & Liu, J. (2012). A Changing-Weight Filter Method for Reconstructing a High-Quality NDVI Time Series to Preserve the Integrity of Vegetation Phenology. *IEEE Transactions on Geoscience and Remote Sensing, 50*, 1085-1094